

The Development of Electrospun Polymer Devices for Drug Delivery to the Oral Mucosa

Katharina Clitherow



Thesis submitted for the degree of Doctor of Philosophy

School of Clinical Dentistry

University of Sheffield

Submitted July 2019

Abstract

Oral health greatly affects our quality of life and there is a clinical need to improve oral disease treatment. Currently high dose systemic drugs are the main treatment option for localised oral lesions and existing treatments such as mouthwashes, gels or creams only have a transient therapeutic effect due to limited drug retention and removal by saliva. Mucoadhesive electrospun fibrous polymer patches for local oral drug delivery are suited to overcome these challenges, where the high surface area to volume ratio of the fibres allows for increased localised drug release. Therefore, the aim of this PhD was to develop an electrospun mucoadhesive drug delivery device to target diseased oral tissue locally.

A mixture of poly(vinyl pyrrolidone) (PVP), Eudragit RS100 and poly(ethylene oxide) in ethanol were used to manufacture the drug-containing electrospun patch layer, whilst a backing layer consisting of poly(ϵ -caprolactone) melted on top of the drug-containing patch was added to aid uni-directional drug release into tissue. Increasing the concentration of polymers in solution greatly increased its viscosity compared to the surface tension and conductivity resulting in proportionally larger fibre diameters. The PCL solutions formed significantly more undulating and fewer straight electrospun fibres compared to the PVP solutions at the same concentration of polymer, where the higher surface tension and lower conductivity of the PCL solutions likely attributed to this observed difference.

The treatment and control of localised oromucosal pain is a largely unmet clinical need. The amorphous form of the anaesthetic, lidocaine was successfully loaded into the electrospun patches and ~80% released from lidocaine-HCl containing patches after 1 h. The flux of lidocaine permeating through 1 mm thick *ex vivo* porcine tissue was $4.47 \pm 0.16 \text{ ng cm}^{-2} \text{ s}^{-1}$. Using mass spectrometry imaging, lidocaine penetrated the tissue within 15 minutes with the drug distribution being localised to tissue directly under the patch. These lidocaine-loaded patches may have applications as analgesic-containing wound dressing or as an anaesthetic patch prior to dental treatments.

Electrospun patches were further tested for the treatment of oral candidiasis. Here the antifungal capabilities of medium-chain saturated fatty acids were tested on *in vitro*-cultured *Candida albicans*. Electrospun patches containing nonanoic (C9) and dodecanoic acid (C12) significantly inhibited yeast and biofilm growth for both wild-type and azole resistant *C. albicans* (C9 had an eight times greater inhibition area on yeast form of azole-resistant strain compared to fluconazole), although at therapeutic levels these fatty acids were also toxic to monolayer cultures of oral keratinocytes (1.4 mM of C12 for 50% cell inhibition). Further toxicity work on full thickness *in vitro* oral mucosa models is required. Overall the work in this thesis showed that electrospun patches have clinical potential for targeted drug delivery at diseased oromucosal sites. It is envisioned that such an electrospun drug delivery device would have wide ranging implications for treatment of a whole range of oral diseases and thereby improve the quality of life for many patients.

Acknowledgements

My PhD would not have been possible and a lot more difficult without the help and support from my colleagues, family and friends throughout the past four years. There are many people and some organisations I need to thank, and I hope to have mentioned them all here.

Firstly, I would like to thank my supervisors Prof Paul Hatton, Prof Craig Murdoch and Dr Sebastian Spain for making this PhD possible. Both for receiving the funding for this PhD from the EPSRC CDT Polymers, Soft Matter and Colloids (Grant EP/K029592/1) and from AFYX Therapeutics and for their continuous supervision, teaching and advice. I have learnt a lot in the past four years, and this can largely be attributed to a great supervision team.

The School of Clinical Dentistry and the University of Sheffield as a whole has been a fantastic place of work and I have a number of people to thank for this. With regards to the scientific PhD work, thank you to: Prof Paul Hatton for continuously underlying the importance on good presentation of data and his general knowledge of lab practice and project management; Prof Craig Murdoch for introducing me to microbiology and tissue culture laboratory work, as well as his teaching and emphasis on statistical analysis of data; Dr Sebastian Spain for welcoming me into the chemistry department and helping me with analytical chemistry method decisions, including discussions on how to best analyse the data afterwards; Dr Martin Santocildes-Romero, a post-doctoral researcher in the group at the start of my PhD, for teaching me electrospinning and on the patch development work that he was doing for AFYX at the time; Dr Helen Colley, for supplying the FNB6 cells for the monolayer studies, for making the 3D oral mucosal models and for her tissue engineering knowledge during the development of the project; Dr Robert Moorehead, technician of the technical/manufacturing labs in the Dental School, for his speedy ordering of consumables and general help in the lab; Mr Jason Heath, technician of the microbiology lab, who was always willing to answer my methodology or equipment questions; Mr Chris Hill, for gold coating samples and teaching me how to use the SEM (and for running TEM samples, that however were unsuccessful and not used in this thesis); Mr Robert Hanson, for teaching and helping me use GC and HPLC; Mr Simon Thorpe, for running the GC-MS samples; Dr Sandra van Meurs, for running the ^1H NMR samples; Dr Thomas Paterson for introducing me to and helping me use Autodesk Maya to create visual models and animations of my work.

During my PhD I was fortunate enough to undertake a three-month placement at the University of Copenhagen Pharmacy Department, from which around half the data in chapter four arises. Here I had another fantastic supervision team, so thank you to: Dr Jette Jacobsen, for always having an open door and for helping me with the *ex vivo* studies; Dr Christian Janfelt and his PhD student Ms Anne-Mette Handler, for the MALDI-MSI advice; Prof Hanne Mørck Nielsen and her PhD student Ms Mai Bay Stie, for their research knowledge input in drug delivery.

My PhD was partly supported financially by AFYX Therapeutics, with whom I had twice yearly meetings. The research in this PhD was to inform them of future potential applications of their product. These meetings were always very thought-provoking and it was interesting to see their company and clinical trial development throughout the PhD. At the end of this PhD I completed a six month industrial placement at their Copenhagen HQ. The team at AFYX has changed since I started my PhD, but the new and former employees I would like to thank for their supervision and interest are: Dr Jens Hansen, Dr Lars Siim Madsen, Dr Lars Hellerung Christiansen, Dr Nishan De Silva and Dr Martin Santocildes-Romero. For the six month placement I am very grateful to have received funding from the National Productivity Investment Fund from the EPSRC which funds CDT students to take innovation placements.

Other groups I would like to thank are: the aforementioned Polymer CDT led by Prof Steve Armes for the industrial, polymer and business seminars and for the multi-disciplinary network of students brought together from such a stimulating academic environment and comradeship; the Bioengineering Health Technologies group, for the interesting big group meetings; the Dental School Research Society, of which I was a committee member for three years, and which made me many friends; the University of Sheffield Triathlon Club, which I only joined in my final year, but enjoyed immensely; and to all other friends I made along the way.

Finally, a big thank you to my parents and sister for their continued love and support throughout my PhD and for looking after me through the multiple sports injuries in the last few years!

The human side of my PhD – a list of firsts during this time in no particular order

First ...

...time running a half marathon

...time completing a triathlon

...time pipetting

...time handling cells in a lab

...love

...heartbreak

...time mourning the passing of a school friend

...major injury (reconstructive knee surgery)

...bone fracture (elbow)

...time being part of a society committee

...time living abroad during my adult life

...conference presentation

...adult language lessons

...time travelling in Japan, Cambodia, Laos, America, Sweden and Norway

...time creating my own animation

...triathlon club membership

...time painting a landscape on a large canvas (of the peak district)

...PhD

“Learning does not make one learned: there are those who have knowledge and those who have understanding. The first requires memory and the second philosophy.”

- Alexandre Dumas, The Count of Monte Christo

List of Outputs

Publications:

M.E. Santocildes-Romero, L. Hadley, **K.H. Clitherow**, J. Hansen, C. Murdoch, H.E. Colley, M.H. Thornhill, P. V. Hatton, Fabrication of electrospun mucoadhesive membranes for therapeutic applications in oral medicine, *ACS Appl. Mater. Interfaces*. 9 (2017) 11557–11567. doi:10.1021/acsami.7b02337.

Submitted to ACS Molecular Pharmaceutics May 2019: **K. H. Clitherow**, C. Murdoch, S. G. Spain, A. M. Handler, H. E. Colley, M. B. Stie, H. M. Nielsen, C. Janfelt, P. V. Hatton, J. Jacobsen, Mucoadhesive electrospun patch delivery of lidocaine to the oral mucosa and spatial distribution in tissue using MALDI mass spectrometry imaging

In Preparation: **K. H. Clitherow**, T. M. Binaljadm, J. Hansen, H. E. Colley, S. G. Spain, P. V. Hatton, C. Murdoch, Medium-chain fatty acids released from polymeric electrospun fibres inhibit *Candida albicans*

Conference presentations:

Warwick Polymer Conference July 2016; Warwick: “Development of electrospun polymer devices for drug delivery to the oral mucosa” (Poster)

United Kingdom Society for Biomaterials (UKSB) June 2017; Loughborough: “Electrospun polymer patches incorporating antifungal agents to inhibit *Candida albicans*” (Oral Presentation)

Europeans Society of Biomaterials (ESB) September 2017; Athens: “Development of electrospun polymer patches incorporating antifungal agents to inhibit *Candida albicans*” (Oral Presentation)

The Biomaterials and Tissue Engineering Group (BiTEG) December 2017; Leeds: “Inhibiting *Candida Albicans* using anti-fungal electrospun patches” (Oral Presentation)

Medical Technologies IKC & Regener8 June 2018; Leeds: “The development of electrospun polymer devices for drug delivery to the oral mucosa” (Media Presentation; Won Dissemination of Research Prize)

International Association of Dental Research (IADR) July 2018; London: “Incorporating anti-fungal agents in electrospun patches to treat oral candidiasis” (Poster)

Tissue Engineering and Regenerative Medicine (TERMIS) September 2018; Kyoto: “Incorporating anti-fungal agents in electrospun patches to treat oral candidiasis” (Poster)

European Association of Oral Medicine (EAOM) September 2018; Gothenburg: “Electrospun fibres deliver lidocaine HCl to porcine buccal mucosa: An *ex vivo* permeation and MALDI-MS imaging study” (Poster)

European Society of Biomaterials (ESB) September 2019; Dresden: “Mucoadhesive electrospun fibre delivery of lidocaine HCl to porcine oral mucosa with drug distribution in tissue analysed by mass spectrometry imaging” (Poster)

Table of Contents

Abstract	i
Acknowledgements.....	ii
List of Outputs.....	v
Table of Contents	vii
List of Figures	xi
List of Tables	xvii
List of Equations	xviii
Abbreviations.....	xx
1. Literature review	1
1.1 Introduction	1
1.2 Anatomy of healthy oral tissue	3
1.3 Oral diseases and oral medicine of soft tissues and respective therapies	5
1.3.1 Treatment of oral pain.....	8
1.3.2 Antifungal therapy for oral candidiasis	10
1.3.3 Oral wound dressings	12
1.4 Electrospinning of polymers	12
1.4.1 Electrospinning process.....	13
1.4.2 Properties of polymer solutions.....	15
1.5 Polymer system.....	19
1.5.1 Biocompatible polymers.....	19
1.5.2 Bioadhesive polymers.....	27
1.6 Drug incorporation in an electrospun patch	28
1.6.1 Review of electrospun polymer-drug systems.....	29
1.7 Drug release and permeation through tissue	34
1.7.1 Quantifying drug release.....	34
1.7.2 Drug permeation into tissue	35
1.8 Summary.....	37
1.9 Hypothesis	38

1.10	Aims and Objectives.....	38
2.	Materials and Methods.....	41
2.1	Materials	41
2.2	Methods: Characterisation of electrospinning polymer solutions and the resulting electrospun mats.....	47
2.2.1	Preparing the polymer solutions.....	47
2.2.2	Viscosity of polymer solutions.....	47
2.2.3	Conductivity of polymer solutions.....	49
2.2.4	Surface tension of polymer solutions	49
2.2.5	Electrospinning parameters	49
2.2.6	Morphology of electrospun mats.....	50
2.3	Methods: <i>Ex vivo</i> permeation of lidocaine released from electrospun patches	53
2.3.1	Manufacture of electrospun mats containing lidocaine	53
2.3.2	Dual layer patch manufacture	53
2.3.3	Differential scanning calimetry	54
2.3.4	pH of electrospun patches containing lidocaine base and lidocaine HCl	54
2.3.5	Isotonic buffer solution.....	54
2.3.6	Ultraviolet scan of lidocaine HCl	55
2.3.7	High-Performance Liquid Chromatography	55
2.3.8	Release of lidocaine in buffer from the electrospun patches	57
2.3.9	Preparation of <i>ex vivo</i> porcine buccal mucosa.....	57
2.3.10	Permeation of lidocaine through porcine buccal mucosa	58
2.3.11	Incubation of the electrospun patches on porcine buccal mucosa.....	60
2.3.12	Cryosectioning.....	61
2.3.13	Matrix application for MALDI-MSI of tissue samples	62
2.3.14	Matrix-Assisted Laser Desorption Ionisation – Mass Spectrometry Imaging ...	63
2.3.15	Using MSiReader software to determine presence of analytes	64
2.3.16	Haemotoxylin and Eosin (H&E) stain	65
2.3.17	Optical microscope images of H&E stained tissue	65

2.4	Methods: Electrospun antifungal mat fabrication	67
2.4.1	Preparation of agar plates and yeast-peptone-dextrose (YPD) broth	67
2.4.2	<i>Candida albicans</i> strains.....	67
2.4.3	Preparation of short- and medium-chain fatty acid stock solutions.....	67
2.4.4	Manufacture of electrospun mats incorporating medium chain fatty acids.....	68
2.4.5	Determination of the concentration of fatty acid in the PCL electrospun patches using nuclear magnetic resonance spectroscopy.....	68
2.4.6	Gas Chromatography – Mass spectrometry to determine concentration of fatty acid in the PVP/RS100 electrospun patches.....	69
2.4.7	Agar disc diffusion	69
2.4.8	Biofilm viability of <i>Candida albicans</i> treated with fatty acid solution.....	74
2.4.9	Biofilm viability assay of <i>Candida albicans</i> treated with fatty acid containing electrospun patches.....	74
2.4.10	Live/Dead stain of <i>C. albicans</i> biofilm	75
2.4.11	Cytotoxicity of fatty acid solutions on oral keratinocyte monolayers	75
2.4.12	Tissue models of 3D oral mucosa.....	76
2.4.13	Infecting 3D tissue models with <i>C. albicans</i> and applying antifungal electrospun patches	76
2.4.14	Lactate dehydrogenase assay	78
2.4.15	Histological processing of oral mucosal models.....	78
2.4.16	Periodic-acid Schiff staining.....	79
3.	Results and Discussion: Characterising electrospinning solutions and resulting electrospun patches.....	81
3.1	Introduction	81
3.2	Rheology of polymer solutions.....	81
3.3	Conductivity of polymer solutions	86
3.4	Surface tension of electrospinning polymer solutions	88
3.5	Morphology and fibre diameters of electrospun mats.....	91
3.6	Discussion.....	98
4.	Results & Discussion: Delivery of lidocaine from electrospun patches	103

4.1 Introduction.....	103
4.2 Incorporating lidocaine into electrospun patches	103
4.3 Lidocaine release from electrospun patches.....	108
4.4 Lidocaine permeation through <i>ex vivo</i> porcine buccal mucosa	109
4.5 Mass spectrometry imaging of lidocaine from electrospun patches permeating into <i>ex vivo</i> tissue	111
4.5 Discussion	117
5. Results & Discussion: Medium-chain fatty acids in electrospun patches inhibit <i>Candida albicans</i>	125
5.1 Introduction.....	125
5.2 Medium chain saturated fatty acids inhibit <i>Candida albicans</i> yeast growth	125
5.3 Medium chain saturated fatty acids show toxicity towards <i>Candida albicans</i> biofilms	128
5.4 Incorporating medium chain saturated fatty acids in electrospun patches.....	131
5.5 Electrospun patches containing fatty acids inhibit <i>C. albicans</i> yeast growth.....	139
5.6 Electrospun patches containing fatty acids reduce metabolic activity of <i>C. albicans</i> biofilms.....	144
5.7 Toxicity of fatty acid solutions on oral keratinocytes.....	147
5.8 Application of fatty acid containing electrospun patches on 3D oral mucosa tissue models	148
5.9 Discussion	153
6. Conclusions	163
7. Future Work.....	167
8. References	171

List of Figures

Figure 1.1. Schematic of the final clinical and commercial aim; where the electrospun polymer patches have the ability of adhering to various oral mucosal tissue surfaces and releasing drugs relevant to the disease it is treating.....	2
Figure 1.2. Schematic of the oral mucosa membrane.	4
Figure 1.3. The electrospinning setup is composed of a) the syringe filled with the polymer solution and any other therapeutic agents or drug compounds, b) the syringe feed pump, c) the grounded high voltage power supply, d) the focussing electrode ring, e) the grounded collector plate.....	14
Figure 1.4. Side-view diagram of the electrospinning set-up and fluid flow terminology for the polymer solution during electrospinning.	16
Figure 2.1. Amplitude sweep test to detect the linear viscoelastic region for 10% PCL in DCM/DMF (93/7 w/w%), 10% PVP in ethanol and a mixture of 10% PVP and 10% RS100 in ethanol (n=1).	48
Figure 2.2. Schematic showing how areas of an electrospun patch were cut out and imaged under the SEM. These 4 cut outs from one patch (A-D) were imaged to measure the range of fibre diameters for one electrospun patch. Using imageJ all fibre diameters were measured in these 8 imaged areas. For one cut out, e.g. section A, the data from the two images is combined.	51
Figure 2.3. Determining the optimal wavelength for lidocaine HCl in PBS, where 1 mL of the solution in a UV-Cuvette at different concentrations of lidocaine is shown (n=1).	55
Figure 2.4. Lidocaine HCl was dissolved in PBS at increasing concentrations and run through the HPLC at a wavelength of 262 nm. The resulting peaks between 9.8 and 10.3 min are shown. Areas under the curve was plotted to show good linearity ($R^2 = 1.0$) across the different concentrations measured.	56
Figure 2.5. The images above show how the buccal mucosa was prepared prior to further experimentation. The following is depicted: A) de-frosted porcine buccal mucosa (ruler only associated to this image), B) porcine buccal mucosa cut to size and mounted on the Ussing slider, C) the addition of an electrospun patch to the porcine cheek, D) the second slider placed on top of the cheek and electrospun patch to sandwich everything together.....	58
Figure 2.6. Overview of the Ussing chamber system and its components.	59
Figure 2.7. Mounting the tissue sample prior to matrix application.	62
Figure 2.8. Matrix application for MALDI-MSI set up.	63
Figure 2.9. Schematic of MALDI-MSI principle, adapted from Hoffman and Strobaant [181].	64
Figure 2.10. Schematic of Agar disc diffusion method.	71

Figure 2.11. Schematic of 3D oral mucosa model growth, infection of model, and electrospun patch treatment.....	77
Figure 3.1. Viscosity of polymer solutions at different concentrations in solvent. PVP (blue) and PVP / RS100 (green) are dissolved in 97% (w/w) ethanol and PCL in DCM/DMF (93/7% w/w) (red and orange) (mean +/- SD, n=3).....	82
Figure 3.2. Viscosity of PVP 10% and RS100 12.5% with additives at different concentrations in 97% ethanol (mean +/- SD, n=3). Adapted from Santocildes-Romero et al. [177].....	83
Figure 3.3. Viscosity of PCL in DCM/DMF (93% / 7%) (red), PVP (blue) and PVP 10%/ with RS100 (green) in 97% ethanol at different concentrations of polymer as recorded at a shear rate of 40 s ⁻¹ (mean +/- SD, n=3). The exponential growth was calculated using non-linear regression in GraphPad Prism. Adapted from Santocildes-Romero et al. [177].....	85
Figure 3.4. Conductivity of PVP in 97% ethanol (blue) and PCL in DCM/DMF (93% / 7%) (red) at different polymer concentrations (mean +/- SD, n=3). Adapted from Santocildes-Romero <i>et al.</i> [177].	87
Figure 3.5. Conductivity of polymers in 97% ethanol (mean +/- SD, n=3). Adapted from Santocildes-Romero <i>et al.</i> [177].....	88
Figure 3.6. Surface tensions of PVP solutions with RS100 and PEO or dextran at different concentrations in 97% ethanol (blue) and the surface tensions of PCL solutions at different concentrations in DCM/DMF (93% / 7%) (red) are shown. (Mean +/- SD, n=5 technical repeats). Significance above SD bar is compared to the respective solvent system (**** p < 0.0001). Significant difference between ethanol and DCM/DMF was ****. Significance between polymer solutions at different concentrations are not shown.	90
Figure 3.7. SEM images of PVP fibres at A) 5% concentration, B) 10% concentration, C) 15% concentration and D) 20% concentration of polymer. Adapted from Santocildes-Romero et al. [177].....	93
Figure 3.8. SEM images of PCL fibres at A) 5% concentration, B) 10% concentration, C) 15% concentration and D) 20% concentration of polymer.	94
Figure 3.9. Fibre diameters derived from SEM images of PVP at concentrations ranging from 5% to 20% and PCL at concentrations 10% to 20% (n = 8 images and > 400 fibres measured per condition). Box and whisker plots show minimum, maximum, 25 th percentile, median and 75 th percentile. Mean is shown by + sign. Adapted from Santocildes-Romero et al. [177]. ...	95
Figure 3.10. SEM images of PVP patches containing RS100, RS100 and dextran and RS100 and PEO, as the description at the top right of the individual images indicates.....	96
Figure 3.11. SEM images of dual-layer electrospun patches. Patches consist of a backing layer (BL), made up of melted PCL fibres and an adhesive layer (AL) made up of PVP, RS100 and PEO fibres and particles.....	97

Figure 4.1. SEM images of electrospun patches made up of 10% PVP, 12.5% RS100 and 10% PEO incorporating A) no addition, B) lidocaine HCl and C) lidocaine base.	104
Figure 4.2. DSC heating profiles of A) an empty pan, B) lidocaine HCl powder, C) lidocaine base powder, D) PVP/RS100/PEO electrospun fibres, E) PVP/RS100/PEO electrospun fibres containing lidocaine HCl and F) PVP/RS100/PEO electrospun fibres containing lidocaine base. The onset melting temperatures of the upward facing enthalpy peaks are given to the nearest 1 °C. The image is representative of n=2 independent experiments...	107
Figure 4.3. pH of electrospun patches dissolved in deionised water measured at 20 °C either as the plain PVP/RS100/PEO patch without drug, the patch containing lidocaine HCl or the patch with lidocaine base (mean ± SD, n=3).	108
Figure 4.4. Accumulative release of lidocaine into PBS from electrospun patches containing either lidocaine base or lidocaine HCl over 1 h. Data presented is the mean ± SD (n=4), where only upward SD is shown. Mann-Whitney U test showed a significant difference in release between the two drugs (p=0.0026).	109
Figure 4.5. Accumulative permeation of lidocaine released from an electrospun patch through ex vivo porcine buccal mucosa. The electrospun patches contained between 0.20 and 0.35 mg lidocaine HCl. Data are mean ± SD (n=6).....	110
Figure 4.6. Accumulative permeation of lidocaine applying 3% (w/v) lidocaine HCl in PBS through ex vivo porcine buccal mucosa. Data are mean ± SD (n=4).	111
Figure 4.7. Mass spectra corresponding to one pixel from the MSI images of porcine buccal tissue with lidocaine HCl solution applied to the surface of the epithelium. The epithelium marker PG (34:1) (m/z 771.5134 [M+Na] ⁺) and lidocaine (m/z 235.1807 [M+Na] ⁺) are circled.	113
Figure 4.8. H&E stained tissue sections and corresponding MALDI-MS images of porcine buccal mucosa with no treatment (control), and exposed to 0.3% (w/v) lidocaine HCl solution (m/z 235.1805 [M+Na] ⁺ ; red) after 15 min, 1 h and 3 h. The epithelium (blue) for each sample is shown using the epithelial marker PG (34:1) (m/z 771.5130 [M+Na] ⁺).....	114
Figure 4.9. H&E stained tissue sections and corresponding MALDI-MS images of porcine buccal mucosa exposed to dual-layer electrospun patches containing 3% (w/v) lidocaine HCl (m/z 235.1805 [M+Na] ⁺ ; red) after 15 min, 1 h and 3 h. The epithelium (blue) for each sample is shown using the epithelial marker PG (34:1) (m/z 771.5130 [M+Na] ⁺). The arrows in the H&E images show the position of the electrospun patch.	115
Figure 4.10. H&E stained tissue sections and corresponding MALDI-MS images of porcine buccal mucosa exposed to dual-layer electrospun patches containing 3% (w/v) lidocaine base (m/z 235.1805 [M+Na] ⁺ ; red) after 15 min, 1 h and 3 h. The epithelium (blue) for each sample is shown using the epithelial marker PG (34:1) (m/z 771.5130 [M+Na] ⁺). The arrows in the H&E images show the position of the electrospun patch.	116

- Figure 5.1.** Inhibition surface areas on *C. albicans* streaked agar plates around filter discs impregnated with fatty acids made up at 0.2 M in DMSO, ranging from butanoic (C5) to dodecanoic acid (C12), with positive controls fluconazole (0.8 mM) in DMSO and miconazole discs (10 µg or 2.4 nmol). DMSO alone was used as the negative control. Results are for *C. albicans* strains BWP17, SC5314 and CAR17. Data are mean +/- SD (n = 3). *p<0.05; **p<0.01, ***p<0.001, ****p<0.0001 compared to DMSO controls. Significant differences of other fatty acids to C5:0 and C6:0 are not shown. Images show representative inhibition zones of commonly used antifungal drug miconazole and nonanoic acid (C9) on *C. albicans* streaked agar plates related to the graphs to the left of the images. 127
- Figure 5.2.** *C. albicans* strain SC5314 biofilm viability when subjected to fatty acids heptanoic acid (C7) to dodecanoic acid (C12) ranging in concentration from 400 mM to 1.56 mM using a metabolic XTT assay. The data is normalised to untreated controls (100% viability) and mean +/- SD over three plates and five wells per concentration is given (n=3). 129
- Figure 5.3.** Fluorescence live/dead stain images of SC5314 biofilm subjected to media control (RPMI media only), 50 mM nonanoic acid (C9) or 50 mM dodecanoic acid (C12). Images show viable cells (green), dead cells (red) and the live/ dead images combined (n=3 wells per treatment). 131
- Figure 5.4.** SEM images of electrospun patches consisting of 10% PCL, alone or with fatty acids heptanoic acid (C7) to dodecanoic acid (C12) incorporated into the patch..... 133
- Figure 5.5.** SEM images of electrospun patches consisting of 10% PVP/ 12.5% RS100, alone or incorporating fatty acids from heptanoic acid (C7) to dodecanoic acid (C12). 134
- Figure 5.6.** ¹H NMR spectra of PCL in pellet form, electrospun PCL fibres, neat dodecanoic acid (C12), and dodecanoic acid (C12) in PCL electrospun fibres, all dissolved in deuterated chloroform. The chemical structures of PCL and dodecanoic acid (C12) are displayed at the top of the figure. The ¹H NMR signals from the PCL and dodecanoic acid structures are alphabetised and numbered, respectively, correlate to the labels in the spectra. The fatty acid peak at 0.8 ppm labelled '11' and the PCL peak at 4.1 ppm labelled 'a' are used for analysis and are circled in red. 136
- Figure 5.7** ¹H NMR spectra of a PCL electrospun patch and of fatty acids heptanoic acid (C7) to dodecanoic acid (C12) incorporated in the PCL fibres and dissolved in deuterated chloroform are given. The fatty acid peak at 0.8 ppm and the PCL peak at 4.1 ppm used for analysis are circled in red..... 137
- Figure 5.8.** Fatty acid concentration of heptanoic acid (C7) to dodecanoic acid (C12) in PCL fibres given in weight % of the total patch weight (n=2). 138

Figure 5.9. Nonanoic acid (C9) and dodecanoic acid (C12) concentration by percentage weight in PVP/RS100 fibres. Mean +/- SD shown for nonanoic acid (n=9) and dodecanoic acid (n=7).....	139
Figure 5.10. Inhibition zone surface areas on <i>C. albicans</i> strain SC5314 for fatty acids incorporated in A-C) PCL electrospun patches and D-F) PVP/RS100 electrospun patches. Mean +/- SD shown (n=3). *p<0.05; **p<0.01, ***p<0.001, ****p<0.0001, where the p value over the SD bar is compared to the plain patch system (PCL or PVP).	140
Figure 5.11. 10% PCL electrospun patches containing octanoic acid (C8) to dodecanoic acid (C12) removed from agar plates streaked with <i>C. albicans</i> after 18 hour.	142
Figure 5.12. 10% PVP and 12.5% RS100 electrospun patches containing octanoic acid (C8) to dodecanoic acid (C12) removed from agar plates streaked with <i>C. albicans</i> after 18 hours.	143
Figure 5.13. Biofilm viability of <i>C. albicans</i> strains A) SC5314 and B) CAR17 when PCL electrospun patches containing fatty acids heptanoic acid (C7) to dodecanoic acid (C12) were placed on the biofilm. Mean +/- SD (n=3). Kruskal-Wallis non-parametric test was used to determine significant differences compared to the plain PCL patch (*p<0.05; **p<0.01, ***p<0.001). Statistical differences between the fatty acids are not shown.....	145
Figure 5.14. Biofilm viability of <i>C. albicans</i> strains A) SC5314 and B) CAR17 when PVP/RS100 electrospun patches containing fatty acids heptanoic acid (C7) to dodecanoic acid (C12) are placed on the biofilm (plain PVP/RS100 patch labelled at PVP). Mean +/- SD (n=3). Kruskal-Wallis non-parametric test was used to determine significant differences compared to the plain PVP/RS100 patch *p<0.05; **p<0.01, ***p<0.001). Statistical differences between the fatty acids are not shown.	146
Figure 5.15. Cytotoxicity of A) nonanoic acid [C9] and B) dodecanoic acid [C12] on FNB6 immortalised oral keratinocyte monolayers using a metabolic activity MTT assay. Graphs shown are the mean +/- SD for 6 wells of one representative experiment. The IC ₅₀ value is given in the top right of the graph (mean +/- SD) for n=3 independent experiments	148
Figure 5.16. Representative light microscope images of PAS stained 3D oral mucosal models with the following treatments: A) nonanoic acid patch applied, B) dodecanoic acid patch applied, C) <i>C. albicans</i> with media only, D) <i>C. albicans</i> with plain patch applied, E) <i>C. albicans</i> with nonanoic acid patch applied, F) <i>C. albicans</i> with dodecanoic acid patch applied. The scale for all images are as shown in H.	151

Figure 5.17. Lactate dehydrogenase assay of media surrounding 3D oral mucosa models with different conditions applied to the models. 'PVP' is the plain PVP/RS100 electrospun patch applied to the models and labels 'C9' and 'C12' are nonanoic and dodecanoic acid containing electrospun patches, respectively. Label 'Ca' is short for Candida, where *C. albicans* strain SC5314 was applied to the surface of the epithelium. Mean +/- SD are of three technical repeats from n=1 biological experiment..... 152

List of Tables

Table 1.1. Clinical applications for a mucoadhesive patch drug delivery system.....	6
Table 1.2. Polymers with potential for electrospinning process.....	21
Table 1.3. Solvent properties.....	23
Table 1.4. Review of electrospun polymer-drug systems.....	30
Table 2.1. Polymers and solvents used in the electrospinning process.....	41
Table 2.2. Reagents used for permeation experiments.....	42
Table 2.3. Culture medium materials used in the microbiology experiments.....	43
Table 2.4. Reagents for antifungal testing.....	43
Table 2.5. Commercial cell viability kits.....	44
Table 2.6. Green's medium components.....	45
Table 2.7. Materials, reagents and cells used in tissue culture.....	46
Table 2.8. Staining solutions.....	46
Table 2.9. Electrospinning setup.....	50
Table 4.1. Concentration of lidocaine in electrospun patches.....	105
Table 5.1. The inhibitory concentration (IC ₅₀) of fatty acids on <i>C. albicans</i> SC5314 biofilm	129

List of Equations

1. Rouse Model of polymer relaxation 17

$$\lambda \approx \frac{6\eta_s[\eta]M}{\pi^2RT}$$

2. Taylor's Critical Electrospinning Voltage 19

$$V_c^2 = \frac{4H^2}{L^2} \left(\ln \frac{2L}{r} - \frac{3}{2} \right) 0.117\pi\gamma r$$

3. Fick's First Law of Diffusion 35

$$J = -D \frac{\delta C}{\delta x}$$

4. The apparent permeability coefficient 36

$$P_{app} = \frac{J_{ss}}{C_{donor}}$$

5. Shear rate of a fluid 48

$$\dot{\gamma} = \frac{4V}{\pi r^3 t}$$

6. Accumulative release 60

$$m = v_s \times \left(\sum_{n=1}^n c_{n-1} \right) + c_n \times v_t$$

7. Steady state flux 60

$$J_{ss} = \frac{dQ}{dt} * \frac{1}{A}$$

8. Determining mass concentration of fatty acid in PCL electrospun fibres from NMR spectra 68

$$\text{Mole ratio} = \frac{\text{Area [PCL]}/N[\text{PCL}]}{\text{Area[Fatty acid]}/N[\text{Fatty acid}]}$$

$$\text{Mass ratio} = \frac{\text{Mole ratio} \times M[\text{PCL}]}{M[\text{Fatty acid}]}$$

$$\% \text{Mass of fatty acid} = 1 - \frac{\text{Mass ratio} \times 100}{\text{Mass ratio} + 1}$$

Definition of symbols used in the equations in order of occurrence:

λ	Relaxation time
$[\eta]$	Intrinsic polymer viscosity
η_s	Solvent viscosity
M	Molecular weight
R	Gas constant
T	Temperature
V_c	Critical voltage
H	Separation distance
L	Length of the syringe tip
r	Radius of inner syringe needle
J	Diffusion flux
D	Diffusion coefficient
$\delta C/\delta x$	Change in concentration gradient over change in position
P_{app}	Apparent permeability coefficient
J_{ss}	Steady state flux
C_{donor}	Concentration in donor chamber
$\dot{\gamma}$	Shear rate
V	Volume of extruded solution
t	Time taken to extrude solution
m	Mass
v_s	Volume of the sampling aliquot
$(\sum_{n=1}^n c_{n-1})$	All previous concentrations determined to n_{th} time point
c_n	Concentration of sample determined at n_{th} time point
v_t	Total volume in the well
$\delta Q/\delta t$	Concentration change over time
A	Diffusion area
N	Number of hydrogens contributing to the NMR signal being integrated
Area[...]	Integral of the PCL or the fatty acid peak in the NMR spectra

Abbreviations

2D	2-dimensional
3D	3-dimensional
ANOVA	Analysis of Variance
c	centi-
<i>C. albicans</i>	<i>Candida albicans</i>
CFU	Colony Forming Units
CMC	Carboxymethyl Cellulose
d	day
Da	Dalton
DCM	Dichloromethane
dH ₂ O	Deionised water
DMAc	Dimethylacetamide
DMEM	Dulbecco's Modified Eagle's Medium
DMF	Dimethylformamide
DMSO	Dimethylsulfoxide
DSC	Differential Scanning Calorimetry
FBS	Fetal Bovine Serum
FDA	Food and Drug Administration
FTIR	Fourier Transform Infrared
g	grams
GC	Gas Chromatography
h	hour
H&E	Haematoxylin and Eosin
HCl	Hydrochloride
HFIP	Hexafluoroisopropanol
HPLC	High-Performance Liquid Chromatography
HWP	Hyphal Wall Protein
IC	Inhibitory Concentration
k	kilo
L	litre
LDH	Lactate Dehydrogenase
m	metre or milli-

M	molar concentration as mol/l		
MALDI	Matrix-Assisted Laser Desorption Ionisation		
min	minute		
mol	moles		
MS	Mass spectrometry		
MSI	Mass spectrometry imaging		
n	nano-		
Na	Sodium		
NMR	Nuclear Magnetic Resonance		
NOF	Normal Oral Fibroblast		
OD	Optical Density		
OH	Hydroxide		
p	Probability		
PAS	Periodic Acid Schiff		
PBS	Phosphate Buffered Saline		
PCL	poly(ϵ -caprolactone)		
PDLA	poly(D,L-lactic acid)		
PEG	poly(ethylene glycol)		
PEO	poly(ethylene oxide)		
PGA	poly(glycolic acid)		
PLA	poly(lactic acid)		
PLGA	poly(lactide glycolic acid)		
PLLA	poly(L-lactic acid)		
PU	poly(urethane)		
PVA	poly(vinyl alcohol)		
PVP	poly(vinyl pyrrolidone)		
RPMI	Roswell Park Memorial Institute (cell culture medium)		
s	seconds		
SEM	Scanning Electron Microscopy		
THF	Tetrahydrofuran		
UV	Ultraviolet		
μ	micro		
V	Volt		
YPD	Yeast	Peptone	Dextrose

1. Literature review

1.1 Introduction

Oral medicine is a clinical speciality in dentistry which involves the diagnosis and non-surgical management of oral diseases. The field of oral medicine faces several challenges in finding an appropriate drug delivery system which can offer sustained release of a drug to directly target the disease site or lesion, not least because the moist environment in the mouth and flexibility of the mucosal tissue surfaces makes adhesion difficult. This represents a major unmet clinical need, as there are currently no effective commercially available drug delivery systems that fully address these problems. The aim of this PhD was therefore to develop a polymer drug delivery device to impress upon these unmet clinical needs in oral medicine, potentially leading to translational research directed towards the development of therapeutic patches. The selected technique to create such a patch is termed electrospinning, which is able to fabricate a patch formed of thin fibres with a very high surface area to volume ratio. This is beneficial in drug release, and is also a feature that might enhance mucoadhesive interaction with the tissue.

In the last two decades, numerous scientific studies have shown that electrospun systems have the ability to act as a drug delivery vehicle. However, few studies have been published on developing an electrospun oromucosal drug delivery vehicle to treat oral diseases locally. Therefore, more specific research in developing a drug delivery vehicle, where the electrospun drug-containing patch should be designed such that it remains within the oral cavity for many minutes or even several hours on the surface of the tissue before being removed, is required. Although the focus for the electrospun patches developed in this study was primarily for buccal drug delivery, the patches have also been shown to adhere to the surface of diseased tissue along the gums or on the tongue [1], as shown in Figure 1.1.

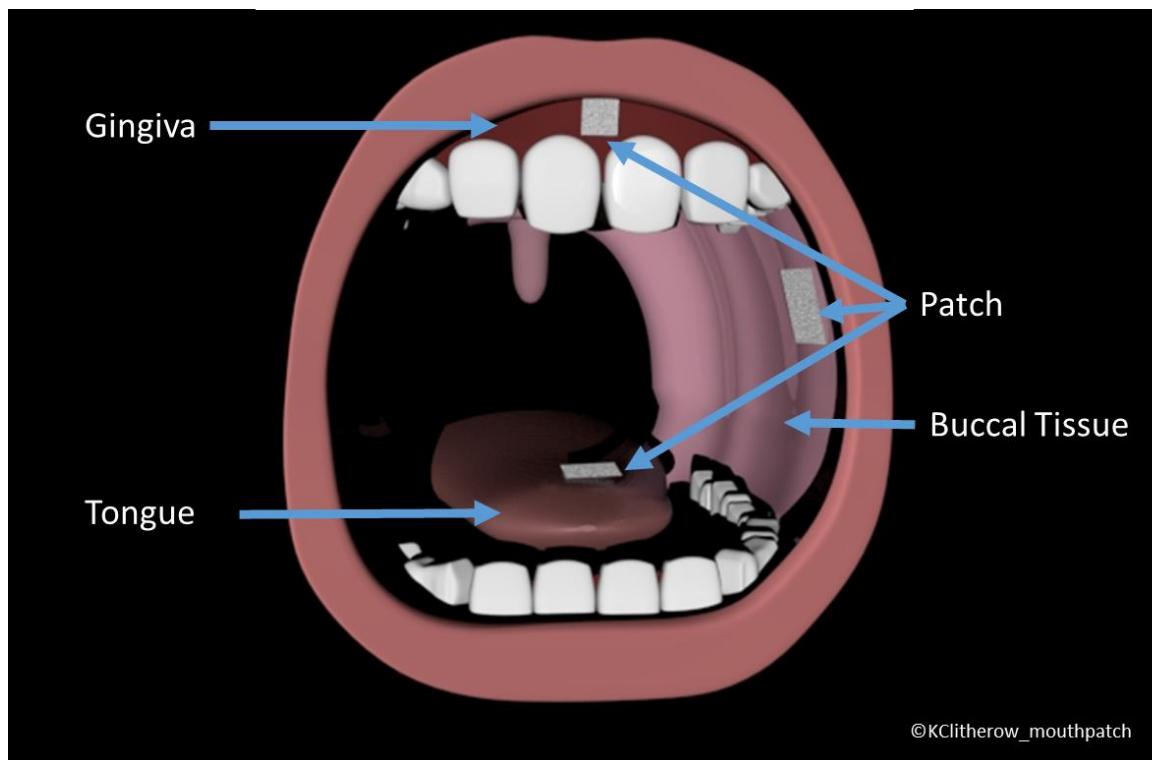


Figure 1.1. Schematic of the final clinical and commercial aim; where the electrospun polymer patches have the ability of adhering to various oral mucosal tissue surfaces and releasing drugs relevant to the disease it is treating.

In preparation for manufacture of a drug delivery device many different considerations need to be made with regards to the material properties. If the device were to be swallowed it needs to be certain that the components used to make the patch are biocompatible and that the material and the by-products of the material are non-toxic. Polymers are an ideal material to be used in manufacturing, specifically electrospinning, a drug delivery system given their relative ease in processing and their good flexibility, toughness, and solubility. The mucoadhesive properties of some polymers also need to be taken into account, as the patch will need to adhere to the oral mucosa. Drug encapsulation efficiency into the polymer patch, drug release from the fibres, drug permeation through *ex vivo* buccal tissue and *in vitro* therapeutic functionality will be researched. Plasticizers and permeation enhancers, which

can affect both the polymer and the mucosal barrier, can be incorporated into the polymer patch to alter the stiffness of the electrospun patch and to increase the drug delivery rate.

Although there are many areas of oral medicine that require attention, two areas of concern that will be focussed on in this research are the major issues of managing oral pain and the increasing resistance of oral *Candida* species to commonly used antifungal drugs. Current available treatments to target these two issues in oral medicine are limited, especially for non-systemic treatment. Therefore, the potential of the electrospun drug delivery vehicle in tackling these issues will be investigated. Before considering this research in detail, the relevant scientific literature will be reviewed to highlight the important research areas and existing knowledge for this PhD work, as well as highlighting knowledge gaps.

1.2 Anatomy of healthy oral tissue

The mouth and oral cavity play a vital role in day-to-day life, including speech, mastication, eating, drinking and other sensory functions. These are all underpinned by healthy oral tissues, where impairment of these tissues due to oral disease can vastly reduce quality of life [2,3]. Oral disease can change the oral tissue structure and as the drug delivery device developed in this research project is intended for direct application to the surface of oral mucosal tissue a basic anatomical understanding of the oral cavity and oral mucosal tissue is required. The oral cavity consists of a number of tissues, including the lips, gingiva, hard palate, soft palate, buccal mucosa, teeth and tongue [4]. The oral mucosa is the mucous membrane lining the oral cavity and consists of stratified squamous epithelium, basement membrane, lamina propria and the submucosa (Figure 1.2). The hard palate, dorsum of the tongue and the gingiva are lined with masticatory mucosa which consists of a keratinised stratified squamous epithelium with different degrees of keratinisation dependent on the location of the tissue (for example more keratinisation may be observed in proximity to teeth). The inner lips, buccal mucosa, soft palate and floor of the mouth are covered in lining mucosa, which consists of a non-keratinised stratified squamous epithelium (Figure 1.2). The

basolateral side of the oral epithelium is attached to the basement membrane followed by the lamina propria, a fibrous connective tissue layer where fibroblast cells produce the extracellular matrix and type I and III collagen fibres. The lamina propria also contains blood vessels, glands and nerves. The submucosa beneath the lamina propria consists of thicker connective tissue that connects the oral mucosa to the underlying muscles.

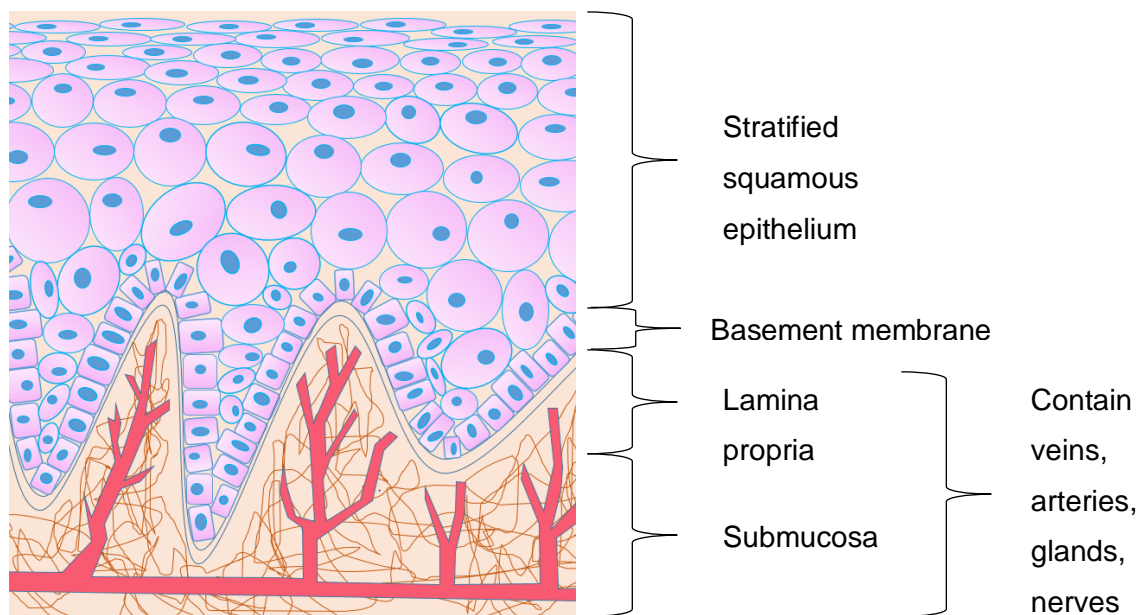


Figure 1.2. Schematic of the oral mucosa membrane.

Healthy oral lining mucosa has a thick epithelium layer of approximately 40 to 50 cell layers thick [5], where previous measurements across 143 healthy volunteers give the mean \pm SD thickness of the buccal epithelium as $294 \mu\text{m} \pm 68 \mu\text{m}$ [6]. Epithelial thickness varies at different mucosal sites with the floor of the mouth having the thinnest mucosa. Unhealthy or diseased tissue may change the thickness of the epithelium, while infection or malignancy may cause lesions to appear on the epithelium [7]. Drug delivery to diseased oral tissue has its challenges and direct local treatment needs to be improved, which will be discussed in greater detail in the next section.

1.3 Oral diseases and oral medicine of soft tissues and respective therapies

For many oral diseases, such as oral infections, ulcers, lesions and cancers, few effective localised therapies are currently available for clinical needs. Delivering therapies systemically does not target the relevant area in the mouth well and large doses are required, having the potential of causing severe side effects. Hence, developing a localised therapy is of great importance. There are a number of reasons why developing a drug delivery system to be administered to the mouth is of medical interest [8–10]:

- a) Ease of administration and repeat administration.
- b) Improved localised dosage and potential reduction of systemic side effects.
- c) Improved patient compliance.
- d) Likely to be cheaper than injections.
- e) Access to the internal jugular vein via the buccal or sublingual mucosa for systemic drug delivery.

There are some obstacles that the drug delivery system must overcome in the oral cavity. Drug retention and absorption is important, and the drug therefore needs to be able to permeate and have a sustained delivery to the oral mucosa. Rapid drug loss due to saliva washing the drug away and mechanical stresses along the mucus barrier need to be avoided to ensure that the necessary therapeutic level of the drug is achieved. To overcome such issues, a bioadhesive drug delivery system which can stick to the oral mucosa is ideal to maintain intimate contact and an increased drug delivery time [10]. A brief overview of diseases or ailments to target locally using a patch system are provided in Table 1.1.



Table 1.1. Clinical applications for a mucoadhesive patch drug delivery system	
<u>Disease</u>	<u>Description of benefits</u>
<p>Immunologically mediated diseases (e.g. oral lichen planus)</p> 	<p>Treatment of immunologically mediated oral mucosal disease, such as oral lichen planus, to improve the drug delivery contact time and to have a localised system in place.</p> <p>(Image reprinted from Olson, M. A., Rogers, R. S. & Bruce, A. J. Oral lichen planus. <i>Clin. Dermatol.</i> 34, 495–504 (2016)[11], with permission from Elsevier)</p>
<p>Diseases surrounding the oral cavity (e.g. oral candidiasis)</p> 	<p>Delivery of drugs into the oral cavity for oral candidiasis, sore throat or delivery of drugs to throat, oesophagus and upper gastrointestinal tract.</p> <p>(Image reprinted from Millsop, J. W. & Fazel, N. Oral candidiasis. <i>Clin. Dermatol.</i> 34, 487–494 (2016)[12], with permission from Elsevier)</p>



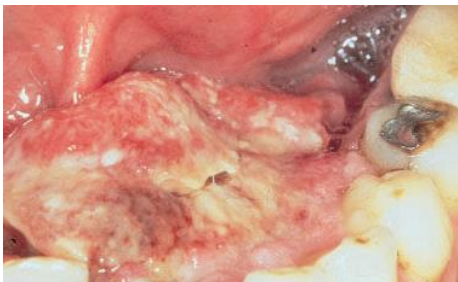
Table 1.1. Continued	
<u>Disease</u>	<u>Description of benefits</u>
<p>Potentially premalignant lesions (e.g. oral leukoplakia)</p> 	<p>Lesions such as actinic keratosis and oral leukoplakia would benefit from a slow release drug system which also improves the localised retention of the drug.</p> <p>(Image reprinted from Amagasa, T., Yamashiro, M. & Ishikawa, H. Oral Leukoplakia Related to Malignant Transformation. <i>Oral Sci. Int.</i> 3, 45–55 (2006)[13], with permission from Elsevier)</p>
<p>Oral mucositis</p> 	<p>Treatment of oral mucositis to improve sustained release of adrenaline to reduce toxic bystander effect and/or analgesics within a patch could reduce the pain.</p> <p>(Image reprinted from Lalla, R. V., Sonis, S. T. & Peterson, D. E. Management of Oral Mucositis in Patients Who Have Cancer. <i>Dent. Clin. North Am.</i> 52, 61–77 (2008)[14], with permission from Elsevier)</p>
<p>Oral carcinoma</p> 	<p>Treating cancerous conditions or providing protective agents in the patch against radiation in cancer treatment.</p> <p>(Image reprinted from Johnson, N. W. & Bain, C. A. Tobacco Intervention: Tobacco and oral disease. <i>Br. Dent. J.</i> 189, 200–206 (2000)[15], with permission from Springer Nature)</p>

Table 1.1. Continued	
<u>Disease</u>	<u>Description of benefits</u>
Cold sores	Cold sores around the lip or on the top of the mouth, some of which may be too difficult to reach with anti-viral cream.
Ulceration and open socket tooth extraction wound	Wound dressing to cover ulcerations or open sockets after tooth extraction (either with or without incorporating drugs).
Pain relief for lesions and/or from injection	Delivery of local anaesthetics to create a topical and local delivery system to reduce the need for widely feared dental injections.

Within this thesis the local delivery of an anaesthetic, to treat either dental pain or to be used prior to dental surgery, was explored. Additionally, an alternative antifungal system was developed to treat oral candidiasis. Therefore, further information on both of these potential applications is given below.

1.3.1 Treatment of oral pain

Treating oral pain locally over a prolonged period of time for numerous oral disease conditions, such as ulceration, mucositis and trauma, is clinically challenging. Anaesthetic injections may be used for some treatments, however this is not possible long term and dental injections are widely feared and the cause of dental anxiety for many patients [16]. One condition that causes pain for many patients is oral mucositis, which is mostly a side effect of chemotherapy agents and radiation therapy disturbing the oral mucosal epithelial

layer leading to painful inflammation and ulceration of the mucosa. Oral mucositis is often observed in patients undergoing head or neck cancer treatment and is sometimes so severe that it prompts early termination of anti-cancer treatment [14].

A large systematic review by Saunders *et al.* (2013) [17] analysed a large number of papers to “develop clinical practice guidelines on the use of antimicrobials, mucosal coating agents, anaesthetics, and analgesics for the prevention and management of oral mucositis in cancer patients”. Within, it was noted that topical anaesthetics have been shown to bring short-term pain relief to some patients, although analgesics are often required to manage the pain. Additionally, the evidence of topical anaesthetics being tested on their own and not in combination with other components (e.g. antimicrobials) to reduce mucositis pain was too low to warrant that anaesthetics alone have a pain reducing effect. The optimal pain relief with minimal side effects were in fact shown by opioids, such as the 2% (w/v) morphine mouth washes [18], as well as anti-depressants such as 0.5% (w/v) of doxepin in a mouth wash providing pain relief [19,20]. The systematic review noted that an improved delivery system which would reside in the mouth for a longer period of time would be desirable and even mentioned that transoral mucosal patches would be beneficial in aiding the healing of ulcers and lesions [17].

Although morphine is suggested as a topical treatment method for oral mucositis pain, there has been an increase in opioid substance abuse and hence using safer alternatives with fewer side effects would be preferable [21,22]. Lidocaine HCl is a relatively safe, well tolerated and effective anaesthetic and the most commonly used in the treatment of local oromucosal pain relief [23,24]. Lidocaine has a quick onset time, which is good for local delivery, where it blocks membrane bound sodium channels to inhibit action potentials and nerve impulse conduction and thereby preventing local sensory functions [25,26]. A number of *ex vivo* studies evaluating the transbuccal permeation of lidocaine, applied as either a solution or in a gel have been reported [27,28]. However, lidocaine has not previously been incorporated into an electrospun patch for transbuccal delivery.

1.3.2 Antifungal therapy for oral candidiasis

Oral candidiasis is a fungal infection that can spread across the whole oral cavity, with the most prevalent *Candida* pathogen being *Candida albicans*. *C. albicans* is a commensal organism in approximately 50% of the population [29] and can grow both in yeast and hyphae form, where the hyphae form shows greater tissue invasiveness and can lead to a systemic infection [30]. Therefore, oral candidiasis infections can vary in severity from acute candida including pseudomembranous candidiasis (thrush) and acute antibiotic stomatitis, to chronic candida infections including denture-induced stomatitis, hyperplastic, mucocutaneous and erythematous candida [12]. Patients presenting with candidiasis are generally immunocompromised, immune-deficient or undergoing prolonged antibiotic treatment or chemotherapy. Individuals with HIV or patients undergoing chemotherapy are at high risk of infection and incidences of oral candidiasis for these patients are 90% - 95% [31,32].

Currently, topical antifungal steroids tend to be the main therapy employed. Some commonly used drugs include fluconazole, miconazole, nystatin, amphotericin B and tetracycline. Depending on the patient and the medication used different side effects may be observed. Nystatin and miconazole tend to be well tolerated, whereas some azoles such as ketoconazole, itraconazole and fluconazole have been shown to have more adverse side effects such as nausea, vomiting, diarrhoea and abdominal pain [33]. Topical delivery methods frequently incorporate fluconazole or clotrimazole and come in the form of gels or creams [33–35]. However, recent rises in antifungal resistance show a need to review alternative antifungal therapies compared to the medicines used currently [36–38]. Some alternative therapies which have been explored for the treatment of *C. albicans* are surfactants [39,40], synthetic peptides [41–43] and fatty acids [44–48]. The size, hydrophilicity and charge of the therapeutic molecules, interaction with the *Candida* cells and inhibition of fungal adhesion influence how well the therapies inhibit *C. albicans* growth or viability. An issue of many surfactants and peptides is their significant toxicity to mammalian

cells, whereas fatty acids in their triglyceride form are less toxic and so have been used as antimicrobial agents in food products, where the toxicity of saturated fatty acids to human endothelial cells is relatively low [49]. A recently developed glycolipid biosurfactant from the sorpholipid family was shown to have good antifungal properties against *C. albicans* whilst displaying low human cell cytotoxicity [39,50]. Free fatty acids do nevertheless have additional benefits, such as their low cost and ability to be effective permeation enhancers due to their lipophilicity [51]. The antimicrobial and antifungal ability of fatty acids are also well known. In fact many short-chain fatty acids are naturally secreted by bacterial microflora to suppress other competing micro-organisms [52,53]. Therefore, within this thesis fatty acids were reviewed as the alternative antifungal agent.

The mechanism by which fatty acids effect *Candida* cell viability is by targeting and disturbing the fungal membrane, such that the cell membrane becomes disorganised and eventually leads to its destruction [44]. A review by Pohl *et al.* (2011) [48] lists numerous saturated and unsaturated fatty acids used in studies for their antifungal properties for human or plant pathogens. Saturated fatty acids which have been highlighted with antifungal properties for *C. albicans* are: decanoic (capric) acid (10:0), dodecanoic (lauric) acid (12:0) and tetradecanoic (myristic) acid (14:0). A number of unsaturated fatty acids have also been referenced with chain lengths: (14:1), (16:1), (18:2), (18:4), (20:5) and (22:5) [48]. The first number in the brackets refers to the total number of carbon atoms, whereas the second number refers to the number of C=C double bonds. Decanoic acid (C10:0) and dodecanoic acid (C12:0) were shown to have the best antifungal effect, especially at a concentration of 10 mM [44]. Although the previous research on the antifungal ability of medium-chain saturated fatty acid proves promising, the majority of antifungal tests were performed only on the yeast and not for the hyphal form of *Candida*. Therefore, testing the antifungal ability of a select range of fatty acids on an already established biofilm of *Candida* would be of interest. Another potential benefit of fatty acids is that they have been shown to act as a plasticiser

[54], as well as being proven penetration and permeation enhancers for transdermal delivery [51,55].

1.3.3 Oral wound dressings

Apart from using a drug-loaded patch system, a placebo patch may also be of benefit as a wound dressing. Wounds such as oral ulcers and lesions can cause various levels of pain as well as frustration to patients. Currently the main medical relief to such pain tends to involve mouth gels, such as Bonjela. Such gels only provide short-term relief and wash away relatively quickly during mastication or even speech. Therefore, having a patch system that would cover the ulcer or lesion over several hours without disturbing mastication and even making such activities more bearable would be of great clinical interest. An oral wound dressing could even be used after tooth removal to seal off the tooth socket, thereby potentially preventing the onset of infection in the socket, which can be very serious (for example postoperative alveolar osteitis [56]), as well as preventing the taste of blood in the mouth as the blood clots in the socket. The main issue with creating a wound dressing for oral use is finding a material system which has suitable mucoadhesive strength to stay attached to the mucosa wall even throughout everyday activities such as eating, where the electrospun patch system may be able to overcome these challenges.

1.4 Electrospinning of polymers

Section 1.3 demonstrates that current therapies in oral medicine need to be improved. An ideal solution is to create a device or dressing that is capable of delivering a therapeutic agent directly to the clinical target and for a sustained length of time. Electrospinning is ideally suited to fabricate such a device as this technique is sufficiently versatile to allow manufacture with a broad range of polymers and drugs and it is capable of producing a mesh structure with a large surface area to volume ratio for increased therapeutic delivery. Before

discussing electrospun polymer-drug combinations in detail, it is important to have a good appreciation of the technique.

1.4.1 Electrospinning process

Electrospinning is a technique used to create thin-fibre mats that have a very high surface area to volume ratio. This high ratio can be very beneficial in medicine as it allows for greater interaction with the target environment, for instance interaction with cells, and if the fibres contain active pharmaceutical ingredients an improved drug dissolution has been observed [57,58]. The porosity present in the resulting mats can also facilitate cell infiltration and nutrient transport which is useful for several cell-based applications such as wound healing [58–60].

Electrospinning requires a high voltage power supply, a syringe filled with the polymer solution, a pump, a grounded collector on which the polymer is spun and a system to hold all items in place (Figure 1.3). The electrospinning process relies on the polymer in the syringe being electrically charged by the electric field emanating from the high voltage power supply and attached to the syringe needle tip, such that the electric force acting on the polymer is greater than the surface tension of the polymer solution causing the polymer to form a fibre jet as it is pulled towards the collector. During this pulling process the solvent evaporates and thin fibres are formed that are then deposited on a collector.

The voltage applied during the process tends to be between 5 and 30 kV depending on the polymer solution and setup used. Other equipment parameters that are simple to alter are: the feeding rate of the pump and the distance between the syringe and collector. Several different types of collectors can be used, where the two most commonly used collectors as seen in literature are a collector plate or a collector drum which is turned at a pre-determined rate. Using different collectors or using additional external field controls can result in different fibre alignment and many different electrospinning set ups are noted in a review article by

Teo *et al.* [61]. Aligned fibres are desirable to encourage tissue or cell growth along the fibres, for neuronal or musculoskeletal tissue for example [62,63]. The electrode focussing ring is commonly used to limit and focus the deposition area of the electrospun fibres.

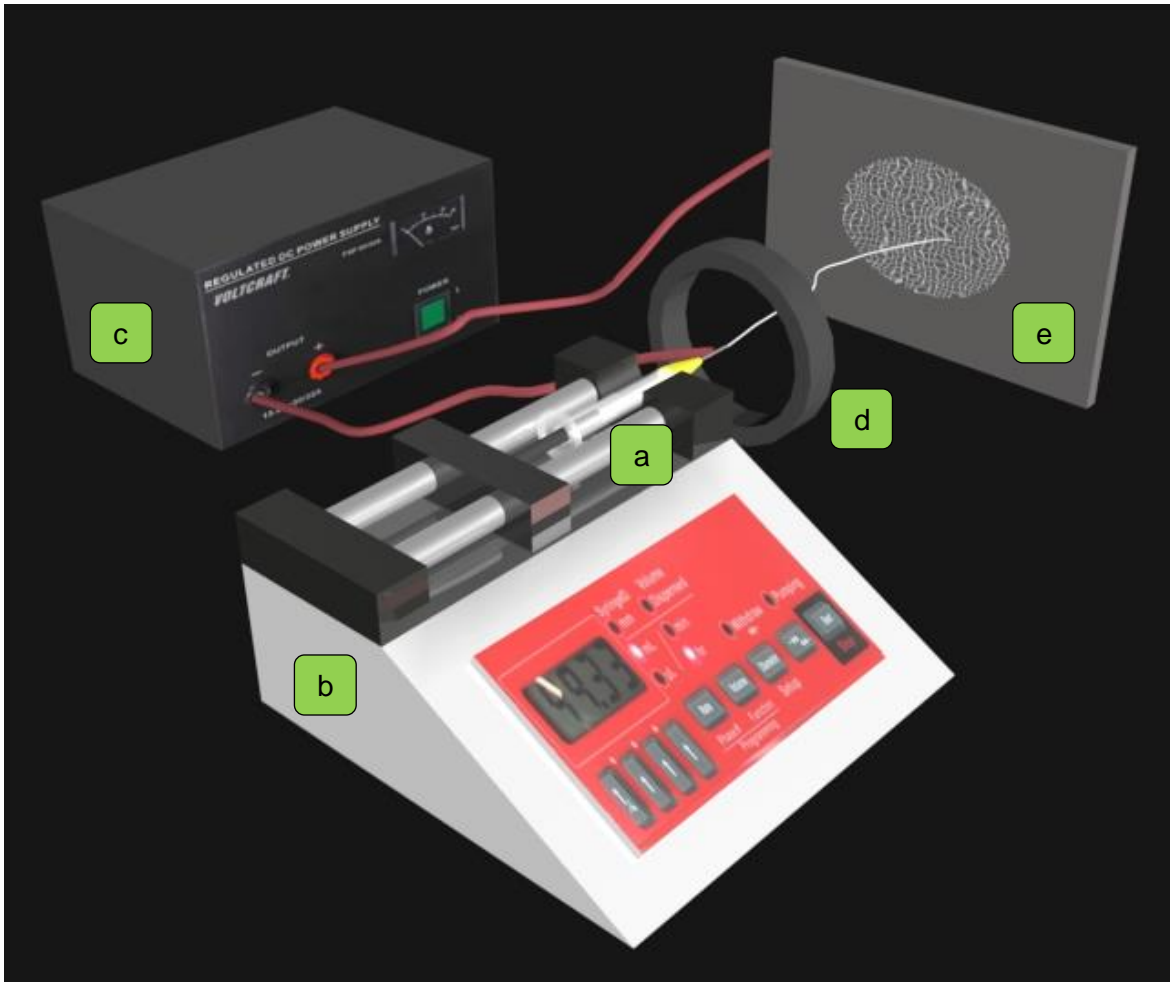


Figure 1.3. The electrospinning setup is composed of a) the syringe filled with the polymer solution and any other therapeutic agents or drug compounds, b) the syringe feed pump, c) the grounded high voltage power supply, d) the focussing electrode ring, e) the grounded collector plate.

Changing equipment parameters changes the resulting fibre characteristics. For instance, increasing the applied electric field generally causes polymer fibres to be stretched to a

greater extent, reducing the fibre diameter [64]. Over a certain voltage some polymers will form beads rather than continuous fibres, however the observations made depend largely on the polymer being spun [60]. The feeding rate will also alter the diameter of the fibres, where a higher feeding rate can cause more bead formation [60] or the polymer may drip at the syringe tip as not all of the polymer is being electrostatically charged, which could also cause the needle tip to clog up. This is due to the effect on the volume-charge-density of the solution as at a faster feed rate the solution would have a shorter contact time with the charged needle and therefore the volume-charge-density of the solution would be lower at a higher flow rate, which could cause instabilities in the solution or increase the fibre diameter depending on the conductivity of the solution [65]. Electrical bending instability can occur if the collector and syringe are far apart and if they are placed too far apart then electrospaying can occur, where the polymer forms droplets and beads rather than fibres on the collector [60,66]. If the collector and syringe are too close together the solvent does not have time to evaporate completely causing the fibres to stick to the collector and to each other [67]. If a rotating collector is used the speed at which the collector rotates greatly influences the alignment of the fibres [61]. The temperature and humidity in the environment in which the spinning is taking place can also affect the resulting fibres [68].

The necessary equipment parameters are largely dictated by the polymer solution used. The properties of the polymer solution and their effect on the electrospun fibres are discussed in the next section.

1.4.2 Properties of polymer solutions

The polymer solution properties largely influence the electrospinning process of the solution. A polymer that electrospins well is one which does not break up or 'splay' during the spinning process and creates a constant stable jet [69]. The influence of the polymer's concentration, molecular weight, viscosity and surface tension on the electrospinning process has been

studied in numerous publications. Some studies have also examined the role of polymer chain entanglement [70,71], elasticity [72,73] and interfacial viscosity [73,74] in creating electrospun fibres. To aid the understanding of terminology used in this section a side-view of the electrospinning process and some of the phenomena occurring during electrospinning is shown in Figure 1.4.

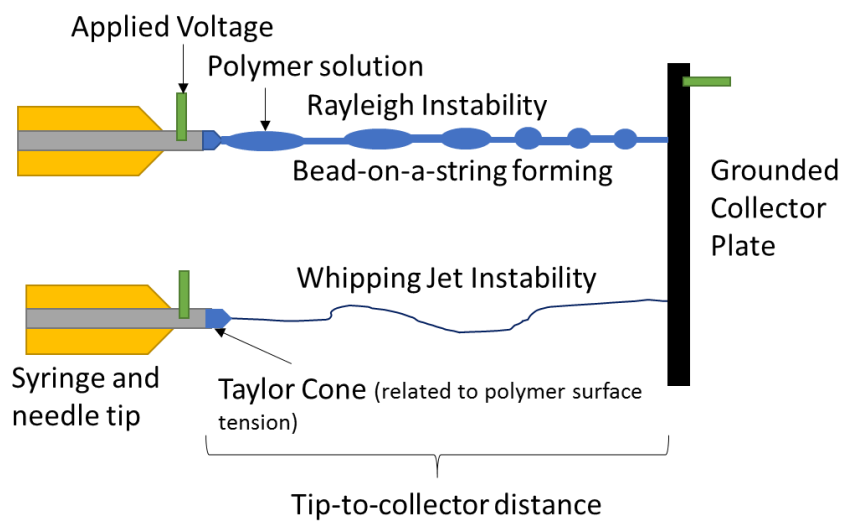


Figure 1.4. Side-view diagram of the electrospinning set-up and fluid flow terminology for the polymer solution during electrospinning.

One of the simplest parameters to test for the polymer solution dependency on electrospun jet stability is observed by varying the polymer concentration. Below a critical polymer concentration, electrospinning or bead formation can be observed mainly due to Rayleigh instability. This is a fluid flow instability reported by Rayleigh (1879), where a falling solution thickens and thins with a reducing surface area until a droplet can be formed [75], as shown in Figure 1.4. This phenomenon is also dependent on the surface tension of the solution and the applied flow rate. If the polymer concentration is too large, Rayleigh instability can cause

non-uniform fibres to be spun or the flow may even be hindered due to the high viscosity causing the droplet to dry out before a constant jet is formed [60,70,76].

The molecular weight of a polymer can change many of its' properties, including the rheological properties, electrical conductivity and surface tension. Various studies relating molecular weight of a polymer to electrospinning fibre formation were reported [77–79]. Studies show that increasing the molecular weight and concentration of a polymer solution increases the electrospun fibre diameter, although at high molecular weights the solution may have too high a viscosity to be able to spin it at particular concentrations. This has been related to an increasing relaxation time in the polymer as the molecular weight is increased [77], where the relaxation time is the time taken for the polymer to recover from an applied, normally elongational, stress. The relaxation time λ can be calculated using the Rouse model [77]:

$$\lambda \approx \frac{6\eta_s[\eta]M}{\pi^2RT} \quad \text{Eq. 1}$$

where η_s is the solvent viscosity, $[\eta]$ the intrinsic polymer viscosity, M the molecular weight of the polymer, R the gas constant and T the temperature.

As the concentration, molecular weight and relaxation time of the polymer all cause the solution viscosity to change this could arguably be one of the most important polymer solution variables in determining the electrospun fibre formation. The importance of solution viscosity in electrospinning has been clearly shown in many papers [65,70,72–74,80–82]. Both the shear and elongational viscosity can be useful in predicting how well the solution can be electrospun, however the elongational viscosity may be more appropriate due to the stretching of the fiber in the electrospinning process. Using the storage modulus, G' , and the loss modulus, G'' , the elasticity of the polymer solution can be reviewed and related to other parameter alterations. Most papers use a rotational rheometer to determine the shear viscosity of a solution, however two papers were found which use a capillary breakup extensional rheometer (CaBER) to determine the extensional viscosity of the solutions

[72,73]. The CaBER technology allows a non-linear response to be created as the solution is pulled into a filament and the changing diameter of the fluid filament is measured as the strain is increased using a laser micrometre. Given that the polymer is being stretched during electrospinning the CaBER method may well be a good method to use in pre-determining the ability of the polymer in being spun before it is used in the electrospinning process.

The interfacial viscosity for polymers used in electrospinning has not been researched in great depth, however in some studies the interfacial viscosity graphs show a clearer cut off point between solutions which can form fibres and those which form beads or beads-on-string than results for the bulk viscosity [74,83]. Other research groups have reviewed polymer chain entanglement, where an increase in chain entanglement is linked to an increase in solution viscosity and the entanglement density increases as either the polymer volume fraction or molecular weight of the polymer is increased [70,71].

The jet shape and its instabilities as well as the surface charge of the spun fluid have been mathematically characterised using fluid mechanics by Ganan-Calvo *et al.* (1998, 2000) [66,84] and Hohman *et al.* (2001) [85,86]. Hohman *et al.* note that the conductivity and charge density of the solution, which is influenced by the surrounding electric field, largely influence the type of flow instability (e.g. whipping jet instability) observed during spinning. Fridrikh *et al.* (2003) [87] claim they have derived an equation which predicts the terminal jet diameter, although it is also noted that the prediction gives a lower bound estimate of diameter and one of the problems with the model is that the solution properties change during the spinning process as the solvent evaporates. Therefore these equations need to be used with consideration towards their limitations, given the many variables such as the equipment parameters, environmental conditions and polymer solution properties that may alter the resulting electrospun fibre morphology and fibre diameter.

A low surface tension allows a Taylor cone and jet to be formed more easily and thus a lower critical voltage can be used. The Taylor cone is the cone formation as the polymer emerges from the syringe tip whilst being drawn into a fibre by the electrostatic forces acting on it

(shown in Figure 1.4). The equation for the critical voltage (V_c) was derived by Taylor (1969) [88]:

$$V_c^2 = \frac{4H^2}{L^2} \left(\ln \frac{2L}{r} - \frac{3}{2} \right) 0.117\pi\gamma r \quad \text{Eq. 2}$$

Where H is the separation distance between the syringe tip and collector, L is the length of the syringe tip, r the radius of the tip and γ the surface tension of the solution.

Changing the solvents in which the polymers are diluted also affects how well the solution is electrospun. Polymer and solvent selection depend on polymer solubility in the solvent and the ease of processability. The solvent should complement the polymer and electrospinning process in terms of its electrical conductivity and surface tension.

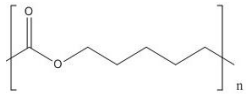
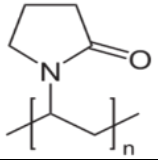
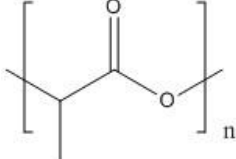
1.5 Polymer system

Having decided on the technique of electrospinning it is important to choose a polymer and solvent system that have desirable properties for the electrospinning process. A number of possible polymer candidates will be reviewed in this section, including a review of the chemical and mechanical properties of the homopolymers prior to electrospinning as well as gathering information on how well the materials could be electrospun from literature. Choosing the polymer system will be of great importance to this PhD and an informed choice on which polymer system for electrospinning a drug delivery vehicle was made by reviewing existing literature and from initial lab work.

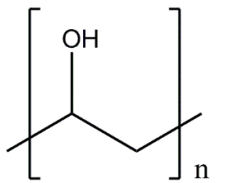
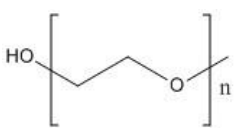
1.5.1 Biocompatible polymers

Both natural and synthetic polymers can be electrospun into a biocompatible scaffold. Various polymers or polymer blends could be used for drug delivery applications, however which polymer or polymer blend will be chosen depends on the resulting properties of the material. A previous review of polymers used in drug delivery gave an overview of the

possible synthesis and drug release mechanisms of many of the polymers listed in Table 1.2 [89]. This section gives an overview of possible polymers which may both electrospinning and as a drug delivery system.

Table 1.2. Polymers with potential for electrospinning process					
Polymer	Formula	Mechanical properties ^a	Previously spun molecular weights ^b (g/mol)	Electrospinning setup (voltage, tip-to-collector distance and flow rate)	Other comments
PCL poly(ϵ -caprolactone)		s: YM: 2.7-4.7 MPa s: TS: 1.2-2.1 MPa Ref: [90]	$M_n = 70,000 - 100,000$ [91–94] (most at M_n 80,000)	14-25 kV, 13-23 cm tip-to-collector distance and 1.5-3.0 ml/h flow rate [93–96]	Hydrophobic; prepared and spun at rtp.; slow degradation
PVP poly(vinyl pyrrolidone)		-	$M_w = 58,000$ [97,98]; 360,000 [99,100]; 1,300,000 [101–103]	15 kV, 12-20 cm tip-to-collector distance and 0.3-2.0 ml/h flow [97–103]	Hydrophilic; prepared and spun at rtp.
PLA poly(lactic acid)		p: YM: 1.5-4 GPa p: TS: 50-70 MPa p: NI: 41 Jm ⁻¹ Ref: [104]	$M_w = 200,000$ [105]	20 kV, 19.4 cm tip-to-collector distance and 10 ml/h flow rate [58]	Slightly hydrophilic
PLLA poly(L-lactic acid)	Stereoisomer of PLA	p: YM: 3.7 GPa p: TS: 55 - 59 MPa p: NI: 26 Jm ⁻¹ Ref: [104]	$M_w = 152,000$ [106,107]; 10,000 [76]	23 or 30 kV, 20 cm tip-to-collector distance and 1-12 ml/h flow rate [107,108]	Selective hydrolysis, mainly hydrophobic. Spun at rtp.
PDLA poly(D,L-lactic acid)	Stereoisomer of PLA	-	$M_w = 109,000$ [76]	30 kV and 15 cm tip-to-collector distance [76]	Prepared and spun at rtp.

a) p: prior to spinning; s: after spinning property; YM: Young's Modulus; TS: Tensile Strength; NI: Notch Izod (impact strength test)
b) M_w for the weight-average molar mass, M_n for the number-average molar mass and M_v for the viscosity-average molar mass.

Table 1.2. (continued)						
PLGA poly(lactide glycolic acid)	Copolymer of PLA and PGA	s-random: YM: 134 MPa s-aligned: YM: 40.4 MPa s-random: TS: 2.6 MPa s-aligned: TS: 2.1 MPa Ref: [109]	$M_w = 75,000-118,000$ [109–112]	20-25 kV, 12-30 cm tip-to-collector distance and 0.06-1 ml/h flow rate [109,112,113]	Both hydrophilic and hydrophobic; processed at 50 °C in one paper [112], however otherwise at rtp. and spun at rtp.	
PVA poly(vinylalcohol)		s: TS: 16.1-16.8 MPa Ref: [114]	$M_w = 72,000$ [115]; $125,000$ [116]; $130,000$ [80]	15-30 kV, 10-15 cm tip-to-collector distance and 0.3-1.2 ml/h flow rate [77,80,114,116,117]	Hydrophilic; processed at ~80 °C ; spun at rtp.	
PEG poly(ethylene glycol) or PEO poly(ethylene oxide)		-	$M_v = 300,000$ [118] $M_w = 400,000$ [74,106,119]	9-30 kV, 6-24 cm tip-to-collector distance and 0.1-5.0 ml/h flow [74,118,119]	Hydrophilic; prepared and spun at rtp.	
PU poly(urethane)	Variable structures	-	$M_w = 110,000$ [120]	12 or 16 kV and 12 or 10 cm tip-to-collector distance [120,121]	Hydrophobic; release properties dependent on functional group	
a) p: prior to spinning; s: after spinning property; YM: Young's Modulus; TS: Tensile Strength; NI: Notch Izod (impact strength test)						
b) M_w for the weight-average molar mass, M_n for the number-average molar mass and M_v for the viscosity-average molar mass.						

Poly(ϵ -caprolactone) - PCL

Poly(ϵ -caprolactone) (PCL) is a semi-crystalline aliphatic polyester with rubbery properties which often improves elasticity [90]. PCL has good mechanical, thermal and chemical stability, has good drug permeability and slow hydrolytic biodegradation [60,92,96].

In electrospinning, PCL tends to be spun in concentrations of 8 – 15 % (w/w) in solvents such as chloroform:acetone (3:1) [91], chloroform:methanol (3:1) [94,96], dichloromethane (DCM):methanol (7:3) [92], or DCM:*N,N*-dimethylformamide (DMF) [90,93,95], DCM only [90] and DCM:toluene [90] tested at varying ratios. As shown in Table 1.2 a large variation of electrospinning setups is given in literature for all polymers as the setup properties depend on the solvent system chosen as well as how the setup variables are combined. The dielectric constants of the chosen solvents change the conductivity [90] of the polymer solution and therefore the required voltage in the electrospinning process, hence the dielectric constants of possible solvents have been reported below in Table 1.3.

Solvent	Solubility	Dielectric constant at 25 °C
Chloroform	Good solvent	4.75
Dichloromethane	Good solvent	9.1
Acetone	Poor solvent	19.10
Methanol	Poor solvent	33.1
Toluene	Poor solvent	2.4
<i>N,N</i> -Dimethylformamide	Non-solvent	36.7

PCL has been shown to produce fibres of relatively uniform size throughout a patch system. Lee *et al.* [90] that a DCM:DMF (40:60) solvent system could produce fibres as small as 200 nm in diameter.

Poly(vinyl pyrrolidone) - PVP

Poly(vinyl pyrrolidone) (PVP) is a biocompatible and hydrophilic polymer which has a wide number of applications in the food, consumer product and pharmaceutical industry. Given its water solubility it has been used in many studies to improve drug dissolution of poorly water-soluble drugs [122].

Solvents which have been used to create PVP solutions for electrospinning purposes are ethanol [97,99,100], *N,N*-dimethylacetamide (DMAc) and ethanol mixtures [98], DMF [102] or a combination of ethanol: water: benzyl alcohol (EtOH:H₂O:BzOH) [101,103]. Ethanol is a good solvent for PVP and its dielectric constant is 24.3 at 20 °C. The average fibre diameter of electrospun mats in literature varies between 200 nm and 1000 nm and was shown to increase with the incorporation of a drug [97–103].

Poly(lactic acids) – PLA, PLLA, PLGA, PDLA

Poly(lactic acid) (PLA), poly(L-lactic acid) (PLLA), poly(D,L-lactic acid) (PDLA) and poly(lactide-co-glycolide) (PLGA) are linear aliphatic polyesters, which are biocompatible and biodegradable. PLA and its copolymers are soluble in a number of solvents such as benzene, chloroform, DCM, DMF, hexafluoroisopropanol (HFIP) and toluene.

Lactic acid molecules can have different stereochemistry and depending on the concentration of the isomers used in polymerisation the properties of the resulting polymer, such as the glass transition temperature, can be altered [89]. The stereochemistry and crystallinity of the polymer will greatly affect the mechanical properties, as well as potentially affecting drug entrapment [104,107]. PLLA tends to be used in its semi-crystalline form whilst PDLA is a completely amorphous polymer. Data on electrospun PLA and PDLA show great dependence on solution viscosities to fabricate uniform fibres without any beading [76,123].

Whereas PLLA takes many months to degrade, PLGA degradation can be adjusted depending on the PLA:PGA co-polymer ratio and hence has been extensively researched for

drug release behaviour [124]. PLA is more hydrophobic than PGA and PGA is a highly crystalline polymer. When PLA and PGA are co-polymerised their crystallinity lowers such that the copolymer crystallinity is far lower than that of the individual polymers. This lower crystallinity of PLGA increases the hydrolysis and hydration of the polymer and a ratio of 50:50 PLA:PGA has the fastest degradation rate, with the degradation rate decreasing as this ratio is altered to either contain more PLA or PGA [124]. For this reason PLGA has been used in a number of electrospun drug delivery systems where a prolonged and controlled drug release was desirable over a few days or weeks [125–127]. Fibre diameters between 800 and 4000 nm were manufactured.

Polyvinyl alcohol - PVA

Poly(vinyl alcohol) (PVA) is a semi-crystalline, hydrophilic polymer which is biodegradable, biocompatible and non-toxic [128,129]. The hydrophilicity of the polymer is one of the main limitations of using this polymer as a drug delivery vehicle, but it has been used in contact lenses and wound dressings as it has good swelling capability and flexibility [115]. Electrospun PVA fibres therefore need to be stabilised if they are to be used in a water rich environment, this can be done by soaking the electrospun mat in alcohol for one day [116]. PVA can also be made less soluble by grafting, co-polymerising or cross-linking PVA with other polymers [115].

For electrospinning the PVA solution needs to be prepared in an oven at 70-80 °C with distilled water for three hours and can then be spun at room temperature [77,80,115,117]. The resulting electrospun fibres tend to be in the nanometre range [80,114–116]. On its own electrospun PVA fibres will burst release a drug very quickly due to its hydrophilicity [107].

Polyethylene glycol - PEG

Polyethylene glycol (PEG) and polyethylene oxide (PEO) are the same material, but for low molecular weights ($\leq 20,000$) the polymer is named PEG and for high molecular

weight (> 20,000) it is called PEO. PEG is a biocompatible, non-toxic polymer with a linear and flexible chain and is found in a large range of food and consumer products. Many papers have investigated theories of electrospinning and the resulting electrospun fibres depending on solution properties using PEO or PEG as the electrospun solution [72,78,106,118,119]. One of the reasons for this may be as one can easily buy a range of molecular weights for PEO or PEG to test. Solvents in which PEG can be dissolved are chloroform, ethanol, DMF and water [118]. PEG behaves as a Newtonian fluid and a review which analyses many variables to evaluate the elasticity of PEG has been conducted by Yu *et al.* [72], which includes measurements for shear viscosity, surface tension and conductivity of the material at different concentrations in de-ionised water.

Polyurethane - PU

Polyurethanes (PU) are synthetic polymers formed by reacting isocyanates with alcohol. Due to their toxic degradation products PU was not used much in the biomaterials field in the past. However, PU with diisocyanate [130] replacements have been developed to overcome issues of toxicity. For drug delivery purposes the material still degrades slowly although polymer blends with PU may be worth considering given its good mechanical properties, especially as a wound dressing [120]. Additionally, due to these material properties, PU may be valuable for the production of tissue engineered scaffolds for numerous applications [131]. PU has been electrospun using DMF and tetrahydrofuran (THF), with fibre diameters around 1 µm for PU concentrations of 20 – 25 % (w/w) in solvent [120,121,132,133].

Polymethacrylic acid derivatives

A number of studies have used polymethacrylic acid derivatives from the Eudragit® (Evonik) range to electrospin drug-containing fibres [99,134–136]. These derivatives consist of copolymers of methacrylic acids and methacrylic acid methyl esters containing quaternary ammonium groups. Eudragit RS100 and RL100 are also popular in oral dosage forms as

they have particular pH sensitive solubilities and the combination of these two polymers at different ratios may modulate drug release as they have different water permeabilities [137]. For electrospinning the Eudragit polymers have been dissolved in ethanol, methanol, or mixtures of either ethanol or methanol with DMAc or DMF, with resulting fibre diameters having been reported between 300 and 2000 nm [99,134–136].

1.5.2 Bioadhesive polymers

As emphasised in section 1.3, one of the difficulties in locally targeting oral diseases is in creating a drug delivery system that can be well retained in the oral cavity. An ideal solution is a mucoadhesive system that will adhere to the target site for a prolonged period of time. A number of polymers with bioadhesive properties that could be incorporated into the electrospun patch system may aid such a purpose.

A number of factors which are said to influence the mucoadhesive properties of polymers have been identified. According to the literature, the molecular weight of the polymer as well as the flexibility of the polymer chain and polymer chain configuration influences the molecular entanglement that can occur between the polymer and the biological substrate and thereby influence the bioadhesiveness. For example greater adhesion of PEO with increasing molecular weights up to 7,000 kDa was observed due to their linear configuration, compared to dextran having similar bioadhesive strengths ranging from molecular weights of 200 kDa to 20,000 kDa as they have a coiled conformation [138,139]. Another reported factor for mucoadhesiveness is that the pH environment may influence the polymer system (for example by dissociation) and thereby alter the resulting charge difference between the polymer substrate and the mucus surface [140]. The contact time of the polymer system to the wet mucus surface also influences polymer swelling and interpenetration between the polymer chains and glycoproteins of the mucus, where the formation of hydrogen bonds and ionic interactions may also increase interpenetration with the mucus layer [138,141]. The

cross-linking density may influence mucoadhesion, as a highly cross-linked polymer will have less chain mobility, a lower diffusion coefficient and decreased swelling would occur, thereby reducing the amount of interpenetration [138]. A number of reviews are available on bioadhesive polymers [9,138,141–144]. Natural polymers that have been widely reported to have bioadhesive properties are chitosan, gelatin and alginates. Some synthetic polymers with bioadhesive properties and which have been mentioned in the previous section are PVP, PVA and PEO. Carboxymethylcellulose and poly(acrylic acid) are other synthetic polymers reported in many studies to have mucoadhesive properties. Some of these polymers have been modified with thiols and reported to have had improved mucoadhesion, where disulphide bridges with cystein domains of glycoproteins in mucus were formed [145].

No one method has been identified to measure mucoadhesion and there is no obvious correlation in results between methods, especially when compared to *in vivo* findings. Shaikh *et al.* [141] have listed a range of tests, mainly *in vitro* tests, which evaluate mucoadhesion. The majority of the tests available measure mucoadhesive strength, which is a measure of the force required to break, pull or tear away the sample from the model membrane.

1.6 Drug incorporation in an electrospun patch

Various methods of drug incorporation into a polymer system and investigation of encapsulation and the drug release kinetics from the polymer have been researched in the past. There are various methods for the incorporation of therapeutics into the polymer solution prior to electrospinning, which can range from simply dissolving the therapeutic in the polymer matrix to creating smart chemical systems where the therapeutic is encapsulated by the polymer and depending on the polymer solution may only be released in certain conditions, for example using temperature, pH or a specific solvent [146].

1.6.1 Review of electrospun polymer-drug systems

Many different electrospun polymer-drug systems for a whole range of diseases (not just in oral medicine) have been previously researched and the information from earlier publications have been collected in Table 1.4. The medicines listed have been either colour coded as follows: analgesic, non-steroidal anti-inflammatory, anti-cancer, antifungal, antibiotic, anaesthetic, or the medicine use has been described in brackets after the name of the medicine.

The 'spinning technique' in Table 1.4 describes how the polymer and drug have been combined in the electrospun system. Many of the terms used are either explained fully in the Meinel *et al.*'s [147] review or are slight adaptations thereof. In brief a 'polymer/drug blend' simply involves dissolving the polymer and drug in the solvent prior to spinning; the 'post-spinning modification' involves electrospinning the polymer on its own and afterwards the drug is absorbed by the polymer matrix; the 'core-shell spinning' technique involves electrospinning two solutions simultaneously such that one fibre is embedded inside the other fibre. The 'photo-polymerisation' method involves subjecting the electrospun mats to ultraviolet (UV) radiation post-spinning to allow crosslinking to occur [148].

Table 1.4. Review of electrospun polymer-drug systems				
Polymer and manufacturing technique	Proposed clinical application	Solution(s) used	Drugs incorporated	Ref.
PCL - Poly (ϵ-caprolactone)				
Polymer/drug blend	Oromucosal delivery of model drugs	Chloroform: Acetone (3:1)	Ibuprofen, Carvedilol (beta-blocker)	[91]
	Sublingual administration for migraines	Acetic Acid: Formic Acid (2:1)	Sumatriptan succinate, Naproxen	[149]
	Antimicrobial activity	Chloroform : Methanol	Amphotericin B	[58]
	Antibiotic wound dressing	Chloroform: Methanol (3:1)	Tetracycline Hydrochloride (HCl)	[96]
	Release proof of concept study	Chloroform: Methanol (3:1)	Naproxen, Chitosan Nanoparticles	[94]
	Cardiovascular implant	Chloroform: Methanol	Cilostazol (anti-platelet medicine)	[150]
	Antibiotic wound dressing	HFIP : Dichloromethane (DCM) (1:3)	Mupirocin	[151]
Core-shell spinning	Release proof of concept study	Chloroform: Methanol	Ampicillin	[152]
Post-spinning modification	Antibiotic for abdominal adhesions	Chloroform and Dimethylformamide (DMF)	Ornidazole	[153]
PVP - Poly(vinyl pyrrolidone)				
Polymer/drug blend	Taste mask bitter taste and to aid drug absorption post-swallowing	b-Cyclodextrin (bCD), 2-Hydroxypropyl- b-cyclodextrin (HPbCD)	Meloxicam	[102]
	Antifungal for oral candidiasis	Ethanol:Water:Benzyl alcohol (7:2:1)	Clotrimazole (CZ)	[101,103]
	Local anaesthetic for dental treatment	Ethanol	Mebeverine HCl	[99]
	Aiding bio-availability and increased release post swallowing	Ethanol	Ibuprofen	[97]
	Anti-inflammatory wound dressing	Ethanol: Methanol (1:1)	Indomethacin	[154]
	Proof of concept study	Dimethylacetamide (DMAc) : Ethanol (1:4)	Ketoprofen	[98]

Table 1.4. (continued)				
PVA - Poly(vinyl alcohol)				
Polymer/drug blend	Transdermal delivery	Water	Meloxicam (insoluble in water)	[114]
	Antifungal for oral candidiasis	CZ-loaded microemulsion-containing chitosan-ethylenediaminetetraacetic acid/polyvinyl alcohol (CS-EDTA/PVA)	Clotrimazole (CZ)	[117]
	Sublingual administration for migraines	Water: Phosphoric acid (99.3:0.7)	Sumatriptan succinate, naproxen	[149]
Photo-polymerisation	Antibacterial properties for wound dressing	Two stages; QCh/PVA by mixing 8% aqueous PVA solution with 8% aqueous solutions of QCh at varying weight ratios of QCh: PVA	Quaternised chitosan (QCh) and photo-cross-linking agent triethylene glycol diacrylate	[148]
PLLA - Poly(L-lactide)				
Polymer/drug blend	Postoperative local chemotherapy	Chloroform: Acetone	Doxorubicin HCl; paclitaxel	[155]
PLGA - Poly(D,L-lactide-co-glycolide)				
Polymer/drug blend	Treating malignant glioma	DCM between 2 and 30% (w/v); or DCM and DMF at 30% (w/v) concentration	Paclitaxel	[156]
	Anaesthetic eluting suture	HFIP	Bupivacaine HCl	[125]
	Anti-inflammatory wound dressing	DCM	Ibuprofen	[157]
Core-shell spinning	Antibiotic for periodontal disease	HFIP	Tetracycline HCl	[127]
Polymer/drug blend	Antibiotic release for wound healing	Lactic acid (LA): Glycolic acid (GA) (1:1); solution tetrahydrofuran (THF): DMF (3:1)	Cefazolin	[64]

Table 1.4. (continued)				
PLLACL - Poly(L-lactid-co-ε-caprolactone)				
Core-shell spinning Co-axial spinning	Anti-bacterial/ antibiotic wound dressing	Poly(L-lactid-co-ε-caprolactone) /2,2,2-Trifluoroethanol (TFE) solutions (as the shell solutions) and Tetracycline HCL/TFE solutions (as the core solutions)	Tetracycline HCl	[158]
PEVA - Poly(ethylene-co-vinyl acetate)				
Polymer/drug blend	Release of antibiotic	Chloroform	Tetracycline HCl	[159]
PAA - Poly(acrylic acid)				
Polymer/drug blend	Sublingual administration for migraines	0.1 M sodium chloride solution with the addition of β-cyclodextrin 1.2% (as a cross-linking agent)	Sumatriptan succinate, naproxen	[149]
PU - Poly(urethane)				
Polymer/drug blend	Anti-hypersensitive agent	DMF or DMAc	Itraconazole and ketanserlin (anti-hypersensitivity)	[121]
	Analgesic via dermal application	DMF	Naproxen	[132]
PLA-PCL - Poly(lactic acid) : Poly(ε-caprolactone)				
Polymer/drug blend	Anti-bacterial/ antibiotic wound dressing	Chloroform: Methanol (2:1)	Tetracycline HCl	[160]
PCL-PEG - Poly(ε-caprolactone): Poly(ethylene glycol)				
Post-spinning modification	Diabetic ulcer healing	DCM used to create block copolymer and Chloroform: Methanol (3:1) used as electrospinning solvent	DNA-binding to electrospun matrix	[161]
PCL-PBS - Poly(ε-caprolactone): Poly(butylene succinate)				
Polymer/drug blend	Anti-bacterial release for ocular infection	DCM, DMF, DMAc and dimethylsulfoxide (DMSO)	Ofloxacin	[162]
PCL-PAMAM: Poly(ε-caprolactone): Poly(amido-amine)				
Polymer/drug blend	Cancer therapy	Star polymer synthesis described in reference	Doxorubicin	[163]

Table 1.4. (continued)				
PLLA-PEVA blend				
Polymer/drug blend	Release of antibiotic	Chloroform	Tetracycline HCL	[159]
PVA core and PLLA or PLGA shell				
Core-shell spinning	Release proof of concept core-shell spinning study	Chloroform and DMF	Metoclopramide hydrochloride (dopamine antagonist)	[107]
PEG-b-PLA diblock copolymer				
Polymer/drug blend	Antimicrobial to prevent post-surgical infection	Polymer synthesis described in reference	MefoxinR (cefoxitin sodium)	[110]
PEG-DA (diacrylate) with gelatin				
Photo-polymerisation	Antifungal oral mucosal delivery for oral candidiasis	HFIP 1% (w/v)	Nystatin	[164]
Chitosan				
Polymer/drug blend	Wound dressing	DCM: Trifluoroacetic acid (3:7)	Lidocaine HCl	[151]

Table 1.4 only lists combinations of the given polymer and drug in an electrospun system, where some literature on electrospun drug delivery systems may have been overlooked and other literature may also discuss these polymer/drug combinations using different manufacturing methods (e.g. films and gels).

The rate at which the polymer fibres release the drug depends largely on the polymer formulation used and their polymer properties, some of which have been described in section 1.5. Other factors such as the binding of the drug to the polymer and whether a core-shell spinning technique has been used will also greatly influence the drug release rate [107,152].

Some of the characterisation methods of the electrospun systems listed in Table 1.4 include:

- Scanning electron microscopy (SEM) to determine the morphology of the fibres.
- Differential scanning calorimetry (DSC) to evaluate the physical state of the polymer and drug.

- Fourier transform infrared (FTIR) spectroscopy to analyse the chemical structure of the polymer and drug on their own compared to when they are combined.
- Wetting and disintegration time (in some instances called 'swelling and weight loss' studies) of electrospun mats.
- Tensile tests to assess the mechanical integrity of the electrospun mats.
- High performance liquid chromatography (HPLC) coupled with a UV spectrophotometer to evaluate drug loading of the electrospun mats and *in vitro* drug release into solution.
- *Ex vivo* permeation tests using permeation chambers.

These tests give a good basis and indication of tests which will need to be performed on the electrospun patches developed for this PhD.

1.7 Drug release and permeation through tissue

1.7.1 Quantifying drug release

Quantifying the release of the drug from the polymer fibres over a period of time will be important to evaluate the drug release. Different experimental *in vitro* set-ups have been used to measure drug dissolution as seen in literature. One such set-up is the paddle-over-disc method which is specific for transdermal patches, measuring one sided patch dissolution in a buffer at a paddle speed of 50 - 100 rpm. At the pre-determined time points, an aliquot is removed from the test solution and replaced with an equivalent volume of fresh buffer solution. The aliquots are then analysed by spectrophotometry techniques [98,99,134,165,166] or HPLC [97,121] to obtain a graph of the drug release over time. A modified and simplified version of this was performed by Illangakoon *et al.* (2014) [100] using a Petri dish, simulated saliva and a magnetic stirrer, although the placement of their electrospun patch in this process was not described. Potrc *et al.* (2015) [91] also used this

simpler approach by rolling their electrospun fibres onto a glass slide and placing this in a phosphate buffer, where the container is also on a magnetic stirrer.

Drug containing polymer matrices often follow either a Fickian or a non-Fickian drug diffusion release profile. Fick's laws of diffusion provide a way of mathematically and theoretically describing the solute transportation from a solid (in this case a polymer) matrix into another medium. Fick's first law of diffusion is given in the following equation:

$$J = -D \frac{\delta C}{\delta x} \quad \text{Eq. 3}$$

Where J is the diffusion flux ($\text{mol cm}^{-2} \text{ s}^{-1}$), D is the diffusion coefficient, δC the negative concentration gradient and δx the change in position. Fickian diffusion is shown by a linear drug release pattern against the square root of time. Various other mathematical diffusion models have also been described by Yao *et al.* (2010) [167] for a number of polymer systems.

1.7.2 Drug permeation into tissue

Drugs may diffuse through tissue via a transcellular or paracellular route. If the drug molecules travel via the extracellular matrix around the epithelial cells the paracellular pathway was taken or alternatively a highly lipophilic drug may diffuse through the cells via the transcellular pathway [168]. The diffusivity of a drug through tissue is dependent on a number of factors, such as the lipophilicity of the drug, the drug molecule size, the degree of ionisation of the drug molecule at a particular pH (pK) and the thickness of the tissue [168,169]. According to the Stokes-Einstein equation, the diffusion coefficient D (Eq.3) is dependent on the size of the solute molecule and the viscosity of the solvent, where the diffusion coefficient decreases with increasing molecule size and increases with the viscosity of the solvent [170]. Another method of increasing the diffusivity of the drug into tissue is by

addition of chemical permeation enhancers, which can alter the lipophilicity and structure of the tissue [171].

Ex vivo drug diffusion may be measured using drug permeation chambers, such as the Ussing chamber or the Franz diffusion cell. In such chambers, the tissue is placed between donor and receptor chambers, where the donor chamber contains the drug in solution or in a delivery system and the receptor chamber holds a physiological relevant buffer solution. These different compartments act as the tissue mucosa model by controlling the temperature, pH, media in the donor and receptor compartments, the dimension of the membrane used and the hydrodynamic conditions. In some instances synthetic membranes may be used to eliminate some variability caused by animal tissue [144]. For these methods the solution is removed from the receptor chamber at pre-determined time points to measure the drug permeation over time using a UV spectrophotometer [165,172] or HPLC [114,173,174].

The rate of drug permeation may also be described by Fick's first law, as in equation 3, although in passive drug diffusion the apparent permeability coefficient P_{app} (cm s^{-1}) for a specific drug molecule crossing a specific tissue is determined. If the concentration gradient between the donor (C_{donor} , mol cm^{-3}) and receptor mediums ($C_{receptor}$, mol cm^{-3}) can be considered constant as $C_{donor} \gg C_{receptor}$, then the flux is also constant, which is referred to as steady state flux J_{SS} ($\text{mol min}^{-1} \text{cm}^{-2}$), therefore the apparent permeability coefficient (cm s^{-1}) can be calculated as:

$$P_{app} = \frac{J_{SS}}{C_{donor}} \quad \text{Eq. 4}$$

1.8 Summary

A wide range of unpleasant oral diseases, such as oral lichen planus, oral mucositis, oral candidiasis and many more, would benefit greatly from an improved drug delivery system which can better target the diseased site locally. A versatile device therefore needs to be developed which can incorporate different medications, for example analgesics, local anaesthetics and antifungals, depending on the disease that is being treated. Furthermore, developing a mucoadhesive protective wound dressing for ulcers and lesions that can cover the diseased epithelium for a longer period of time is also an important area of research.

Electrospinning is potentially an ideal manufacturing method for this project for a number of reasons. One such reason being that a range of polymers and medications can be used in the manufacturing process and these can be combined in a simple solvent system to be then electrospun to fabricate a drug delivery device. Another reason is that the resulting thin-fibre patch may have mucoadhesive interaction at the tissue surface as well as having an improved drug release compared to other devices, such as films, because of the high surface area to volume ratio of the fibres.

When choosing a polymer and a solvent for the electrospinning process some important material characteristics to be aware of are the molecular weight and concentration of the polymer and the viscosity, conductivity and surface tension of the polymer/solvent system. These properties will influence the resulting fibre morphology, as well as influencing the necessary electrospinning equipment parameters (such as the voltage, pump feed rate and needle tip to collector distance). Having a polymer matrix as the main component gives good flexibility and toughness to the electrospun patch and some of the polymers which have previously been used to electrospin a drug delivery device for various applications are PCL, PVP, PLLA and PVA. Depending on the application of the drug delivery device and the properties of the drug in question a specific polymer may be best suited to manufacture the patch. To improve mucoadhesion various polymers or additives may also be added to the electrospinning polymer solution. When evaluating the electrospun drug delivery device

research should include measuring the drug encapsulating efficiency, drug stability, drug release from the patch and drug permeation into tissue. Although various electrospun drug delivery systems with different combinations of polymers and therapeutic agents have been previously researched, as shown in Table 1.4, only very few of these systems were developed to treat oral mucosal diseases, which will be addressed in this thesis.

Two clinical challenges in oral medicine highlighted in section 1.3 of the literature review were to improve the control of localised oral pain and to treat oral candidiasis with alternative antifungal therapies due to an increase in antifungal drug resistance. The improved local delivery of a safe and effective anaesthetic may benefit a wide variety of patients experiencing oral pain, including the treatment of painful ulcerative conditions. For the treatment of oral candidiasis the potential of short- to medium-chain fatty acids as an alternative antifungal therapy was highlighted. With the findings from this literature review taken into account the hypothesis, aims and objectives for the thesis can be formed, as discussed in the following sections.

1.9 Hypothesis

Mucoadhesive electrospun patches may be successfully fabricated to incorporate and release an active pharmaceutical ingredient or therapeutic agent to target specific areas of the oral mucosa for treatment of oral diseases.

1.10 Aims and Objectives

This literature review concludes that an improved localised drug delivery device is needed for oral diseases. Whilst electrospinning has been around for the past century as a manufacturing method only more recently has electrospinning been used as a means to encapsulate drugs in polymeric fibres. Currently only a few detailed publications have explored the potential for an electrospun drug delivery device to locally target oral diseases by adhering to the oral mucosa, and mainly from the research group working on this project

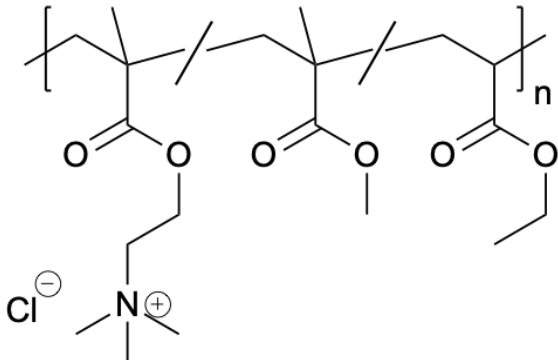
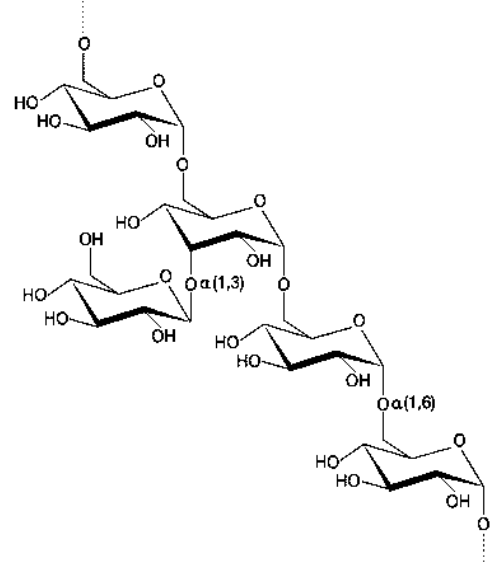
at the University of Sheffield. Therefore, the aim of this PhD is to develop and evaluate a systematic series of electrospun patches that may be loaded with therapeutic molecules for the purposes of adhering to the oral mucosa over several hours and deliver a drug locally to the diseased site for a sustained period. The specific objectives are:

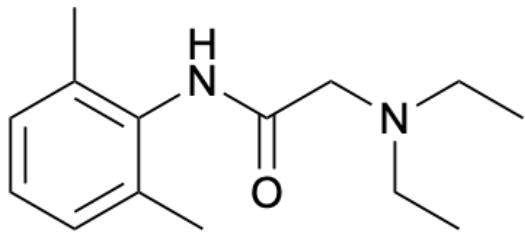
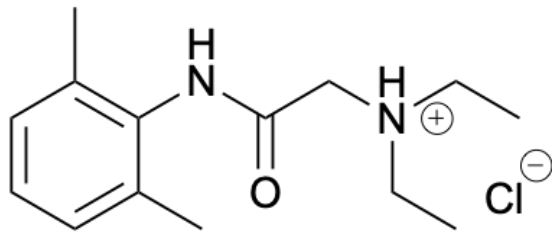
1. To select a suitable polymer-solvent system for electrospinning a drug delivery device and then characterising the viscosity, conductivity and surface tension of the polymer solutions. The resulting electrospun patches will be analysed for their fibre diameters and morphology using SEM.
2. To load a drug molecule, specifically lidocaine, into the electrospun polymer fibres and analyse the drug stability, drug encapsulation efficiency in the fibres, the drug release in buffer and the *ex vivo* permeation through porcine buccal tissue. This includes setting up a robust HPLC method to measure the lidocaine concentrations in the release and permeation tests. Additionally drug spatial distribution in tissue will be evaluated using mass spectrometry imaging.
3. To test the patches for their therapeutic potential by treating an oral fungal disease, oral candidiasis. This includes testing the therapeutic ability of short- to medium-chain saturated fatty acid solutions against several *C. albicans* strains (one of which is resistant to commonly used antifungal drugs) in its yeast and biofilm form; assessing the cytotoxicity of the fatty acids on mammalian cell; evaluating the encapsulation efficiency of the fatty acids in the electrospun patches; measuring *C. albicans* inhibition from the fatty acid containing electrospun patches; and testing the fatty acid containing patches on a more physiologically relevant *C. albicans* infected 3D oral mucosal model.

The findings from this thesis should inform on the potential of electrospun patches as a local oromucosal drug delivery device. The methodologies to determine the outlined objectives are described in full in the following chapter.

2. Materials and Methods

2.1 Materials

Table 2.1. Polymers and solvents used in the electrospinning process			
Polymers	Weight-average molecular mass M_w (g/mol)	Density (g/mL)	Supplier
Poly(ϵ -caprolactone) (PCL) ^a	70,000 - 90,000	1.15	Sigma Aldrich, UK
Poly(vinyl pyrrolidone) (PVP); Kollidon 90 ^a	1,000,000 - 1,500,000	0.40 – 0.55	BASF, Germany
Eudragit RS100 ^b	32,000	Unknown	Evonik, Germany
Poly(ethylene oxide) (PEO) ^a	400,000	Unknown	Sigma Aldrich, UK
Dextran T2000 ^c	1,500,000 - 2,500,000	1.8	Pharmacosmos, Denmark
^a Structures shown in Table 1.2 on pages 20-21			
^b Structure of RS100		^c Structure of Dextran	
			
Solvents			
Ethanol	46.07	0.79	Fischer Scientific, UK
Dichloromethane (DCM)	84.93	1.33	
Dimethylformamide (DMF)	73.09	0.94	

Reagent	Molecular Weight M_w (g/mol)	Water solubility (g/100mL) at 20 °C to 25 °C	Supplier
Lidocaine base ^a	234.30	Not soluble	Abcam, UK
Lidocaine HCl ^b	270.80	2.7	
Carboxymethylcellulose (CMC) sodium	Not given. Viscosity given as 400-1000 mPa.s, 2% in H ₂ O (25 °C) (dry substance)	0.2-0.5	Sigma Aldrich, DK
2,5-dihydroxybenzoic acid (DHB)	154.02	Soluble	
Disodium hydrogen phosphate	141.96	7.7	
Potassium dihydrogen phosphate	136.09	Approx. 25	
Methanol	32.04	Miscible	Th. Geyer GmbH & Co. KG, Germany
Acetonitrile	41.05	80	Fischer Scientific, UK
^a Lidocaine base structure		^b Lidocaine HCl structure	
			

Reagents	Supplier
Yeast	Oxoid Ltd, UK
Peptone	
Dextrose	
Agar	
Phosphate Buffer Saline (PBS) tablets	
Roswell Park Memorial Institute (RPMI)-1640 Media	Sigma Aldrich, UK
Poly-L-lysine	

Reagents	Molecular Weight (g/mol)	Water solubility (g/100mL) at 20°C/ 25°C	Supplier
Pentanoic acid	102.13	4	Sigma Aldrich, UK
Hexanoic acid	116.16	1.03	
Heptanoic acid	130.18	0.28	
Octanoic acid	144.21	6.8 E-2	
Nonanoic acid	158.24	3.0 E-2	
Decanoic acid	172.26	6.2 E-3	
Undecanoic acid	186.29	2.8 E-4	
Dodecanoic acid	200.32	4.8 E-4	
Dimethyl sulfoxide (DMSO)	78.13	1	
Fluconazole	306.27	1	Mast Diagnostics, UK
Miconazole discs (10 µg)	416.14	Not known	

Kit name	Type of assay	Supplier
Cell proliferation kit II, (2,3-bis-(2-methoxy-4-nitro-5-sulfophenyl)-2H-tetrazolium-5-carboxanilide) (XTT)	Colorimetric	Sigma Aldrich, UK
<i>In vitro</i> toxicology assay kit, 3-[4,5-dimethylthiazol-2-yl]-2,5-diphenyl tetrazolium bromide (MTT) based	Colorimetric	
LIVE/DEAD™ BacLight™ Bacterial Viability Kit	Fluorescent	ThermoFischer Scientific, UK
CytoTox 96® Non-radioactive Cyto-toxicity assay, lactose dehydrogenase (LDH) kit	Colorimetric	Promega, UK

Reagent	Making stock instructions/ concentration	Final concentration (of total)	Quantity for 500 mL media	Supplier	
Adenine (>99%)	0.5 mg in 70 mL dH ₂ O. Add up to 3 mL 1 M HCl and make up to 80 mL (6.25 µg/mL)	12.5 µg/mL (4%)	2 mL	Sigma Aldrich, UK	
Dulbecco's modified Eagle medium (DMEM) – High Glucose	As purchased.	(66%)	330 mL		
Epidermal growth factor	2 mg with 2 mL 10 mM acetic acid and add 20 mL PBS (100 µg/mL)	10 ng/mL (<0.5%)	50 µL		
Fetal Calf Serum	As purchased	(10%)	50 mL		
Amphotericin B	250 µg/mL	312.5 µg/mL (<0.5%)	1.25 mL		
Ham's F12 medium	As purchased.	(22%)	108 mL		
Hydrocortisone	25 mg in 1 mL dH ₂ O and 9 mL PBS.	200 µg/mL (<0.5%)	80 µL		
Insulin	As purchased.	(<0.5%)	233 µL		
Penicillin Streptomycin	100x conc. Includes 10 mg/mL Streptomycin and 10,000 units of penicillin.	10 mL/L (1%)	5 mL		
3,3,5-Tri-iodothyronine (T3)/ apotransferrin	13.6 mg T3 dissolved in 0.02 M NaOH and made up to 100 mL in dH ₂ O. 250 mg apo-transferrin in 30 mL PBS and add 0.5 mL of T3 solution and make up to 50 mL in PBS.	22 ng/mL T3 83 µg/mL of apo-transferrin (<0.5%)	500 µL		
Total (100%)			497.11 mL		-

Material, reagent or cells	Brief description	Supplier
12, 24 or 96 well plates	Used as a vessel for cell growth.	Greiner Bio-One, UK
Flasks	Used as a vessel for cell growth.	
Trypsin-EDTA solution	Used to dissociate adherent cells from the flasks in which they have been grown up.	Sigma Aldrich, UK
Rat tail collagen	Provides structure for the models and aids the 3D proliferation of the fibroblasts.	Provided by Dr Emma Bird at the University of Sheffield.
Normal oral fibroblasts (NOF)	Obtained via oral biopsies from the buccal mucosa of healthy volunteers with informed consent by the Sheffield Ethics Committee (ref09/H1308/66).	Provided by Dr Helen Colley at the University of Sheffield.
FNB6 oral keratinocytes	Normal immortalised oral keratinocyte cell line isolated from the buccal mucosa.	Obtained from Glasgow Dental Hospital and School [176].
Acetic acid	For collagen stock.	Fisher Scientific, UK
pH buffer	To calibrate the pH meter prior to use.	
Sodium chloride (NaCl)	To adjust the pH.	Sigma Aldrich, UK
Hydrochloric acid (HCl)		

Stain or reagent	Supplier
Xylene	Fisher scientific, UK
Schiff's reagent	
Periodic acid	VWR Prolab
Haematoxylin	Thermoscientific, UK
Eosin	
DPX mountant	
Sodium hydrogen carbonate	Merck KGaA, Germany

2.2 Methods: Characterisation of electrospinning polymer solutions and the resulting electrospun mats

This section describes the polymer and solvent systems, and the methodology used to manufacture and characterise electrospun patches.

2.2.1 Preparing the polymer solutions

For both electrospinning and material characterisation the polymer solutions were prepared as follows: PCL was dissolved in a DCM and DMF solution at a w/w ratio of 93:7 DCM to DMF at various concentrations and left on a magnetic stirrer for four hours before being used for electrospinning. PVP was dissolved in 97% (w/w) ethanol in deionised water at various concentrations and was left on a magnetic stirrer for 18 h. For some further experiments RS100, PEO and dextran were added to the PVP solution at different concentrations and stirred for up to 24 h.

2.2.2 Viscosity of polymer solutions

Rotational rheology tests were performed on the polymer solutions using an MCR 301 rheometer (Anton Paar, Austria) with a cone-plate measuring system CP50-1 (50 mm diameter and 1° cone) at a constant temperature of 25 +/- 0.2 °C with a sample volume of approximately 1 mL. The linear viscoelastic region of the polymer solutions was pre-determined with an amplitude sweep test. The selected polymer solutions remained in the linear viscoelastic region as the strain was increased from 0.1% to 100%, as shown by the linear storage modulus G' in Figure 2.1. This means that within this region of strain the material structure is not destroyed or altered, and the viscosity test will be run within this viscoelastic region.

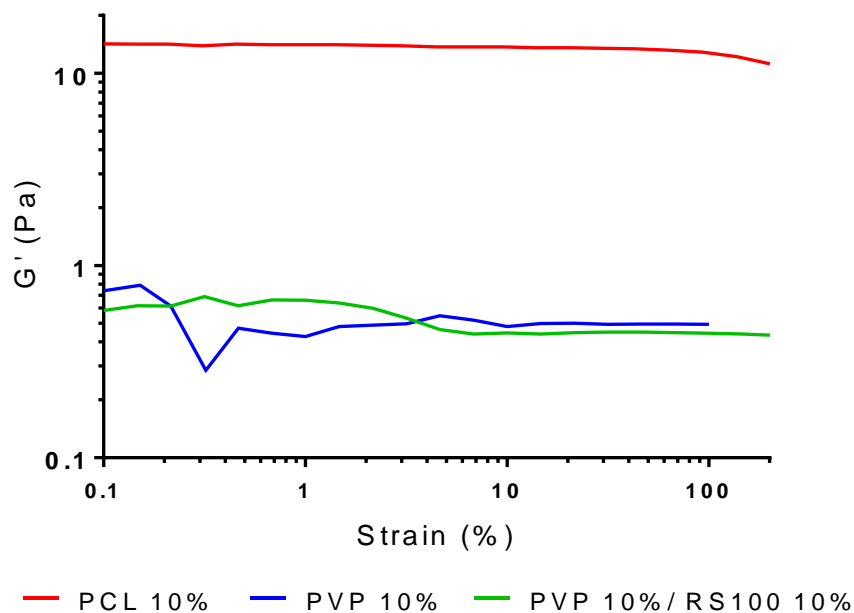


Figure 2.1. Amplitude sweep test to detect the linear viscoelastic region for 10% PCL in DCM/DMF (93/7 w/w%), 10% PVP in ethanol and a mixture of 10% PVP and 10% RS100 in ethanol ($n=1$).

The shear rate in the shear sweep tests to determine the solution viscosities ranged from 1 to 100 s^{-1} . The shear rate of the solution being pushed from the electrospinning needle was estimated to be 40 s^{-1} , using the following equation [177]:

$$\dot{\gamma} = \frac{4V}{\pi r^3 t} \quad \text{Eq. 5}$$

Where $\dot{\gamma}$ is the shear rate (s^{-1}), V is the volume of extruded solution (m^3), r is the radius of the nozzle (in m) and t is the time taken to extrude the volume of solution (s).

A parallel-plate measuring system with a 0.5 mm gap (PP-50) was used when adding PEO particles to the PVP/RS100 solution as these non-soluble particles did not fit under the CP50-1 plate. For all experiments a solvent trap was used, with the solvent system in which the respective polymer was dissolved in, to prevent evaporation of the solvent from the polymer solution.

2.2.3 Conductivity of polymer solutions

Conductivity of solutions was measured using a Mettler Toledo FG3 conductivity meter (Mettler Toledo, Switzerland) with a conductivity standard of 1413 $\mu\text{S}/\text{cm}$. The conductivity meter was cleaned with solvent and deionised water between each use.

2.2.4 Surface tension of polymer solutions

The surface tension of polymer solutions was measured using a Lauda tensiometer TD3 with a De Noüy ring (Lauda-Brinkman, Germany). Prior to the experiment and between each test the De Noüy ring was cleaned by dipping it in ethanol, heating it by blow-torch and dipping it in water, followed by blow-torching it again before placing it on the equipment stanchion. The ring was calibrated and tested with deionised water, for which a surface tension of 72 \pm 1 mN m^{-1} was expected. The polymer solutions were made up to 60 mL and poured into a glass dish that was placed on the stage below the ring. The stage was operated upwards until the ring just dipped below the surface of the polymer solution. The surface tension was recorded by taking five to six measurements per solution.

2.2.5 Electrospinning parameters

The electrospinning setup consisted of a pump (KD Scientific, US), which expelled polymer from a 1 mL syringe with internal diameter of 0.584 mm (BD Plastipack, Spain) through a 20-gauge blunt metallic needle (Intertronics, UK). The Alpha IV Brandenburg power supply was connected to the needle supplying a voltage between 10 and 30 kV. The polymer was collected on a metallic collector plate a specified distance from the tip of the needle (see Table 2.9). The following electrospinning parameters were used, with slight alterations to previously published work [178]:

<i>Polymer</i>	<i>PVP solution</i>	<i>PCL solution</i>
<i>Voltage (kV)</i>	17-19	17
<i>Feed pump speed (mL/h)</i>	3	3
<i>Collector-to-syringe tip distance (cm)</i>	14-18	21
<i>Collector covered in</i>	baking paper	aluminium foil

The flow rate was decreased to 1.5 mL/h with the addition of PEO or dextran particles, as otherwise the polymer solution would overflow from the tip of the needle rather than being directly drawn into a fibre. As the rig was not temperature or humidity controlled, the voltages were increased slightly during hot summer days where the temperature in the laboratory was over 25 °C, as this resulted in better drawing of the polymer solution into a fibre.

The same set up as in Table 2.9 was used when therapeutic agents were added to the PVP or PCL polymer solutions, with the before mentioned decrease in flow rate if the PEO particles were also added. The PVP solution with the addition of dextran or PEO particles required a larger syringe tip (Intertronics, UK) with an inside diameter of 1.372 mm (15-gauge) tip.

2.2.6 Morphology of electrospun mats

Electrospun scaffold samples were prepared for scanning electron microscopy (SEM) by placing cut out areas of the electrospun membranes onto stubs with carbon sticky tape followed by gold coating using Edwards S150B Gold Sputter Coater (BOC Edwards, UK) prior to the microscopy process. The morphology of the fibres was imaged using a Philips XL-20 (Philips, Netherlands) SEM set at 15 kV. The diameters of the electrospun fibres were measured using imageJ (National Institute of Health, US [179]). The method of how the fibre diameter data was obtained for one electrospun patch is shown in Figure 2.2.

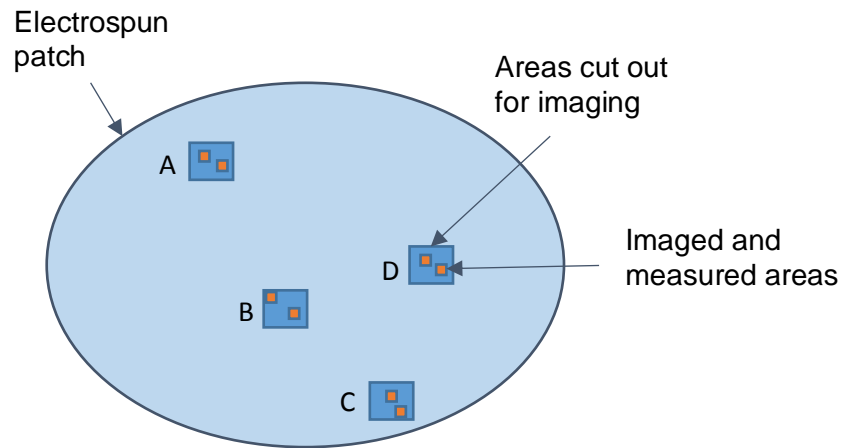


Figure 2.2. Schematic showing how areas of an electrospun patch were cut out and imaged under the SEM. These 4 cut outs from one patch (A-D) were imaged to measure the range of fibre diameters for one electrospun patch. Using imageJ all fibre diameters were measured in these 8 imaged areas. For one cut out, e.g. section A, the data from the two images is combined.

2.3 Methods: *Ex vivo* permeation of lidocaine released from electrospun patches

An important consideration when developing a local drug delivery device is to understand whether the drug is not only being released from the electrospun patch but whether it is also able to permeate the local tissue. This section includes methodology of the drug being incorporated into the electrospun patches and the characterisation thereof, the drug release from the electrospun patches in buffer, drug permeation through oral mucosal tissue using diffusion chambers and the use of mass spectrometry imaging to determine drug distribution in tissue.

2.3.1 Manufacture of electrospun mats containing lidocaine

Lidocaine base or lidocaine HCl was added at 3% (w/w) of the dry polymer in the dope solution (e.g. 0.1 g of lidocaine in 3.26 g of polymer in a 10 g polymer dope solution). The polymer dope consisted of 10% (w/w) PVP, 12.5% (w/w) Eudragit RS100 and 10% (w/w) PEO in 97% (w/w) ethanol prepared in deionised water. The solutions were mixed at room temperature using a magnetic stirrer for 24 h or until they were dissolved. Then the solutions were electrospun as described in section 2.2.5.

2.3.2 Dual layer patch manufacture

A strip of plain PCL patch and either the plain or lidocaine containing PVP/RS100/PEO patch were sandwiched together between two glass slides and placed in an oven at 70 °C for 3 min. Backing paper was placed between the glass and the PCL to prevent the PCL sticking to the glass. PCL has a lower melting point than the PVP layer and so melts onto the top of the PVP fibres. The dual-patch was then punched using a 10 mm diameter punch. If the PCL layer peeled from the top of the PVP layer slightly because of the punching process, the mat

was placed back in the oven for a few more minutes to ensure that the two layers were stuck together.

2.3.3 Differential scanning calimetry

Differential scanning calimetry (DSC) was used to determine whether the lidocaine was amorphous in the electrospun mat. After the liquid nitrogen flow was turned on the DSC (Pyris 1, Perkin Elmer) was left to equilibrate to 25 °C prior to the start of the experiment. The samples were weighed out to 0.001 mg accuracy and placed in an aluminium pan that was crimped shut with an aluminium cover. The DSC heating profile was from 25 °C to 200 °C with a heating rate of 10 °C/min.

2.3.4 pH of electrospun patches containing lidocaine base and lidocaine HCl

After fully dissolving the electrospun patches either containing no drug, lidocaine HCl or lidocaine base (n = 3 patches for each condition, 110 ± 4 mg patch weight; mean \pm SD) in 10 mL of deionised water the pH was measured using a FiveGo pH meter (Mettler Toledo, Switzerland) at 20.5 °C.

2.3.5 Isotonic buffer solution

Isotonic phosphate buffered saline (PBS) at pH 7.4 and an osmotic pressure of 290 mOsm/kg was prepared by dissolving 2.38 g of disodium hydrogen with 0.19 g potassium dihydrogen phosphate and 8 g sodium chloride in 1 L of deionised water. The pH was adjusted to pH 7.4 with concentrated sodium hydroxide solution or hydrochloric acid solution if necessary and the osmotic pressure was adjusted to 290 mOsm/kg using sodium chloride.

2.3.6 Ultraviolet scan of lidocaine HCl

Lidocaine HCl 3% (w/v) in PBS was scanned using a UV-cuvette on a NanoDrop 2000 Spectrophotometer (ThermoFisher Scientific, US). The optimal wavelength was determined to be 262 nm (Figure 2.3).

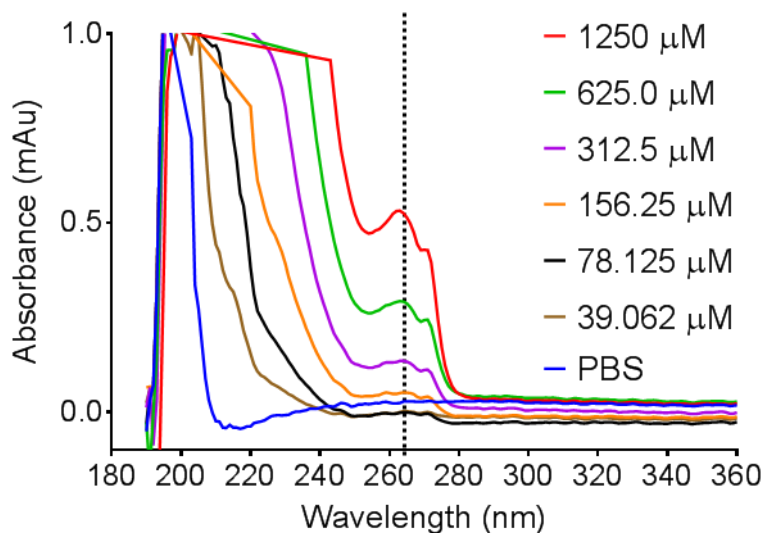


Figure 2.3. Determining the optimal wavelength for lidocaine HCl in PBS, where 1 mL of the solution in a UV-Cuvette at different concentrations of lidocaine is shown (n=1).

2.3.7 High-Performance Liquid Chromatography

HPLC analysis was performed to detect the presence of lidocaine using a XBridge BEH-C18 column (4.6mm × 250 mm, 130 Å pore size) (Waters, UK) and a mobile phase composed of acetonitrile (ACN): water (1:1 v/v) containing 0.1% (v/v) ammonia, run for 12 min at a flow rate of 1 mL/min. The UV detector was set to 262 nm, and a single injection of 20 μL per sample was performed to obtain the concentration results. A standard curve was achieved using known concentrations of lidocaine HCl in buffer. Good linearity was achieved ($R^2=1.00$) and the limit of quantitation was determined to be 1.8 μM (ten times the background reading created by PBS in the lidocaine peak region). The validation of this method is shown in Figure 2.4, where the retention time peak was approximately 10.1 min.

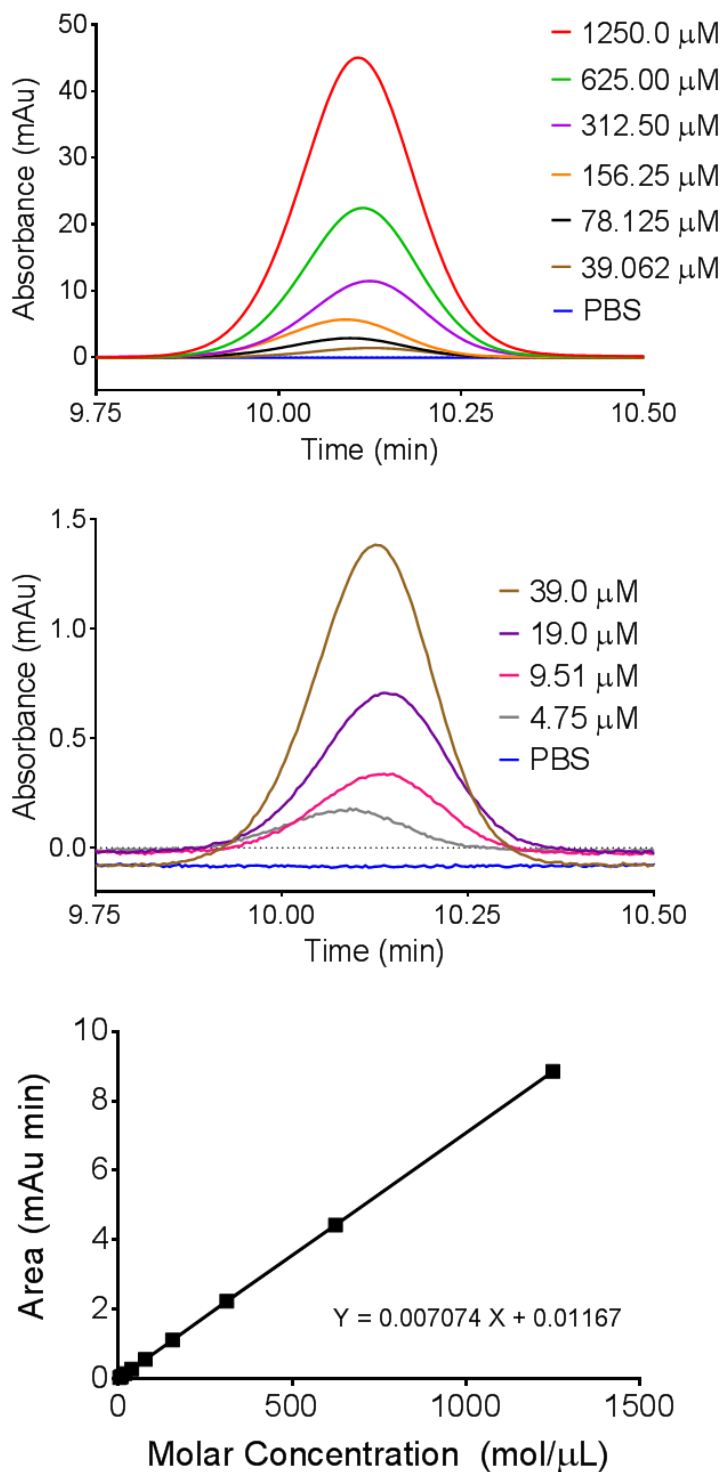


Figure 2.4. Lidocaine HCl was dissolved in PBS at increasing concentrations and run through the HPLC at a wavelength of 262 nm. The resulting peaks between 9.8 and 10.3 min are shown. Areas under the curve was plotted to show good linearity ($R^2 = 1.0$) across the different concentrations measured.

2.3.8 Release of lidocaine in buffer from the electrospun patches

Single layer drug containing patches (\varnothing 10 mm) were weighed and placed in a 12 well plate, which was then filled with 2 mL PBS and gently stirred at room temperature. Samples of 200 μ L were taken every 2 min for the first 10 min and then every 5 min up to 1 h and the amount removed was replaced by fresh PBS. The samples were analysed using the HPLC (see section 2.3.7) to determine the accumulative release over time.

2.3.9 Preparation of *ex vivo* porcine buccal mucosa

Porcine buccal cheeks, purchased from the University of Copenhagen Veterinary School, were stored in cryomedium (40% (w/v) glycerol and 20% (w/v) sucrose in PBS pH 7.4) at -80 °C. In preparation for further experiments requiring porcine cheeks, the required number of cheeks were removed from the freezer and placed in a glass vial with PBS which had been stored at 4 °C. The glass vial was placed on a shaker with a cool plate that had been stored in the freezer to allow gentle defrosting of the tissue. The cheek was moved to three different glass vials with fresh PBS every 10 min to allow the cryomedium to be washed from the tissue (Figure 2.5.A). The porcine cheeks were cut to size using surgical scissors and the height measured between two glass slides using a custom made height measurement equipment (Carl Zeiss, DK). The tissue sample was stretched across the Ussing slider (P2413, Physiologic instruments, US) with the epithelium side of the tissue facing upwards (Figure 2.5.B). The slider had an aperture diameter of 9.5 mm and a surface area of 0.71 cm². Next, the cheek was slightly wetted with 20 μ L of PBS before adding an electrospun patch to the top of the cheek with the drug loaded slide of the patch resting on the epithelium (Figure 2.5.C). Controls received placebo or no patch. To ensure a tight fit of the electrospun patch to the buccal mucosa parafilm was also placed across the patch prior to sandwiching the two sliders together (Figure 2.5.D).

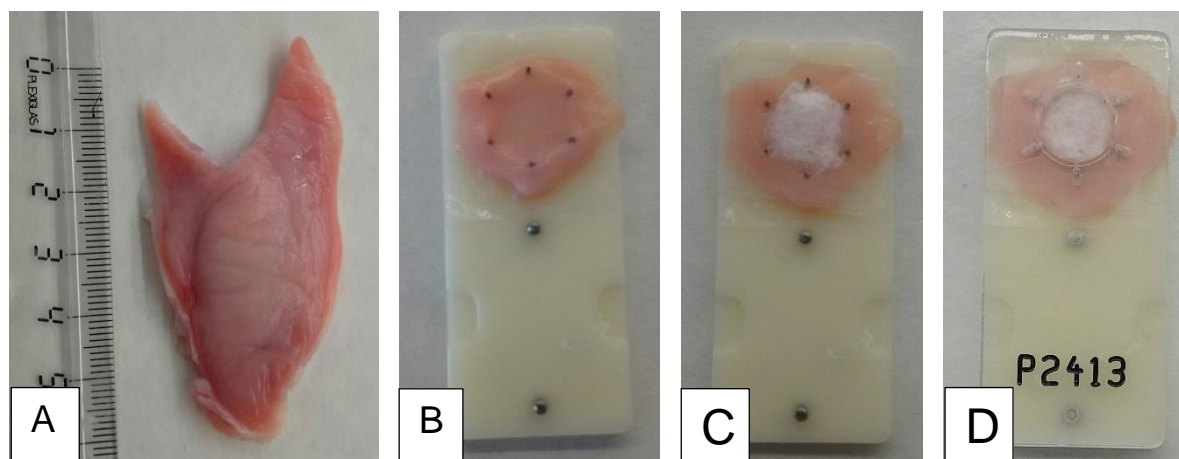


Figure 2.5. The images above show how the buccal mucosa was prepared prior to further experimentation. The following is depicted: A) de-frosted porcine buccal mucosa (ruler only associated to this image), B) porcine buccal mucosa cut to size and mounted on the Ussing slider, C) the addition of an electrospun patch to the porcine cheek, D) the second slider placed on top of the cheek and electrospun patch to sandwich everything together.

2.3.10 Permeation of lidocaine through porcine buccal mucosa

The Ussing chamber set up is shown in Figure 2.6. Heated water flowed through the blue outer chambers to regulate the temperature of the receptor and donor chambers. The water bath for the temperature control was set to 37.4 °C. The receptor and donor chambers were slotted in place between the blue heated chamber holders and the active transport measurement portals were closed off and not used in this experiment as the tissue was not fresh. The chambers were filled with 2 mL PBS to allow for the chambers to warm up whilst preparing the porcine tissue as described in section 2.3.9. Once the tissue samples were prepared the chambers were emptied of PBS and dried using paper tissue. The Ussing sliders containing the samples, either with or without the electrospun patch, were then slotted inbetween the two Ussing chambers with the epithelium facing towards the donor chamber.

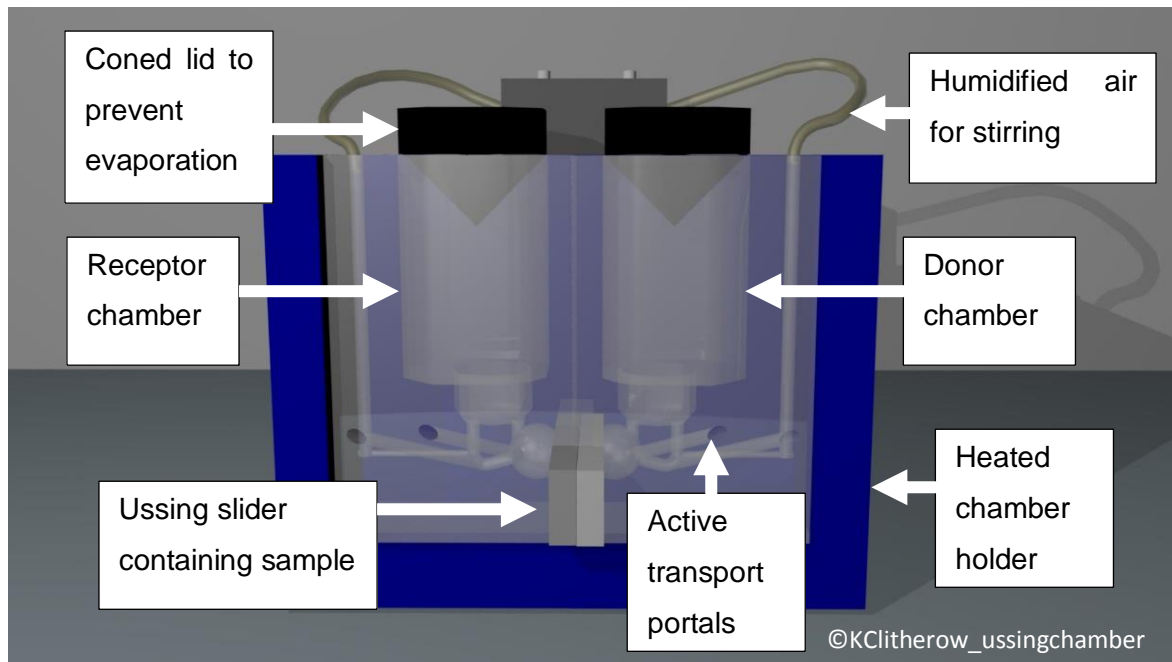


Figure 2.6. Overview of the Ussing chamber system and its components.

The Ussing chamber experiments were performed for three separate conditions:

1. The porcine tissue alone in the Ussing slider with 2 mL PBS in the receptor chamber and 2 mL of lidocaine HCl at 30 mg/mL in PBS in the receptor chamber. The moment the lidocaine HCl solution was added to the donor chamber the stop watch was started.
2. The porcine mucosa has a dual layer lidocaine HCl-loaded electrospun patch added to it, with the drug-loaded side of the patch facing the epithelium. In this case the donor chamber was left empty and the moment the receptor chamber was filled with 2 mL PBS the stopwatch was started.
3. The porcine mucosa has a dual layer lidocaine base-loaded electrospun patch added to it, with the drug-loaded side of the patch facing the epithelium. Again, the donor chamber was left empty and the moment the receptor chamber was filled with 2 mL PBS the stopwatch was started.

For all three experimental conditions 200 μL samples from the receptor chamber were taken every 15 to 30 min over 5 h and the removed liquid was replaced with fresh buffer. The temperature and pH in the donor and receptor chamber were recorded towards the start and the end of the experiment. The samples are analysed using the HPLC method described in section 2.3.7 and the accumulative release was calculated using the following equation:

$$m = v_s \times \left(\sum_{n=1}^n c_{n-1} \right) + c_n \times v_t \quad \text{Eq. 6}$$

Where m is the weight of the lidocaine released, v_s is the volume of the sampling aliquot, $(\sum_{n=1}^n c_{n-1})$ are all previous concentrations determined to n^{th} time point, c_n concentration of sample determined at n^{th} time point, v_t is the complete volume in the well.

The accumulated permeated amount (J_{SS} , $\mu\text{g min}^{-1} \text{cm}^{-2}$) was plotted against time (t , min) using GraphPad Prism. The steady state flux (dQ/dt , $\mu\text{g min}^{-1}$) was determined by taking the linear part of the slope between 180 and 300 min using the equation for steady state flux (J_{SS}), where A is the diffusion area (0.71 cm^2):

$$J_{SS} = \frac{dQ}{dt} * \frac{1}{A} \quad \text{Eq. 7}$$

For lidocaine HCl in PBS the apparent permeability (P_{app} , cm s^{-1}) was calculated using equation 4, as given in section 1.7.2, with the donor concentration given in μg .

2.3.11 Incubation of the electrospun patches on porcine buccal mucosa

The porcine tissue was prepared for this experiment as described in section 2.3.9, although for one condition the porcine tissue was mounted on a P2405 Ussing slider (Physiologic instruments, US), which has a square aperture size of 4.5 x 9.2 mm and an area of 0.4 cm^2 .

The following conditions were used:

1. Lidocaine HCl dissolved in PBS at 0.3% (w/w) of which 70 μ L was added to porcine tissue mounted in a P2405 Ussing slider.
2. A dual layer electrospun patch containing lidocaine HCl, which had been previously weighed, was applied to a slightly wetted porcine tissue mounted in a P2413 Ussing slider and parafilm was used to hold the patch in place.
3. A dual layer electrospun patch containing lidocaine base, which had been previously weighed, was applied to a slightly wetted porcine tissue mounted in a P2413 Ussing slider and parafilm was used to hold the patch in place.

All Ussing sliders were tightly held together using tape at the bottom end of the slider. The sliders were placed in a high humidity chamber with the epithelium side facing upwards. The chamber contained supersaturated NaCl solution to provide high humidity and the lower half of the Ussing sliders were lying in PBS solution. The chamber was placed in a 37.4 °C incubator. At different time points of 15 min, 1 h and 3 h the samples were removed from the chamber and the tissue samples were gently taken off the slider and placed onto aluminium foil. The tissue samples were covered in 5% CMC gel (made up in water). The samples were then placed in the -80 °C freezer in preparation for cryosectioning.

2.3.12 Cryosectioning

The cryostat (Leica Microsystems A/S, Germany) chamber and cutting arm was kept at -20 °C during the cryosectioning procedure. The tissue samples were removed from the -80 °C freezer and stored in the cryostat chamber until they were needed for cryosectioning. The frozen tissue samples were mounted in the cryostat using deionised water. Initially the sample was trimmed at 100 μ m until the centre of the sample was reached. The samples were then cut into 30 μ m slices and thaw mounted onto microscope glass slides. Once the cryosectioning was completed the glass slides were stored in the -80 °C freezer.

2.3.13 Matrix application for MALDI-MSI of tissue samples

Prior to matrix application the cryosectioned samples on the glass slides were defrosted by placing the slide under vacuum for 5 min. A sample was selected and the area desirable for imaging was selected using a red marker pen on the opposite side of the glass to where the tissue is (having an area of epithelium and submucosa), and the glass containing the sample was cut to a smaller size and placed on a metal tissue mount using sticky tabs, as shown in Figure 2.7. The matrix was made up of 30 mg 2,5-dihydroxybenzoic acid (DHB, MW=154.03) with a 1mL 1:1 methanol : water mixture containing 1% trifluoroacetic acid.

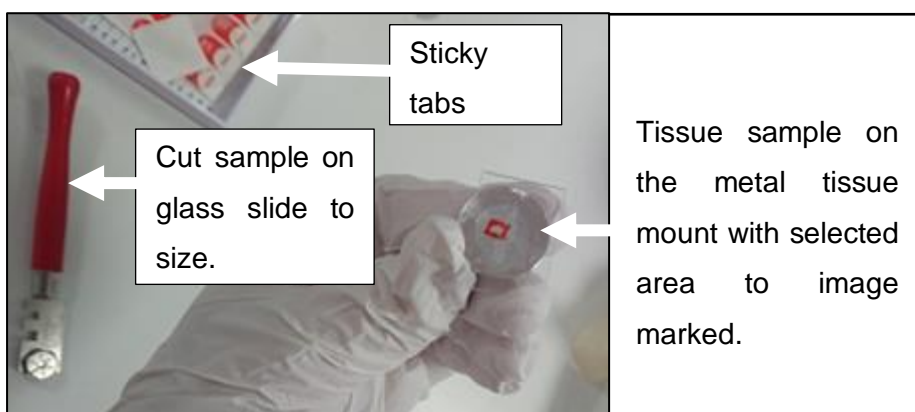


Figure 2.7. Mounting the tissue sample prior to matrix application.

The matrix application set-up is shown in Figure 2.8, which consists of a syringe pump, a syringe filled with the matrix solution, a tube attached to the syringe leading to the top of a stand, a gas attachment to the needle to allow for matrix spraying, a rotating top with a central hole to hold the sample mount and a plastic cup with a hole to hold the syringe needle that has a height of 13.5 cm which was placed centrally over the rotating sample.

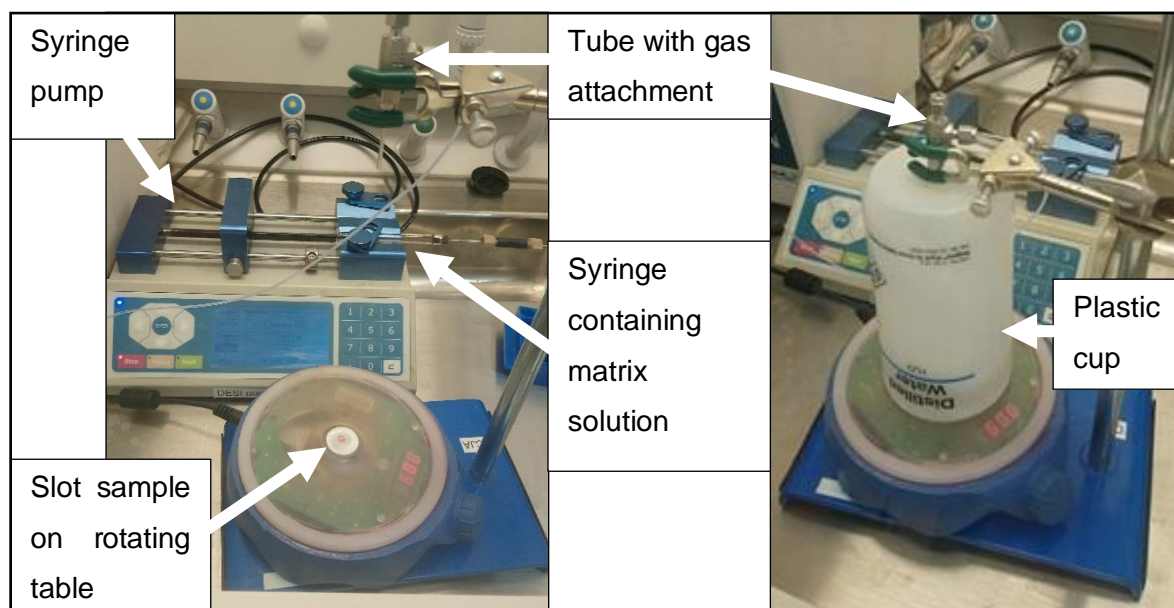


Figure 2.8. Matrix application for MALDI-MSI set up.

The sample was rotated at 600 rpm, the nitrogen flow was set to 2 bar and 300 μL of the matrix was applied at a rate of 30 $\mu\text{L}/\text{min}$. The sample was then ready for the imaging procedure.

2.3.14 Matrix-Assisted Laser Desorption Ionisation – Mass Spectrometry Imaging

To obtain spatial information of the presence of lidocaine in the tissue samples MALDI-MSI was utilised. A schematic of how the mass spectra by ‘scanning’ an area of tissue using a laser beam was obtained is shown in Figure 2.9. A Thermo QExactive Orbitrap mass spectrometer (Thermo Fisher Scientific GmbH, Bremen, Germany) coupled with a AP-SMALDI10 Ion source (TransMIT Gesellschaft für Technologietransfer GmbH, Germany) was used for imaging. Positive ionisation mode was utilised with a 200-800 m/z scan range and a mass resolving power of 140,000@ m/z . An m/z 295.02131 signal of the DHB matrix was used as a lock mass, thereby ensuring a mass accuracy of 2 ppm or better throughout the entire image. The images have a spatial resolution of 20 μm resolution. The mass

spectrum data was converted to an imzML file so that the mass spectroscopy image of the analytes present in the sample can be generated in MSiReader v. 0.09 [180,181].

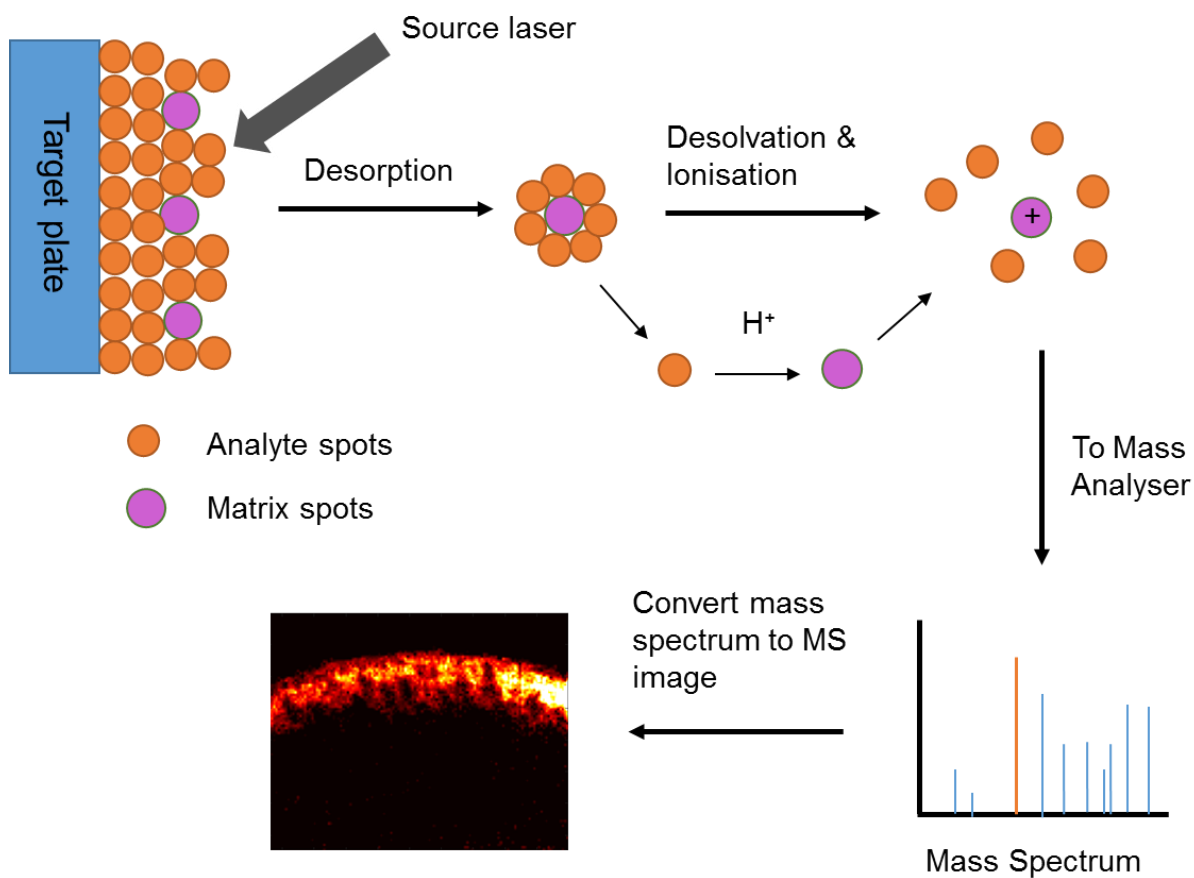


Figure 2.9. Schematic of MALDI-MSI principle, adapted from Hoffman and Strobaant [182].

2.3.15 Using MSiReader software to determine presence of analytes

The mass spectrum data collected from MALDI-MS over the sample surface from each laser point can be put together to show the presence and distribution of the analytes in the sample. The MSiReader v. 0.09 is an open source Matlab plugin that was used to open the imzML files and to attain the MALDI images, where a bin width of 0.002 Th was used [181].

2.3.16 Haematoxylin and Eosin (H&E) stain

Post-MALDI-MSI the glass slide was carefully removed from the tissue mount and the matrix on the tissue sample was removed by spraying ethanol directly onto the glass slide. The sample was then left to dry in the fume hood for 10 min after which 200 μL of haematoxylin was added to the sample, covering the tissue and was left for 12 min. Following this the haematoxylin was removed by pouring 0.1% NaHCO_3 over the sample. The glass slide was then placed in a Petri dish with fresh 0.1% NaHCO_3 covering the sample and incubated on a tipping table for 15 min. After removing the NaHCO_3 one to two drops of eosin were applied to the sample for 1 min. The eosin was removed with distilled water, after which fresh distilled water was left covering the sample for 1 min.

2.3.17 Optical microscope images of H&E stained tissue

Images of the H&E stained sample were taken under the optical microscope (Olympus, Japan) equipped with an AxioCam ERc5s camera (Zeiss, Germany) and then Image Composite Editor (Microsoft, US) was used to stitch the images together. This image can then be used to overlay it with the MALDI images using MSiReader.

2.4 Methods: Electrospun antifungal mat fabrication

To show the potential of electrospun patches to be used in the treatment of oral diseases, antifungal agents were loaded into the electrospun patches and *in vitro* tests using the most prevalent pathogen of oral candidiasis, *Candida albicans*, were performed. The methodologies for these tests are given below.

2.4.1 Preparation of agar plates and yeast-peptone-dextrose (YPD) broth

Yeast extract (2%), peptone (2%), dextrose (1%) and 2% agar were added to de-ionised water, autoclaved and transferred to a 55 °C water bath to cool before pouring into Petri dishes to solidify for approximately 1 h prior to storing the plates in the fridge. YPD broth was prepared using the same ratio as before, but without the addition of agar.

2.4.2 *Candida albicans* strains

The wild type strains used were BWP17 (provided by Prof. Julian Naglik, Kings Collage London) and SC5314 (provided by Dr Steven Saville, University of Texas San Antonio). An antifungal azole resistant clinical strain (CAR17; provided by Prof. David Williams, University of Cardiff) was also used. All strains were cultured on YPD agar at 37 °C and stored at 4 °C.

2.4.3 Preparation of short- and medium-chain fatty acid stock solutions

Stock solutions of a range of short- to medium-chain fatty acids were made up in DMSO. The fatty acids ranged from butanoic acid (C5:0) to dodecanoic acid (C12:0) and were made up as 8 M stock solutions that were diluted prior to use in experiments.

2.4.4 Manufacture of electrospun mats incorporating medium chain fatty acids

Fatty acids were incorporated in both 10% (w/w) PCL and 10% (w/w) PVP/ 12.5% (w/w) RS100 electrospun mats. The fatty acids were incorporated into the polymer dopes as purchased (not from the stock solutions) and added to make up 0.2 M concentration in the solvent mixture of the polymer solution. Otherwise the polymer solutions were made up as described in section 2.2.1 and electrospun as described in section 2.2.5.

2.4.5 Determination of the concentration of fatty acid in the PCL electrospun patches using nuclear magnetic resonance spectroscopy

Nuclear magnetic resonance (NMR) ^1H spectra of fatty acids and PCL electrospun patches dissolved in 0.7 mL to 1 mL deuterated chloroform (CDCl_3) and sealed in a 5 mm tube were recorded using a Bruker AVANCE III or Bruker AVANCE III HD spectrometer at 298 K and 400.2 MHz or 500.13 MHz. The quantitative spectra were recorded with eight transients using a 90° pulse and a relaxation delay of 40 s (having previously determined the longest T_1 within the mixtures to be ~ 6.5 s), over an acquisition window of 20 ppm and 64 k acquisition points. The spectra were analysed using Bruker TopSpin version 3.2 software. The NMR peaks are representative of the number of hydrogens present at a particular resonance, where the normalised integrated signals give the relative number of hydrogens at a particular resonance. By comparing the normalised integrals of distinguishable PCL signals versus fatty acid signals the mole ratio of the two components could be calculated and thereby the mass concentration of fatty acid present in the PCL electrospun fibres was established. The step by step equations to determine the mass concentration are given below:

$$\text{Mole ratio} = \frac{\text{Area [PCL]}/N[\text{PCL}]}{\text{Area[Fatty acid]}/N[\text{Fatty acid}]} \quad \text{Eq. 8 (a)}$$

Where Area[PCL] or Area[Fatty acid] was the integral of the PCL or the fatty acid peak, and N[PCL] and N[Fatty acid] are the number of hydrogens contributing to the signal being integrated, where N[PCL] = 2 and N[Fatty acid] = 3.

The mass ratio was calculated using the known molecular weights of M[PCL] and M[Fatty acid]:

$$\text{Mass ratio} = \frac{\text{Mole ratio} \times M[\text{PCL}]}{M[\text{Fatty acid}]} \quad \text{Eq. 8 (b)}$$

The percentage mass of fatty acid in the sample was:

$$\% \text{Mass of fatty acid} = 1 - \frac{\text{Mass ratio} \times 100}{\text{Mass ratio} + 1} \quad \text{Eq. 8 (c)}$$

2.4.6 Gas Chromatography – Mass spectrometry to determine concentration of fatty acid in the PVP/RS100 electrospun patches

Electrospun patches were weighed and dissolved in 1 mL 97% (v/v) ethanol. Standards of the fatty acids were also made up in 97% (v/v) ethanol, ranging from 0.01 M to 1 M. An Aligent DB-WAX-UI (30 m × 0.25 mm × 0.25 μm) column was used with helium flowing through the column at 1.2 mL min⁻¹ with a pressure of 9.15 psi. The injection volume of the sample was 1 μL and the temperature of the column was increased from 50 °C to 250 °C at 10 °C min⁻¹ intervals. The mass spectrometer scan range was between 25-500 m/z.

2.4.7 Agar disc diffusion

C. albicans strains were inoculated overnight at 37 °C in YPD broth with shaking. Disk diffusion tests on YPD agar plates were performed using 200 μL of 2 × 10⁵ colony forming

units (CFU) of *C. albicans* diluted in phosphate buffered saline (PBS) (Sigma Aldrich, US), which were then spread across YPD agar. Fatty acids with chain length C5:0 to C12:0 were diluted from the stock solutions to 0.2 M concentration in DMSO and 20 μ L pipetted onto 0.62 mm diameter filter discs (Thermo Scientific, US). The filter discs were placed on the *C. albicans* streaked YPD plate in triplicate per concentration. Fluconazole (0.8 mM) and miconazole discs (10 μ g or 2.4 nmol) were used as a positive controls and neat DMSO was used as the negative control. The YPD plates were incubated at 37 °C for 24 h then the YPD plate imaged and the zone of inhibition around the filter disc measured using ImageJ software (National Institute of Health, US [179]). Electrospun patches (12.7 mm diameter) incorporating fatty acid were also placed onto the *C. albicans* spread YPD plate and 37 °C for 24 h before measuring the zone of inhibition using the same method as for the filter discs. The agar disc diffusion methodology is shown schematically in Figure 2.10.

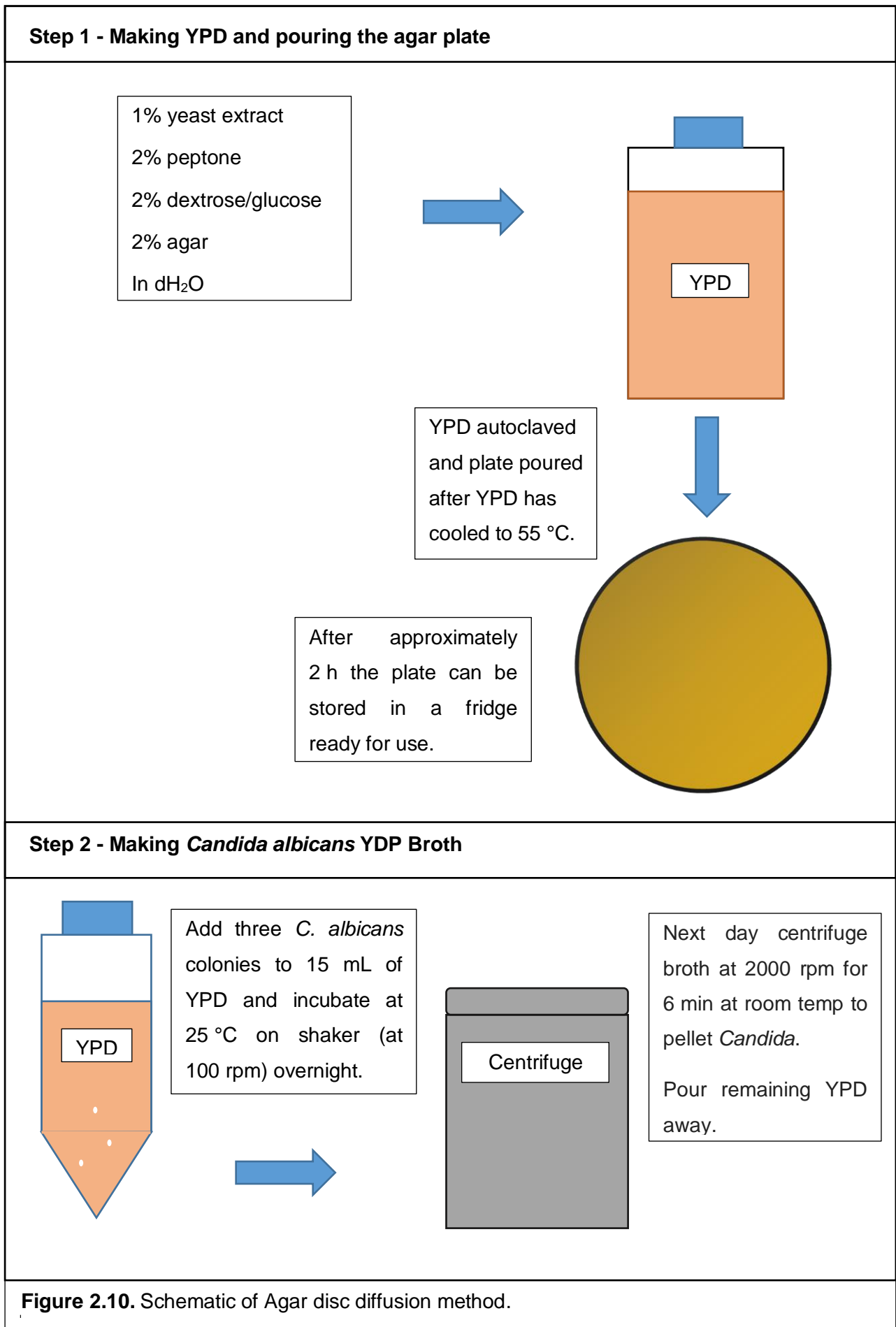


Figure 2.10. Schematic of Agar disc diffusion method.

Step 3 - Counting *Candida* Cells

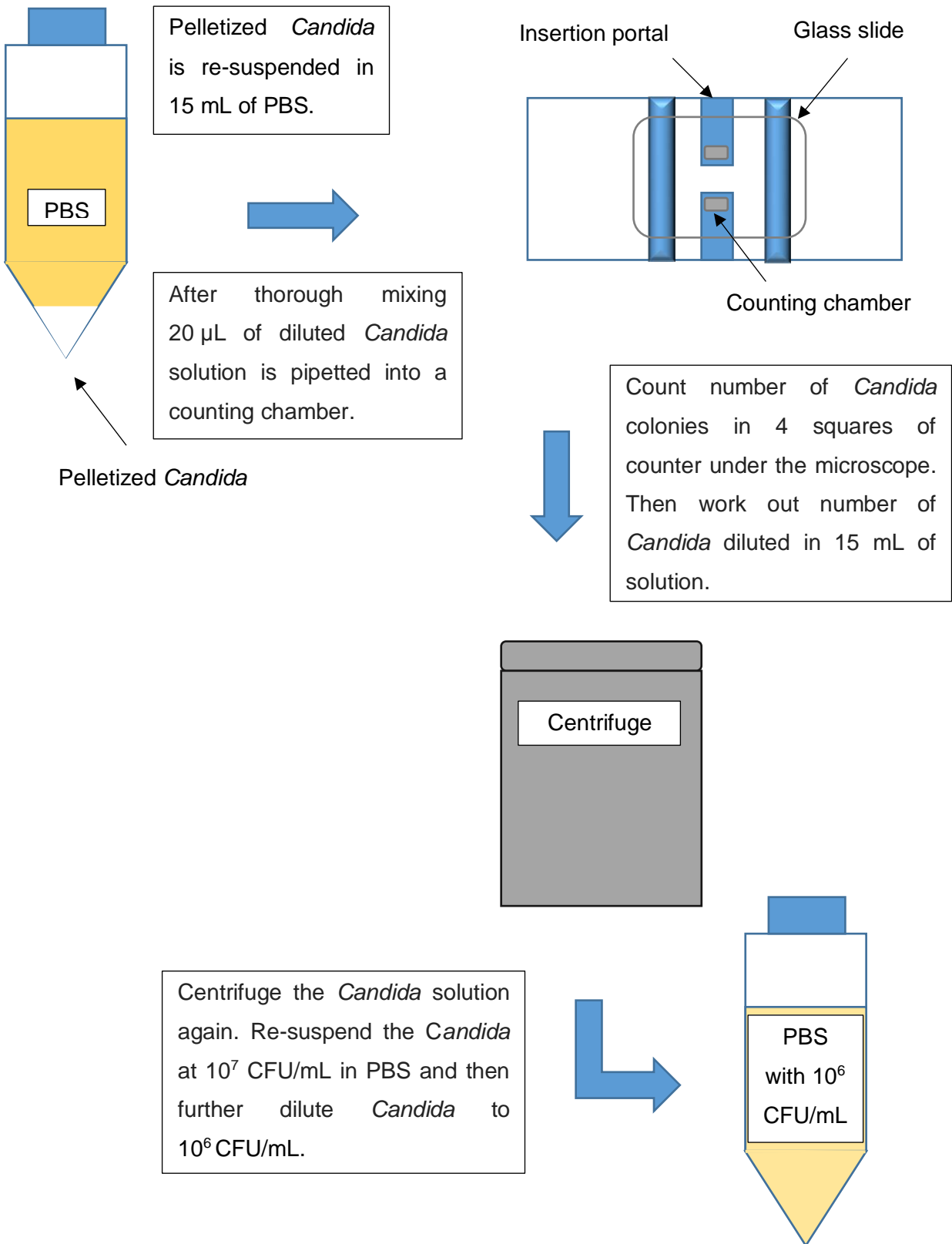
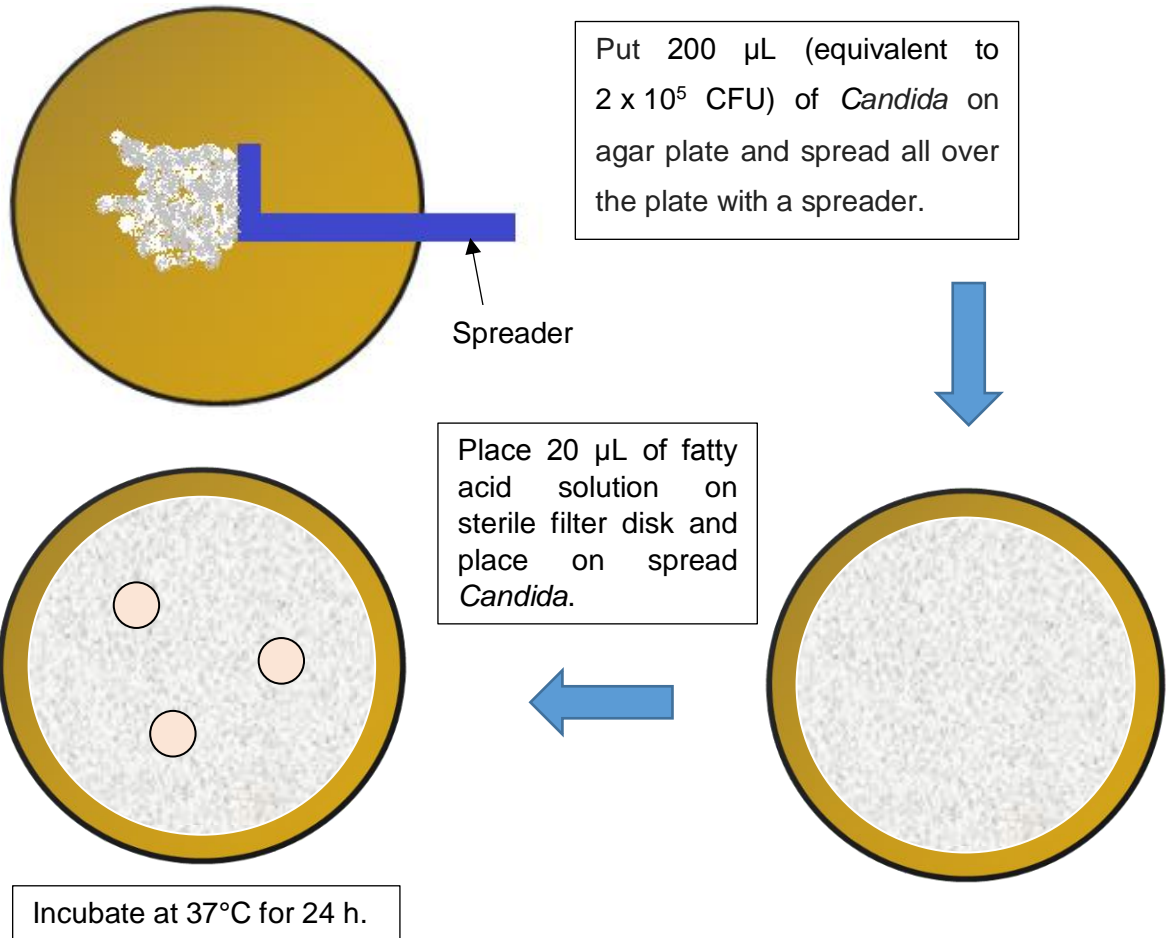


Figure 2.10 continued. Schematic of Agar disc diffusion method

Step 4 - Spreading *Candida* on agar plates



Step 5 - Measure *Candida* inhibition zone

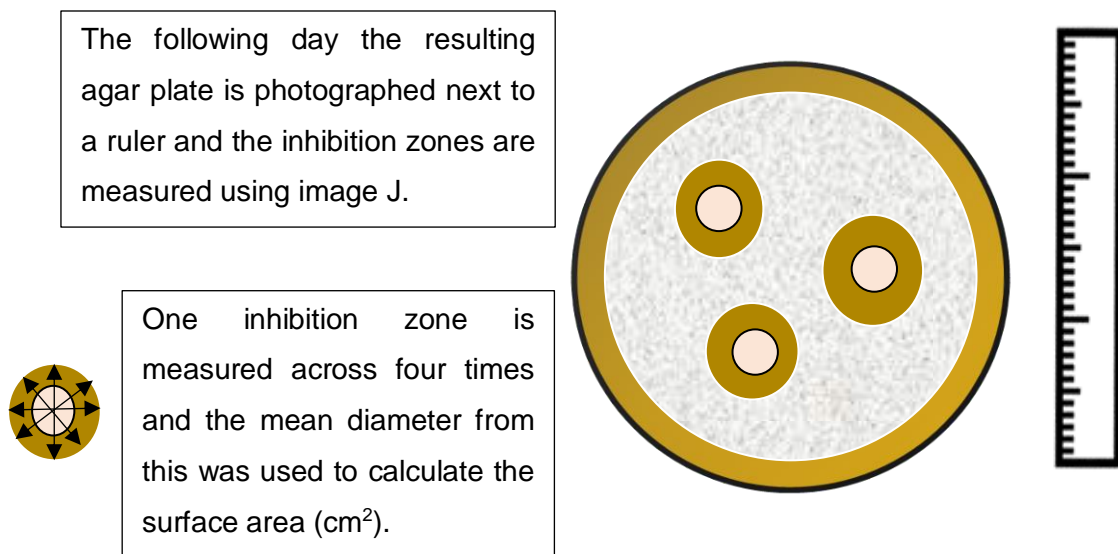


Figure 2.10 continued. Schematic of Agar disc diffusion method

2.4.8 Biofilm viability of *Candida albicans* treated with fatty acid solution

The effect of fatty acid treatment on *C. albicans* biofilms was measured using an XTT metabolism assay. 100 μL of 1×10^5 CFU/mL *C. albicans* (SC5314) was prepared in serum-free RPMI and pipetted into each well of a 96-well plate and the plate incubated at 37 °C for 24 h to enable the *Candida* to form a biofilm. The wells were washed once with PBS to remove any non-adherent cells. Fatty acids were prepared in DMSO and RPMI at increasing concentrations with 0.4 M being the highest concentration and 1:1 serial dilutions performed in RPMI. 100 μL of the fatty acid solutions was added to the wells (6 wells per treatment) and incubated at 37 °C for 18 h. RPMI was removed and 50 μL of freshly prepared XTT solution was added to the wells and the plate was incubated for a further 2 h. When the XTT is metabolised by the *C. albicans* a colour change occurs that is directionally proportional to the number of *Candida* in the well. 40 μL of the XTT solution was removed to a new 96-well plate and the absorbance read in a plate reader (Infinite 200 Pro, Tecan, Switzerland) at 450 nm with a correction reading taken at 690 nm. The results were plotted in Graphpad Prism (US) such that the control (no treatment) shows 100% biofilm viability and the concentration of the fatty acid on the x-axis is log-scale. The IC_{50} values were calculated using GraphPad Prism.

2.4.9 Biofilm viability assay of *Candida albicans* treated with fatty acid containing electrospun patches

24-well plates were pre-treated with poly-L-lysine (0.01% w/v) to increase the adherence of the *C. albicans* cells to the well surface. *C. albicans* strains SC5314 and CAR17 were cultured in YPD broth overnight, centrifuged, the pellet resuspended at 1×10^6 CFU/mL in RPMI and 1 mL pipetted into each well of a 24-well plate, which was then incubated at 37 °C for 24 h to form a biofilm. The wells were washed once with PBS and then electrospun discs (12.7 mm \varnothing) were placed in the individual wells along with 200 μL RPMI so that the biofilm

did not dry out. Three wells were used per electrospun patch condition (e.g. three wells used for electrospun patches containing C7:0). After 18 h incubation at 37 °C the RPMI was removed and 200 µL of XTT in PBS was added to each well and then returned to the incubator for 1 h at 37 °C. 40 µL of the XTT solution per well was removed and placed in a 96-well plate. The absorbance was read at 450 nm with a deducted background absorbance of 690 nm using the plate reader (Infinite 200 Pro, Tecan, Switzerland). The biofilm viability of each fatty acid electrospun patch condition was plotted using GraphPad Prism.

2.4.10 Live/Dead stain of *C. albicans* biofilm

The Live/Dead BacLight viability kit consisted of SYTO-9 and propidium iodine stains and were used on *C. albicans* biofilms grown as described in section 2.4.9 and treated with 50 mM of the fatty acid in RPMI solutions. The plate was washed twice and microscopic images were acquired using the Zeiss Axiovert 200 M inverted fluorescence microscope and AxioVision software.

2.4.11 Cytotoxicity of fatty acid solutions on oral keratinocyte monolayers

Monolayers of FNB6 cells were prepared in 96-well plates using 10^4 cells/mL (100 µL/well) and cultured in Green's medium at 37 °C, 5% CO₂ for 24 h. The monolayers were treated with nonanoic (C9:0) and dodecanoic (C12:0) acid with the highest concentration being at 0.1 M prepared in Green's medium and then 1:1 serial dilutions were performed across the plate. After 24 h incubation at 37 °C, 5% CO₂ the medium was removed, the cell monolayers were washed twice with PBS and 100 µL/well MTT solution (0.5 mg/mL) applied and incubated for 2 h at 37 °C, 5% CO₂. The MTT was removed and 50 µL/well acidified isopropanol was added, mixed to lyse the cells and the absorbance was read at 570 nm in a plate reader (Infinite 200 Pro, Tecan, Switzerland).

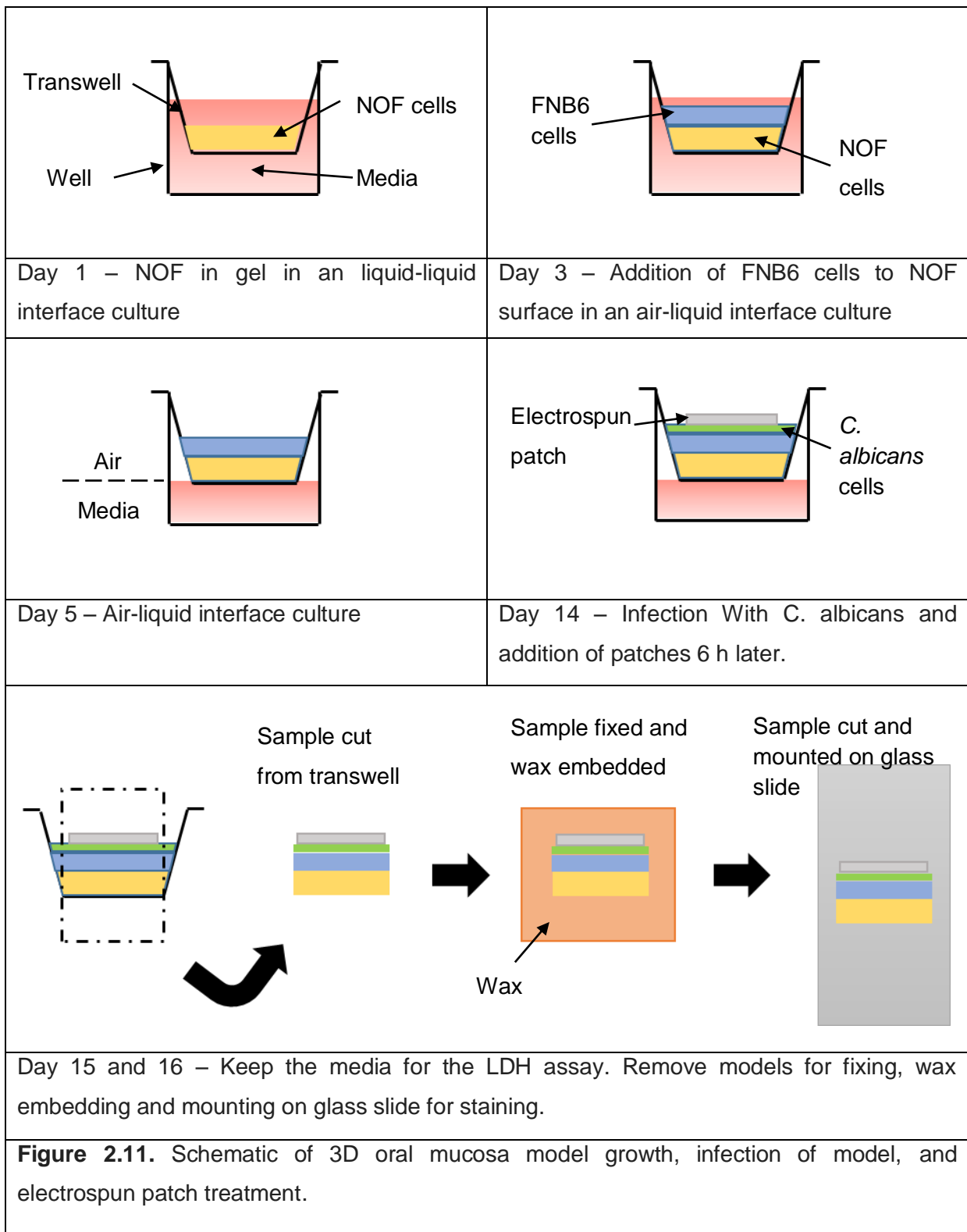
2.4.12 Tissue models of 3D oral mucosa

3D tissue engineered oral mucosal models using FNB6 keratinocytes were prepared as described previously [183], and a schematic of these tests is given in Figure 2.11. Rat tail collagen (5 mg/mL in 0.1 M acetic acid) was used as a connective tissue scaffold. Normal oral fibroblasts (NOF) were detached from tissue culture flasks using trypsin and resuspended at 1×10^6 cells/mL in Green's medium [175]. FBS, 10 × DMEM, L-Glutamine, and reconstitution buffer (2.2% sodium bicarbonate, 4.8% HEPES, 0.248% NaOH in dH₂O) were added to the collagen and the pH was adjusted to 7.4 with the addition of 1 M NaOH. NOF were added to the collagen mixture at a concentration of 2.5×10^5 cells/mL before adding 1 mL to each 12 mm cell culture transwell inserts (0.4 μm pore; Millipore) and allowed to solidify in a humidified atmosphere at 37 °C for 2 h. NOF-populated gels were submerged in Green's media and incubated for 2 d, after which 500 μL of 5×10^5 FNB6 oral keratinocytes per model were seeded onto the surface and further cultured for 2 d. Models were then cultured at an air-to-liquid interface for 14 d at 37 °C, 5% CO₂.

2.4.13 Infecting 3D tissue models with *C. albicans* and applying antifungal electrospun patches

Two days prior to using the mucosal models for infection experiments the culture medium was removed and replaced with fresh Green's medium without fungizone or penicillin/streptomycin. *C. albicans* (SC5314) were grown in YPD broth as described in section 2.4.7, centrifuged, washed twice with 25 mL PBS and resuspended in PBS at 5×10^7 CFU/mL. The Green's medium underneath the transwell inserts was removed and replaced with fresh medium (without fungizone or penicillin/streptomycin) and either 100 μL of SC5314 *C. albicans* (5×10^6 CFU/mL per model) or PBS control was applied to the surface of the model. Models were incubated for 6 h at 37 °C, 5% CO₂. Then 10 mM discs containing the following molecules were applied to the surface of the keratinocytes: placebo PVP/RS100

patch, PVP/RS100 patch containing nonanoic acid, PVP/RS100 patch containing dodecanoic acid, no patch control. Models were further incubated at 37 °C for 18 h.



2.4.14 Lactate dehydrogenase assay

The medium from under the 3D models was pipetted into an Eppendorf tube and centrifuged at 12,000 *g* for 3 min to pellet the cell debris. The supernatant was pipetted into a fresh Eppendorf and 50 μ L then transferred to each well of a 96-well plate for the LDH assay; the remainder was frozen down at -20 °C for later use. Cytotox 96® Reagent was prepared as described in the product assay protocol, then 50 μ L of the reagent was added to the cell culture conditioned medium and the plate incubated at room temperature for 30 min in the dark. 50 μ L stop solution was added and the OD measured using a spectrophotometer at 492 nm.

2.4.15 Histological processing of oral mucosal models

Oral mucosal models were washed twice in PBS and fixed in 10% PBS-buffered formalin, where 2 mL of the fixative was placed underneath the inserts and 500 μ L on top of the epithelial surface. The samples were left to fix for at least 5 h at 4 °C. After fixing, the insert along with the 3D model were removed and sandwiched in a processing cartridge before being placed in the wax embedding processor. The Leica TP tissue processor takes the tissue samples through several different graded alcohol baths over several hours and the sample becomes infiltrated with paraffin wax. The following day the models were bisected and the tissue halves placed upright in metal containers, hot paraffin wax was added and cooled making sure that the samples stay in an upright position. The wax was left to solidify, then removed from the metal container. Wax-embedded mucosal were sectioned (5 μ m) using a Leica microtome, floated on 40 °C water, mounted on high-adhesive microscope slides and then dried in an oven at 50 °C for 15 min.

2.4.16 Periodic-acid Schiff staining

Microscope slides were loaded into a Shandon Automated Linear Stainer (ThermoFisher, US), where slides were automatically taken through 3 × xylene, decreasing alcohol gradients (2 × 100%, 1 × 70%) then to water. The slides were kept in each bath for 15 s before moving onto the next one. The slides were removed from the stainer and flooded with 1% periodic acid for 10 min and then washed with distilled water. Next the sections were stained with Schiff's reagent for 15 min and again rinsed with distilled water. Following this the samples were counterstained in the automated stainer with Mayer's haematoxylin followed by 1 × Scott's tap water, 1 × 95% alcohol, 4 × absolute alcohol, 1 × absolute alcohol/xylene (50/50) and finally 2 × xylene. The slides were removed from the automated stainer, dried and mounted using DPX mountant, adding a coverslip in the process. Once dried images of the tissue samples were taken using a light microscope (Leica microscope Olympus, UK).

3. Results and Discussion: Characterising electrospinning solutions and resulting electrospun patches

3.1 Introduction

Choosing the material for a drug delivery device was critical, as a bioinert and non-toxic material was desired, which could adhere to the oral mucosa for several hours without eliciting an undesired inflammatory response from the tissue. Polymers dissolved in solvent were used to manufacture the delivery device, as they can be electrospun into a fibrous, flexible, drug-containing patch with mucoadhesive properties. For this study, PCL and PVP were chosen as the main electrospinning polymers on the basis that they are considered safe and are already used as medical materials in industry. Hence, they are highly likely to be FDA approved, which was also an important consideration in reducing the time needed to take the patches to clinic. Additionally, dextran and PEO particles were added to the PVP polymer solution and electrospun, as previous research in the group had shown increased mucoadhesion of the electrospun patches with these inclusions [1,178]. To gain a better understanding of some material parameters that influenced the final morphology of the electrospun patches, the polymer solutions were characterised and SEM images of the patches were analysed.

3.2 Rheology of polymer solutions

Electrospinning conditions, such as the voltage and flow rate, were adjusted depending on the solution that was electrospun. These necessary adjustments were related to the polymer solution properties, which may also affect the resulting morphology and fibre diameter of the electrospun fibres. Here, PCL at different concentrations in DCM/DMF and PVP in ethanol at different concentrations with a range of additives were tested using a shear viscosity test. The viscosity results in Figure 3.1 show that the polymer solutions are Newtonian fluids as the viscosity remains the same despite the change in external force acting on the fluid (n=3). For clarity, only the maximum and minimum concentrations of the different polymer solutions

are shown, however the polymers behaved as Newtonian fluids at all concentrations tested (Figure 3.1). With the addition of dextran particles, the polymer solutions still show Newtonian behaviour (Figure 3.2). However, the addition of PEO particles results in a higher viscosity at lower shear rates and a reduction in viscosity with increased shear stress (Figure 3.2). This is attributed to the PEO particles not dissolving in ethanol and hence as the shear stresses act on the solution both mixing of the particles into the solution and potential breaking of the particles may be occurring.

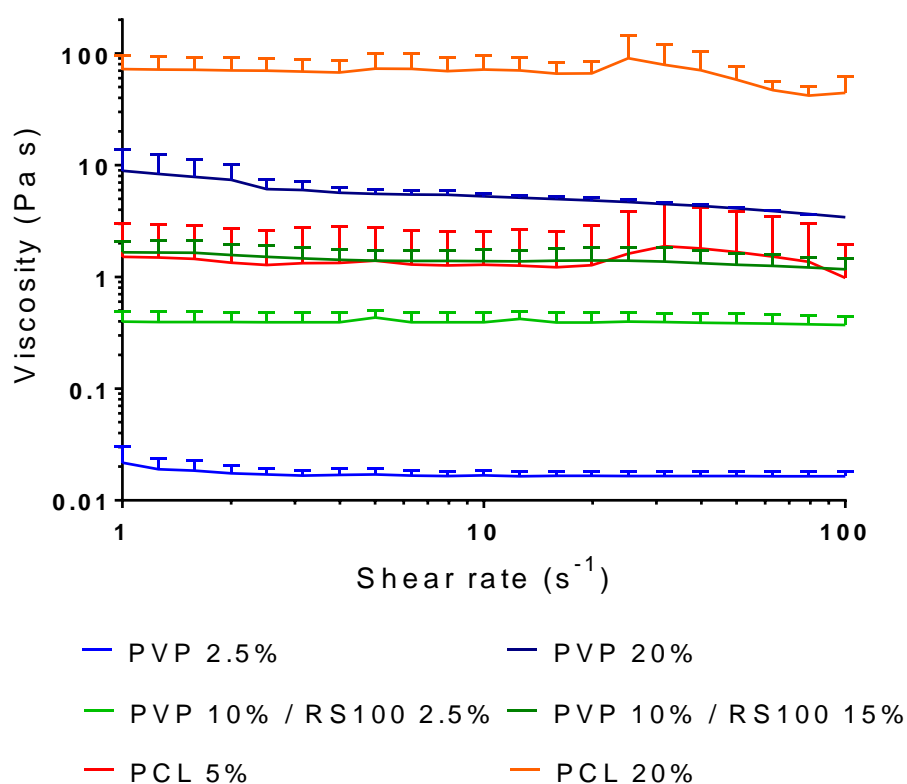


Figure 3.1. Viscosity of polymer solutions at different concentrations in solvent. PVP (blue) and PVP / RS100 (green) are dissolved in 97% (w/w) ethanol and PCL in DCM/DMF (93/7% w/w) (red and orange) (mean +/- SD, n=3).

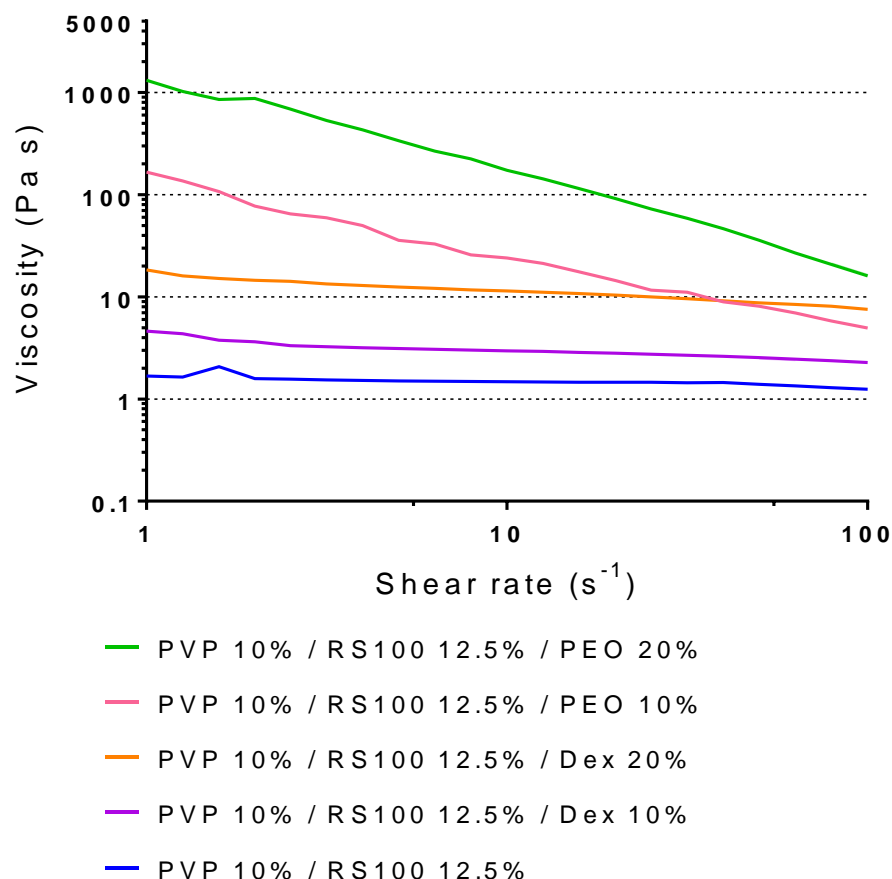


Figure 3.2. Viscosity of PVP 10% and RS100 12.5% with additives at different concentrations in 97% ethanol (mean +/- SD, n=3). Adapted from Santocildes-Romero *et al.* [178].

The shear rate of the solution being pushed from the electrospinning needle was estimated to be 40 s^{-1} , using Eq. 5 given in section 2.2.2. Hence the viscosity at a shear rate of 40 s^{-1} for the polymer solutions was selected to compare the PCL dope and PVP dope solutions chosen for electrospinning (Figure 3.3). It was shown that PCL at the same concentration in DCM/DMF compared to PVP in 97% (w/w) ethanol has a viscosity approximately 10-fold greater (Figure 3.4). Both the PCL and PVP solutions followed an exponential trend in increasing viscosity as the polymer concentration in solution was increased, with $R^2 = 0.96$ and $R^2 = 0.98$, respectively. As PVP is a hydrophilic polymer another polymer was added to

the electrospinning dope to make the electrospun patch more hydrophobic so that it does not dissolve too rapidly in the oral cavity once used as a drug delivery device. This polymer was Eudragit RS100, a copolymer of ethyl acrylate and a methacrylic acid ester, although this polymer also has quaternised amine side groups meaning it also has some hydrophilic properties. The addition of RS100 to 10% (w/w) PVP in the polymer dope solution did not greatly change the viscosity even as the concentration of RS100 was increased, which was also reflected by $R^2 = 0.52$. However, as there were two polymers in this mixture, and the PVP concentration was kept at 10% (w/w), the solution was not expected to follow the same exponential trend as the PCL and PVP solutions on their own. The polymer solution viscosity is only one of the material properties that can influence the resulting electrospun polymer fibres and hence further material characteristics were measured in the following sections.

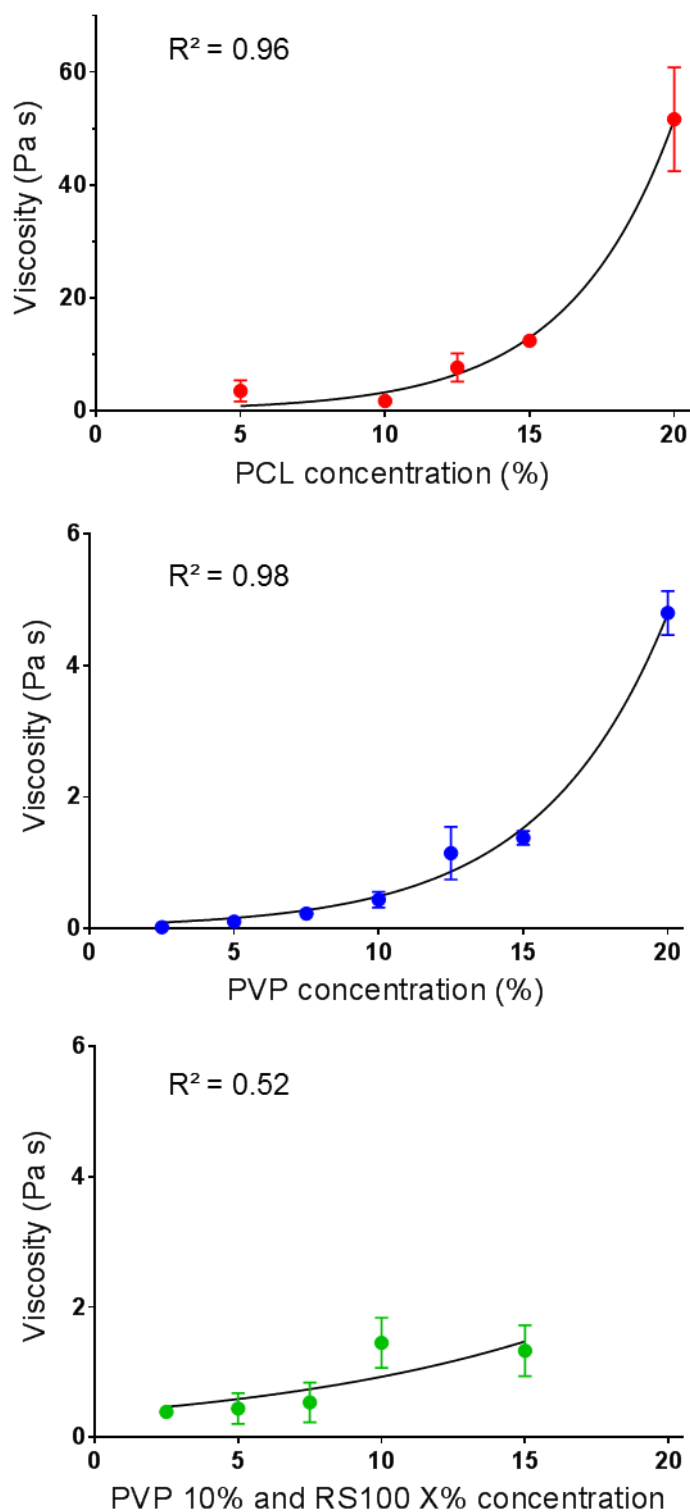


Figure 3.3. Viscosity of PCL in DCM/DMF (93% / 7%) (red), PVP (blue) and PVP 10%/ with RS100 (green) in 97% ethanol at different concentrations of polymer as recorded at a shear rate of 40 s^{-1} (mean \pm SD, $n=3$). The exponential growth was calculated using non-linear regression in GraphPad Prism. Adapted from Santocildes-Romero *et al.* [178].

3.3 Conductivity of polymer solutions

Electrospinning is performed in a controlled electrical field and the polymer solution is drawn by the electrical forces into a fibre. Therefore, the conductivity of the polymer solution will influence how well the solutions are drawn into a fibre. The results for the conductivity of PVP at different concentrations in ethanol and of PCL at different concentrations in DCM/DMF are shown in Figure 3.4. Here it is shown that the PVP solutions have a far higher conductivity than the PCL solutions and that this is not related to the solvent conductivity. One-way ANOVA reported statistically significant differences between the polymer solution and the respective solvent ($p < 0.0001$), apart from PCL 5% compared to DCM/DMF ($p = 0.0008$). There was no significant difference between the conductivities of ethanol and DCM/DMF. The addition of RS100 to the PVP dope resulted in a large increase in solution conductivity and the further addition of PEO or dextran particles reduced the conductive effect of RS100 (Figure 3.5). In Figure 3.5 almost all solution conductivities were significantly different to each other ($p < 0.0001$) using one-way ANOVA, apart from PVP 10% RS100 10% to PVP 10% RS100 10% with either the addition of dextran 10% or PEO 10%. Solutions including either dextran 20% or PEO 20% were also not significantly different to each other.

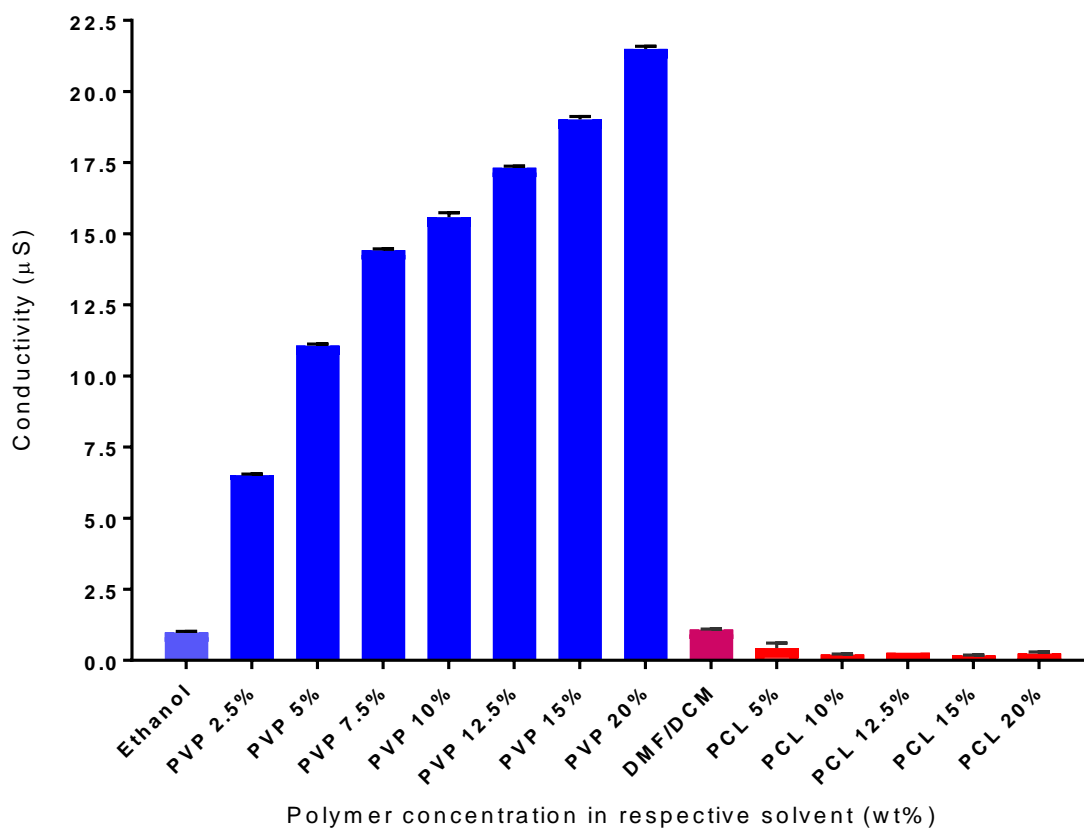


Figure 3.4. Conductivity of PVP in 97% ethanol (blue) and PCL in DCM/DMF (93% / 7%) (red) at different polymer concentrations (mean \pm SD, $n=3$). Adapted from Santocildes-Romero *et al.* [178].

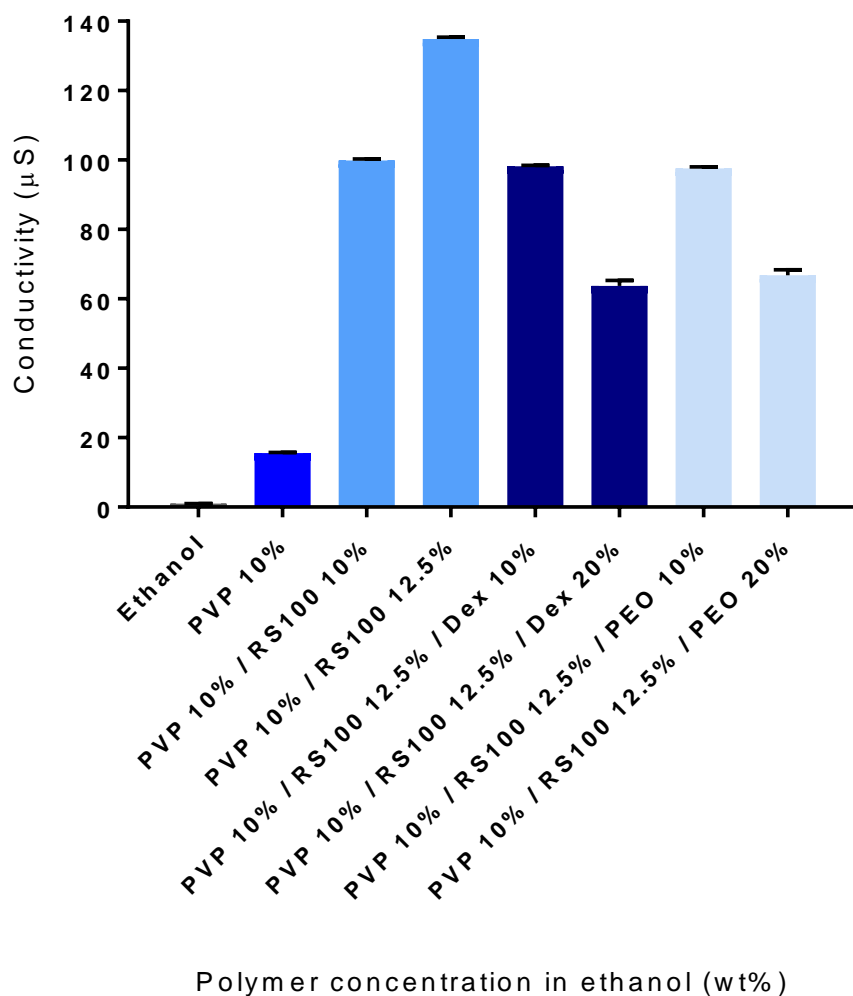


Figure 3.5. Conductivity of polymers in 97% ethanol (mean +/- SD, n=3). Adapted from Santocildes-Romero *et al.* [178].

3.4 Surface tension of electrospinning polymer solutions

The formation of the Taylor cone in electrospinning is described as the shape formed when a polymer solution in an electric field is drawn into a cone which is dependent on the surface tension of the solution. Geoffrey Taylor, who first discovered this phenomenon whilst researching electrospaying, developed an equation (Eq. 2 in section 1.4.2) for the critical voltage required to achieve this coning and subsequent electrospaying [88]. The surface tensions of PVP in ethanol at different concentrations and with the addition of RS100 were all relatively similar to each other, although there were some statistically significant differences

between some of the polymer solutions compared to ethanol on its own and especially with the addition of PEO or dextran particles, as shown in Figure 3.6 using one-way ANOVA (**** $p < 0.0001$). In contrast, the PCL solutions had slightly higher surface tensions than the PVP solutions, where the surface tension for the solvent systems were 22.07 ± 0.01 for 97% ethanol and 28.60 ± 0.02 for DCM/DMF (93% / 7%) (mean \pm SD; $N=1$; $n=6$), which are significantly different to each other ($p < 0.0001$). For the PCL solutions, there was a significant difference between the solvent on its own and the PCL/solvent mixtures at 15% and 20% concentration ($p < 0.0001$, one-way ANOVA). Significant differences between polymer solutions at different concentrations are not shown, although PVP 5% and PVP 10% were significantly different to the same PVP polymer solutions as ethanol, but to a lesser extent ($p < 0.01$). Similarly, PCL 5% and PCL 10% were significantly different to PCL 15% and PCL 20%. The critical voltages were determined using Eq. 2 (chapter 1.4.2), where for the PVP solutions, with and without other polymer additives, the critical voltages ranged from 9.7 kV to 10.3 kV and for the PCL solutions the critical voltages ranged from 11.0 to 11.7 kV. It is noted that higher voltages between 17 kV and 19 kV were used for the electrospinning conducted in this thesis as electrospun fibres and not electrospayed beads were desired.

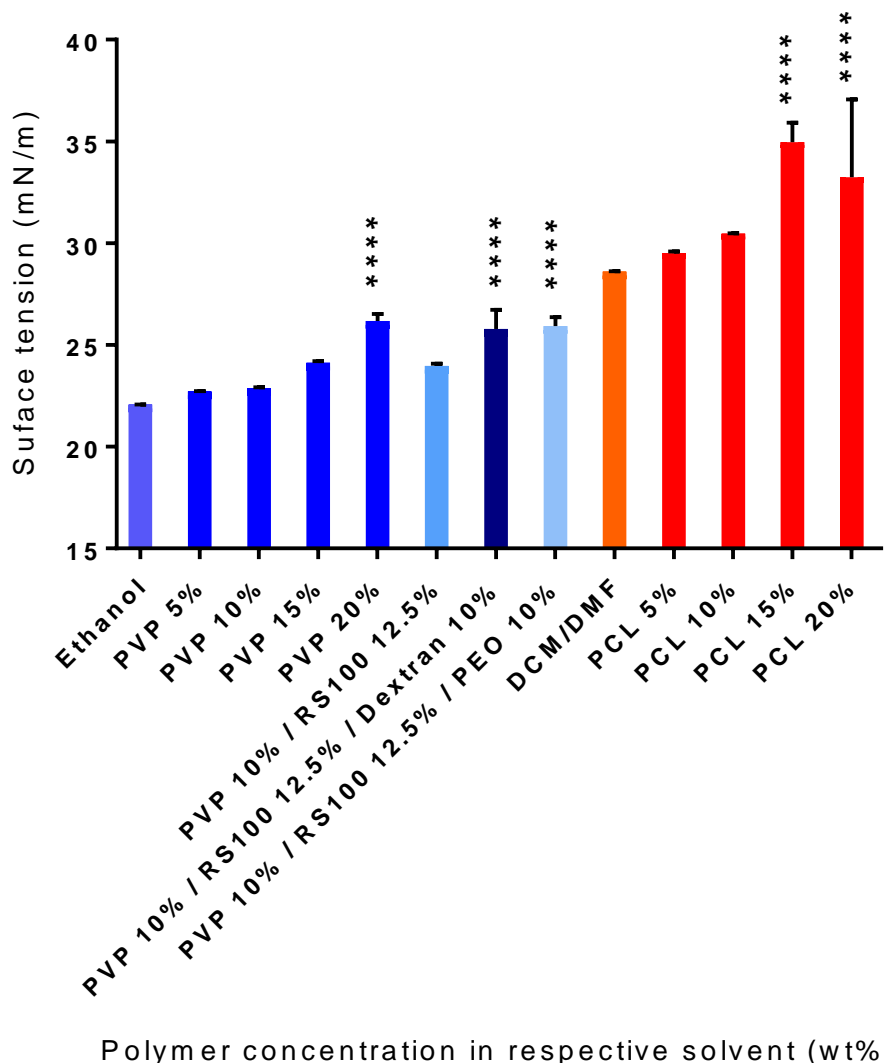


Figure 3.6. Surface tensions of PVP solutions with RS100 and PEO or dextran at different concentrations in 97% ethanol (blue) and the surface tensions of PCL solutions at different concentrations in DCM/DMF (93% / 7%) (red) are shown. (Mean +/- SD, n=5 technical repeats). Significance above SD bar is compared to the respective solvent system (**** p < 0.0001). Significant difference between ethanol and DCM/DMF was ****. Significance between polymer solutions at different concentrations are not shown.

3.5 Morphology and fibre diameters of electrospun mats

Fibres with smaller diameters have a greater surface area to volume ratio and therefore should increase the rate of drug release. However, trying to reduce the fibre diameter, either by changing the equipment parameters or reducing the polymer concentration in the solution, can cause instabilities in the electrospinning processes and result in fibre inconsistencies. Such inconsistencies could include beading along the fibre or the collection of electrospayed beads rather than fibre formation occurring [72,184]. In this project a consistent fibre diameter was desired, as a drug delivery product was being developed and large variation in the fibre morphologies may influence several material and drug release properties of the electrospun patch.

The morphology of the electrospun patches of PVP and PCL prepared at different concentrations are shown in representative SEM images in Figure 3.7 and Figure 3.8, respectively. The fibre diameters in these images were measured by image analysis and are shown in Figure 3.9, where the mean diameter for PVP fibres was less than for the PCL fibres at the same concentration. Additionally, PVP fibres have a smaller range of diameters at the same concentration of polymer compared to the PCL fibres. Beading along the polymer fibres occurred in PCL patches spun from dope containing 5% PCL, as shown in Figure 3.8.A. The fibre diameters of the 5% PCL patches were therefore not measured due to the beading effect and hence the absence of 5% PCL fibre diameter data in Figure 3.9. One difference that can be observed when comparing the PVP fibres and PCL fibres in the SEM images was that, although random fibre alignment was seen for both polymers, the PVP fibres look to be straighter (Figure 3.7) and less undulating than the PCL fibres (Figure 3.8), which may be related back to the polymer solution characteristics determined in previous sections of this chapter.

Representative SEM images of the electrospun fibres consisting of PVP with additions of RS100, RS100 and PEO, and RS100 and dextran are shown in Figure 3.10. Here, it is shown that the addition of RS100 does not greatly alter the morphology of the patch,

although the fibres flatten slightly. With the inclusion of dextran or PEO particles, occasional particle shapes were detected in the electrospun patch, which may be undissolved dextran or PEO particles, as they are not soluble in 97% ethanol, as was observed during the mixing of the polymer solution. From images at higher magnification, it is shown that the particles in the PVP/RS100/PEO patches have a diameter of up to 15 μm . It was noted that in the patches containing dextran very few particle shapes were observed, however particle shapes were more frequently detected for patches containing PEO.

PCL electrospun patches were melted on top of a PVP/RS100/PEO patch to manufacture a dual-layer patch, with representative SEM images thereof shown in Figure 3.11. This was to create a barrier for any drug contained within the PVP layer to not simply be washed away into the oral cavity. This should also improve drug release into the target tissue. The thermal treatment of the patches at 70 °C caused the PCL fibres to melt into each other and develop a relatively smooth surface, whereas no change to the PVP fibre layer was observed. The PCL layer will from here on be referred to as the 'backing layer'. This concludes the characterisation of the developed electrospun patches, where the influence of the polymer solution characteristics on the patch morphologies will be discussed in the next section.

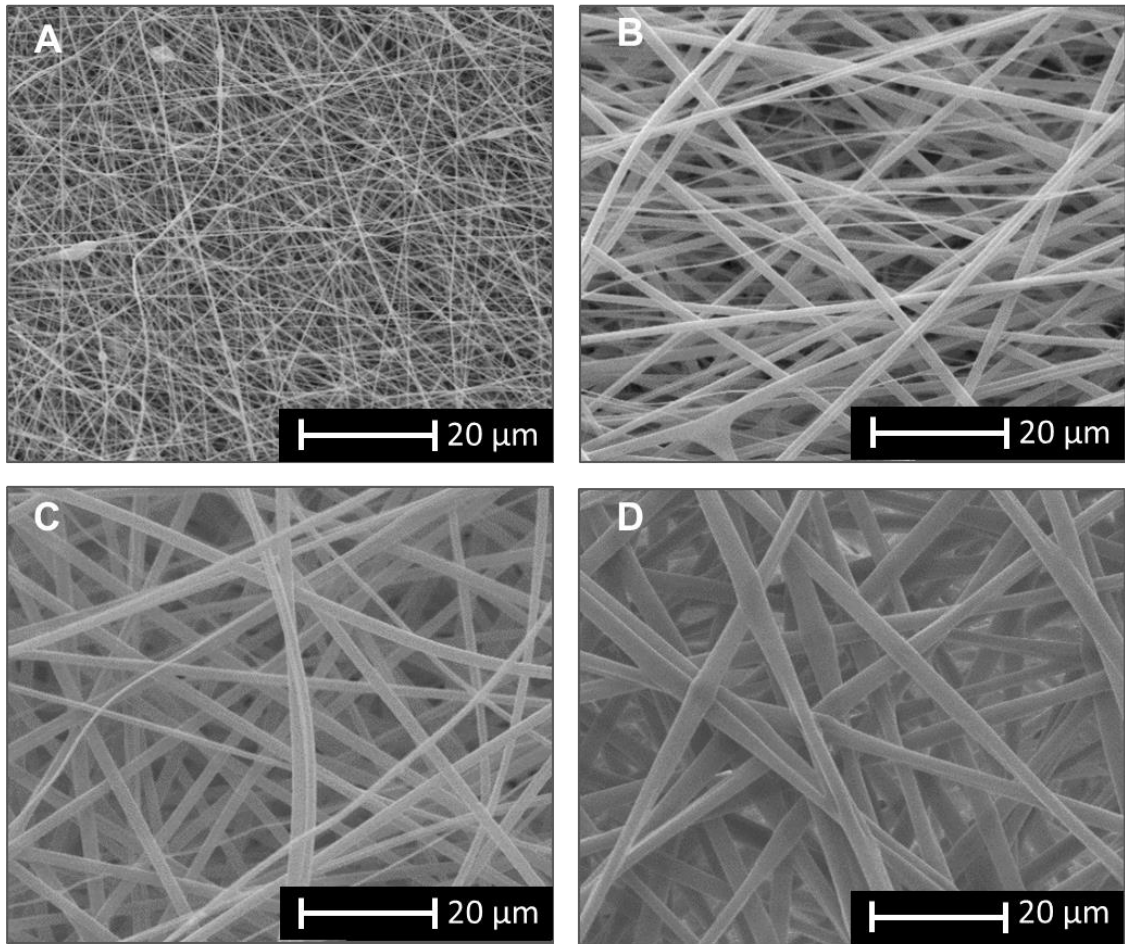


Figure 3.7. SEM images of PVP fibres at A) 5% concentration, B) 10% concentration, C) 15% concentration and D) 20% concentration of polymer. Adapted from Santocildes-Romero *et al.* [178].

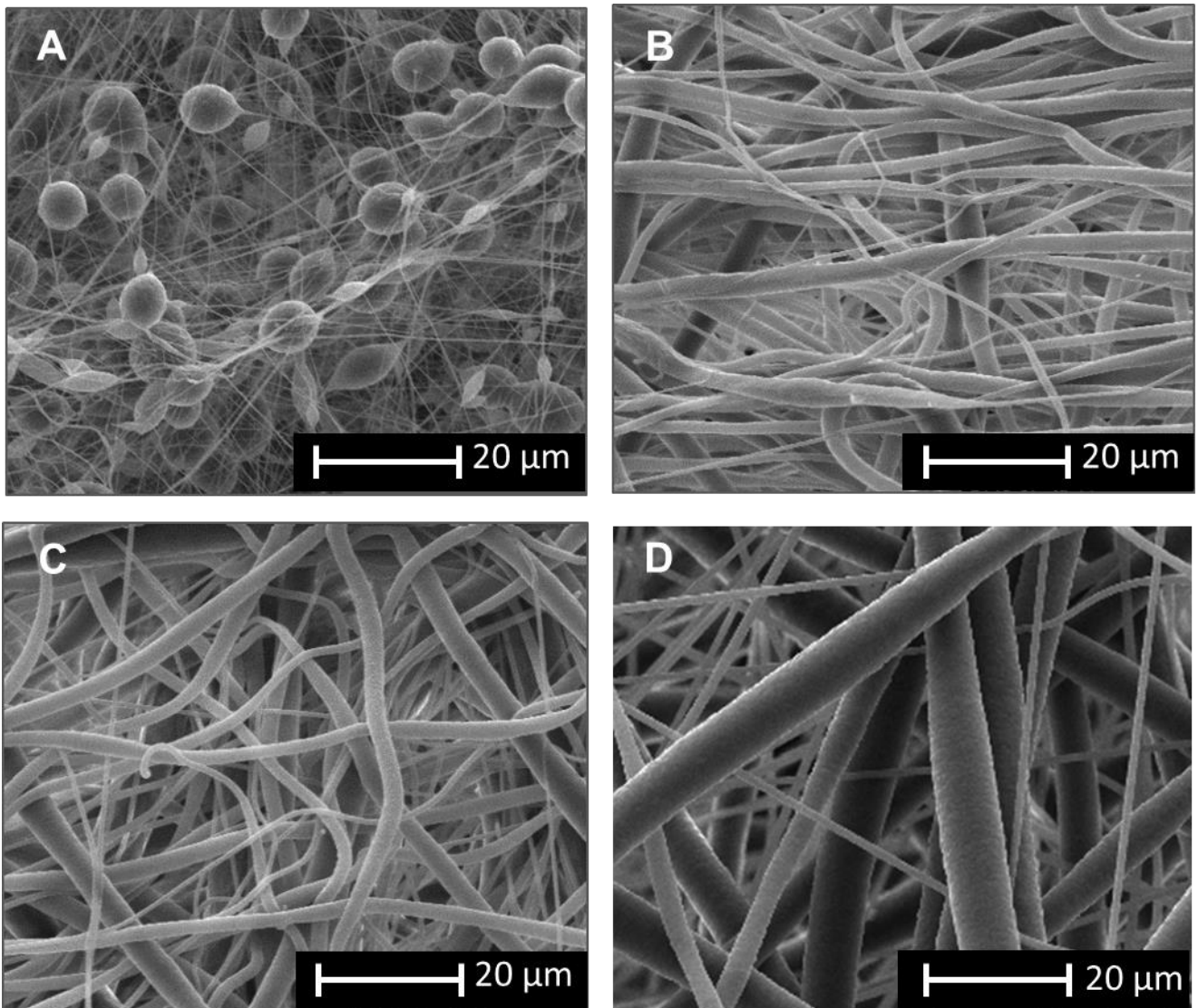


Figure 3.8. SEM images of PCL fibres at A) 5% concentration, B) 10% concentration, C) 15% concentration and D) 20% concentration of polymer.

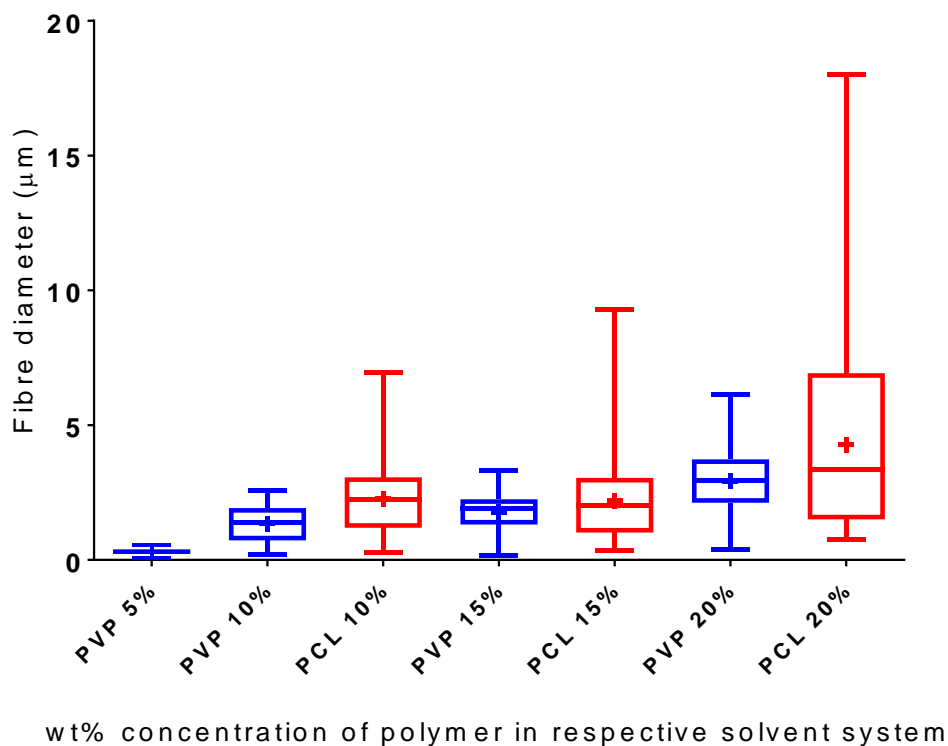


Figure 3.9. Fibre diameters derived from SEM images of PVP at concentrations ranging from 5% to 20% and PCL at concentrations 10% to 20% ($n = 8$ images and > 400 fibres measured per condition). Box and whisker plots show minimum, maximum, 25th percentile, median and 75th percentile. Mean is shown by + sign. Adapted from Santocildes-Romero *et al.* [178].

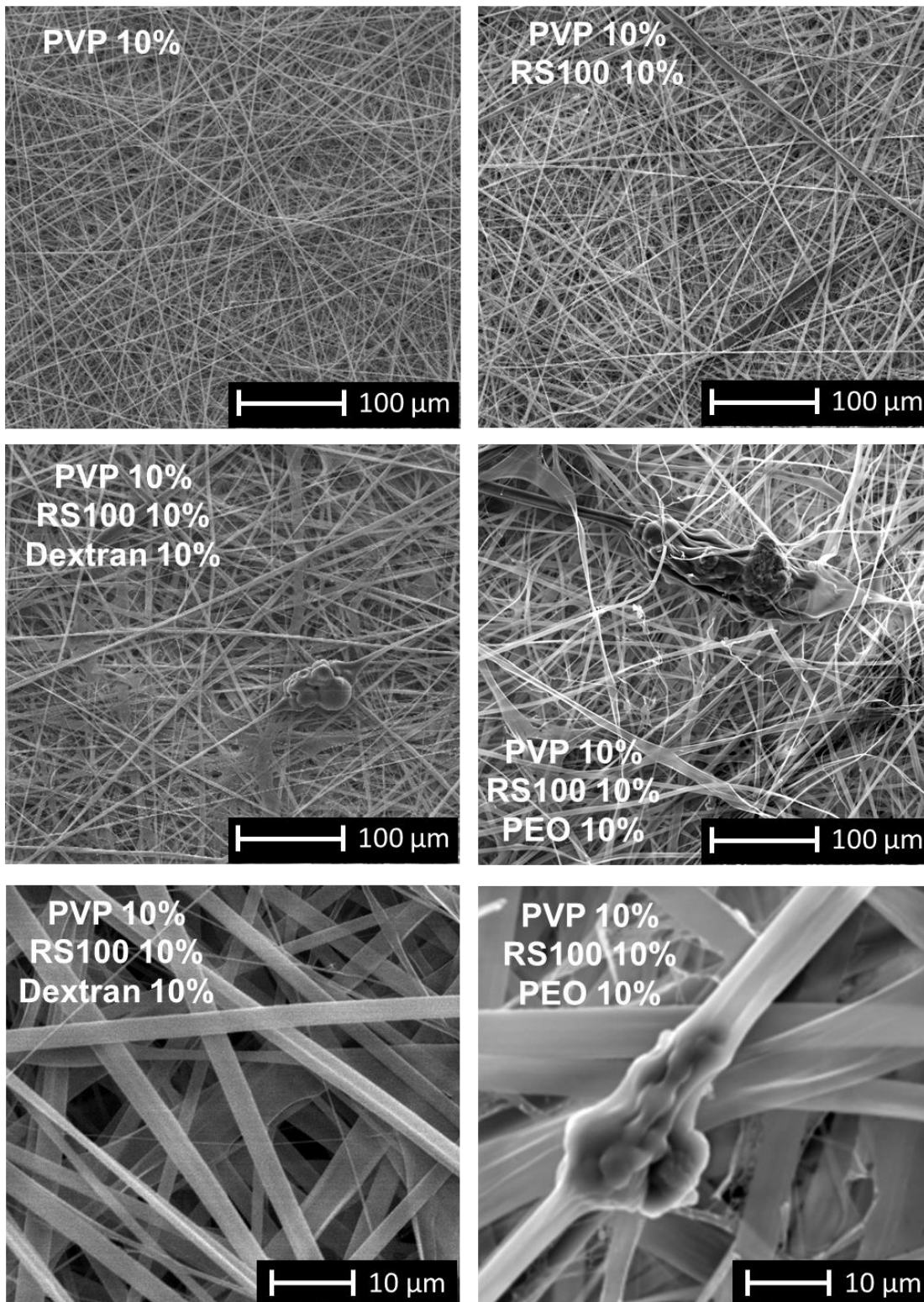


Figure 3.10. SEM images of PVP patches containing RS100, RS100 and dextran and RS100 and PEO, as the description at the top right of the individual images indicates.

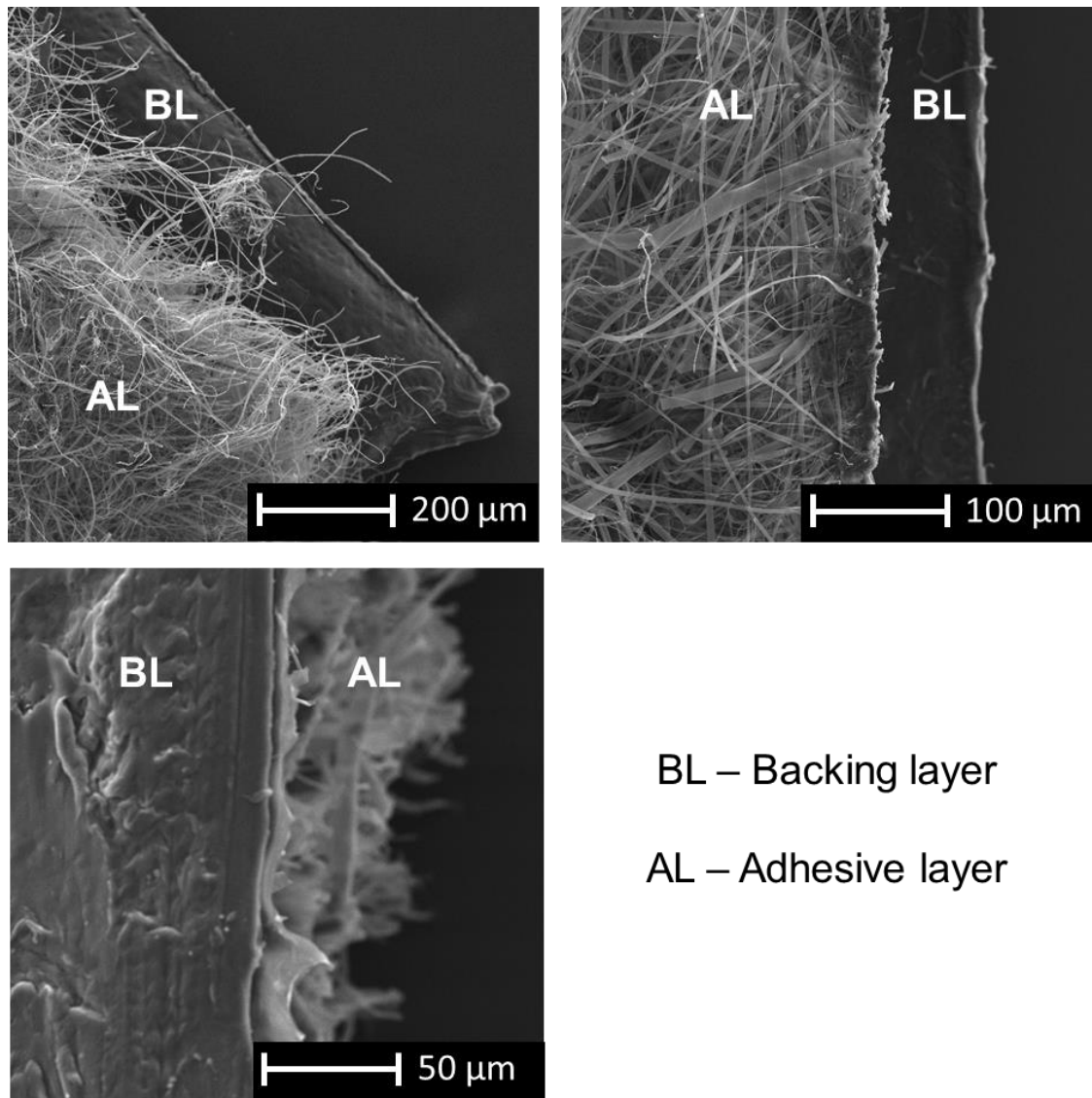


Figure 3.11. SEM images of dual-layer electrospun patches. Patches consist of a backing layer (BL), made up of melted PCL fibres and an adhesive layer (AL) made up of PVP, RS100 and PEO fibres and particles.

3.6 Discussion

This chapter reviews the chosen polymer-solvent systems for electrospinning by analysing the polymer solution properties and the resulting electrospun fibre patches. The polymer mixtures that were used were PCL in DCM/DMF and PVP with RS100 and either PEO or dextran in ethanol. Polymer solution characteristics which are likely to influence the resulting fibre morphology most are the viscosity, conductivity and surface tension of the solutions, as highlighted in chapter 1.4 in the literature review.

As the polymer concentration was increased, the largest material change observed was in the solution viscosity. The viscosity of the electrospinning solutions with one polymer in a solvent mixture was found to increase exponentially as the polymer concentration increased. The difference in viscosity between the PVP and PCL solutions was 10-fold for the same concentration of polymer in solvent. A previous study showed how the solution viscosity of 10.5% (w/w) PCL in DCM/DMF was dependent on the ratio of DCM to DMF, where the standard deviation for 10% (w/w) PCL in this chapter with DCM/DMF (93/7% w/w) was however far larger and within the range of viscosities for all the ratios of DCM/DMF used by Zamani *et al.* [93]. The larger standard deviation in this experiment could relate to greater solvent evaporation having occurred during the experiment and thereby changing the DCM/DMF ratio. Two other studies using PCL dissolved at similar ratios in DCM/DMF reported viscosities around 10 times lower, even though the polymers were purchased from the same manufacturer and had similar molecular weights [90,95]. However, their mean fibre diameters were also significantly smaller, while similar conductivities and surface tensions were reported [90,95]. There were some fundamental differences, where in one study the viscosity was measured at 20 °C rather than the 25 °C in this work, and in the electrospinning set up higher voltages and a mandrel were used. Only one other comparable study of PCL dissolved in a mixture of DCM/DMF was found, in which the intrinsic viscosity of PCL was measured [185], although given the popularity of PCL as an electrospinning polymer in a variety of different solvents [186] other relevant literature may have been

overlooked. PVP in ethanol solutions have been used in a number of studies to manufacture electrospun fibres for drug delivery [97,99–101,103,154,187–189], however, the majority of these papers have not reviewed the viscosities of the solution. Viscosity measurements were recorded in two of these publications (both of which used PVP with a similar weight-average molecular mass): one recorded the viscosities for a range of PVP concentrations in 100% ethanol and also showed an exponential increase [154], where the measurements agreed with the results in this study; the other study measured the viscosity for 8% PVP in an ethanol/water (70/30% v/v) mixture with a viscosity of 0.22 Pa·s [101], where an 8% PVP in 97% (w/w) ethanol solution, as read from Figure 3.3, would have a similar mean viscosity of 0.3 Pa·s. Rasekh *et al.* [154] also reported similar conductivities and surface tensions for their PVP in neat ethanol. Here, the PVP and PCL solution characteristics were compared to results found in literature, next the trends for the polymer solution characteristics with an increase of polymer concentration will be compared to each other and how they may have affected the resulting fibre morphologies.

As the PVP solution concentrations increased from 5% to 20% the viscosity, conductivity and surface tension of the solution increased and the resulting mean fibre diameters, as well as the range of fibre diameters, also increased. Between the 10% and 20% concentrations of PVP the viscosity increased 12-fold from 0.4 Pa·s to 4.8 Pa·s, the conductivity increased 1.4-fold from 15.6 μS to 21.5 μS , the surface tension increased 1.14-fold from 22.9 mN/m to 26.2 mN/m, and the mean fibre diameter increased from 1.3 μm to 2.9 μm . These results, including the size and range of fibre diameters, are relatable to another study where PVP solutions in ethanol were characterised [154]. In comparison to the PVP fibres, the mean fibre diameter for 10% PCL was 2.3 μm , which was similar for 15% PCL at 2.2 μm , but doubled for 20% PCL. As the concentration of PCL increased from 10%, to 15% to 20%, the viscosity increased from 1.7 Pa·s to 12 Pa·s to 52 Pa·s, the conductivity went from 0.21 μS to 0.18 μS to 0.24 μS , and the surface tension went from 30 mN/m to 35 mN/m to 33 mN/m. As the electrospinning set up, including the voltage, feed rate and needle-to-collector distance,

was kept the same for all polymer concentrations, the viscosity of the polymer solution seemed to have the greatest influence on the change in fibre diameter. However, the surface tension and conductivity of the solution influence how well the solution can be drawn into a fibre, as reflected by the 5% PCL versus 5% PVP solution. At a concentration of 5% of PCL a 'bead-on-string' morphology was observed, which has often been reported to occur for low polymer concentration solutions with low viscosities [59,60], although the viscosity of the 5% PVP solution was lower and no bead-on-string formations were observed. This indicates that the higher surface tension and lower conductivity of 5% PCL compared to 5% PVP added instabilities to the electrospinning process. Additionally, the surface tension and conductivity may affect the orientation of the fibres, as the PVP solution had a higher conductivity and lower surface tension than the PCL solutions, where the PVP fibres were straighter and had a less curved formation than the PCL fibres as observed in the SEM images. One publication theorised using a mathematical electrospinning model that the surface tension had the least effect on the electrospinning jet radius [190], although the forming of the initial jet is dependent on the surface tension and the applied voltage, where a low viscoelastic solution is more likely to form unstable jets if the solution has a high surface tension.

The morphology of the electrospun fibres is also dependent on the electrospinning conditions, such as the voltage, feed rate and plate-to-collector distance, as well as factors such as temperature and humidity. It is additionally noted that electrospinning rigs are currently not standardised and therefore some variation in results of similar experiments in literature are likely. The electrospinning rig in this thesis was put together in-house and the temperature and humidity were not controlled during electrospinning, where on a warm day the solutions were noticeably less viscous. Temperature and humidity not only influence the viscosity of the solution, but also the solvent evaporation during electrospinning, thereby affecting the resulting fibre morphology. One study using PVP in ethanol showed how an increase in temperature resulted in a less viscous solution, thereby manufacturing thinner fibres, although at a low temperature with a more viscous solution (10 °C) the ethanol

evaporation was reduced, thereby also producing thinner fibres [68]. An increase in humidity resulted in less well-defined 'fused' fibres as the PVP-ethanol system absorbed water during the electrospinning process [68]. Thus, the polymer took longer to solidify into a fibre whilst drawn to the collector plate, resulting in some thinner fibres, although this trend was different for another polymer in a non-water soluble solvent, where precipitation was observed [68,191]. A change in temperature and humidity may therefore affect the PCL solution differently to the PVP solution. PCL made up in chloroform/THF in an earlier publication did not change the diameter of the fibres as the humidity and temperature was increased, but pores were observed along the surface of the fibres [192]. Therefore, it is important to be aware of such possible changes to the electrospun patches in an uncontrolled manufacturing environment such as in this project. The voltage, feed rate and plate-to-collector distance in this thesis were chosen with a view to previously reported values, reviewing by eye whether a stable jet was formed and looking at the SEM images to determine what set up worked well on the electrospinning rig at the University of Sheffield, School of Clinical Dentistry. The effects of modifying the process parameters as reported in literature were reviewed in chapter 1.4.1.

RS100 was added to the PVP electrospun patches to increase the hydrophobicity of the patches, as otherwise the PVP patch dissolve into a gel-like structure within a few seconds of water application. Dextran and PEO particles were added and successfully electrospun into the patches as they have previously been shown to markedly increase the adhesion residence time of the PVP/RS100 patches on both tissue culture plastic and *ex vivo* porcine tissue [178]. Data on the adherence residence time on human volunteers using placebo patches consisting of PVP/RS100/PEO at 10/12.5/20% (w/w) were also recently published, where the patches adhered to the buccal mucosa from 50 min up to the maximum time the study was run at 120 min [1]. This study especially shows the potential of these electrospun patches as an adherent oral mucosal wound dressing, as well as a potential oromucosal drug delivery vehicle.

The hydrophobic PCL backing layer was added to the surface of the PVP electrospun patch, which would consist of the drug containing fibres. The melted backing layer formed a relatively smooth, non-porous layer on the PVP electrospun fibres, where the two layers adhered to each other. However, the dual-patch needed to be handled carefully to avoid separation of the two layers. This backing layer should aid uni-directional release into the tissue, which is considered important to avoid the drug being washed into the oral cavity and away from the target diseased tissue.

As active pharmaceutical ingredients are incorporated into the electrospun fibres, the morphologies of the fibres may change, which may be related back to changes in the polymer solution properties reviewed in this chapter. Morphological changes, such as increased porosity or flattening of fibres, have previously been reported with the inclusion of therapeutic molecules into the fibres [91,92,99]. The next step in this project will be to incorporate a drug molecule into the electrospun patch relevant to oromucosal tissue treatment. Therefore, in the next chapter a lidocaine containing electrospun patch was analysed to test the effectiveness of the electrospun patch as a drug delivery vehicle.

4. Results & Discussion: Delivery of lidocaine from electrospun patches

4.1 Introduction

Oral pain may greatly affect a person's quality of life as it can influence basic day to day activities such as drinking, eating and speech [193]. Controlling oral pain, especially chronic pain, is challenging and are either treated via in injection of lidocaine to the oral mucosa or using benzydamine HCl or lidocaine mouthwashes. However, anaesthetic injections are not feasible over prolonged periods of time and furthermore many patients fear needle injections, which can cause dental anxiety and have further dental health repercussions [16]. Local anaesthetic gels and mouthwashes are available and are relatively successful for short term treatments [194,195], however the local drug retention could be improved upon. Additionally, an electrospun patch system may act as wound dressing covering painful oral lesions.

The aim of this chapter was to show the potential of the electrospun patch developed in chapter three as a drug delivery device, by loading the patches with a drug and determining drug release and uptake into tissue. Specifically, in this chapter lidocaine was incorporated into the electrospun patches, the concentration of lidocaine in the patches was determined and the release of lidocaine from the patches into buffer and the permeation of lidocaine through *ex vivo* oral mucosal buccal tissue was established. To conclude this chapter, mass spectrometry imaging was used to visualise the time-dependent permeation of lidocaine through buccal tissue. This work demonstrates the potential of an anaesthetic loaded electrospun patch to improve the control of localised oral pain, where uncontrolled oral pain is a major unmet clinical problem.

4.2 Incorporating lidocaine into electrospun patches

Lidocaine HCl and lidocaine base were electrospun into the fibrous polymer patches. SEM images of the resulting patches were taken, representatives of which are shown in Figure 4.1. The morphology of the PVP/RS100/PEO electrospun patches remained very similar with

the incorporation of lidocaine, where a range of fibre diameters can be observed. The fibre diameters for PVP/RS100/PEO only patches were $2.28 \pm 1.35 \mu\text{m}$, the lidocaine HCl loaded fibres were $1.98 \pm 1.50 \mu\text{m}$ and the lidocaine base loaded fibres were $2.42 \pm 2.09 \mu\text{m}$ (~100 fibres in total measured from $n=3$ patches per condition; mean \pm SD). Occasional particle like structures may be observed as in Figure 4.1.A, which may be the PEO particles as discussed in chapter 3.

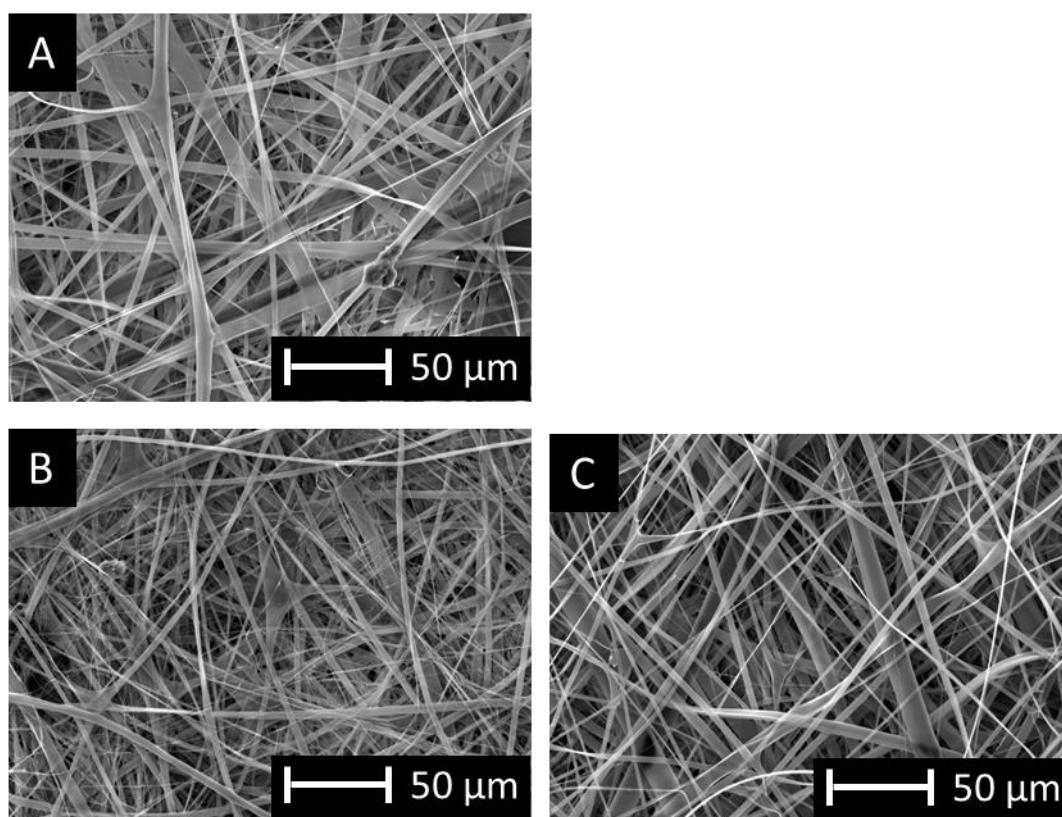


Figure 4.1. SEM images of electrospun patches made up of 10% PVP, 12.5% RS100 and 10% PEO incorporating A) no addition, B) lidocaine HCl and C) lidocaine base.

Lidocaine was added at 3% (w/w) to the polymer dope prior to electrospinning, however, low molecular weight compounds that are to be incorporated within the polymer fibres may be lost during the electrospinning process [91,93]. Therefore, the amount of lidocaine

encapsulated in an electrospun patch was determined using an HPLC method. A robust HPLC method was first developed, as presented in section 2.3.7. The concentration of lidocaine in the electrospun patches is shown in Table 4.1. Batch variation was taken into consideration and three samples from three separately spun patches were tested. Here, it can be observed that for batch 3 of the lidocaine HCl patches less lidocaine was detected within the patch. For the three batches tested, greater batch consistency was observed for the lidocaine base patches. It is noted that, for later experiments, the exact content of lidocaine within the patches is unknown due to batch inconsistency and therefore percentage release or percentage permeation cannot accurately be determined.

Table 4.1. Concentration of lidocaine in electrospun patches.					
		Batch no. 1	Batch no. 2	Batch no. 3	Mean \pm SD from three batches
Patches containing lidocaine HCl	Patch weight (mg)	5.0	6.0	7.7	6.2 \pm 1.2
	Drug loading (wt%)	2.5	2.9	1.7	2.4 \pm 0.5
Patches containing lidocaine base	Patch weight (mg)	5.0	10.7	12.3	9.3 \pm 3.3
	Drug loading (wt%)	2.2	2.5	2.7	2.5 \pm 0.2

It is desirable for the drug to be kept in a high-energy amorphous form within the fibres to improve drug solubility and thereby bioavailability [196]. To determine whether or not the drug is amorphous in the electrospun fibres, DSC analysis was performed. The onset melting temperatures and enthalpy peaks of lidocaine HCl or lidocaine base in their, as purchased, powder form were not present once incorporated in the electrospun patches, as shown in Figure 4.2. An onset melting temperature of PEO at 59 °C was observed for the plain polymer electrospun patch (thermogram D), which was similar in the drug containing electrospun patches. For the electrospun fibres alone or containing lidocaine HCl (thermograms D and E) a less pronounced, but wider endothermic peak can also be observed between 80 °C and 135 °C, which is consistent with a previously published DSC thermogram of PVP K90 particles and an electrospun PVP K90 patch [197]. The lack of sharp endothermic peaks for the lidocaine complexes in the electrospun patch samples, or any significant change to the endothermic peak resulting from the polymer component of the patch (between 59 °C and 75 °C for samples D-F in Figure 4.2), concludes that lidocaine is amorphous within the polymer fibres.

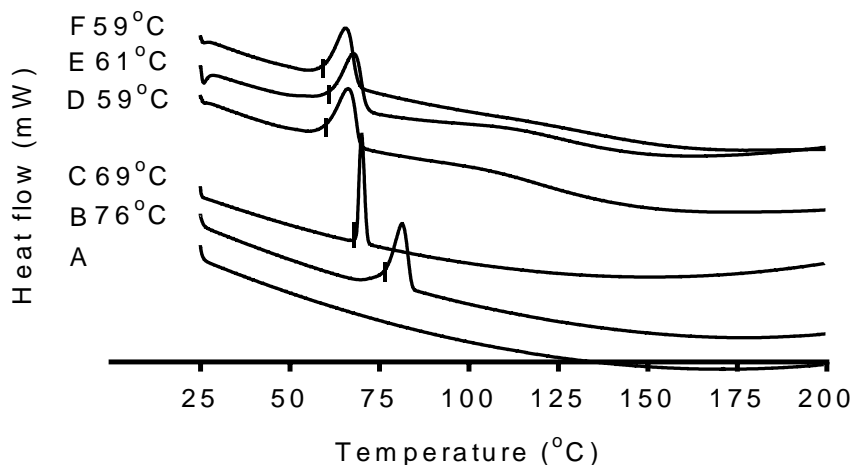


Figure 4.2. DSC heating profiles of A) an empty pan, B) lidocaine HCl powder, C) lidocaine base powder, D) PVP/RS100/PEO electrospun fibres, E) PVP/RS100/PEO electrospun fibres containing lidocaine HCl and F) PVP/RS100/PEO electrospun fibres containing lidocaine base. The onset melting temperatures of the upward facing enthalpy peaks are given to the nearest 1 °C. The image is representative of n=2 independent experiments.

As drug release from a system can be dependent of the pH microenvironment, and as the acid and base complex of lidocaine were incorporated into the patches, the pH of the electrospun patches dissolved in deionised water was measured. The mean pH of the plain patch was pH 7.78 and as expected the addition of lidocaine HCl made the patch more acidic, reducing the pH by about 0.5, and the addition of lidocaine base increased the pH by about 0.5 (Figure 4.3).

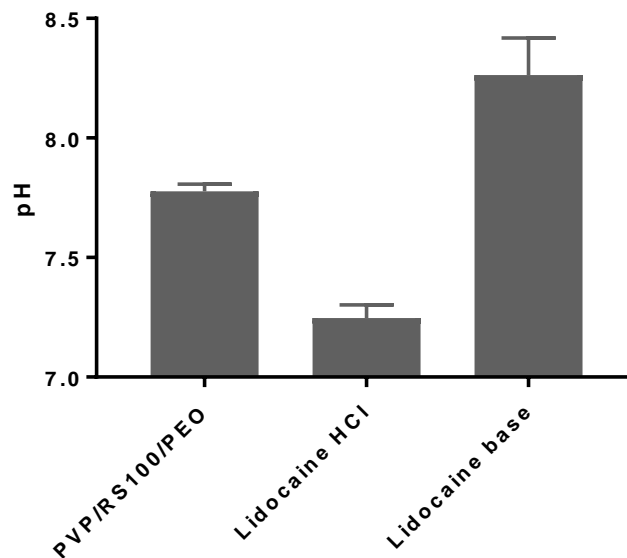


Figure 4.3. pH of electrospun patches dissolved in deionised water measured at 20 °C either as the plain PVP/RS100/PEO patch without drug, the patch containing lidocaine HCl or the patch with lidocaine base (mean \pm SD, n=3).

4.3 Lidocaine release from electrospun patches

To ensure that the electrospun patches can be utilised as an anaesthetic delivery system, drug release from the patches needed to be determined. As there was variation in patch weight, with 10.8 ± 3.9 mg for lidocaine HCl containing patches and 11.0 ± 2.7 mg for lidocaine base containing patches (mean \pm SD, n=4), the accumulative drug release per 10 mg of patch was calculated in PBS over 1 h (Figure 4.4). Lidocaine from lidocaine HCl patches released more rapidly from the electrospun fibres with 0.16 ± 0.04 mg released over the first 15 min, compared to lidocaine base where 0.06 ± 0.01 mg was released within 15 min. At 60 min, 0.21 ± 0.02 mg of lidocaine from the lidocaine HCl patches was released compared to 0.11 ± 0.02 mg of lidocaine base. This corresponds to approximately 81% and 40% of total lidocaine content released from the lidocaine HCl-containing and lidocaine base-containing patches, respectively. Overall, the release of lidocaine from the lidocaine HCl-

containing patches was significantly quicker than that from the lidocaine base-containing electrospun patches ($p < 0.0001$).

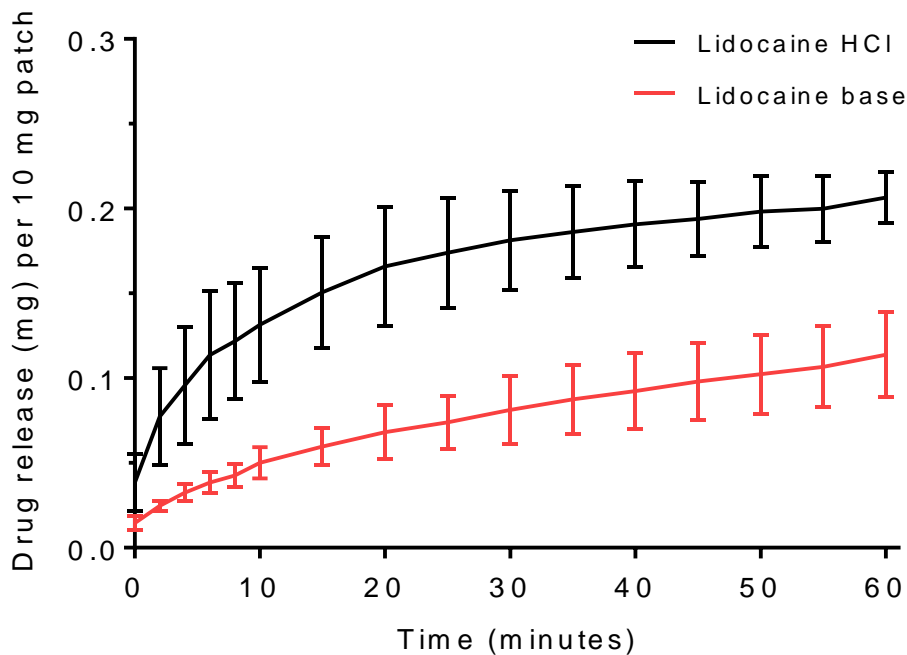


Figure 4.4. Accumulative release of lidocaine into PBS from electrospun patches containing either lidocaine base or lidocaine HCl over 1 h as measured by UV-HPLC. Data presented is the mean \pm SD ($n=4$), where only upward SD is shown. Mann-Whitney U test showed a significant difference in release between the two drugs ($p < 0.0001$).

4.4 Lidocaine permeation through *ex vivo* porcine buccal mucosa

Lidocaine release from the electrospun patches into PBS has been established, however permeation of lidocaine into oral mucosal tissue is required for it to have an anesthetic effect. To determine whether released lidocaine did permeate tissue, patches were assessed in an *ex vivo* model using porcine buccal mucosa. Dual-layer electrospun patches were used in the permeation studies to ensure uni-directional release of lidocaine directly into the mucosal tissue, thereby preventing release into the donor chamber which is simulating the oral cavity. The lidocaine HCl loaded electrospun patches were placed onto the surface of *ex vivo* porcine buccal epithelium and the permeation through $1011 \pm 133 \mu\text{m}$ thick tissue (mean \pm

SD, n=10) over 5 h using permeation chambers was measured. Consistent accumulative permeation of lidocaine was observed for all repeats and lidocaine was detected by HPLC in the permeation chamber after only 15 min (Figure 4.5). It is difficult to estimate the concentration of lidocaine in the patches as the dual layer system was used, however it was estimated that a minimum of 0.20 mg to a possible maximum of 0.35 mg of lidocaine HCl was present per patch. The average resulting flux, calculated using equation 7 (see section 2.3.10), was $4.47 \pm 0.16 \text{ ng cm}^{-2} \text{ s}^{-1}$ (mean \pm SD; n= 6). In comparison, applying 3% (w/v) lidocaine HCl in solution resulted in a flux of $68.20 \pm 1.03 \text{ ng cm}^{-2} \text{ s}^{-1}$ and an apparent permeability (P_{app} , equation 4 in section 1.7.2) value of $2.27 \pm 0.03 (\times 10^{-6}) \text{ cm s}^{-1}$ (mean \pm SD; n= 4) (Figure 4.6.). The two experiments are not directly comparable as lidocaine HCl in solution does not require a release step from solid polymer fibres and additionally a very large concentration of lidocaine HCl (60 mg in 2 mL PBS) was present in the chamber. Electrospun patches containing between 0.25 mg and 0.39 mg lidocaine base per patch were tested in the same model, however, no lidocaine could be detected in the receptor buffer.

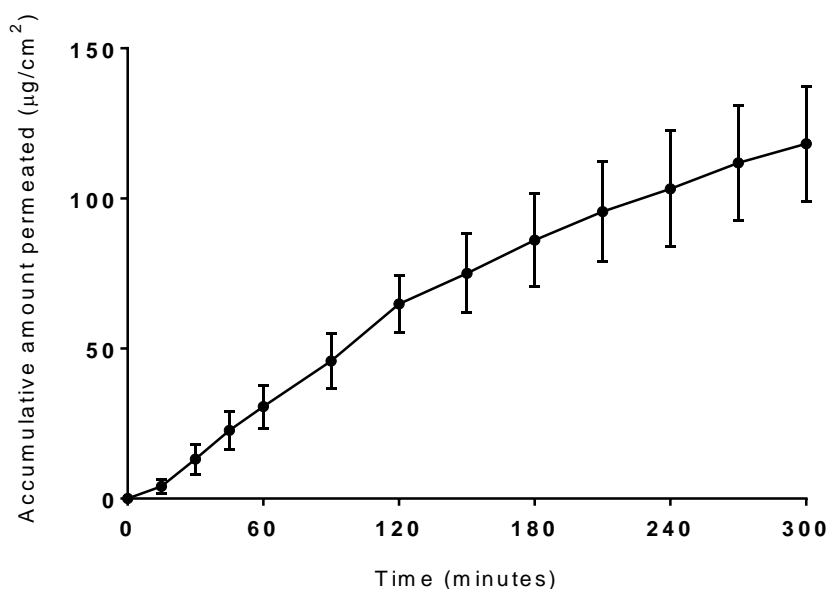


Figure 4.5. Accumulative permeation of lidocaine released from an electrospun patch through ex vivo porcine buccal mucosa as measured by UV-HPLC. The electrospun patches contained between 0.20 and 0.35 mg lidocaine HCl. Data are mean \pm SD (n=6).

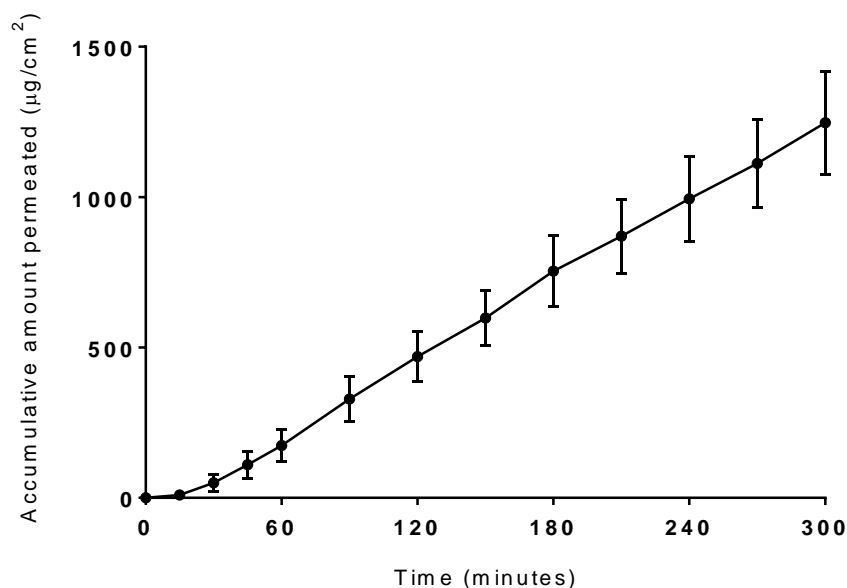


Figure 4.6. Accumulative permeation of lidocaine applying 3% (w/v) lidocaine HCl in PBS through ex vivo porcine buccal mucosa as measured by UV-HPLC. Data are mean \pm SD (n=4).

4.5 Mass spectrometry imaging of lidocaine from electrospun patches permeating into ex vivo tissue

One method more recently used for detecting the spatial distribution of drug in tissue is the use of mass spectrometry imaging (MSI). Matrix-assisted laser desorption ionisation-MSI (MALDI-MSI) was used to detect the distribution of lidocaine in tissue after it had been applied to the surface of the epithelium, either in PBS solution or within an electrospun patch. An AP-SMALDI10 Ion source was used allowing imaging with 10 μm spatial resolution and a high-resolution mass analyser, a QExactive Orbitrap mass spectrometer with high mass resolving power of current, was used to give sub ppm mass accuracy [198–200]. The 2,5-DHB matrix provided a lock mass at m/z 295.0213 giving an internal standard in the mass spectrum that re-calibrates any drift in the electrical field, thereby maintaining mass accuracy of the spectrum. An example mass spectrum to show that the lidocaine signal was best detected in the protonated form at m/z 235.1807 with a mass accuracy of 1.0 ppm, and

the mass used to detect the epithelium marker at m/z 751.5134, is shown in Figure 4.7. Over 10,000 mass spectra were recorded to create each MSI, as the images were around 125×100 pixels in size. In the MSI images, lipid phosphatidylglycerol (PG) (34:1) with an m/z of 771.513 was used as the epithelium marker and is false-coloured blue, whereas lidocaine with m/z 235.181 was false-coloured red. After a MALDI-MSI was recorded the same tissue was H&E stained, to make the epithelium layer and lamina propria clearly visible (Figures 4.8-4.10).

Firstly, drug distribution after exposure to a solution of lidocaine HCl (3 mg mL^{-1} , approximately 0.21 mg applied) for up to 3 h was investigated (Figure 4.8), where a clear time-dependent permeation was observed. The control shows that no lidocaine signal present was when the drug was not applied. In the first 15 min, lidocaine was visible exclusively within the epithelium, where it was evenly distributed throughout the stratified structure of the upper epithelium and extending into the rete ridges. After 1 h, lidocaine was detected throughout the epithelium and was shown to progress into the lamina propria. At 3 h, lidocaine was shown in the entire imaged section of the tissue, including lidocaine distribution in the epithelium, lamina propria and submucosa.

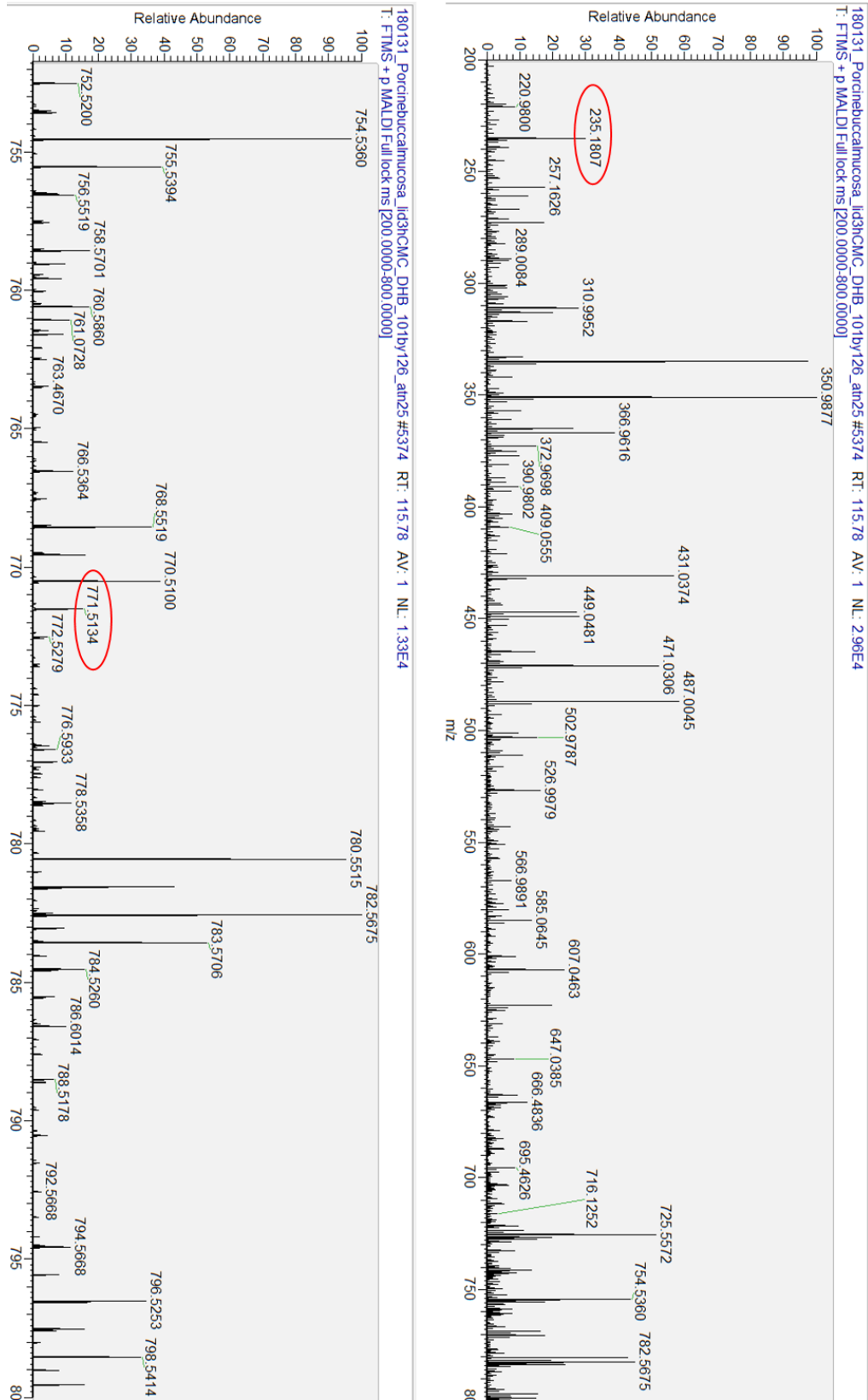


Figure 4.7. Mass spectra corresponding to one pixel from the MSI images of porcine buccal tissue with lidocaine HCl solution applied to the surface of the epithelium. The epithelium marker PG (34:1) (m/z 771.5134 $[M+Na]^+$) and lidocaine (m/z 235.1807 $[M+Na]^+$) are circled.

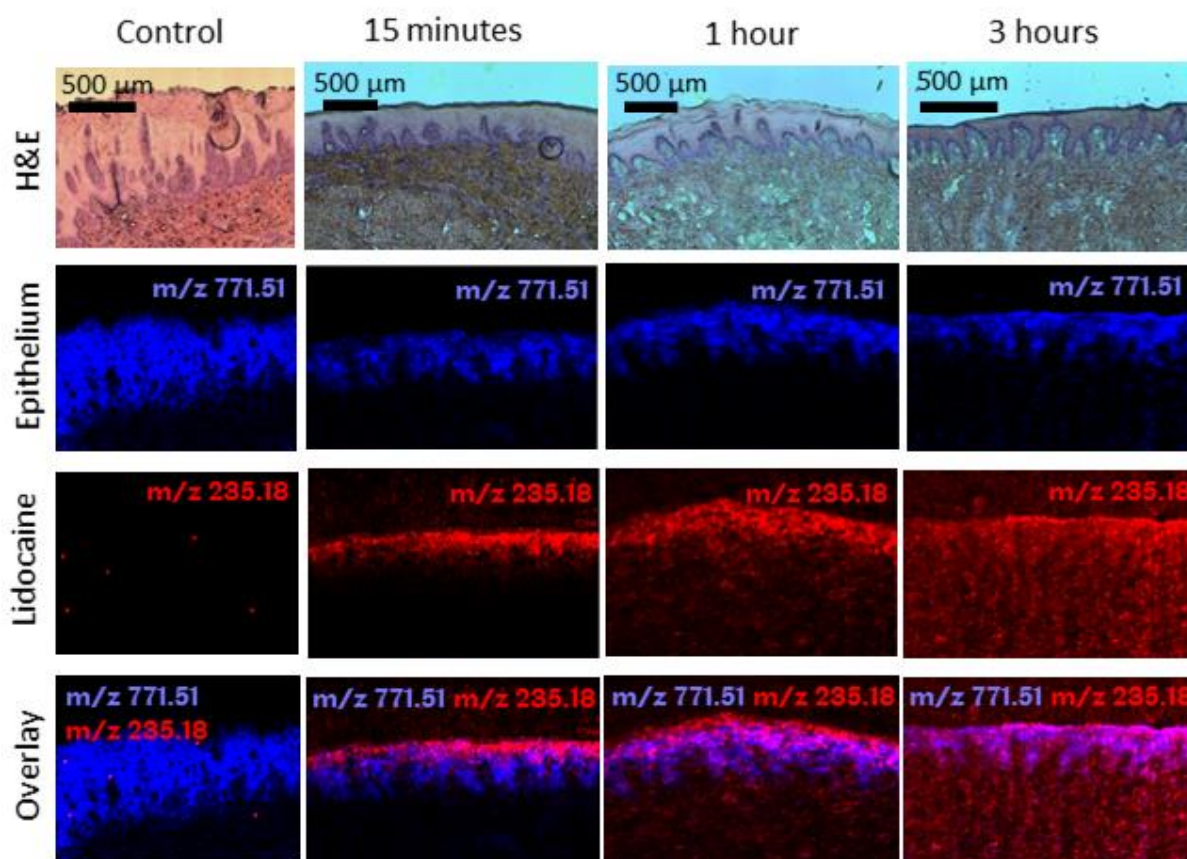


Figure 4.8. H&E stained tissue sections and corresponding MALDI-MS images of porcine buccal mucosa with no treatment (control), and exposed to 0.3% (w/v) lidocaine HCl solution (m/z 235.1807 [M+Na]⁺; red) after 15 min, 1 h and 3 h. The epithelium (blue) for each sample is shown using the epithelial marker PG (34:1) (m/z 771.5130 [M+Na]⁺).

The placement of the electrospun patch on top of the surface of the epithelium is shown by the blue arrows in the H&E images (Figure 4.9 and 4.10). Lidocaine released from the lidocaine HCl-containing electrospun patches was shown to permeate into the epithelium layer in the first 15 min, with the m/z signal being most abundant in the area local to where the patch was placed (Figure 4.7). After 1 h, slightly more lidocaine was shown in the lamina propria and at 3 h it spread through both the epithelium and lamina propria.

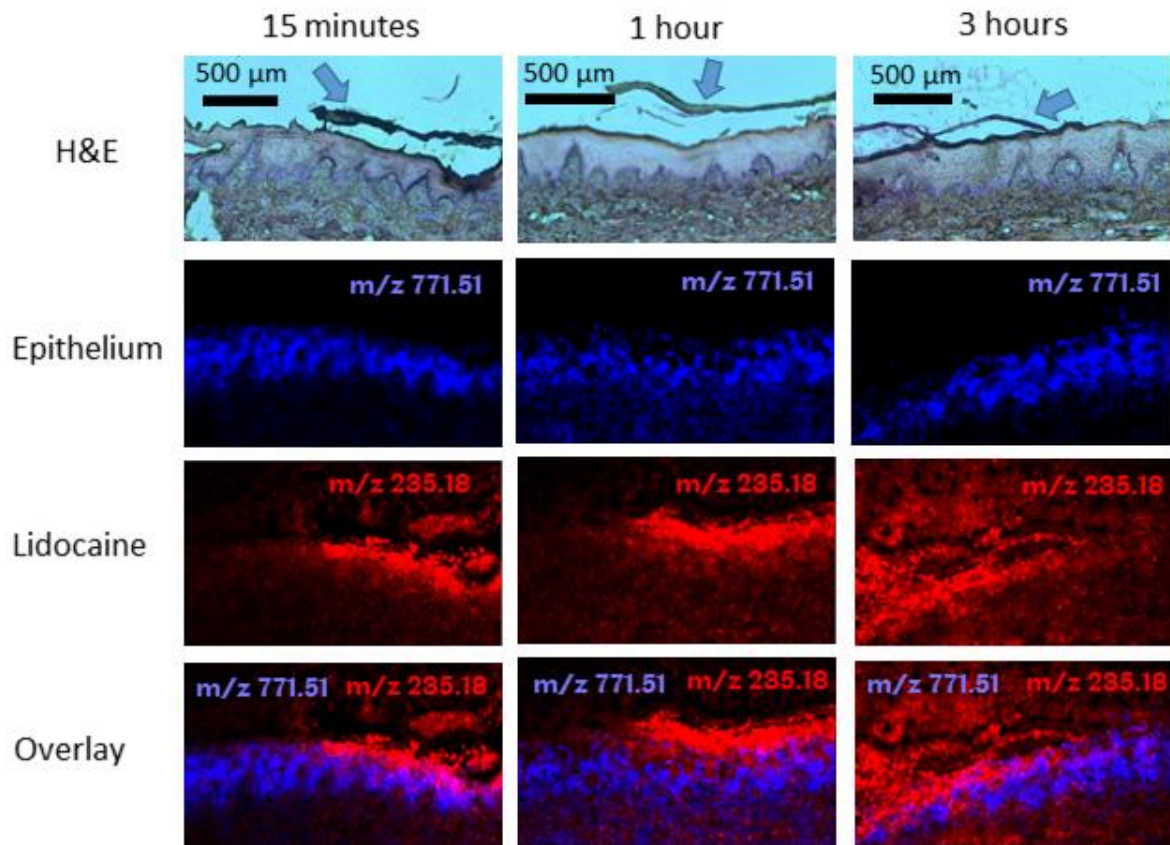


Figure 4.9. H&E stained tissue sections and corresponding MALDI-MS images of porcine buccal mucosa exposed to dual-layer electrospun patches containing 3% (w/v) lidocaine HCl (m/z 235.1807 [M+Na]⁺; red) after 15 min, 1 h and 3 h. The epithelium (blue) for each sample is shown using the epithelial marker PG (34:1) (m/z 771.5130 [M+Na]⁺). The arrows in the H&E images show the position of the electrospun patch.

For the lidocaine base containing patches some lidocaine was detected in the lamina propria at 15 min, and at 1 h and 3 h it was seen throughout the imaged parts of the tissue (Figure 4.10). Overall, the mucosal distribution of lidocaine was more widespread and homogeneous when lidocaine HCl was applied as a solution compared to the electrospun patches. However, unlike administering a solution in the oral cavity, the electrospun patches will maintain local contact to the tissue and, as can be seen in Figure 4.9 and 4.10, lidocaine was not depleted from the patch over a period of 3 h.

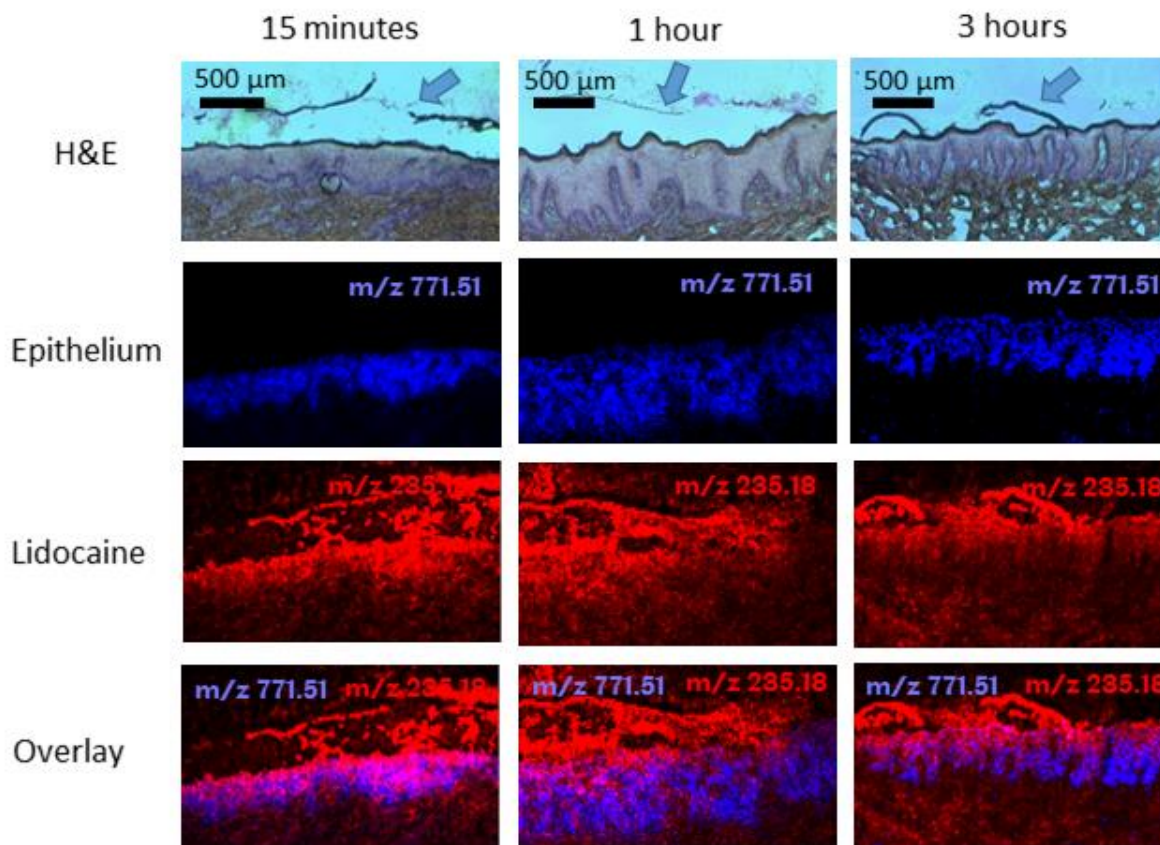


Figure 4.10. H&E stained tissue sections and corresponding MALDI-MS images of porcine buccal mucosa exposed to dual-layer electrospun patches containing 3% (w/v) lidocaine base (m/z 235.1807 [M+Na]⁺; red) after 15 min, 1 h and 3 h. The epithelium (blue) for each sample is shown using the epithelial marker PG (34:1) (m/z 771.5130 [M+Na]⁺). The arrows in the H&E images show the position of the electrospun patch.

4.5 Discussion

The aim of this chapter was to demonstrate the application of an electrospun patch as a vehicle for a small molecule drug to be delivered directly to oral mucosal tissue. Although transbuccal drug delivery has been studied for formulations, such as tablets, gels, creams and films [144,173,195,201–203], only limited data on electrospun fibrous patches as oromucosal drug delivery vehicles has been recorded to date. Some of the most relevant studies to the work in this chapter have been published in the past two years. The most related study was largely performed by the same research group in Sheffield, where corticosteroids were directly incorporated into a polymer dope prior to electrospinning the patch, and the patch was used for transbuccal delivery of the steroid [1]. In that study data using *in vitro*, *ex vivo* and *in vivo* models to show the potential of the drug-loaded patch were produced. Another study used the same drug as in this project, where lidocaine was additively printed onto the surface of an electrospun patch for the purpose of oromucosal delivery, although the delivery system was only characterised for its material properties and did not study the application of the device on tissue or any other biological assay [204]. As highlighted in the literature review, and by other published review articles [10,205], improving local oromucosal drug delivery to treat oral diseases is desirable as the tissue is easily accessible for self-administration, sustained release is achievable and it could reduce side effects experienced from taking drugs systemically. Additionally, the reason for choosing lidocaine was as it could benefit a wide range of patients experiencing oromucosal pain.

Although lidocaine has not previously been electrospun into patches for the application of transbuccal delivery, it has been electrospun into patches for wound dressing applications [151,174,206–209]. Various polymer/solvent mixtures were used, with a number of studies using PLGA, but PCL and PLLA were also used. In this study, lidocaine was incorporated into PVP/RS100/PEO fibres, where the incorporation of the drug did not appear to alter the fibre morphology. The drug encapsulation into PLGA was previously shown by FTIR spectroscopy [208,209], although as the lidocaine content in the electrospun

PVP/RS100/PEO patches here were measured by HPLC, no FTIR or X-ray diffraction was performed. However, DSC was used to determine the crystallinity of the drug in the fibres. In PLLA fibres, it was noted that there were areas of crystalline lidocaine [174]. This crystallinity is not desired, as an amorphous drug form should be higher energy, and therefore more soluble, to allow drug release from the patch and into tissue [196]. The DSC results in section 4.2, however, showed that lidocaine HCl and lidocaine base were both amorphous within the PVP/RS100/PEO fibres. This is consistent with other active pharmaceutical ingredients in electrospun polymer fibres [97,121,146], where this amorphous form was shown to increase drug solubility and bioavailability.

The release of lidocaine from lidocaine HCl and lidocaine base containing electrospun patches was measured in PBS over 1 h (Figure 4.4). Lidocaine in the lidocaine HCl patches was released significantly quicker from the fibres than the basic form of the drug and released 70-80% of the total drug concentration in the patch over 1 h, similar to previously reported release data for lidocaine HCl in PLLA and PCL electrospun fibres [151,174]. Lidocaine base previously electrospun into CMC/PEO and prepared in a hydroxypropylcellulose film had 50-60% of the total drug concentration released over 1 h [206,210], which was also similar to the release observed in this project. The difference in release between the two lidocaine complexes incorporated into the patch were likely due to a difference in pH microenvironment of the fibres, as shown in Figure 4.3, and the acidity of the drug complexes. The acidic and protonated salt, lidocaine HCl, releases more quickly than lidocaine base from the surface of the fibres. The solubility of weakly basic drugs are increased by lower pH environments and hence acidity modifiers within the delivery vehicle may be used to increase their solubility [211].

The subsequent uptake of lidocaine released from the electrospun patch into buccal mucosa was determined using *ex vivo* porcine tissue. Prior to experimentation, the porcine tissue was kept at -80 °C in cryopreservants, where an earlier study using the same tissue and cryopreservant, showed no change in the permeation barrier properties between fresh and

de-frosted tissue [212]. Unchanging permeation properties have also been reported for fresh and frozen porcine oesophageal tissue [203]. A research group at the University of Parma has previously performed a number of permeation studies of lidocaine HCl-containing poly(vinyl alcohol) films on oesophageal porcine tissue [203] and rabbit ear skin [55,213], where the permeation profiles were similar to lidocaine across porcine buccal mucosa released from the lidocaine HCl-containing patches in this study. The flux was calculated to be $4.47 \pm 0.16 \text{ ng cm}^{-2} \text{ s}^{-1}$ (mean \pm SD; $n=6$) for the lidocaine released from the electrospun patch, which was 15 times less than the flux measured from a high concentration of lidocaine in PBS. However, the two systems cannot be directly compared as the release medium and concentrations were different. Films that contained 19 times more lidocaine had a flux between 0.7 and $20.7 \text{ } \mu\text{g cm}^{-2} \text{ s}^{-1}$ in porcine buccal tissue, showing how polymer composition, enhancers and drug dosing can have a large influence on drug release and permeability [214]. The apparent permeability for lidocaine in solution crossing oesophageal porcine epithelium was previously reported as $7.25 \pm 0.75 (\times 10^{-6}) \text{ cm s}^{-1}$ [203], which is similar to the P_{app} value of $2.27 \pm 0.03 (\times 10^{-6}) \text{ cm s}^{-1}$ (mean \pm SD; $n=4$) of lidocaine crossing the porcine buccal tissue in this study. The P_{app} for just crossing the buccal epithelium (with no underlying lamina propria unlike the tissue in this study) was reported to be over seven times greater at $17.0 \pm 1.8 (\times 10^{-6}) \text{ cm s}^{-1}$ [27]. This would suggest that the lamina propria in this study greatly reduces the permeation rate, however this is highly unlikely as the epithelium is known to be the greater permeation barrier and the lamina propria consists of loose connective tissue. In fact the top one third of the epithelium has been shown to cause the greatest permeation barrier in buccal tissue, as the squamous epithelium cells extrude lipids into the extracellular space [215,216]. Therefore, biological tissue variation between the pigs in the different studies, or potentially the handling of the tissue, was more likely to have caused the difference in apparent permeability.

Two studies were found to have previously incorporated lidocaine base into a film and to have subsequently measured the release and permeation through buccal tissue [165,210].

One of the films contained approximately 100 times more lidocaine base than the electrospun patches, and, unlike in this study where no permeation of lidocaine from the electrospun patches over 5 hours (n=4) was observed, the lidocaine was detected in the receptor chamber after only 5 min [165]. The permeation in the study was surprisingly quick, especially as the release rate into PBS was similar and the tissue thickness was reported to be 1.3 cm. Therefore, the state of the tissue was slightly in question. The other study had 6 mg of lidocaine base (200 times the amount in this study) in the film and over two hours 0.4 mg or 500 $\mu\text{g}/\text{cm}^2$, similar to the lidocaine HCl in solution as shown in Figure 4.6, permeated through hamster oral mucosa. However, this is only 6% of the original concentration and a lot less compared to 75% of lidocaine that was reported to release from the films into buffer over the same amount of time. If only 6% of lidocaine base permeated through the tissue from the electrospun patches, this would only be around 20 μg , which would however have been measureable using the HPLC. One plausible explanation for not detecting the lidocaine permeation in this instance is related to the low water-solubility and higher lipid-solubility of the uncharged lidocaine when present as the free-base, where stable lipid binding with the oral keratinocyte cells in the lamina propria may have occurred [217]. In comparison, the more water-soluble and positively charged lidocaine molecules dissociated from lidocaine HCl permeate through the lamina propria in a paracellular manner and were therefore detected in the Ussing chamber permeation experiments [217]. The more alkaline microenvironment of the free lidocaine base also influences the water solubility of the molecules resulting in a slower permeation of the molecules through the various tissue layers, where the tissues layers also have their own different pH microenvironments.

Although the *ex vivo* permeation data provides valuable quantitative information on the amount of lidocaine permeated, it does not inform us on the spatial distribution of drug within the tissue. MSI is a powerful technique which can detect a multitude of compounds, including lipids, small molecules and metabolites, to a high resolution and can be used to form a visual image of the tissue and presence of drug molecules. Desorption electrospray ionisation –

MSI has been previously used to detect the presence of lidocaine, and metabolites thereof, in skin [218–220] and MALDI-MSI was used to detect nicotine and mannitol permeation through porcine buccal mucosa [221,222]. This was however, the first time that MALDI-MSI was used to detect release of a small drug molecule from an electrospun patch system. Specifically, the spatial distribution of lidocaine within porcine buccal mucosa after delivery from an electrospun patch was shown. The images show that in the first 15 min the lidocaine penetration into the buccal mucosa was mainly focussed in the local area of patch placement (Figure 4.9 and 4.10). For the lidocaine HCl patches the lidocaine signal was strongest in the region of patch placement and in the epithelium directly adjacent to the patch, especially at 15 min and 1 h time points (Figure 4.9). The reason for the electrospun patches having stronger lidocaine signals in the patch compared to the tissue at the lower time points can be explained by reviewing the permeation data, as only 20 µg of potentially up to 300 µg of lidocaine contained in the patch permeated through the mucosa after 1 h. This concentration of lidocaine in the electrospun patch should reduce over time as it is released, although after 3 h the lidocaine patches were not entirely depleted of the drug (Figure 4.9 and 4.10). Care should however be taken when comparing ion signals within MS images and comparing separate MS images in terms of signal intensity and correlating this to drug concentration. The signal intensity is dependent on a number of variables which make quantification and direct comparison between images difficult and is a challenge many researchers are currently confronting [223–225]. Such variables include ion suppression, the heterogeneity of the tissue and matrix application, the matrix crystal size, analyte stability and fluctuations in the detector response [226].

Despite not being able to detect lidocaine permeation from a lidocaine base containing patch in a 5 h period using UV-HPLC, MALDI-MSI Figure 4.10 clearly shows the presence of lidocaine in tissue. Figure 4.10 shows that even after 15 min of patch application to the tissue, lidocaine was present in both the epithelium and the lamina propria. As lidocaine is a fairly lipophilic molecule, upon release from the patch, it is expected to permeate through the

epithelium, into the lamina propria and submucosa over time, as shown in Figures 4.9 and 4.10, although the rate of permeation will depend on the charge state and water- and lipid-solubility of the lidocaine ions [217]. The time-dependent penetration of the drug was observed especially clearly when lidocaine HCl in solution was applied to the surface of the epithelium, where a homogenous distribution in the tissue was shown at 3 h. The tissue penetration depth may also be controlled by the dose of the drug, as was shown for lidocaine on skin [219]. Hence, if the patch were left on the tissue over a prolonged period of time with a greater concentration of lidocaine loaded into the electrospun patch, increased tissue penetration would be expected. Clinically, 2% lidocaine is often reported for topical administration, which indicates a 20 mg/mL drug loading. Xylocaine (lidocaine HCl) 2% viscous oral solution by Frensius Kabi, where the product has been discontinued, recommends in the usage instructions that a single dose for an adult should not exceed 4.5 mg/kg of body weight and should not exceed 300 mg in total [227]. In these instructions it is recommended for an adult to swirl 15 mL of the solution in the mouth, which corresponds to 300 mg. This is clearly a lot higher than the 0.3 mg incorporated in the patches in this study, however, compared to a mouthwash, the patches would be directly adhering to the mucosa for a prolonged period for sustained drug delivery. Furthermore a 10-fold increase to incorporate 30% (w/w) instead of 3% (w/w) of lidocaine HCl in the electrospun patch was later achieved. This 30% (w/w) loading is similar to previous film patches which were used in an *in vivo* study [214]. This *in vivo* study was of films containing 4.71 mg of lidocaine HCl adhered to the buccal pouch of rabbits and slightly over 2 µg/mL of lidocaine were found in the plasma after 2 h, where the therapeutic range has been reported to be greater than 1.5 µg/mL [228]. Another *in vivo* study using PLGA electrospun nanofibers incorporating an assumed 56 mg of lidocaine HCl (although the concentration for the *in vivo* study was unclear) was used as an eluting implant on incised rat abdomen [208]. Over fourteen days, samples of plasma contained 10-100 µg/mL of lidocaine. However, it has previously been reported that at plasma concentrations over 6 µg/mL the risk of cardiac arrhythmias increases [229]. The electrospun patch in this project, however, will be used for a shorter

application time of a few hours with a smaller dose of lidocaine. Therefore, a next step would be to test the 30% (w/w) lidocaine HCl-loaded electrospun patches in a similar *in vivo* study as Abu-Huwaij *et al.* [214].

To summarise the results in this chapter, electrospun patches containing lidocaine base and lidocaine HCl were successfully manufactured using electrospinning, and the release profiles of these drugs were demonstrated. Lidocaine uptake and permeation through *ex vivo* porcine buccal mucosa was shown following release from a lidocaine HCl-loaded patch. This was confirmed using MALDI-MS, where for the first time, the distribution of electrospun delivered lidocaine within oral soft tissues was depicted. The data in this chapter shows the potential of electrospun patches as a delivery vehicle for lidocaine to buccal mucosa, with the aim of improving current local treatment of oral pain. However, *in vivo* studies and clinical investigation are first required to determine the feasibility of using this patch system as a topical dental anaesthetic or as an analgesic for patients with painful oral mucosal disease conditions.

5. Results & Discussion: Medium-chain fatty acids in electrospun patches inhibit *Candida albicans*

5.1 Introduction

Oral candidiasis is a major risk factor for immunocompromised patients and can range from chronic mucocutaneous conditions to severe, invasive systemic infections with high morbidity and mortality [230]. Antimicrobial resistance has increased in the last decade, including resistance to commonly used antifungal drugs such as fluconazole and miconazole to treat candidiasis [38]. It is key that alternative antifungal agents are discovered to reduce the risk of resistance. The most prevalent human pathogen of *Candida* species is *Candida albicans*, for which a large increase in azole drug resistance has been reported [37]. Alternative therapies that have previously been researched are surfactants[39,40], synthetic peptides[41–43] and fatty acids[44–48]. For the purpose of this study *C. albicans* was selected as a fungal model organism and a range of short- to medium-chain saturated fatty acids were tested for their antifungal properties.

The research in this chapter aimed to determine whether short- to medium-chain saturated fatty acids could be used as an alternative antifungal agent to treat oral candidiasis and on the potential of electrospun patches as an antifungal drug delivery vehicle.

5.2 Medium chain saturated fatty acids inhibit *Candida albicans* yeast growth

The antifungal ability of a range of short- to medium-chain saturated fatty acids, from butanoic (C5:0) to dodecanoic acid (C12:0), were first tested on two wild-type (BWP17 and SC5314) strains and one azole resistant (CAR17) strain of *C. albicans* grown in their yeast form using an agar disc diffusion assay as described in section 2.4.7. Octanoic (C8) and nonanoic (C9) acid at 0.2 M applied onto filter discs had the highest inhibitory response on *C. albicans* wild type strain growth, significantly preventing growth of *C. albicans* wild-type compared to the DMSO control as well as undecanoic acid (C11) on BWP17 and heptanoic

acid (C7) on SC5314 ($p < 0.05$) (Figure 5.1.A&B). The inhibition zones of the positive controls, fluconazole (0.8 mM) or miconazole (10 μg disc or 2.4 nmol) were similar to those of octanoic (C8) and nonanoic acid (C9) on the wild type strains. Disc diffusion data using the CAR17 strain confirmed that this was an azole resistant strain as these antifungal agents failed to prevent fungal growth with similar levels to the DMSO control (Figure 5.1.C). In contrast, when applied to CAR17, not only did octanoic acid (C8) and nonanoic (C9) acid show a similar inhibition area as for BWP17 and SC5314, but their killing efficiency was significantly different ($p < 0.0001$) to the positive controls, suggesting that these fatty acids are able to kill azole resistant strains of *C. albicans* (Figure 5.1.C). Hexanoic (C6) and heptanoic (C7) acid were also shown to have an increased inhibitory effect on CAR17 compared to inhibition on the wild type strains, although with greater standard deviation.

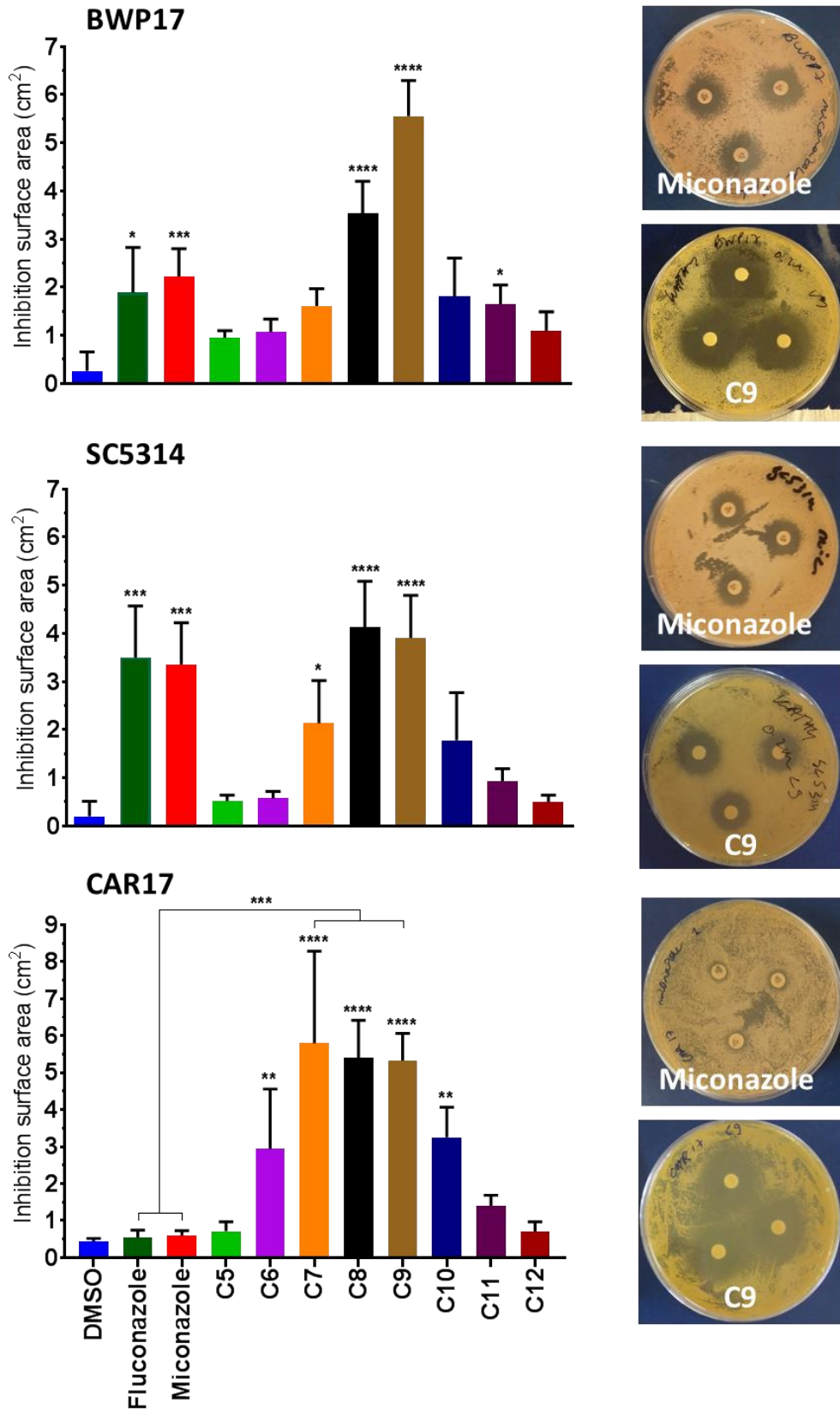


Figure 5.1. Inhibition surface areas on *C. albicans* streaked agar plates around filter discs impregnated with fatty acids made up at 0.2 M in DMSO, ranging from butanoic (C5) to

dodecanoic acid (C12), with positive controls fluconazole (0.8 mM) in DMSO and miconazole discs (10 µg or 2.4 nmol). DMSO alone was used as the negative control. Results are for *C. albicans* strains BWP17, SC5314 and CAR17. Data are mean +/- SD (n = 3). *p<0.05; **p<0.01, ***p<0.001, ****p<0.0001 compared to DMSO controls. Significant differences of other fatty acids to C5:0 and C6:0 are not shown. Images show representative inhibition zones of commonly used antifungal drug miconazole and nonanoic acid (C9) on *C. albicans* streaked agar plates related to the graphs to the left of the images.

5.3 Medium chain saturated fatty acids show toxicity towards *Candida albicans* biofilms

The drug diffusion assay determines the toxic effect of substances to a forming *C. albicans* colony. However, it is likely that *C. albicans* in a pre-existing biofilm state is the target for therapeutic intervention. Therefore, the inhibitory effect of heptanoic (C7) to dodecanoic (C12) acid on pre-formed SC5314 biofilms was tested using a metabolic/XTT assay as a surrogate measure of toxicity. Butanoic (C5) and hexanoic (C6) acid were not tested here as they showed almost no inhibitory response on the previous agar disc diffusion experiments. The results show that as the carbon chain length of fatty acids increases from C7:0 to C12:0 the required concentration to inhibit 50% of the biofilm (IC₅₀) decreases (Figure 5.2), meaning that the SC5314 biofilm is more susceptible to dodecanoic acid (C12). The IC₅₀ of the fatty acids is given in table 5.1, where it was shown that the IC₅₀ of dodecanoic acid (C12) was 10-fold less compared to heptanoic acid (C7). In fact a large decrease in fatty acid concentration required to achieve IC₅₀ is observed for undecanoic (C11) and dodecanoic (C12) acid compared to the other saturated fatty acids tested with shorter carbon chain lengths.

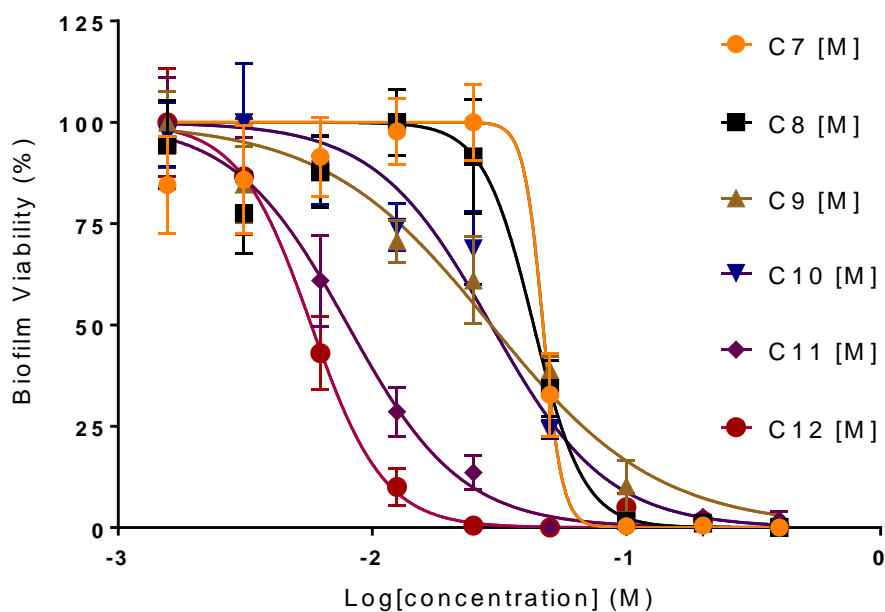


Figure 5.2. *C. albicans* strain SC5314 biofilm viability when subjected to fatty acids heptanoic acid (C7) to dodecanoic acid (C12) ranging in concentration from 400 mM to 1.56 mM using a metabolic XTT assay. The data is normalised to untreated controls (100% viability) and mean \pm SD over three plates and five wells per concentration is given (n=3).

IC ₅₀ of fatty acids on SC5314 biofilm (n=3)	
Fatty acid chain length	Average (mM)
C7	47.3 \pm 1.9
C8	47.5 \pm 2.7
C9	36.5 \pm 8.5
C10	26.0 \pm 8.2
C11	5.4 \pm 1.3
C12	4.7 \pm 1.1

The XTT assay measures cell mitochondrial metabolism and not cell viability *per se*, with the rationale that metabolism is directly linked to the number of viable cells (non-viable cells do not metabolise). To confirm the XTT findings an additional experiment was performed using fluorescent viability stains that directly distinguish live (green) or dead (red) cells (Figure 5.3). Similar to the XTT data, the live/dead stained images in Figure 5.3 show direct *C. albicans* killing by the fatty acids (50 mM), as observed by an increase in red fluorescence staining. Only biofilm killing for nonanoic acid (C9) and dodecanoic acid (C12) are shown, however live/dead images for SC5314 biofilms subjected to heptanoic acid to dodecanoic acid were tested. At this concentration the fatty acids such as heptanoic (C7), octanoic (C8) and nonanoic (C9) acid with shorter chain lengths showed little killing activity, whereas decanoic (C10), undecanoic (C11) and dodecanoic (C12) acid showed markedly greater killing activity. The fluorescence images also suggest that mainly yeast cells were killed by nonanoic acid treatment, given the more rounded structure of the dead cells, whereas dodecanoic acid treatment lead to both yeast and hyphae cell death.

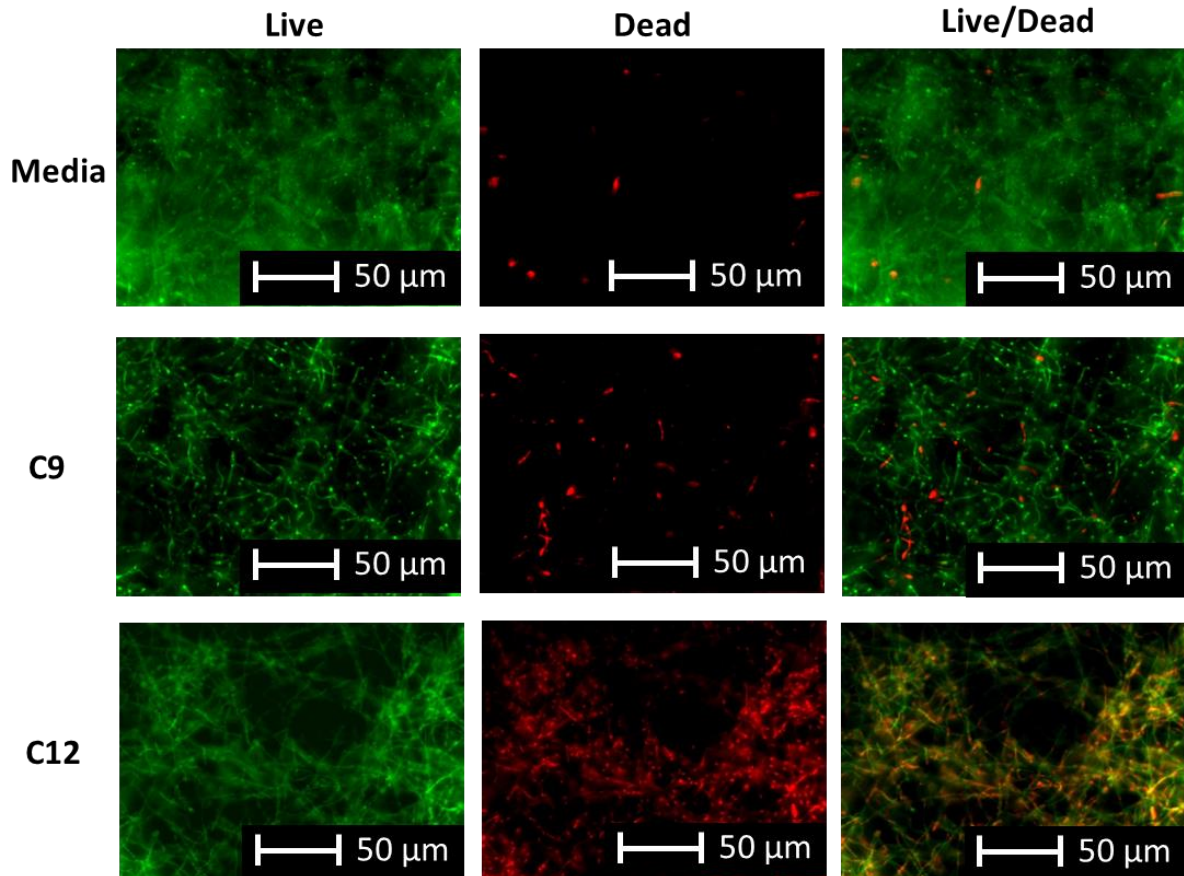


Figure 5.3. Fluorescence live/dead stain images of SC5314 biofilm subjected to media control (RPMI media only), 50 mM nonanoic acid (C9) or 50 mM dodecanoic acid (C12) in a 24 h incubation. Images show viable cells (green), dead cells (red) and the live/ dead images combined (n=3 wells per treatment).

5.4 Incorporating medium chain saturated fatty acids in electrospun patches

Fatty acids incorporated into an electrospun oromucosal drug delivery system could have multiple applications. One potential application could be as an antifungal delivery system for oral candidiasis. Another may be as a drug permeation enhancer as capric acid (C10) and lauric acid (C12), as well as sodium caprate and sodium laurate, are well known drug absorption enhancers through mucosal and dermal tissue [51,203,231–233]. The inclusion of medium chain saturated fatty acids in the electrospun system may therefore have applicability in both these processes. For example, the inclusion of fatty acids as an

antifungal into the backing layer of the patch may be useful for dual treatment with corticoid steroids, which have been previously incorporated into the PVP layer by researchers at Sheffield [1], where a potential side-effect of steroidal treatment is oral candidiasis. If an antifungal patch as a stand-alone product were to be developed the fatty acid could be incorporated directly into the PVP layer (without a backing layer). For this reason fatty acids were incorporated both into PCL and PVP/RS100 electrospun patches. Representative SEM images for PCL and PVP/RS100 fatty acid containing patches are shown in Figure 5.4 and Figure 5.5, respectively. The fibres containing fatty acids, both for PCL and PVP/RS100 fibres, look to be flatter and ribbon-like with more variable fibre diameters observed.

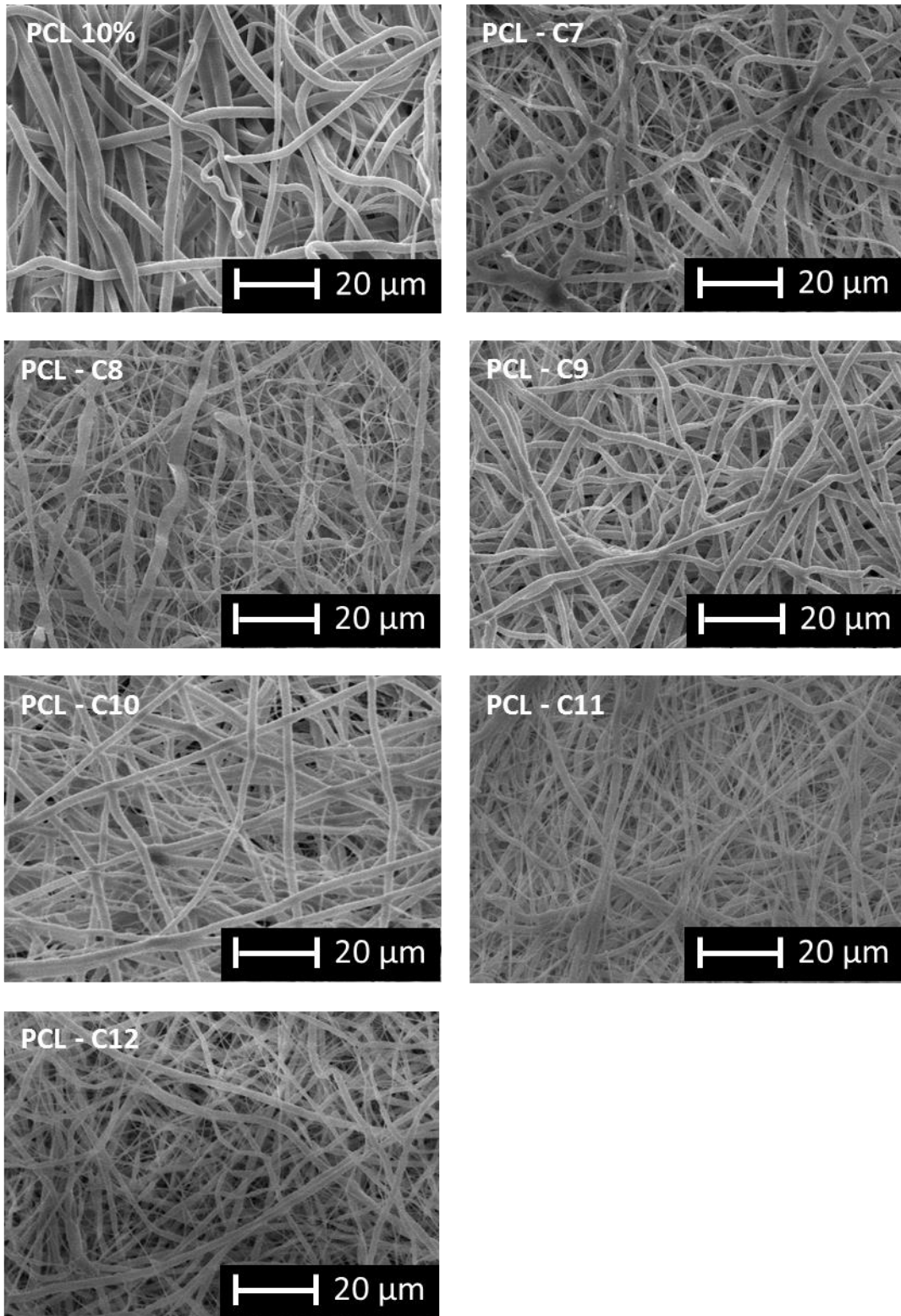


Figure 5.4. SEM images of electrospun patches consisting of 10% PCL, alone or with fatty acids heptanoic acid (C7) to dodecanoic acid (C12) incorporated into the patch.

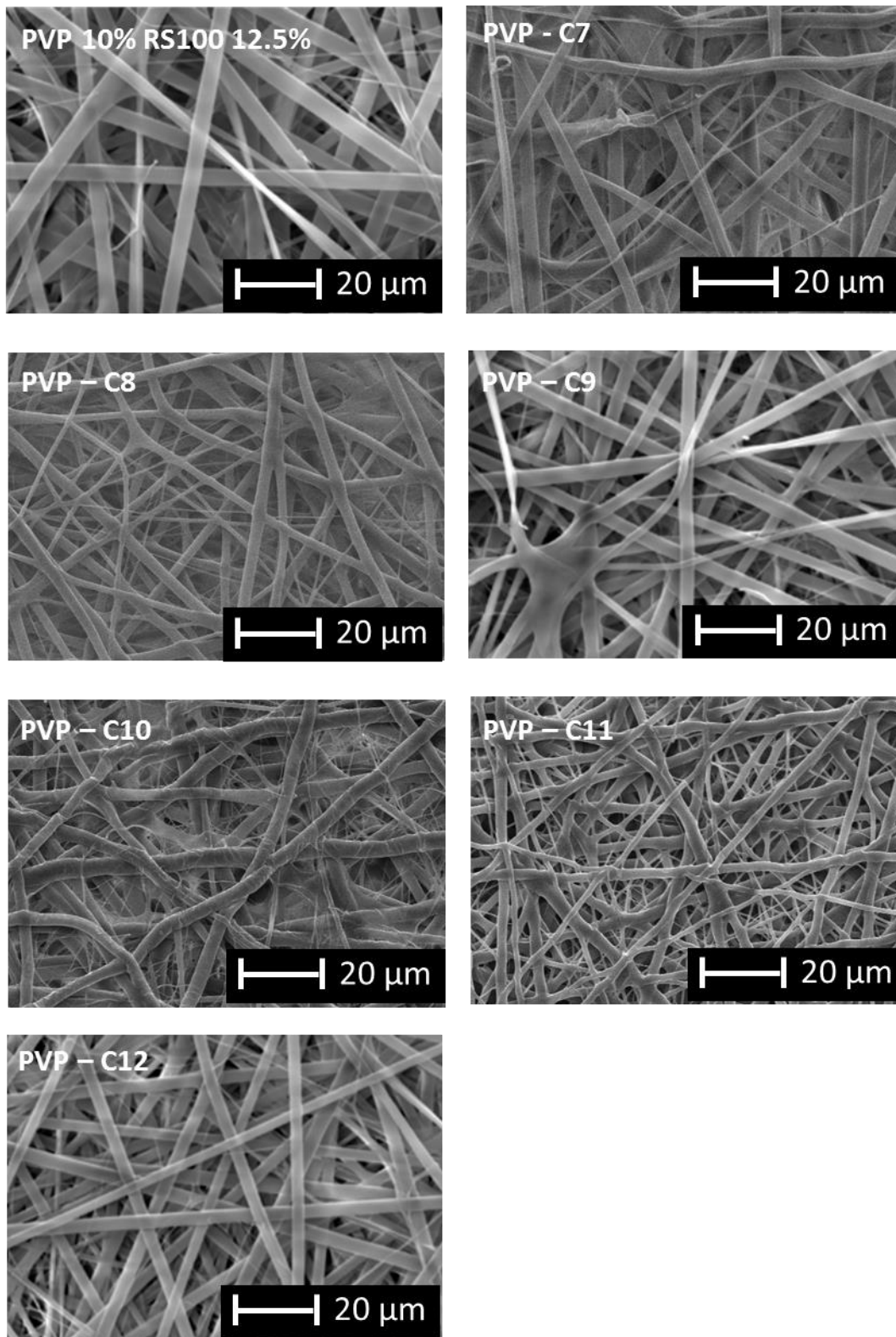


Figure 5.5. SEM images of electrospun patches consisting of 10% PVP/ 12.5% RS100, alone or incorporating fatty acids from heptanoic acid (C7) to dodecanoic acid (C12).

To establish the concentration of fatty acid present in the electrospun patches two different techniques were used for the PCL and PVP/RS100 fibres. ^1H NMR spectroscopy required little sample preparation or method development, hence this technique was used for the PCL fatty acid containing fibres. In contrast to the PVP/RS100 fatty acid fibres, there were distinguishable peaks in the ^1H NMR spectra for the PCL and fatty acid components. Specifically, there were no overlapping peaks for the PCL CH_2 group next to the $-\text{COO}$ group at 4.1 ppm and the fatty acid CH_3 group at the end of the chain at 0.8 ppm (Figure 5.6). The method and calculations outlined in section 2.4.5 were used to determine the percentage mass for all fatty acids shown in Figure 5.7 and these were plotted in Figure 5.8. Comparing the NMR spectra for different fatty acids incorporated into the electrospun patch in Figure 5.7 it is noticeable that fatty acids with shorter carbon chain lengths than decanoic acid (C10) were barely detectable in the PCL fibres at 0.8 ppm (circled in red), which is also reflected in Figure 5.8. PCL electrospun patches cut in a 12.7 mm diameter weighed between 5 - 8 mg, which means patches in this weight range containing 22 wt% dodecanoic acid (C12) contain 1.1 - 1.8 mg dodecanoic acid (C12) equivalent to 5 - 9 μmol .

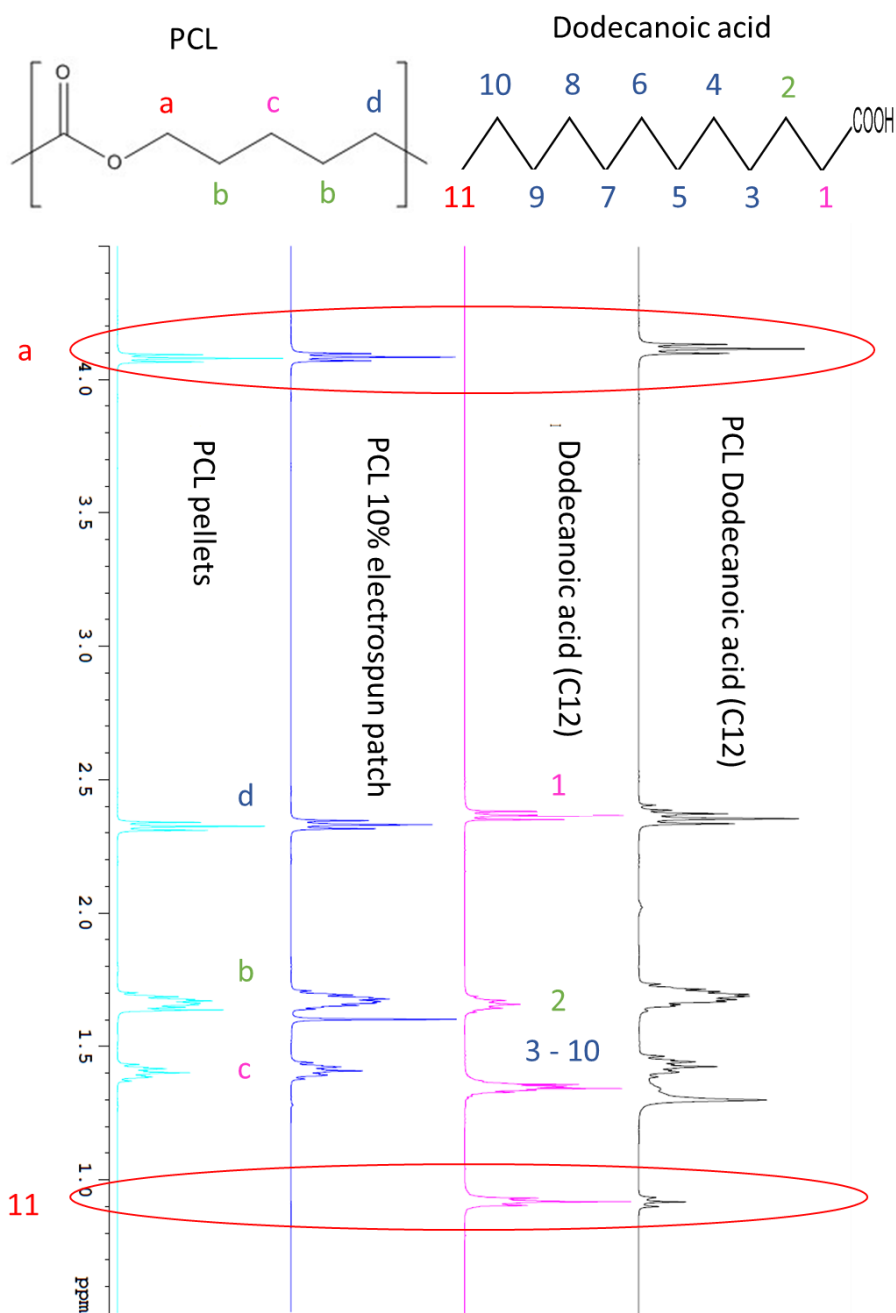


Figure 5.6. ¹H NMR spectra of PCL in pellet form, electrospun PCL fibres, neat dodecanoic acid (C12), and dodecanoic acid (C12) in PCL electrospun fibres, all dissolved in deuterated chloroform. The chemical structures of PCL and dodecanoic acid (C12) are displayed at the top of the figure. The ¹H NMR signals from the PCL and dodecanoic acid structures are alphabetised and numbered, respectively, correlate to the labels in the spectra. The fatty acid peak at 0.8 ppm labelled '11' and the PCL peak at 4.1 ppm labelled 'a' are used for analysis and are circled in red.

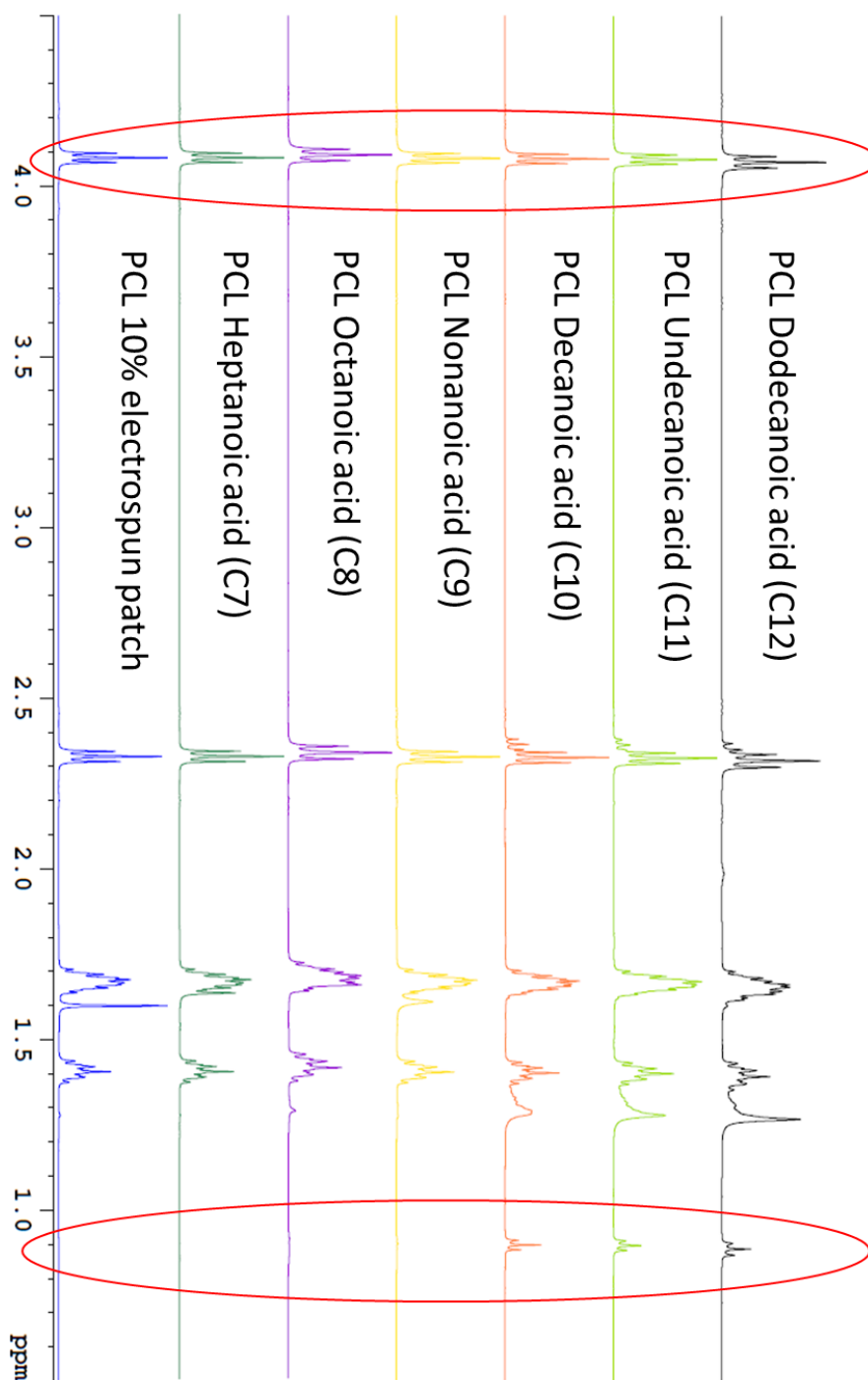


Figure 5.7 ^1H NMR spectra of a PCL electrospun patch and of fatty acids heptanoic acid (C7) to dodecanoic acid (C12) incorporated in the PCL fibres and dissolved in deuterated chloroform are given. The fatty acid peak at 0.8 ppm and the PCL peak at 4.1 ppm used for analysis are circled in red.

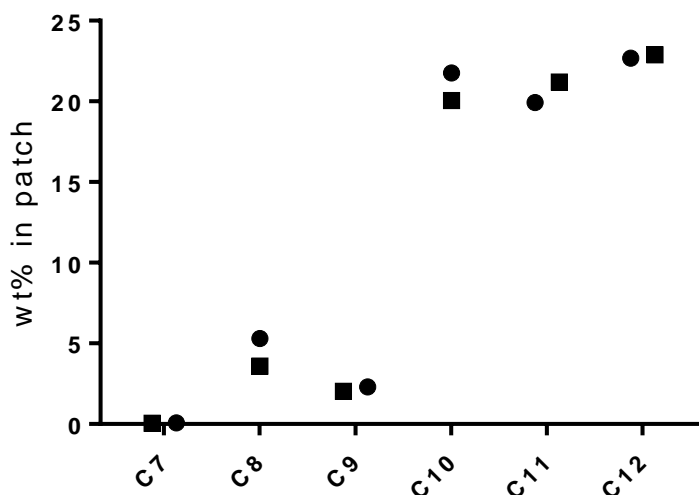


Figure 5.8. Fatty acid concentration of heptanoic acid (C7) to dodecanoic acid (C12) in PCL fibres given in weight % of the total patch weight (n=2).

For the PVP/RS100 fibres, GC-MS was used to quantify the amount of fatty acid encapsulated into the fibres, where only nonanoic (C9) and dodecanoic acid (C12) containing patches were analysed due to the time required to complete analysis. Similar to the PCL patches, more dodecanoic acid (C12) was retained within the patches after electrospinning compared to nonanoic acid (C9). However, only around 12 wt% compared to 22 wt% dodecanoic acid (C12) was present in the PVP/RS100 fibres compared to the PCL fibres. In contrast 8.1 +/- 2.7 wt% nonanoic acid (C9) in PVP/RS100 was retained in the patches compared to 2.2 wt% in the PCL patch. The PVP/RS100 patches contained 3.3 +/- 0.9 mM nonanoic acid (C9) with patch weights 6.8 +/- 1.3 mg and 5.2 +/- 1.7 mM dodecanoic acid (C12) with patch weights 8.6 +/- 2.8 mg (mean +/- SD, n=7 for C9 and n=7 for C12). Patches with ten times less dodecanoic acid (C12) in the polymer dope solution at 0.02 M (or 1.7 wt% in the dope) were electrospun and the resulting electrospun patches also showed a ten-fold decrease in the concentration of fatty acid present in the fibres with a concentration of 1.3 +/- 0.1 wt% and 0.23 +/- 0.04 mM for patches weighing 3.5 +/- 0.3 mg (mean +/- SD, n=3).

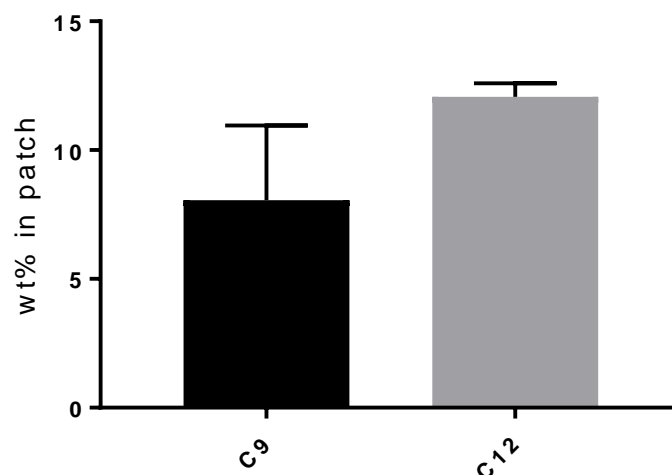


Figure 5.9. Nonanoic acid (C₉) and dodecanoic acid (C₁₂) concentration by percentage weight in PVP/RS100 fibres. Mean +/- SD shown for nonanoic acid (n=9) and dodecanoic acid (n=7).

5.5 Electrospun patches containing fatty acids inhibit *C. albicans* yeast growth

Electrospun patches containing fatty acids (C₅-C₁₂) were placed on *C. albicans* streaked agar plates and the inhibition zones were measured in a similar manner to the disc diffusion assay previously described in section 2.4.7. As shown in Figure 5.10 PCL patches showed no inhibition zones at all for patches containing butanoic (C₅) to octanoic (C₈) fatty acids, with levels similar to those for PCL patches containing no fatty acid (Figure 5.10.A). For nonanoic (C₉) to dodecanoic acid (C₁₂) an inhibition zone around the PCL patch was observed (Figure 5.10.B&C) where C₉ displayed the most significant difference compared to a plain PCL patch and many of the other fatty acids tested. Decanoic (C₁₀) and undecanoic (C₁₁) acids also displayed marked zones of inhibition that were not significantly different from those observed with C₉ (Figure 5.10A). Interestingly, PVP/RS100 patches containing no fatty acid displayed a small zone of inhibition (Figure 5.10.D&E) that may be related to the more hydrophilic PVP/RS100 patches almost instantaneously shrinking on placement of the patches on the moist, *C. albicans* streaked, agar plates. Similar observations were found for PVP/RS100 patches containing C₅ – C₇ (Figure 5.10.D). Only patches containing C₈ and C₉

were significantly different ($p \leq 0.001$) to the plain PVP/RS100 patch. Some of the PVP/RS100 patches containing fatty acid shrank more than the plain PVP/RS100 patch (Figure 5.10 E & F).

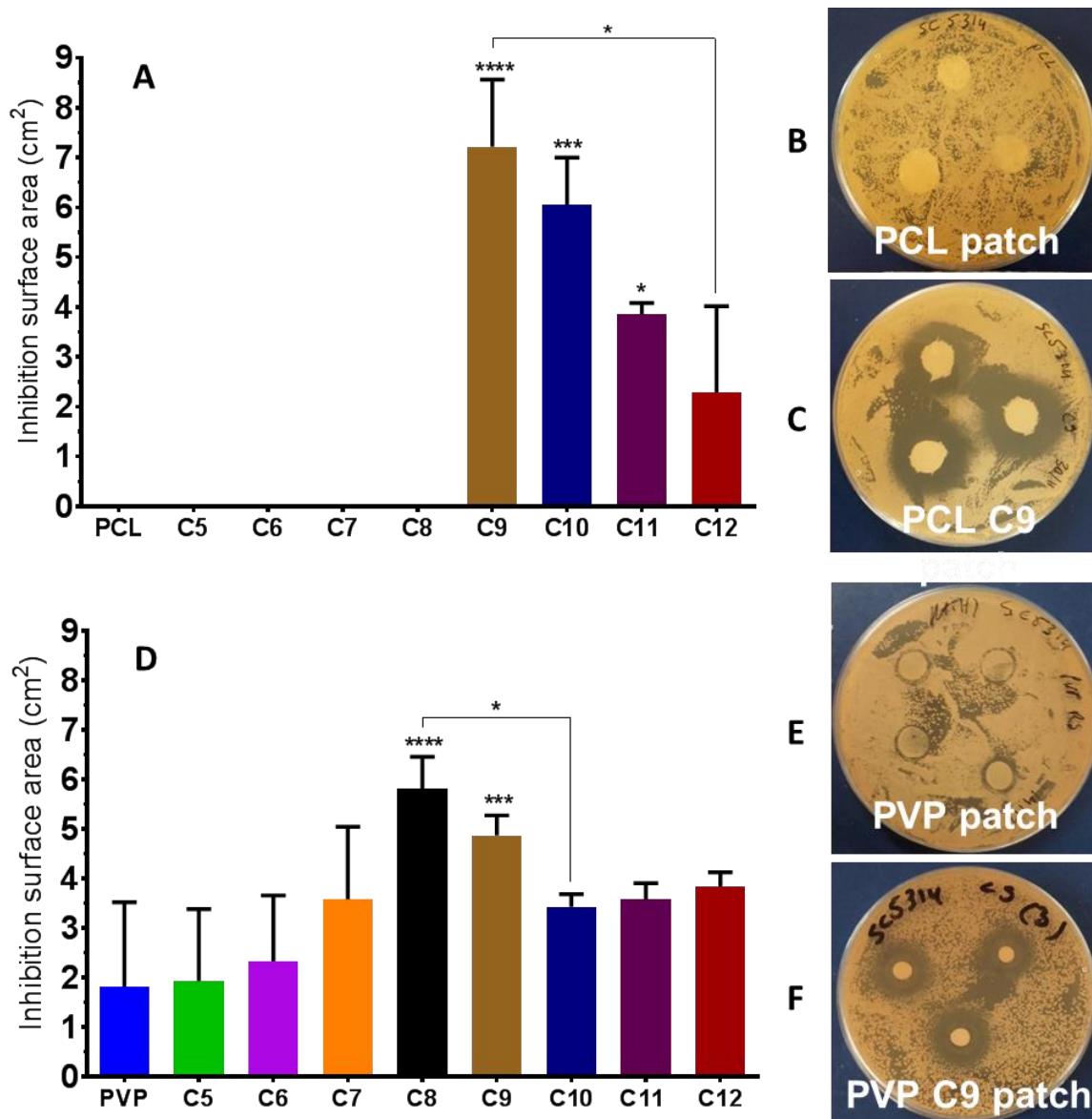


Figure 5.10. Inhibition zone surface areas on *C. albicans* strain SC5314 for fatty acids incorporated in A-C) PCL electrospun patches and D-F) PVP/RS100 electrospun patches. Mean +/- SD shown (n=3). * $p < 0.05$; ** $p < 0.01$, *** $p < 0.001$, **** $p < 0.0001$, where the p value over the SD bar is compared to the plain patch system (PCL or PVP).

SEM images of the PCL patches that were removed from the agar plate and turned upside down are shown in Figure 5.11. In these representative images *C. albicans* yeast cells are present between the fibres. Fewer yeast cells were found on patches containing nonanoic (C9) and decanoic acid (C10), yet this observation was from a single biological experiment (n=1), although three individual patches were analysed. The difference in hydrophilicity between the PVP/RS100 patches in Figure 5.12 compared to the PCL patches in Figure 5.11 was clearly visible since most of the PVP/RS100 patches had lost their fibrous structure compared to the PCL patches. *C. albicans* yeast cells were observed only on the PVP/RS100 plain patches, although due to the structure of these patches any yeast cells that may have been present could have been removed during the SEM processing procedure.

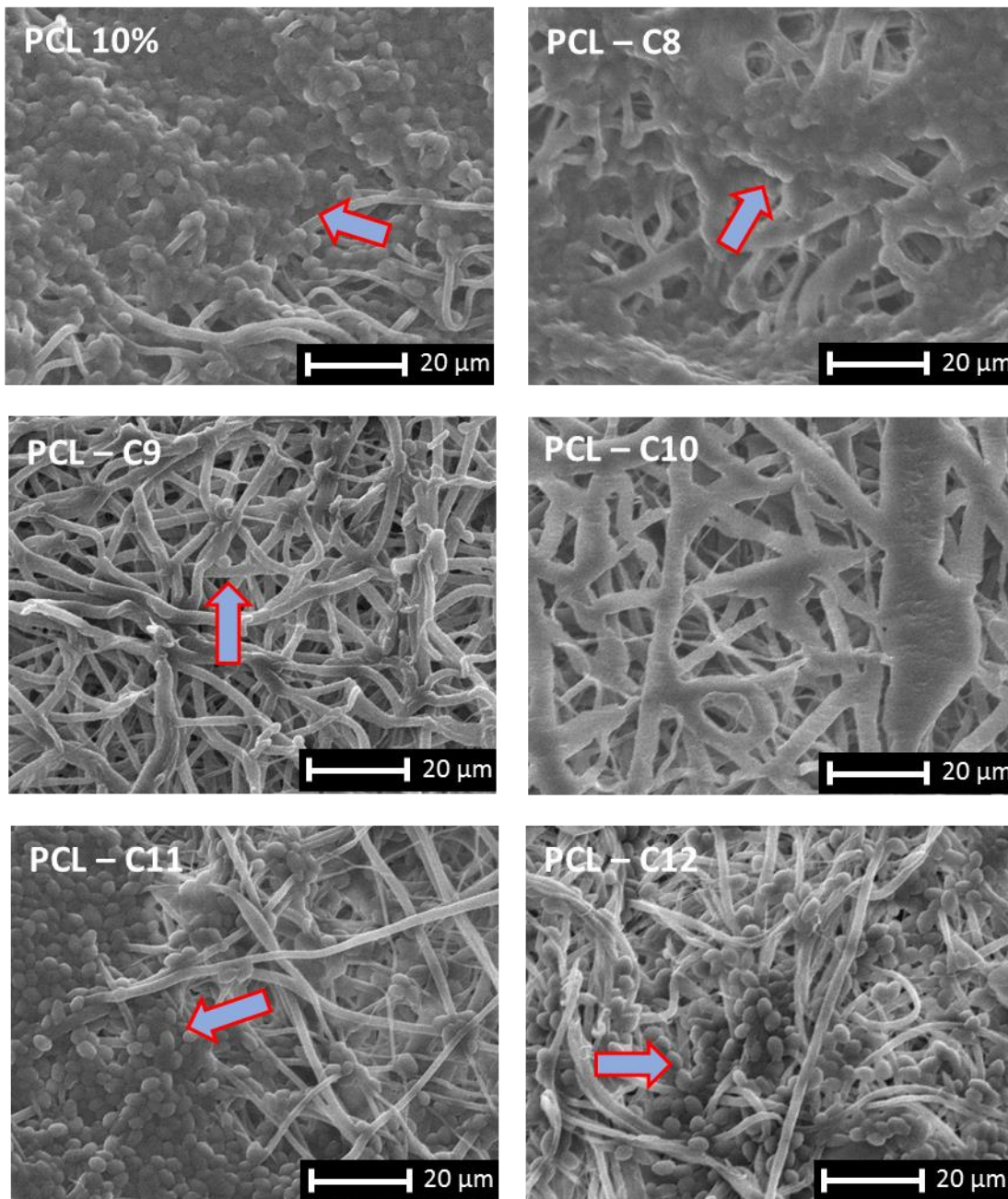


Figure 5.11. 10% PCL electrospun patches containing octanoic acid (C8) to dodecanoic acid (C12) removed from agar plates streaked with *C. albicans* after 18 hour.

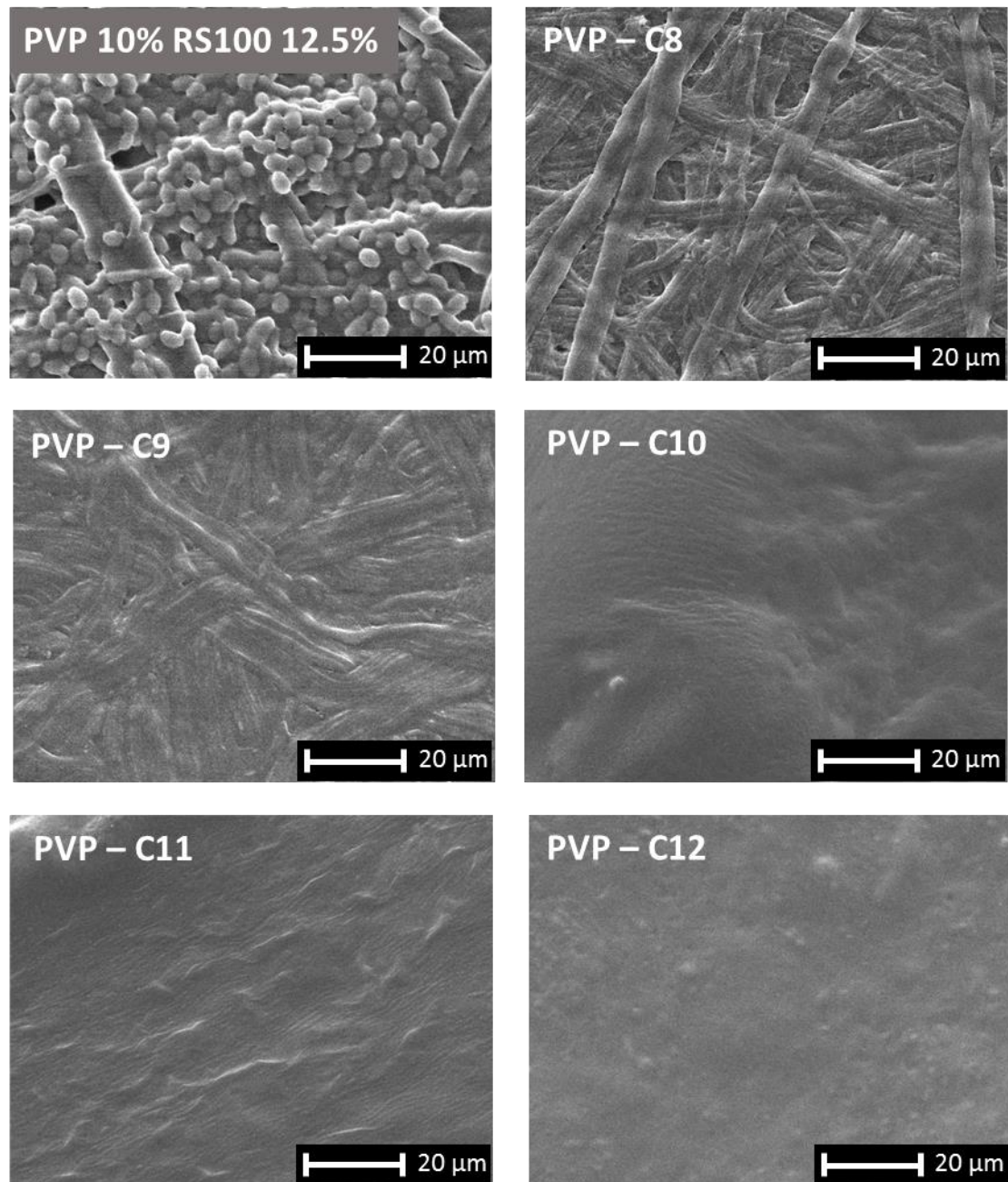


Figure 5.12. 10% PVP and 12.5% RS100 electrospun patches containing octanoic acid (C8) to dodecanoic acid (C12) removed from agar plates streaked with *C. albicans* after 18 hours.

5.6 Electrospun patches containing fatty acids reduce metabolic activity of *C. albicans* biofilms

PCL and PVP/RS100 electrospun patches with the inclusion of fatty acids were now tested on pre-existing *C. albicans* biofilms for both SC5314 (section A) and CAR17 (section B) strains, as shown in Figures 5.13 and 5.14. For both PCL and PVP/RS100 electrospun patches decanoic (C10), undecanoic (C11) and dodecanoic (C12) acids displayed the greatest effect on metabolic activity/viability on both SC5314 (Figure 5.13 & 5.14 A) and CAR17 (Figure 5.13 & 5.14 B) biofilms. Nonanoic acid (C9) also showed good biofilm killing from both electrospun polymer patches, more so on CAR17 than SC5314. The PCL patches displayed no significant difference on biofilm viability compared to media alone, labelled 'Blank' in Figure 5.13. However, the addition of PVP/RS100 patches without fatty acid to the CAR17 biofilm appeared to reduce the biofilm viability (Figure 5.14.B), although this was not statistically significant ($p = 0.7004$). The reason as to why this occurred on three separately run experiments for these patches on only this *C. albicans* strain was not established.

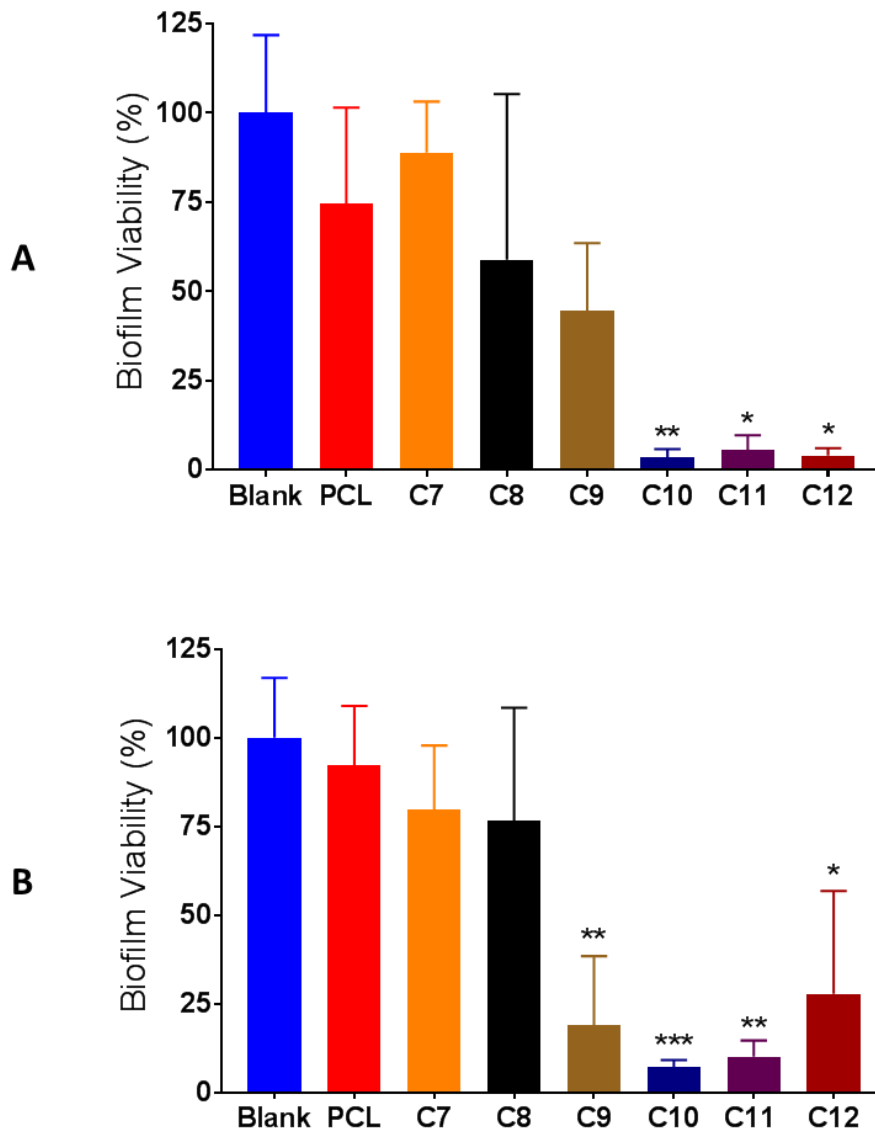


Figure 5.13. Biofilm viability of *C. albicans* strains A) SC5314 and B) CAR17 when PCL electrospun patches containing fatty acids heptanoic acid (C7) to dodecanoic acid (C12) were placed on the biofilm. Mean \pm SD (n=3). Kruskal-Wallis non-parametric test was used to determine significant differences compared to the plain PCL patch (*p<0.05; **p<0.01, ***p<0.001). Statistical differences between the fatty acids are not shown.

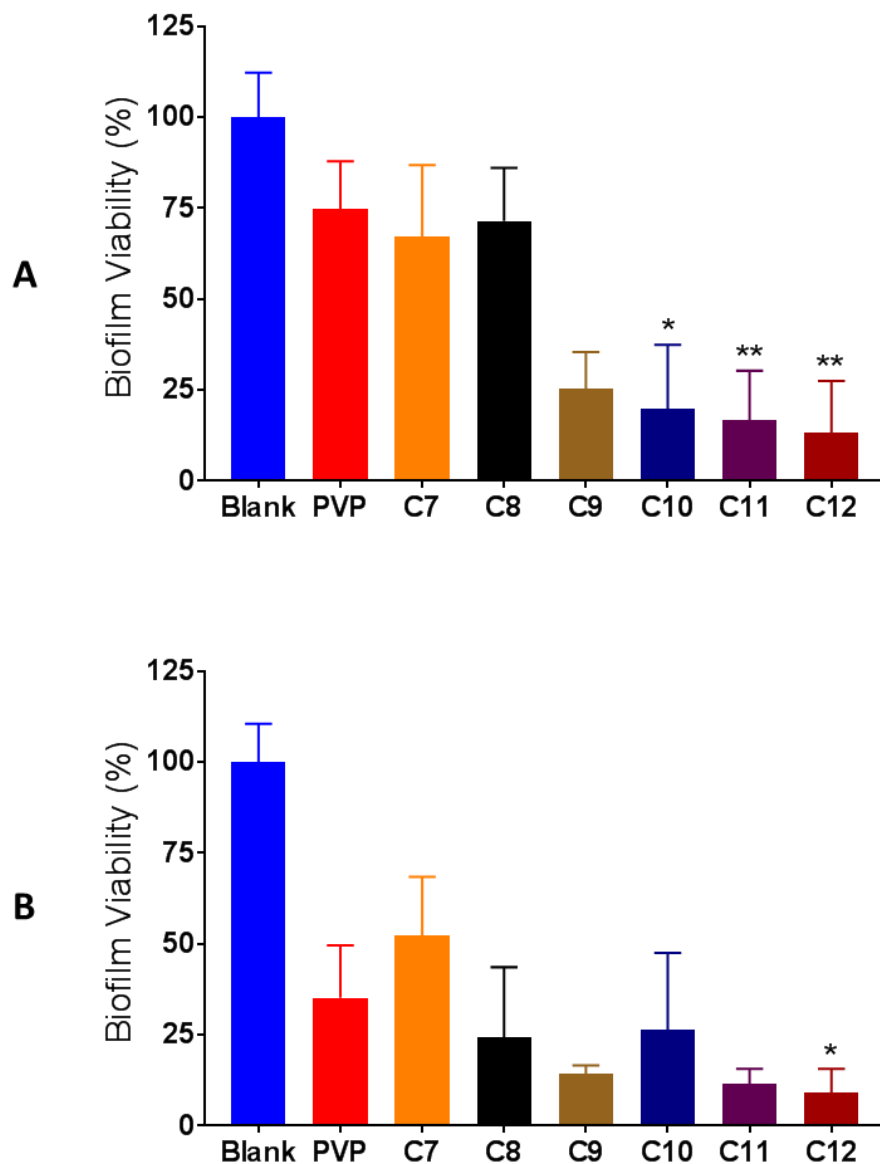


Figure 5.14. Biofilm viability of *C. albicans* strains A) SC5314 and B) CAR17 when PVP/RS100 electrospun patches containing fatty acids heptanoic acid (C7) to dodecanoic acid (C12) are placed on the biofilm (plain PVP/RS100 patch labelled at PVP). Mean +/- SD (n=3). Kruskal-Wallis non-parametric test was used to determine significant differences compared to the plain PVP/RS100 patch (*p<0.05; **p<0.01, ***p<0.001). Statistical differences between the fatty acids are not shown.

5.7 Toxicity of fatty acid solutions on oral keratinocytes

The two most potent fatty acids, nonanoic acid (C9) and dodecanoic acid (C12), for *C. albicans* yeast and biofilm inhibition were selected to evaluate their cytotoxic effect on a monolayer of oral keratinocytes. Nonanoic acid (C9) was found to be three times less cytotoxic than dodecanoic acid (C12), as shown by the IC_{50} values in Figure 5.15. The mean IC_{50} value for oral keratinocyte monolayers was seven times smaller for nonanoic acid (C9), and four times smaller for dodecanoic acid (C12), than for *C. albicans* biofilm (Table 5.1). These data suggest that the concentrations used to kill *C. albicans* would also be toxic to oral keratinocytes, with no therapeutic window established.

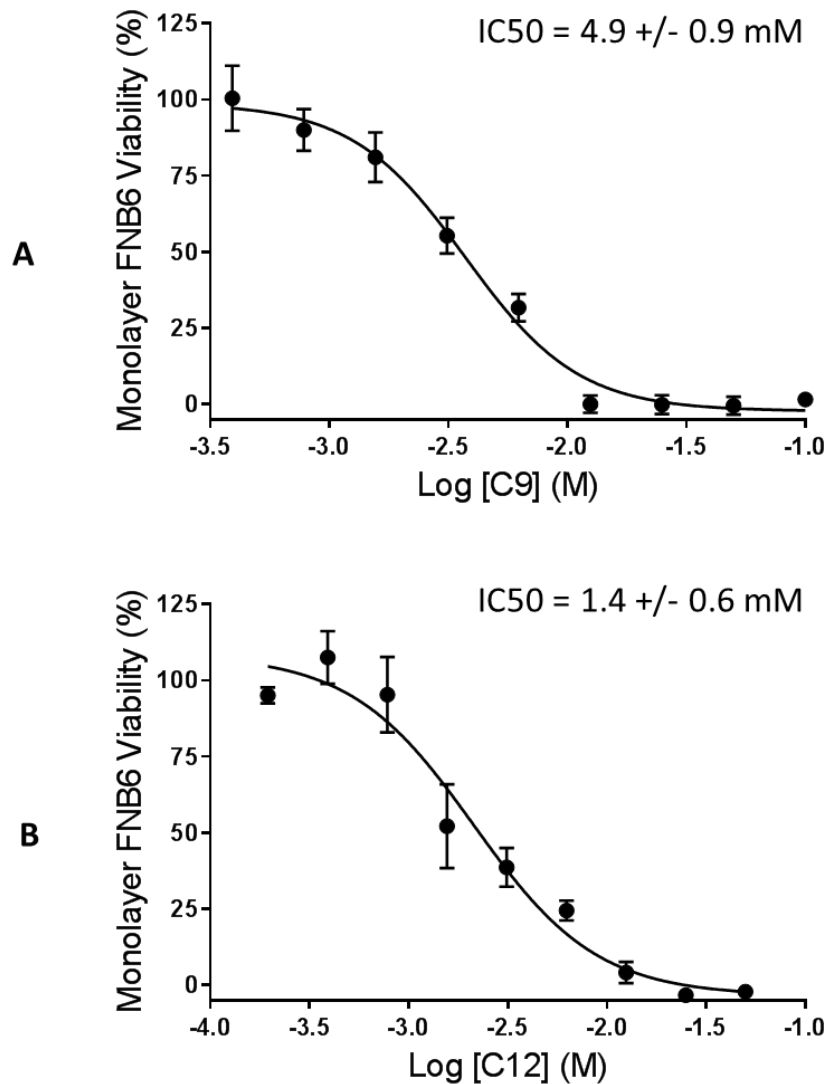


Figure 5.15. Cytotoxicity of A) nonanoic acid [C9] and B) dodecanoic acid [C12] on FNB6 immortalised oral keratinocyte monolayers using a metabolic activity MTT assay. Graphs shown are the mean \pm SD for 6 wells of one representative experiment. The IC₅₀ value is given in the top right of the graph (mean \pm SD) for $n=3$ independent experiments

5.8 Application of fatty acid containing electrospun patches on 3D oral mucosa tissue models

Fatty acids C9 and C12 were shown to be toxic to monolayers of oral keratinocytes cells at the therapeutic dose required to kill *C. albicans* biofilms. However, a one cell thick monolayer does not take into account the complex and multi-layered structure of the oral mucosal

tissue. It is well known that toxicity data obtained in 2D cell culture models does not reflect toxicity in 3D or native tissue [234], with levels of toxicity always greater for monolayers compared to 3D tissue when a substance is applied at the same concentration [235]. Therefore, 3D *in vitro* models of the oral mucosa that better represent the native oral tissue structure were used. The effects of electrospun patches, either without or containing nonanoic or dodecanoic acid were used on this model. The mucosal model consists of a stratified squamous epithelium that are several cell layers thick, with epithelial desquamation occurring at the most superficial layers, and a fibroblast-populated collagen lamina propria (Figure 5.16.A) and uninfected models were used as controls. Addition of a PVP/RS100 plain electrospun patch or a patch containing nonanoic acid (Figure 5.16.A), did not alter the epithelium thickness on uninfected tissue, whereas addition of the dodecanoic acid patch visibly reduced the epithelium thickness and the presence of a crystalline structure was observed on the surface of the epithelium that may be the fatty acid (Figure 5.16.B). Electrospun patches used weighed ~5 mg suggesting that ~600 µg (3.8 µmol) of nonanoic acid and 1100 µg (5.5 µmol) of dodecanoic acid were present within the patches. If this entire fatty acid content releases into 100 µL of media at the site of patch application, the concentration of nonanoic acid is ~8 times more than on the IC₅₀ concentration on the keratinocyte monolayers (which was 4.9 mM) and ~39 times more than that of dodecanoic acid (1.4 mM). It was assumed that the majority of fatty acid from the patches would be released over the 18 h treatment period.

C. albicans was grown on the surface of the epithelium over 4 h prior to the application of the electrospun patches to obtain a biofilm on the epithelium surface in order to represent oral candidiasis. *Candida*, (coloured purple by PAS staining) had formed hyphae and was observed invading into the epithelium as occurs clinically. However, it was noted that *C. albicans* biofilm was not widely spread across the epithelium surface of the model and was mainly found in dips along the epithelium surface. This indicates that the method required optimisation, perhaps using a greater volume of media in which the *C. albicans* would be

suspended on the epithelium surface. The epithelium thickness was drastically reduced for all *C. albicans*-infected models, although fewer *C. albicans* cells were detected with the application of the electrospun patches (Figure 5.16.G&H). This was however also true for the models with plain patches applied (Figure 5.16.F).

Keratinocyte cell lysis was measured using an LDH assay. OD readings were very high for all conditions, including models receiving medium alone (Figure 5.17). OD values were approximately eight times greater than expected when compared to similar experiments in the literature [236], suggesting that for some reason cell lysis was occurring for all conditions. Only two conditions were markedly different to the untreated tissue model; namely there was a reduction in cell lysis with the application of the plain electrospun patch on the tissue without any *Candida* and an increased LDH response when the nonanoic acid patch was applied on the tissue without *Candida*. Although, it must be noted that due to time constraints this experiment was performed only once and so it is difficult to come to any firm conclusions without performing more optimised, repeat experiments.

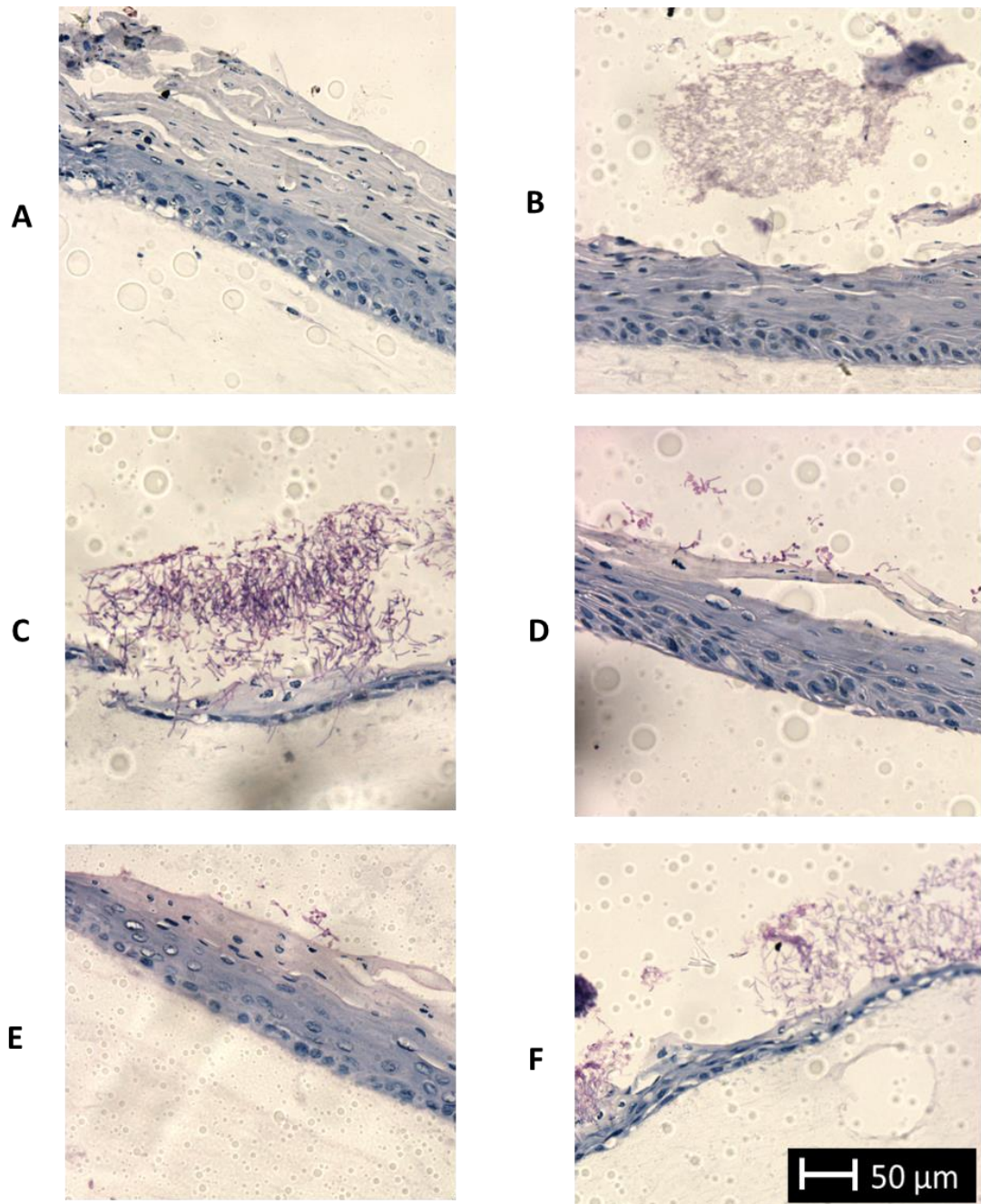


Figure 5.16. Representative light microscope images of PAS stained 3D oral mucosal models with the following treatments: A) nonanoic acid patch applied, B) dodecanoic acid patch applied, C) *C. albicans* with media only, D) *C. albicans* with plain patch applied, E) *C. albicans* with nonanoic acid patch applied, F) *C. albicans* with dodecanoic acid patch applied. The scale for all images are as shown in H.

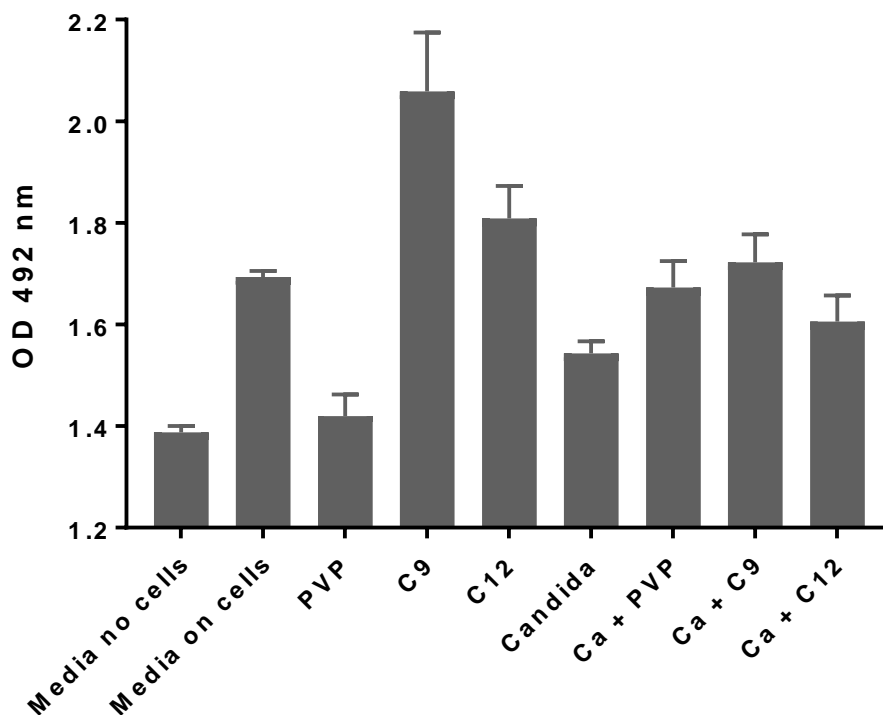


Figure 5.17. Lactate dehydrogenase assay of media surrounding 3D oral mucosa models with different conditions applied to the models. 'PVP' is the plain PVP/RS100 electrospun patch applied to the models and labels 'C9' and 'C12' are nonanoic and dodecanoic acid containing electrospun patches, respectively. Label 'Ca' is short for *Candida*, where *C. albicans* strain SC5314 was applied to the surface of the epithelium. Mean \pm SD are of three technical repeats from n=1 biological experiment.

5.9 Discussion

The aim of this chapter was to determine the capability of the electrospun patches as an antifungal vehicle to treat oral candidiasis. This condition was chosen as oral fungal infections are relatively common amongst mainly immuno-compromised individuals and is also a side-effect following steroidal treatment for oral lichen planus, which was the original electrospun device application fabricated by the research group at the School of Clinical Dentistry in Sheffield [1]. Two *in vitro* methods to test fatty acids incorporated into electrospun patches against candidiasis were employed. First *C. albicans* was streaked on agar plates to test the ability of fatty acids to inhibit fungal cell growth and secondly *C. albicans* was grown into a biofilm to test the ability of fatty acids in killing an already existing biofilm. *C. albicans* yeast form tends to be associated with the commensal organism that occurs in approximately 50% of the adult healthy population [29]. In contrast, the biofilm form contains a mixture of yeast and hyphae where the latter are associated with penetration and invasion into the oral epithelium causing tissue damage and disease [30]. Therefore, testing fatty acids on both of these forms of *C. albicans* was of interest.

In the last few decades there has been a rise in antifungal resistance and hence testing for alternative therapies to common antifungal drugs is important. The reason for choosing short- to medium-chain saturated fatty acids was as they have known antimicrobial and antifungal properties [45,237]. Additionally, a number of bacteria use short-chain fatty acids as their own antimicrobial defense mechanism against other organisms [52]. However, the majority of earlier studies were performed using tests in broth culture, which are not clinically relevant as this method does not resemble *C. albicans* growth or biofilm formation in the oral cavity [45,237]. Other benefits of using fatty acids as the therapeutic agent are their low production cost and that they are known to be permeation enhancers and aid penetration of other therapeutic molecules into tissues due to their lipophilicity [51].

As well as comparing the antifungal potential of a range of short- to medium-chain fatty acids on both yeast and biofilm states of *C. albicans*, it is important to test inhibition on a number of

C. albicans strains as some are likely to be less susceptible to inhibition than others. Tests were therefore performed on two wild types of *C. albicans*, SC5314 and BWP17, as well as a clinical isolate, CAR17, known to be resistant to azole drugs. On both wild type strains tested the fatty acids in solution showed a similar pattern of inhibition. The most notable difference in results between the wild type strains was that SC5314 was more susceptible to the positive controls, fluconazole and miconazole, than BWP17. For both strains octanoic (C8) and nonanoic (C9) acid showed the greatest inhibition by disc diffusion test. Previous studies showed that only even numbered carbon chain length fatty acids were effective against *C. albicans* [44–47]. This is the first study to show that nonanoic acid displays inhibitory capabilities on *C. albicans*. Additionally, no previously published agar disc diffusion results were found for short- to medium-chain fatty acids on *C. albicans*. Earlier studies using fatty acids as an antifungal measured *C. albicans* yeast inhibition in broth dilutions using a number of different *C. albicans* strains, either recording the minimum inhibitory concentration (MIC) by the turbidity of the broth or by diluting the broth and counting CFU/mL on agar plates [44–47]. In every one of these earlier studies decanoic acid had the best inhibition on the yeast *C. albicans* cells in broth. Huang *et al* showed that hexanoic, octanoic and dodecanoic acid all gave similar inhibition results [45], whilst Kabara *et al.* [47] and Bergsson *et al.* [44] reported that octanoic acid had very low inhibitory responses on *C. albicans* yeast cells in broth. Hayama *et al.* [46] reported the MIC of octanoic acid, decanoic acid and dodecanoic acid as 34.7 mM, 29.0 mM, and 49.9 mM on a *C. albicans* clinical isolate strain in broth culture. Therefore, given the larger inhibition zone for octanoic acid compared to decanoic acid in this study (Figure 5.1), it would suggest that octanoic acid diffuses better on the agar plates than decanoic acid. This is likely as the water solubility of octanoic acid is around 10-fold higher than for decanoic acid and as the carbon chain length of the fatty acid increases the water solubility decreases further. The fatty acids were all prepared in DMSO prior to adding them to filter discs, which would also aid the elution of the fatty acid into the agar environment as DMSO is miscible in water.

Fluconazole resistance of *Candida* strains (of different species) has been previously defined using an agar disc diffusion method, where an inhibition diameter smaller than 14 mm with an MIC greater than 32 µg/mL was termed resistant by two separate studies that acquired large data sets (one study used 250 strains and another 1407 strains) [238,239]. In comparison the concentration of fluconazole used on the clinical isolate CAR17 in this thesis was 245 µg/mL and the mean inhibition zone was 8.4 mm (Figure 5.1), showing that this strain was very resistant to fluconazole. Additionally, fluconazole and miconazole had non-significant inhibition zones on CAR17 and were similar to that of the negative control DMSO. The fatty acids, however, had similarly high inhibition zones as on the wild type strains, with octanoic and nonanoic acid again having the largest inhibition zones on the agar plate, along with heptanoic acid (although the standard deviation was very large for heptanoic acid). This shows for the first time that medium-chain saturated fatty acids have potential as an alternative therapy for azole-resistant *Candida* strains.

Metabolic tests conducted on the pre-existing *C. albicans* biofilm showed a different fatty acid to be the most toxic to the hyphae *C. albicans* cells (Figure 5.2) compared to on the yeast cells in the agar disc diffusion tests (Figure 5.1). Here, dodecanoic acid (C12) showed the best biofilm inhibition compared to the other fatty acids with an IC₅₀ of 4.7 mM. As the carbon chain length of the fatty acid increases the metabolic activity of the biofilm is reduced for the same concentration of fatty acid. Only one previous study reported hyphal IC₈₀ for fatty acids octanoic, decanoic and dodecanoic acid at 205 µM, 16.7 µM and 61.0 µM respectively [46]. These values are surprisingly low and very different to the IC₅₀ values obtained in this study. The main reason for this large difference in inhibitory concentration may be that a different strain of *C. albicans* was used, however, substantial differences in the methodology are also apparent, where far fewer CFU were used (5×10^3 compared to 1×10^5 cells/mL used in this study) and the IC₈₀ was measured using a crystal violet staining assay, where the MIC was defined as a reduction in biofilm growth by 80% measured using the optical density (OD) compared to the OD of a non-treated biofilm. In crystal violet staining the entire biomass is

stained (including live cells, dead cells and extracellular mass), compared to only the viable cells by XTT assay used in this thesis. A study which has previously compared the two methods to study *C. albicans* biofilm growth found that far better experimental reproducibility was achieved using the XTT method compared to crystal violet staining [240].

Compared to the yeast cells in the agar disc diffusion test the biofilm contains a variety of structures of the polymorphic fungus *C. albicans*, where both yeast and hyphae cells are present, as can be observed in the live/dead stain images (Figure 5.3). In the biofilm the cells also excrete extracellular matrix and glycoproteins to make a denser, more invasive structure that is much more resistant to therapy. It was observed that the biofilm was less thick after fatty acids at 50 mM had been applied to the biofilm, as there was a reduction in the live (green) area of cells in the images, and more dead (red) cells present as well. With the application of dodecanoic acid a greater number of dead cells were present compared to when nonanoic acid was applied at the same concentration, as seen visually in the live/dead stain images. This data confirms the metabolic assay data and shows that actual cell death and not just a decrease in metabolic activity occurred. Previous literature has analysed the mechanism in which fatty acids kill the *C. albicans* cells, where a TEM image of a yeast candida cell to which decanoic acid (C10) had been applied showed that the whole cytoplasm was disrupted, although no difference to the size of the cell wall was observed [44]. This is very similar to the observations made by TEM for *C. albicans* cells treated with miconazole, where several fat globules forming within the cytoplasm and vesicles on the outer cell wall theorised to be remnants of cytoplasm were also shown [241]. Previous studies on *C. albicans* virulence and the gene expression responsible for the yeast to hyphae change also give information on how the application of fatty acids may lead to fungal cell death. There are a number of hyphae-associated genes that allow the *Candida* cells to be transformed from yeast to hyphae cells, one of which is the hyphal wall protein HWP1 [242]. Hyphae cells also release adhesins and cell surface glycoproteins so that they can adhere to a variety of surfaces and to other microorganisms, of which HWP1 is also one. Reduced

HWP1 expression upon addition of decanoic acid has previously been determined, along with the reduction of another glycolipid, INO1, which is also related to *C. albicans* virulence [52]. Genes related to azole resistance in *C. albicans* strains have been previously reported to have an upregulation of INO1 proteins [243]. Therefore, using antifungals such as fatty acids to downregulate proteins related to hyphal switching and which have an increased presence in azole resistant strains are desirable.

No previous literature on incorporating medium-chain fatty acids into electrospun patches for medical purposes has been reported, although a number of papers have incorporated lauric acid (C12) into electrospun polymer fibres to phase change the polymer material for thermal energy storing uses [244,245]. A more related study to the work in this thesis incorporated monolaurin, a monoester formed of glycerol and lauric acid, into shellac (a resin) electrospun fibres to test antimicrobial properties on *C. albicans*, *Staphylococcus aureus* and *Escherichia coli* [246]. Another research group has also incorporated the antifungal drug clotrimazole into electrospun patches, which successfully eradicated *C. albicans* viability within a few hours in broth dilutions [101,103,117]. Therefore, given the potential of medium-chain saturated fatty acids as an antifungal even for azole drug resistant strains of *Candida*, and of electrospun patches as a drug delivery vehicle, these two systems were combined and researched in the second half of this chapter.

Heptanoic to dodecanoic acid were electrospun into both PCL and PVP/RS100 fibres, where 0.2 M of the respective fatty acids were incorporated into the polymer dope solution. Although both the PCL (Figure 5.4) and the PVP/RS100 fibres (Figure 5.5) look slightly flatter with the incorporation of fatty acids, the morphology of the PCL fatty acid fibres look more different than the PVP/RS100 fatty acid fibres when compared to the plain patches with a greater range of thin and thick fibres. This would suggest that the material dope properties may be more different when fatty acids were added to the PCL dope than to the PVP/RS100 dope, although there was also more variation in the plain PCL dope properties as observed in chapter 3. As the fatty acids have different degrees of solubility and volatility it was

expected that some fatty acid might be lost in the electrospinning process. Therefore, ^1H NMR spectroscopy data was obtained to find the fatty acid concentration in PCL, whereas GC-MS was used to detect the amount of fatty acid present in the PVP/RS100 fibres. The less volatile fatty acids, decanoic to dodecanoic acid, which were solids prior to being dissolved into the polymer dope, were present in the PCL fibres at a similar wt% as in the polymer dope. However, the more volatile fatty acids with shorter carbon-chain lengths, heptanoic to nonanoic acid, were barely present in the PCL fibres. In the PVP/RS100 fibres more nonanoic acid was present than in the PCL fibres, however more dodecanoic acid was present in the PCL fibres. Reasons for this were not explored, however it is assumed that the different chain-length fatty acids interact differently with the polymer complexes. Hydrogen bonding between the (-OH) group in lauric acid and (C=O) in PLGA (a bond which is also present in PCL, but not in PVP) has previously been theorised using FTIR spectroscopy data to explain the plastizing effects that occurred when the polymer and fatty acid were combined to manufacture an electrospun patch [54]. Both the PCL and PVP/RS100 electrospun patches in this study also became noticeably stiffer with the addition of the medium chain fatty acids, also suggesting plasticisation occurring.

The agar disc diffusion tests to measure the inhibition of *C. albicans* growth were repeated for the fatty acid containing electrospun patches on strain SC5314. Although PCL patches did not contain much nonanoic acid from the NMR results, they still produced the greatest inhibition zone on the *C. albicans* lawn (Figure 5.10). This would indicate that nonanoic acid is far more toxic to the *C. albicans* yeast cells, even at lower concentrations, than the other fatty acids tested. PVP/RS100 patches containing octanoic and nonanoic acid displayed the most significant inhibition compared to the plain patches, despite the GC-MS results also showing less nonanoic acid than dodecanoic acid to have been retained in the patches. The plain PVP/RS100 patches also inhibited the *C. albicans* growth in the disc diffusion assay, which was likely due to the hydrophilicity of these patches. The difference in hydrophilicity between the PCL and PVP/RS100 patches was shown by comparing SEM images after the

patches had been removed from the *C. albicans* streaked agar plates, where the PVP/RS100 patches did not retain clear fibrous structure compared to the PCL fibres. The PCL patch containing nonanoic and decanoic acid had the fewest yeast cells visible among the fibres, whereas on the PVP/RS100 patches yeast cells were only visible on the plain patch. This may however be related to the loss in fibrous structure and the patches therefore not retaining the yeast cells during the SEM processing procedure. For PVP/RS100 patches with octanoic acid and nonanoic acid the outline of the fibres could still be determined, whereas no fibre outlines are visible for patches that contained decanoic to dodecanoic acid. This is likely to be related to the increase in lipophilicity of the higher end fatty acids, which have been reported on databases for chemical substances and for metabolites as logP [247,248].

The biofilm viability tests with electrospun patches containing fatty acids were performed on strains SC5314 and CAR17 (Figure 5.13 and 5.14). For both the PCL and PVP/RS100 patches on both strains decanoic to dodecanoic acid gave the best reduction in biofilm viability, similar as for the fatty acid solution only results. The patches containing nonanoic acid also showed significant inhibition, apart from in PCL on strain SC5314. The data in chapter 5.6 therefore shows that electrospun patches incorporating fatty acids could be used to treat *C. albicans* biofilms.

The two fatty acids that were most potent against the yeast and hyphae *C. albicans* cells were selected to test their cytotoxicity on a monolayer of oral keratinocytes (FNB6 cell line). It was shown that dodecanoic acid was more toxic to the cells than nonanoic acid, as was the case for the *C. albicans* biofilms (Figure 5.2). The IC₅₀ values were similar to previous values reported for a human endothelial cell line (EA.hy 926), where an IC₅₀ of 1.72 mM for decanoic acid and 2.95 mM for lauric acid were recorded [49]. The IC₅₀ for the two fatty acids were lower on the oral keratinocytes than on *C. albicans* biofilm and therefore from this data no therapeutic window could be established, especially as an IC₉₀ of fatty acid to make sure that the majority of the *Candida* would be killed is desired. The IC₉₀ was around 10 mM for dodecanoic acid to kill *C. albicans* and the IC₉₀ for the monolayer of oral keratinocytes was a

similar concentration. The reason for the *C. albicans* cell being more resistant to treatment than an oral keratinocyte can be related to the difference in the cell wall structures of the respective cells. A *Candida* cell wall is mainly composed of a thick layer of chitin with several layers of mainly glycosylated and mannosylated proteins on the cell surface creating a considerable barrier for the fatty acids to penetrate [249]. In comparison, oral keratinocytes have just a plasma membrane as a biological barrier for the fatty acids to pass into the cell and to disrupt the cytoplasm leading to cell death. There are several limitations in using a monolayer of keratinocytes as an *in vitro* cytotoxicity test. Cell monolayers are one cell in thickness and so do not replicate the oral epithelium tissue structure, thickness, mechanical or biomechanical cues. In monolayer culture the keratinocytes have basal and stem cell features and are all actively proliferating, whereas oral mucosa is a stratified epithelium with multiple cell layers where only the most basolateral basal cells proliferate. In a 2D *in vitro* model interaction with the other, non-proliferating cell layers is not replicated. It is also difficult to model the flow of saliva and the presence of other excipients on the surface of the oral mucosa that create additional therapeutic barriers. Therefore on multi-layered oral mucosa and even in a 3D *in vitro* tissue model an increase in inhibitory concentration of the fatty acid on the oral mucosal tissue would be expected.

Initial tests on 3D oral mucosa models were performed to replicate oral candidiasis so as to test the antifungal electrospun patches on this model. *C. albicans* biofilms have previously been successfully grown and characterised on 3D oral mucosa models [236,250]. The oral mucosa models in this thesis were infected as described by Yadev *et al.* [236], however an even biofilm growth along the surface of the epithelium was not achieved. For this reason a modification of the Yadev *et al.* [236] method, could be used by applying a greater volume of *C. albicans* to the model surface in the infection stage to try and obtain a more even *C. albicans* biofilm across the surface of the epithelium. An alternative method was described by Morse *et al.* [250] where the biofilm was first grown separately in acrylic coupons for several days then the coupons were applied to the oral mucosal model by inverting the coupon onto

the surface of the model and leaving it for 12 hours. This produced good biofilm growth and biofilm invasion into the model, however the coupon was only carefully removed post-infection and the model was straight processed for histology. Therefore, this method could be difficult to replicate as the electrospun patches also need to be applied to the infected model over several hours. Another issue with the initial pilot study was the high concentration of fatty acid within the electrospun patches. Future experiments would focus on the dodecanoic acid electrospun patches as the difference in toxicity between the *Candida* and oral keratinocytes was less than when using nonanoic acid (four fold difference versus a seven fold difference in IC_{50}) and as dodecanoic acid was the most potent fatty acid on the biofilm experiments. Testing patches containing between 0.5 μmol and 1 μmol dodecanoic acid would also optimise experimental conditions in future experiments. One μmol dodecanoic acid in 100 μL of solution (10 mM) would kill around 90% of the *C. albicans* biofilm, but would also be toxic to the oral keratinocytes according to data presented in this chapter. From table 5.1 the mean IC_{50} of dodecanoic acid for *C. albicans* was 4.7 mM, which is however four times the mean IC_{50} on the oral keratinocytes. Therefore, this concentration would be toxic to the *C. albicans* cells but much less toxic to the oral mucosa tissue model than for oral keratinocyte monolayers.

Taken together the data in this chapter suggests that medium-chain saturated fatty acids have potential as an antifungal agent to inhibit *C. albicans* yeast or biofilm. Octanoic and nonanoic acid were most suited as a preventative for oral candidiasis growth and dodecanoic acid to treat an already existing biofilm of *Candida*. These fatty acids were also shown to have similar inhibition on an azole resistant strain of *C. albicans*, which is very promising given the rise in antifungal resistance. Additionally, the medium-chain fatty acids were successfully electrospun into patches and had similar inhibitory responses as for the fatty acid solutions. An electrospun patch would therefore be an ideal vehicle to deliver the fatty acids directly to the locally infected candidiasis sites on the oral mucosa. Further research on the toxicity of the fatty acids on mammalian tissue needs to be conducted, with suggested *in*

vitro testing on 3D models, so that a therapeutic dose can be determined without it being harmful to tissue.

6. Conclusions

As highlighted in the literature review, there is an existent clinical need in oral medicine to improve local drug delivery to oral diseases with improved drug retention at the disease site. This is challenging given the moist and malleable mucosal tissue in the oral cavity. Therefore, the aim of this thesis, as presented in section 1.10, was to evaluate an electrospun polymer patch as a drug delivery vehicle for direct treatment of oral diseases. The electrospun patch system was successfully developed, manufactured and analysed for such purposes. Specific objectives for this project were determined in section 1.10 and the main conclusions of the research are presented here:

1. In chapter 3 two main polymer systems for electrospinning a drug delivery device were chosen and the polymer solution and resulting electrospun patches were characterised. PVP in ethanol and PCL in DCM/DMF (93/7 w/w%) could be electrospun well, especially at 10 – 15% (w/w) of the polymer in solvent, to form fibrous mats with some variations in fibre diameter. Differences in material solution properties, such as the viscosity, surface tension and conductivity, could be related back to the difference in fibre diameters and morphologies observed at different polymer concentrations and between the two polymer systems. The main difference between the PVP and PCL solutions was that the mean polymer solution viscosity and the mean fibre diameters for PVP were less than for PCL at the same concentration of polymer. The higher surface tension and lower conductivity for PCL solutions at the same concentrations of PVP were theorised to be the reason for the less straight and more undulating PCL fibres compared to PVP fibres. RS100 and PEO particles were added to the PVP solution and successfully electrospun at 10/12.5/10% (w/w) PVP/RS100/PEO to form a less hydrophilic and mucoadhesive patch (as shown in a previously published study by another member of the research group). The PVP/RS100/PEO layer and PCL layer were molten together at 70 °C to

form a smooth PCL backing layer on the fibrous PVP layer, which should aid uni-directional drug release into tissue if an active pharmaceutical ingredient were added into the PVP fibres.

2. In chapter 4 a small drug molecule, lidocaine, was incorporated into the electrospun patch and uptake into tissue was evaluated to show the potential of the electrospun system characterised in chapter 3 as a drug delivery vehicle. Lidocaine in its base and hydrochloride salt form were incorporated into the PVP/RS100/PEO electrospun fibres at 2.9 ± 0.3 % (w/w) and 2.4 ± 0.5 % (w/w) of the dry patch, respectively. Lidocaine in both the salt and basic forms were shown by DSC to be amorphous within the electrospun fibres, where the amorphous state is known to improve drug solubility from the fibres and into tissue. A robust HPLC method to measure lidocaine concentrations in buffer, including determining the limit of quantitation, was established in section 2.3.7. It was shown that the acidic lidocaine HCl released more quickly from the electrospun fibres than lidocaine base and were shown to have around 80% and 50% of total drug content released in buffer over 1 h, respectively. Lidocaine from the lidocaine HCl containing patches was shown to release from the electrospun fibres and permeate through around 1 mm thick *ex vivo* porcine mucosa within the first 15 min and had a flux of 4.47 ± 0.16 ng cm⁻² s⁻¹. Although, lidocaine permeation from the lidocaine base electrospun patches was not detected using the same HPLC method. However, the lidocaine uptake from the electrospun patches into tissue was confirmed by MALDI-MSI, where the spatial distribution of lidocaine in buccal tissue was visualised post-release from both lidocaine HCl and lidocaine base containing patches. The time-dependent penetration of lidocaine into tissue was also clearly shown by MALDI-MSI, where lidocaine was mainly present in the epithelium layer in the first hour, however, over three hours the lidocaine was distributed in the epithelium and lamina propria. For

the condition where lidocaine was applied to the epithelium surface as a solution lidocaine was also visible in the submucosa after 3 h. Therefore, this data shows great promise for the application of electrospun patches as anaesthetic and/or analgesic vehicle of lidocaine to buccal tissue. Further validation work of the system is suggested in the following chapter.

3. In chapter 5 medium-chain saturated fatty acids were shown to have therapeutic ability in treating oral candidiasis strain *C. albicans*, including a strain resistant to common azole antifungal drugs. Octanoic (C8) and nonanoic (C9) acid were shown to have the greatest inhibition effect on *C. albicans* growth from the range of fatty acids tested, whereas dodecanoic acid (C12) was the best treatment option for an already existing biofilm of *C. albicans*. The fatty acids were incorporated into PVP/RS100 and PCL polymer dopes and electrospun into fibrous mats, where the higher carbon-chain length fatty acids (C10 and over) were better encapsulated in the PCL fibres. In the PVP/RS100 fibres only nonanoic (C9) and dodecanoic (C12) acid were tested for their encapsulation efficiency, where C12 was also better encapsulated in the fibres than C9, but not as well as in the PCL fibres. The inhibition zones on the *C. albicans* streaked agar plates were similar for the fatty acids eluting from electrospun patches as for when they were applied as solutions, showing the potential of the electrospun patches as an antifungal fatty acid delivery vehicle. Fatty acid containing electrospun patches placed on biofilms of *C. albicans* also showed decanoic (C10) to dodecanoic (C12) acids being the most potent of the fatty acids tested against the biofilms. Cytotoxicity tests on a monolayer of oral keratinocytes showed that the therapeutic concentration at which the fatty acids killed *C. albicans* was also toxic for the monolayer. However, as a monolayer is more susceptible to therapeutic treatments than live and thick oral mucosal tissue an initial study using a more physiologically relevant *C. albicans* infected 3D oral mucosal model was performed. Here, nonanoic (C9) and dodecanoic (C12) acid

containing patches on the infected 3D oral mucosal models were applied. However, this study needed further development to obtain a greater *C. albicans* infection along the epithelium surface of the mucosa model and a lower concentration electrospun patch to provide valuable and conclusive data. The necessary additional work for this study will be proposed in the next chapter. Overall, medium-chain saturated fatty acids were shown to be a good alternative antifungal therapy to treat *C. albicans* compared to current antifungal drugs, for which *C. albicans* is becoming increasingly resistant. Additionally, the use of an electrospun polymer patch was shown to be an effective delivery method for these antifungals. Combining the two systems provides a promising solution to targeting oral candidiasis locally.

In conclusion, this thesis demonstrated the development of electrospun devices for delivery of therapeutics to treat and target oral diseases. Loading of therapeutics into the electrospun fibres was demonstrated, as well as release of these therapies from the fibres in the presence of moisture or when directly applied to mucosal tissue. Both drug uptake into tissue from the electrospun system as well as disease treatment via electrospun patch was shown in this work. This suggests that electrospun drug delivery devices could be a viable alternative local delivery method for sustained treatment of oromucosal diseases, where a real clinical need to improve such treatment methods exists. For this reason further studies of the electrospun devices developed, including clinical work, are recommended as highlighted in the following chapter.

7. Future Work

The research in this thesis demonstrates the value of electrospun devices for oral drug delivery; however, some additional validation work will be recommended here:

1. The electrospinning process in this work was performed without any environmental controls, where humidity and temperature can have an effect on the electrospinning solution and resulting electrospun fibres. Therefore, one improvement, especially if such a device were to be manufactured for a commercial pharmaceutical purpose, would be to control the electrospinning environment. This could be achieved either by using a more specialised electrospinning rig or by having the rig in an environmentally controlled room.
2. As highlighted in the literature review, a multitude of other bioadhesive polymers may aid mucoadhesion of the electrospun patches. Therefore, a systematic review of such polymers could be performed, however, first a study to differentiate between the mucoadhesive strengths of electrospun systems would need to be established, especially where only small differences can be observed, which would be a large project of its own.
3. Establishing the maximum possible loading of lidocaine into the electrospun fibres may be of interest to increase the amount of lidocaine that can be delivered to tissue within the area of patch application. This would also require the experiments in chapter 4 to be repeated to observe how drug concentration changes the release rate from the patches and the permeation rate into tissue.
4. The research in chapter 4 was performed using the dual-layer electrospun patch. However, whether the backing layer does in fact aid uni-directional release and penetration of the drug into tissue was not tested due to time constraints. This may also be difficult to show using the Ussing permeation chambers as in this study, where the chambers are vertical and if the donor chamber had been filled with buffer the patch would have most likely degraded into this chamber. Therefore, using the

horizontal Franz Diffusion chambers with simulated saliva flow on the epithelium surface where the patch is applied, and taking aliquots from both the donor and receptor sides, could be one way of testing whether the backing layer does in fact aid uni-directional release. For this study a dual-layer and single-layer patch with the same drug content would need to be manufactured and the results compared.

5. In literature it has been shown via MALDI-MSI that drug penetration depth in tissue was dose-dependent [219]. As a quick response of the anaesthetic along the tissue is desirable, especially if the patches were to be used prior to dental surgery, a dose-dependent MALDI-MSI study would be interesting.
6. In this thesis it was not shown whether lidocaine was still biologically active after it was electrospun into the polymer fibres. As lidocaine functions by blocking voltage-gated sodium channels, a biological assay to show this effect could be employed. A previous study using a neuroblastoma cell line showed the functionality of the voltage-gated sodium channels using a neurotoxin (veratridine) to open these channels and a fluorescence kit to show calcium ion release once the channels were opened [25]. Applying lidocaine elutant to the cells prior to adding veratridine should dampen the fluorescence signal, indicating that fewer calcium ions were released and that therefore the voltage-gated sodium channels were blocked.
7. *In vivo* animal studies using electrospun patches with different concentrations of lidocaine would be of interest to validate the anaesthetising effect of the patches. Such studies could potentially be performed in the buccal pouches of hamsters or rabbits, as have been previously shown in literature, and the lidocaine concentration in plasma over a number of hours could be recorded [214].
8. Finding a therapeutic window in which fatty acids, such as nonanoic and dodecanoic acid, inhibit *C. albicans* growth or biofilm formation without being highly toxic to tissues in the oral cavity is required if they were to be a viable treatment option for oral candidiasis. First the *C. albicans* infected 3D oral mucosa method used in chapter 5.8 needs to be amended to obtain a more even biofilm spread across the

epithelium surface of the model. It will need to be reviewed whether this could be achieved by increasing the CFU or volume of solution added to the epithelium surface. Once the infection method has been improved an electrospun patch containing a lower concentration of dodecanoic acid should be added to the model compared to what was performed in this work, where a 0.5 μmol and 1 μmol dodecanoic acid patch are suggested.

9. Recent work on infecting the oral cavity of mice with *C. albicans* for antifungal treatment tests have been reported [251,252]. Adapting these methods for the application of dodecanoic acid patches would be possible, although another animal, such as rabbits or hamsters, may be better suited for electrospun patch application.

8. References

- [1] H.E. Colley, Z. Said, M.E. Santocildes-Romero, S.R. Baker, K. D'Apice, J. Hansen, L.S. Madsen, M.H. Thornhill, P. V. Hatton, C. Murdoch, Pre-clinical evaluation of novel mucoadhesive bilayer patches for local delivery of clobetasol-17-propionate to the oral mucosa, *Biomaterials*. 178 (2018) 134–146. doi:10.1016/j.biomaterials.2018.06.009.
- [2] R. Baiju, E. Peter, N. Varghese, R. Sivaram, Oral health and quality of life: Current concepts, *J. Clin. Diagnostic Res.* 11 (2017) ZE21–ZE26. doi:10.7860/JCDR/2017/25866.10110.
- [3] C. Yang, L. Liu, H. Shi, Y. Zhang, Psychological problems and quality of life of patients with oral mucosal diseases: A preliminary study in Chinese population, *BMC Oral Health*. 18 (2018) 1–7. doi:10.1186/s12903-018-0696-y.
- [4] C.A. Squier, M.J. Kremer, Biology of oral mucosa and esophagus, *J. Natl. Cancer Inst. Monogr.* 29 (2001) 7–15. doi:10.1093/oxfordjournals.jncimonographs.a003443.
- [5] D. Harris, J.R. Robinson, Drug Delivery via the Mucous Membranes of the Oral Cavity, *J. Pharm. Sci.* 81 (1992) 1–10. doi:10.1002/jps.2600810102.
- [6] S. Prestin, S.I. Rothschild, C.S. Betz, M. Kraft, Measurement of epithelial thickness within the oral cavity using optical coherence tomography, *Head Neck*. 34 (2012) 1777–1781. doi:10.1002/hed.22007.
- [7] P.M. Speight, Update on Oral Epithelial Dysplasia and Progression to Cancer, *Head Neck Pathol.* 1 (2007) 61–66. doi:10.1007/s12105-007-0014-5.
- [8] V. Hearnden, V. Sankar, K. Hull, D.V. Juras, M. Greenberg, A.R. Kerr, P.B. Lockhart, L.L. Patton, S. Porter, M.H. Thornhill, New developments and opportunities in oral mucosal drug delivery for local and systemic disease, *Adv. Drug Deliv. Rev.* 64 (2012) 16–28. doi:10.1016/j.addr.2011.02.008.
- [9] Y. Sudhakar, K. Kuotsu, A.K. Bandyopadhyay, Buccal bioadhesive drug delivery — A promising option for orally less efficient drugs, *J. Control. Release*. 114 (2006) 15–40. doi:10.1016/j.jconrel.2006.04.012.
- [10] C. Paderni, D. Compilato, L.I. Giannola, G. Campisi, Oral local drug delivery and new perspectives in oral drug formulation, *Oral Surg. Oral Med. Oral Pathol. Oral Radiol.* 114 (2012) e25–e34. doi:10.1016/j.oooo.2012.02.016.
- [11] M.A. Olson, R.S. Rogers, A.J. Bruce, Oral lichen planus, *Clin. Dermatol.* 34 (2016) 495–504. doi:10.1016/j.clindermatol.2016.02.023.

- [12] J.W. Millsop, N. Fazel, Oral candidiasis, *Clin. Dermatol.* 34 (2016) 487–494. doi:10.1016/j.clindermatol.2016.02.022.
- [13] T. Amagasa, M. Yamashiro, H. Ishikawa, Oral Leukoplakia Related to Malignant Transformation, *Oral Sci. Int.* 3 (2006) 45–55. doi:10.1016/S1348-8643(06)80001-7.
- [14] R. V. Lalla, S.T. Sonis, D.E. Peterson, Management of Oral Mucositis in Patients Who Have Cancer, *Dent. Clin. North Am.* 52 (2008) 61–77. doi:10.1016/j.cden.2007.10.002.
- [15] N.W. Johnson, C.A. Bain, Tobacco Intervention: Tobacco and oral disease, *Br. Dent. J.* 189 (2000) 200–206. doi:10.1038/sj.bdj.4800721.
- [16] A.J. van Wijk, J. Hoogstraten, Anxiety and pain during dental injections, *J. Dent.* 37 (2009) 700–704. doi:10.1016/j.jdent.2009.05.023.
- [17] D.P. Saunders, J.B. Epstein, S. Elad, J. Allemanno, P. Bossi, M.D. Van De Wetering, N.G. Rao, C. Potting, Systematic review of antimicrobials, mucosal coating agents, anesthetics, and analgesics for the management of oral mucositis in cancer patients, *Support. Care Cancer.* 21 (2013) 3191–3207. doi:10.1007/s00520-013-1871-y.
- [18] L.C.A. Cerchietti, A.H. Navigante, M.R. Bonomi, M.A. Zaderajko, P.R. Menéndez, C.E. Pogany, B.M.C. Roth, Effect of topical morphine for mucositis-associated pain following concomitant chemoradiotherapy for head and neck carcinoma, *Cancer.* 95 (2002) 2230–2236. doi:10.1002/cncr.10938.
- [19] J.B. Epstein, E.L. Truelove, H. Oien, C. Allison, N.D. Le, M.S. Epstein, Oral topical doxepin rinse: Analgesic effect in patients with oral mucosal pain due to cancer or cancer therapy, *Oral Oncol.* 37 (2001) 632–637. doi:10.1016/S1368-8375(01)00005-7.
- [20] J.B. Epstein, J.D. Epstein, M.S. Epstein, H. Oien, E.L. Truelove, Doxepin rinse for management of mucositis pain in patients with cancer: One week follow-up of topical therapy, *Spec. Care Dent.* 28 (2008) 73–77. doi:10.1111/j.1754-4505.2008.00015.x.
- [21] R.C. Dart, H.L. Surratt, T.J. Cicero, M.W. Parrino, S.G. Severtson, B. Bucher-Bartelson, J.L. Green, Trends in Opioid Analgesic Abuse and Mortality in the United States, *N. Engl. J. Med.* 372 (2015) 241–249. doi:10.1056/NEJMsa1406143.
- [22] W.M. Compton, N.D. Volkow, Major increases in opioid analgesic abuse in the United States: Concerns and strategies, *Drug Alcohol Depend.* 81 (2006) 103–107. doi:10.1016/J.DRUGALCDEP.2005.05.009.
- [23] A.R. Gammaitoni, N.A. Alvarez, B.S. Galer, Safety and tolerability of the lidocaine patch 5%, a targeted peripheral analgesic: A review of the literature, *J. Clin. Pharmacol.* 43 (2003) 111–117. doi:10.1177/0091270002239817.

- [24] H.-S. Lee, Recent advances in topical anesthesia, *J. Dent. Anesth. Pain Med.* 16 (2016) 237–244. doi:10.17245/jdapm.2016.16.4.237.
- [25] I. Vetter, C.A. Mozar, T. Durek, J.S. Wingerd, P.F. Alewood, M.J. Christie, R.J. Lewis, Characterisation of Na^v types endogenously expressed in human SH-SY5Y neuroblastoma cells, *Biochem. Pharmacol.* 83 (2012) 1562–1571. doi:10.1016/j.bcp.2012.02.022.
- [26] B.G. Covino, Pharmacology of local anaesthetic agents, *Br. J. Anaesth.* 58 (1986) 701–716. doi:10.1093/bja/58.7.701.
- [27] A. Kokate, X. Li, B. Jasti, Effect of drug lipophilicity and ionization on permeability across the buccal mucosa: a technical note., *AAPS PharmSciTech.* 9 (2008) 501–504. doi:10.1208/s12249-008-9071-7.
- [28] L. Hu, S.M.C. Silva, B.B. Damaj, R. Martin, B.B. Michniak-Kohn, Transdermal and transbuccal drug delivery systems: Enhancement using iontophoretic and chemical approaches, *Int. J. Pharm.* 421 (2011) 53–62. doi:10.1016/j.ijpharm.2011.09.025.
- [29] L.P. Scully C, El-kabir, M, Samaranayake, Candida and Oral Candidosis: A Review, *Crit Rev Ord Biol Med.* 5 (1994) 125–157. doi:10.1177/10454411940050020101.
- [30] M. Hertel, A.M. Schmidt-Westhausen, F.-P. Strietzel, Local, systemic, demographic, and health-related factors influencing pathogenic yeast spectrum and antifungal drug administration frequency in oral candidiasis: a retrospective study, *Clin. Oral Investig.* 20 (2016) 1477–1486. doi:10.1007/s00784-015-1631-0.
- [31] B. Rodu, J.T. Carpenter, M.R. Jones, The pathogenesis and clinical significance of cytologically detectable oral Candida in acute leukemia, *Cancer.* 62 (1988) 2042–2046. doi:10.1002/1097-0142.
- [32] B. Dupont, J. Graybill, D. Armstrong, R. Laroche, J. Touzé, L. Wheat, Fungal infections in AIDS patients, *J. Med. Vet. Mycol.* 30 (1992) 19–28. doi:10.1080/02681219280000731.
- [33] C. Garcia-Cuesta, M. Sarrion-Perez, J. Bagan, Current treatment of oral candidiasis: A literature review, *J. Clin. Exp. Dent.* 6 (2014) 576–582. doi:10.4317/jced.51798.
- [34] H.M. Nairy, N.R. Charyulu, V.A. Shetty, P. Prabhakara, A pseudo-randomised clinical trial of in situ gels of fluconazole for the treatment of oropharyngeal candidiasis, *Trials.* 12 (2011) 99–104. doi:10.1186/1745-6215-12-99.

- [35] N. Harish, P. Prabhu, R. Charyulu, M. Gulzar, E.V.. Subrahmanyam, Formulation and evaluation of in situ gels containing clotrimazole for oral candidiasis, *Indian J. Pharm. Sci.* 71 (2009) 421–427. doi:10.4103/0250-474X.57291.
- [36] F. Lamoth, S.R. Lockhart, E.L. Berkow, T. Calandra, Changes in the epidemiological landscape of invasive candidiasis, *J. Antimicrob. Chemother.* 73 (2018) 4–13. doi:10.1093/jac/dkx444.
- [37] J. Loeffler, D.A. Stevens, Antifungal Drug Resistance, *Clin. Infect. Dis.* 36 (2003) 31–41. doi:10.1086/344658.
- [38] D. Sanglard, Emerging Threats in Antifungal-Resistant Fungal Pathogens, *Front. Med.* 3 (2016) e11. doi:10.3389/fmed.2016.00011.
- [39] F. Haque, K. Ganesan, M.S. Bhattacharyya, Inhibitory Effect of Sophorolipid on *Candida albicans* Biofilm Formation and Hyphal Growth, *Sci. Rep.* 6 (2016) 23575–23585. doi:10.1038/srep23575.
- [40] Q. Yu, B. Zhang, F. Ma, C. Jia, C. Xiao, B. Zhang, L. Xing, M. Li, Novel mechanisms of surfactants against *Candida albicans* growth and morphogenesis, *Chem. Biol. Interact.* 227 (2015) 1–6. doi:10.1016/J.CBI.2014.12.014.
- [41] K.Y. Lum, S.T. Tay, C.F. Le, V.S. Lee, N.H. Sabri, R.D. Velayuthan, H. Hassan, S.D. Sekaran, Activity of Novel Synthetic Peptides against *Candida albicans*, *Sci. Rep.* 5 (2015) 9657–9668. doi:10.1038/srep09657.
- [42] S. Paulone, A. Ardizzoni, A. Tavanti, S. Piccinelli, C. Rizzato, A. Lupetti, B. Colombari, E. Pericolini, L. Polonelli, W. Magliani, S. Conti, B. Posteraro, C. Cermelli, E. Blasi, S. Peppoloni, The synthetic killer peptide KP impairs *Candida albicans* biofilm in vitro, *PLoS One.* 12 (2017) e0181278. doi:10.1371/journal.pone.0181278.
- [43] P. Morici, R. Fais, C. Rizzato, A. Tavanti, A. Lupetti, Inhibition of *Candida albicans* Biofilm Formation by the Synthetic Lactoferricin Derived Peptide hLF1-11, *PLoS One.* 11 (2016) e0167470. doi:10.1371/journal.pone.0167470.
- [44] G. Bergsson, J. Arnfinnsson, H. Arnfinnsson, In Vitro Killing of *Candida albicans* by Fatty Acids and Monoglycerides, *Antimicrob. Agents Chemother.* 45 (2001) 3209–3212. doi:10.1128/AAC.45.11.3209.
- [45] C.B. Huang, Y. Alimova, T.M. Myers, J.L. Ebersole, Short- and medium-chain fatty acids exhibit antimicrobial activity for oral microorganisms, *Arch. Oral Biol.* 56 (2011) 650–654. doi:10.1016/j.archoralbio.2011.01.011.

- [46] K. Hayama, M. Takahashi, S. Yui, S. Abe, Inhibitory effects of several saturated fatty acids and their related fatty alcohols on the growth of *Candida albicans*, *Drug Discov. Ther.* 9 (2015) 386–390. doi:10.5582/ddt.2015.01062.
- [47] J.J. Kabara, D.M. Swieczkowski, a. J. Conley, J.P. Truant, Fatty acids and derivatives as antimicrobial agents., *Antimicrob. Agents Chemother.* 2 (1972) 23–28. doi:10.1128/AAC.2.1.23.
- [48] C.H. Pohl, J.L.F. Kock, V.S. Thibane, Antifungal free fatty acids: a review, *Sci. against Microb. Pathog. Curr. Res. Technol. Adv.* 3 (2011) 61–71.
- [49] T. Kitahara, N. Koyama, J. Matsuda, Y. Aoyama, Y. Hirakata, S. Kamihira, S. Kohno, M. Nakashima, H. Sasaki, Antimicrobial Activity of Saturated Fatty Acids and Fatty Amines against Methicillin-Resistant *Staphylococcus aureus*, *Biol. Pharm. Bull.* 27 (2004) 1321–1326. doi:10.1248/bpb.27.1321.
- [50] Y. Hirata, M. Ryu, Y. Oda, K. Igarashi, A. Nagatsuka, T. Furuta, M. Sugiura, Novel characteristics of sophorolipids, yeast glycolipid biosurfactants, as biodegradable low-foaming surfactants, *J. Biosci. Bioeng.* 108 (2009) 142–146. doi:10.1016/j.jbiosc.2009.03.012.
- [51] S. a Ibrahim, S.K. Li, Efficiency of Fatty Acids as Chemical Penetration Enhancers: Mechanisms and Structure Enhancement Relationship, *Pharm. Res.* 27 (2011) 115–125. doi:10.1007/s11095-009-9985-0.Efficiency.
- [52] A. Murzyn, A. Krasowska, P. Stefanowicz, D. Dziadkowiec, M. Łukaszewicz, Capric acid secreted by *S. boulardii* inhibits *C. albicans* filamentous growth, adhesion and biofilm formation, *PLoS One.* 5 (2010) e12050. doi:10.1371/journal.pone.0012050.
- [53] J. Oever, M.G. Netea, The bacteriome – mycobiome interaction and antifungal host defense, *Eur. J. Immunol.* 44 (2014) 3182–3191. doi:10.1002/eji.201344405.
- [54] K. Jamuna-Thevi, N.N. Saarani, M.R. Abdul Kadir, H. Hermawan, Triple-layered PLGA/nanoapatite/lauric acid graded composite membrane for periodontal guided bone regeneration, *Mater. Sci. Eng. C.* 43 (2014) 253–263. doi:10.1016/j.msec.2014.07.028.
- [55] C. Padula, S. Nicoli, P. Colombo, P. Santi, Single-layer transdermal film containing lidocaine: Modulation of drug release, *Eur. J. Pharm. Biopharm.* 66 (2007) 422–428. doi:10.1016/j.ejpb.2006.11.014.

- [56] P.G. Fotos, G.F. Koerbusch, D.S. Sarasin, R.J. Kist, Evaluation of intra-alveolar chlorhexidine dressings after removal of impacted mandibular third molars, *Oral Surg. Oral Med. Oral Pathol.* 73 (1992) 383–388. doi:10.1016/0030-4220(92)90140-I.
- [57] T.E. Borbás, A. Balogh, K. Bocz, J. Müller, É. Kiserdei, T. Vigh, B. Sinkó, A. Marosi, A. Halász, Z. Dohányos, L. Szente, G.T. Balogh, Z.K. Nagy, In vitro dissolution–permeation evaluation of an electrospun cyclodextrin-based formulation of aripiprazole using μ FluxTM, *Int. J. Pharm.* 491 (2015) 180–189. doi:10.1016/j.ijpharm.2015.06.019.
- [58] G. Buschle-Diller, J. Cooper, Z. Xie, Y. Wu, J. Waldrup, X. Ren, Release of antibiotics from electrospun bicomponent fibers, *Cellulose.* 14 (2007) 553–562. doi:10.1007/s10570-007-9183-3.
- [59] T.J. Sill, H. a. von Recum, Electrospinning: Applications in drug delivery and tissue engineering, *Biomaterials.* 29 (2008) 1989–2006. doi:10.1016/j.biomaterials.2008.01.011.
- [60] D. Kai, S.S. Liow, X.J. Loh, Biodegradable polymers for electrospinning: Towards biomedical applications, *Mater. Sci. Eng. C.* 45 (2014) 659–670. doi:10.1016/j.msec.2014.04.051.
- [61] W.E. Teo, S. Ramakrishna, A review on electrospinning design and nanofibre assemblies, *Nanotechnology.* 17 (2006) 89–106. doi:10.1088/0957-4484/17/14/R01.
- [62] M. Behbehani, A. Glen, C.S. Taylor, A. Schuhmacher, F. Claeysens, J.W. Haycock, Pre-clinical evaluation of advanced nerve guide conduits using a novel 3D in vitro testing model, *Int. J. Bioprinting.* 4 (2018) 123–134. doi:10.18063/ijb.v4i1.123.
- [63] A. Huber, A. Pickett, K.M. Shakesheff, Reconstruction of spatially orientated myotubes in vitro using electrospun, parallel microfibre arrays, *Eur. Cells Mater.* 14 (2007) 56–63. doi:10.22203/eCM.v014a06.
- [64] D.S. Katti, K.W. Robinson, F.K. Ko, C.T. Laurencin, Bioresorbable nanofiber-based systems for wound healing and drug delivery: Optimization of fabrication parameters, *J. Biomed. Mater. Res.* 70 (2004) 286–296. doi:10.1002/jbm.b.30041.
- [65] S.A. Theron, E. Zussman, A.L. Yarin, Experimental investigation of the governing parameters in the electrospinning of polymer solutions, *Polymer (Guildf).* 45 (2004) 2017–2030. doi:10.1016/j.polymer.2004.01.024.
- [66] A. Gañán-Calvo, Generation of Steady Liquid Microthreads and Micron-Sized Monodisperse Sprays in Gas Streams, *Phys. Rev. Lett.* 80 (1998) 285–288. doi:10.1103/PhysRevLett.80.285.

- [67] Z.M. Huang, Y.Z. Zhang, M. Kotaki, S. Ramakrishna, A review on polymer nanofibers by electrospinning and their applications in nanocomposites, *Compos. Sci. Technol.* 63 (2003) 2223–2253. doi:10.1016/S0266-3538(03)00178-7.
- [68] S. De Vrieze, T. Van Camp, A. Nelvig, B. Hagström, P. Westbroek, K. De Clerck, The effect of temperature and humidity on electrospinning, *J. Mater. Sci.* 44 (2009) 1357–1362. doi:10.1007/s10853-008-3010-6.
- [69] Y.M. Shin, M.M. Hohman, M.P. Brenner, G.C. Rutledge, Electrospinning: A whipping fluid jet generates submicron polymer fibers, *Appl. Phys. Lett.* 78 (2001) 1149–1151. doi:10.1063/1.1345798.
- [70] S.L. Shenoy, W.D. Bates, H.L. Frisch, G.E. Wnek, Role of chain entanglements on fiber formation during electrospinning of polymer solutions: good solvent, non-specific polymer–polymer interaction limit, *Polymer (Guildf)*. 46 (2005) 3372–3384. doi:10.1016/j.polymer.2005.03.011.
- [71] P.K. Bhattacharjee, J.P. Oberhauser, G.H. McKinley, L.G. Leal, T. Sridhar, Extensional rheometry of entangled solutions, *Macromolecules*. 35 (2002) 10131–10148. doi:10.1021/ma0118623.
- [72] J.H. Yu, S. V. Fridrikh, G.C. Rutledge, The role of elasticity in the formation of electrospun fibers, *Polymer (Guildf)*. 47 (2006) 4789–4797. doi:10.1016/j.polymer.2006.04.050.
- [73] O. Regev, S. Vandebriel, E. Zussman, C. Clasen, The role of interfacial viscoelasticity in the stabilization of an electrospun jet, *Polymer (Guildf)*. 51 (2010) 2611–2620. doi:10.1016/j.polymer.2010.03.061.
- [74] R. Rošic, J. Pelipenko, P. Kocbek, S. Baumgartner, M. Bešter-Rogač, J. Kristl, The role of rheology of polymer solutions in predicting nanofiber formation by electrospinning, *Eur. Polym. J.* 48 (2012) 1374–1384. doi:10.1016/j.eurpolymj.2012.05.001.
- [75] R.G. Larson, Instabilities in viscoelastic flows, *Rheol. Acta.* 31 (1992) 213–263. doi:10.1007/BF00366504.
- [76] X. Zong, K. Kim, D. Fang, S. Ran, B.S. Hsiao, B. Chu, Structure and process relationship of electrospun bioabsorbable nanofiber membranes, *Polymer (Guildf)*. 43 (2002) 4403–4412. doi:10.1016/S0032-3861(02)00275-6.

- [77] a. Koski, K. Yim, S. Shivkumar, Effect of molecular weight on fibrous PVA produced by electrospinning, *Mater. Lett.* 58 (2004) 493–497. doi:10.1016/S0167-577X(03)00532-9.
- [78] R.P. Mun, J. a Byars, D. V Boger, The effects of polymer concentration and molecular weight on the breakup of laminar capillary jets, *J. Nonnewton. Fluid Mech.* 74 (1998) 285–297. doi:10.1016/S0377-0257(97)00074-8.
- [79] P. Gupta, C. Elkins, T.E. Long, G.L. Wilkes, Electrospinning of linear homopolymers of poly(methyl methacrylate): Exploring relationships between fiber formation, viscosity, molecular weight and concentration in a good solvent, *Polymer (Guildf)*. 46 (2005) 4799–4810. doi:10.1016/j.polymer.2005.04.021.
- [80] C. Kriegel, K.M. Kit, D.J. McClements, J. Weiss, Nanofibers as Carrier Systems for Antimicrobial Microemulsions. Part I: Fabrication and Characterization, *Am. Chem. Soc.* 25 (2009) 1154–1161. doi:10.1016/j.polymer.2008.09.041.
- [81] R. Rošic, J. Pelipenko, J. Kristl, P. Kocbek, M. Bešter-Rogač, S. Baumgartner, Physical characteristics of poly (vinyl alcohol) solutions in relation to electrospun nanofiber formation, *Eur. Polym. J.* 49 (2013) 290–298. doi:10.1016/j.eurpolymj.2012.11.013.
- [82] Q.P. Pham, U. Sharma, A.G. Mikos, Electrospinning of polymeric nanofibers for tissue engineering applications: a review., *Tissue Eng.* 12 (2006) 1197–1211. doi:10.1089/ten.2006.12.ft-65.
- [83] J. Pelipenko, J. Kristl, R. Rošic, S. Baumgartner, P. Kocbek, Interfacial rheology: An overview of measuring techniques and its role in dispersions and electrospinning, *Acta Pharm.* 62 (2012) 123–140. doi:10.2478/v10007-012-0018-x.
- [84] A. Gañán-Calvo, Cone-Jet Analytical Extension of Taylor's Electrostatic Solution and the Asymptotic Universal Scaling Laws in Electrospinning, *Phys. Rev. Lett.* 79 (1997) 217–220. doi:10.1103/PhysRevLett.85.4193.
- [85] M.M. Hohman, M. Shin, G. Rutledge, M.P. Brenner, Electrospinning and electrically forced jets. I. Stability Theory, *Phys. Fluids.* 13 (2001) 2201–2220. doi:10.1063/1.1384013.
- [86] M.M. Hohman, M. Shin, G. Rutledge, M.P. Brenner, Electrospinning and electrically forced jets. II. Applications, *Phys. Fluids.* 13 (2001) 2221–2236. doi:10.1063/1.1384013.

- [87] S. V. Fridrikh, J.H. Yu, M.P. Brenner, G.C. Rutledge, Controlling the Fiber Diameter during Electrospinning, *Phys. Rev. Lett.* 90 (2003) 144502. doi:10.1103/PhysRevLett.90.144502.
- [88] G. Taylor, Electrically driven jets, *Proc. R. Soc. A.* 313 (1969) 453–475.
- [89] K.E. Uhrich, S.M.C. And, R.S. Langer, K.M. Shakesheff, Polymeric Systems for Controlled Drug Release, *Chem. Rev.* 99 (1999) 3181–3198. doi:10.1021/CR940351U.
- [90] K.H. Lee, H.Y. Kim, M.S. Khil, Y.M. Ra, D.R. Lee, Characterization of nano-structured poly(ϵ -caprolactone) nonwoven mats via electrospinning, *Polymer (Guildf).* 44 (2003) 1287–1294. doi:10.1016/S0032-3861(02)00820-0.
- [91] T. Potrc, S. Baumgartner, R. Roškar, O. Planinšek, Z. Lavric, J. Kristl, P. Kocbek, Electrospun polycaprolactone nanofibers as a potential oromucosal delivery system for poorly water-soluble drugs, *Eur. J. Pharm. Sci.* 75 (2015) 101–113. doi:10.1016/j.ijpharm.2014.12.024.
- [92] E. Luong-Van, L. Grøndahl, K.N. Chua, K.W. Leong, V. Nurcombe, S.M. Cool, Controlled release of heparin from poly(ϵ -caprolactone) electrospun fibers, *Biomaterials.* 27 (2006) 2042–2050. doi:10.1016/j.biomaterials.2005.10.028.
- [93] M. Zamani, M. Morshed, J. Varshosaz, M. Jannesari, Controlled release of metronidazole benzoate from poly ϵ -caprolactone electrospun nanofibers for periodontal diseases, *Eur. J. Pharm. Biopharm.* 75 (2010) 179–185. doi:10.1016/j.ejpb.2010.02.002.
- [94] Y. Wang, B. Wang, W. Qiao, T. Yin, A Novel Controlled Release Drug Delivery System for Multiple Drugs Based on Electrospun Nanofibers Containing Nanoparticles, *J. Pharm. Sci.* 99 (2010) 4215–4227. doi:10.1002/jps.
- [95] D. Paneva, N. Manolova, M. Argirova, I. Rashkov, Antibacterial electrospun poly(ϵ -caprolactone)/ascorbyl palmitate nanofibrous materials, *Int. J. Pharm.* 416 (2011) 346–355. doi:10.1016/j.ijpharm.2011.06.032.
- [96] P. Karuppuswamy, J. Reddy Venugopal, B. Navaneethan, A. Luwang Laiva, S. Ramakrishna, Polycaprolactone nanofibers for the controlled release of tetracycline hydrochloride, *Mater. Lett.* 141 (2015) 180–186. doi:10.1016/j.matlet.2014.11.044.

- [97] D.-G. Yu, X.-X. Shen, C. Branford-White, K. White, L.-M. Zhu, S.W. Annie Bligh, Oral fast-dissolving drug delivery membranes prepared from electrospun polyvinylpyrrolidone ultrafine fibers, *Nanotechnology*. 20 (2009) 055104. doi:10.1088/0957-4484/20/5/055104.
- [98] D.-G. Yu, G.R. Williams, X. Wang, X.-K. Liu, H.-L. Li, S.A. Bligh, Dual drug release nanocomposites prepared using a combination of electrospinning and electrospinning, *RSC Adv*. 3 (2013) 4652–4658. doi:10.1039/c3ra40334c.
- [99] U.E. Illangakoon, T. Nazir, G.R. Williams, N.P. Chatterton, Mebeverine-loaded electrospun nanofibers: Physicochemical characterization and dissolution studies, *J. Pharm. Sci.* 103 (2014) 283–292. doi:10.1002/jps.23759.
- [100] U.E. Illangakoon, H. Gill, G.C. Shearman, M. Parhizkar, S. Mahalingam, N.P. Chatterton, G.R. Williams, Fast dissolving paracetamol/caffeine nanofibers prepared by electrospinning, *Int. J. Pharm.* 477 (2014) 369–379. doi:10.1016/j.ijpharm.2014.10.036.
- [101] P. Tonglairoum, T. Ngawhirunpat, T. Rojanarata, S. Panomsuk, R. Kaomongkolgit, P. Opanasopit, Fast-Acting Clotrimazole Compositated PVP/HP β CD Nanofibers for Oral Candidiasis Application, *Pharm. Res.* 31 (2014) 1893–1906. doi:10.1007/s11095-013-1291-1.
- [102] W. Samprasit, P. Akkaramongkolporn, T. Ngawhirunpat, T. Rojanarata, R. Kaomongkolgit, P. Opanasopit, Fast releasing oral electrospun PVP/CD nanofiber mats of taste-masked meloxicam, *Int. J. Pharm.* 487 (2015) 213–222. doi:10.1016/j.ijpharm.2015.04.044.
- [103] P. Tonglairoum, T. Ngawhirunpat, T. Rojanarata, S. Panomsuk, R. Kaomongkolgit, P. Opanasopit, Fabrication of mucoadhesive chitosan coated polyvinylpyrrolidone/cyclodextrin/clotrimazole sandwich patches for oral candidiasis, *Carbohydr. Polym.* 132 (2015) 173–179. doi:10.1016/j.carbpol.2015.06.032.
- [104] K.K.S. Anderson, K.K.M. Schreck, M.A. Hillmyer, Toughening polylactide, *Polym. Rev.* 48 (2008) 85–108. doi:10.1080/15583720701834216.
- [105] C.-C. Qin, X.-P. Duan, L. Wang, L.-H. Zhang, M. Yu, R.-H. Dong, X. Yan, H.-W. He, Y.-Z. Long, Melt electrospinning of poly(lactic acid) and polycaprolactone microfibers by using a hand-operated Wimshurst generator, *Nanoscale*. 7 (2015) 16611–16615. doi:10.1039/c5nr05367f.
- [106] T. Han, D.H. Reneker, A.L. Yarin, Buckling of jets in electrospinning, *Polymer (Guildf)*. 48 (2007) 6064–6076. doi:10.1016/j.polymer.2007.08.002.

- [107] S.K. Tiwari, R. Tzezana, E. Zussman, S.S. Venkatraman, Optimizing partition-controlled drug release from electrospun core-shell fibers, *Int. J. Pharm.* 392 (2010) 209–217. doi:10.1016/j.ijpharm.2010.03.021.
- [108] J. Zeng, X. Xu, X. Chen, Q. Liang, X. Bian, L. Yang, X. Jing, Biodegradable electrospun fibers for drug delivery, *J. Control. Release.* 92 (2003) 227–231. doi:10.1016/S0168-3659(03)00372-9.
- [109] A. Subramanian, U.M. Krishnan, S. Sethuraman, Fabrication of uniaxially aligned 3D electrospun scaffolds for neural regeneration, *Biomed. Mater.* 6 (2011) 025004. doi:10.1088/1748-6041/6/2/025004.
- [110] K. Kim, Y.K. Luu, C. Chang, D. Fang, B.S. Hsiao, B. Chu, M. Hadjiargyrou, Incorporation and controlled release of a hydrophilic antibiotic using poly(lactide-co-glycolide)-based electrospun nanofibrous scaffolds, *J. Control. Release.* 98 (2004) 47–56. doi:10.1016/j.jconrel.2004.04.009.
- [111] H. Jiang, D. Fang, B.S. Hsiao, B. Chu, W. Chen, Optimization and characterization of dextran membranes prepared by electrospinning, *Biomacromolecules.* 5 (2004) 326–333. doi:10.1021/bm034345w.
- [112] T. Elsarnagawy, H. Fouad, F.N. Almajhdi, Y.A. Elnakady, M.F. Al Rez, S. Abuelreich, A. Mahmood, S.G. Ansari, Thermo-Mechanical, Osteoblastic Cell Growth and Attachment Behavior of Electrospun Poly(D, L-lactide-co-glycolide) Nano-Fibers: In Vitro Study, *Sci. Adv. Mater.* 7 (2015) 396–405. doi:10.1166/sam.2015.2251.
- [113] H.G. Şenel Ayaz, A. Perets, H. Ayaz, K.D. Gilroy, M. Govindaraj, D. Brookstein, P.I. Lelkes, Textile-templated electrospun anisotropic scaffolds for regenerative cardiac tissue engineering., *Biomaterials.* 35 (2014) 8540–8552. doi:10.1016/j.biomaterials.2014.06.029.
- [114] T. Ngawhirunpat, P. Opanasopit, T. Rojanarata, P. Akkaramongkolporn, U. Ruktanonchai, P. Supaphol, Development of meloxicam-loaded electrospun polyvinyl alcohol mats as a transdermal therapeutic agent, *Pharm. Dev. Technol.* 14 (2009) 70–79. doi:10.1080/10837450802409420.
- [115] M. Jannesari, J. Varshosaz, M. Morshed, M. Zamani, Composite poly(vinyl alcohol)/poly(vinyl acetate) electrospun nanofibrous mats as a novel wound dressing matrix for controlled release of drugs, *Int. J. Nanomedicine.* 6 (2011) 993–1003. doi:10.2147/IJN.S17595.

- [116] J. Pelipenko, P. Kocbek, B. Govedarica, R. Rošic, S. Baumgartner, J. Kristl, The topography of electrospun nanofibers and its impact on the growth and mobility of keratinocytes, *Eur. J. Pharm. Biopharm.* 84 (2013) 401–411. doi:10.1016/j.ejpb.2012.09.009.
- [117] P. Tonglairoum, T. Ngawhirunpat, T. Rojanarata, R. Kaomongkolgit, P. Opanasopit, Fabrication of a novel scaffold of clotrimazole-microemulsion-containing nanofibers using an electrospinning process for oral candidiasis applications, *Colloids Surfaces B Biointerfaces.* 126 (2015) 18–25. doi:10.1016/j.colsurfb.2014.12.009.
- [118] W.K. Son, J.H. Youk, T.S. Lee, W.H. Park, The effects of solution properties and polyelectrolyte on electrospinning of ultrafine poly(ethylene oxide) fibers, *Polymer (Guildf).* 45 (2004) 2959–2966. doi:10.1016/j.polymer.2004.03.006.
- [119] J.M. Deitzel, J.D. Kleinmeyer, J.K. Hirvonen, N.C. Beck Tan, Controlled deposition of electrospun poly(ethylene oxide) fibers, *Polymer (Guildf).* 42 (2001) 8163–8170. doi:10.1016/S0032-3861(01)00336-6.
- [120] M.-S. Khil, D.-I. Cha, H.-Y. Kim, I.-S. Kim, N. Bhattarai, Electrospun nanofibrous polyurethane membrane as wound dressing, *J. Biomed. Mater. Res. B. Appl. Biomater.* 67 (2003) 675–679. doi:10.1002/jbm.b.10058.
- [121] G. Verreck, I. Chun, J. Rosenblatt, J. Peeters, A. Van Dijck, J. Mensch, M. Noppe, M.E. Brewster, Incorporation of drugs in an amorphous state into electrospun nanofibers composed of a water-insoluble, nonbiodegradable polymer, *J. Control. Release.* 92 (2003) 349–360. doi:10.1016/S0168-3659(03)00342-0.
- [122] A. Bhakay, M. Rahman, R.N. Dave, E. Bilgili, Bioavailability Enhancement of Poorly Water-Soluble Drugs via Nanocomposites: Formulation – Processing Aspects and Challenges, *Pharmaceutics.* 10 (2018) E86. doi:10.3390/pharmaceutics10030086.
- [123] Z. Jun, H. Hou, A. Schaper, J.H. Wendorff, A. Greiner, Poly-L-lactide nanofibers by electrospinning – Influence of solution viscosity and electrical conductivity on fiber diameter and fiber morphology, *E-Polymers.* 3 (2003) 102–110. doi:10.1515/epoly.2003.3.1.102.
- [124] H. Makadia, S. Siegel, Poly Lactic-co-Glycolic Acid (PLGA) as Biodegradable Controlled Drug Delivery Carrier, *Polymers (Basel).* 3 (2011) 1377–1397. doi:10.3390/polym3031377.Poly.
- [125] C.B. Weldon, J.H. Tsui, S.A. Shankarappa, V.T. Nguyen, M. Ma, D.G. Anderson, D.S. Kohane, Electrospun drug-eluting sutures for local anesthesia, *J. Control. Release.* 161 (2012) 903–909. doi:10.1016/j.jconrel.2012.05.021.

- [126] S.H. Ranganath, C.-H. Wang, Biodegradable microfiber implants delivering paclitaxel for post-surgical chemotherapy against malignant glioma, *Biomaterials*. 29 (2008) 2996–3003. doi:10.1016/j.biomaterials.2008.04.002.
- [127] M. Ranjbar-Mohammadi, M. Zamani, M.P. Prabhakaran, S.H. Bahrami, S. Ramakrishna, Electrospinning of PLGA/gum tragacanth nanofibers containing tetracycline hydrochloride for periodontal regeneration, *Mater. Sci. Eng. C*. 58 (2016) 521–531. doi:10.1016/j.msec.2015.08.066.
- [128] J. Bonilla, E. Fortunati, L. Atarés, A. Chiralt, J.M. Kenny, Physical, structural and antimicrobial properties of poly vinyl alcohol-chitosan biodegradable films, *Food Hydrocoll.* 35 (2014) 463–470. doi:10.1016/j.foodhyd.2013.07.002.
- [129] C.. DeMerlis, D.R. Schonker, Review of the oral toxicity of polyvinyl alcohol (PVA), *Food Chem. Toxicol.* 41 (2003) 319–326. doi:10.1016/S0278-6915(02)00258-2.
- [130] D. Ozdil, H.M. Aydin, Polymers for medical and tissue engineering applications, *J. Chem. Technol. Biotechnol.* 89 (2014) 1793–1810. doi:10.1002/jctb.4505.
- [131] M. Sokolsky-Papkov, K. Agashi, A. Olaye, K. Shakesheff, A.J. Domb, Polymer carriers for drug delivery in tissue engineering, *Adv. Drug Deliv. Rev.* 59 (2007) 187–206. doi:10.1016/j.addr.2007.04.001.
- [132] C. Akduman, I. Özgüney, E.P.A. Kumbasar, Preparation and characterization of naproxen-loaded electrospun thermoplastic polyurethane nanofibers as a drug delivery system, *Mater. Sci. Eng. C*. 64 (2016) 383–390. doi:10.1016/j.msec.2016.04.005.
- [133] D. Hua, Z. Liu, F. Wang, B. Gao, F. Chen, Q. Zhang, R. Xiong, J. Han, S.K. Samal, S.C. De Smedt, C. Huang, pH responsive polyurethane (core) and cellulose acetate phthalate (shell) electrospun fibers for intravaginal drug delivery, *Carbohydr. Polym.* 151 (2016) 1240–1244. doi:10.1016/j.carbpol.2016.06.066.
- [134] X. Shen, D. Yu, L. Zhu, C. Branford-White, K. White, N. Chatterton, Electrospun diclofenac sodium loaded Eudragit® L 100-55 nanofibers for colon-targeted drug delivery, *Int. J. Pharm.* 408 (2011) 200–207. doi:10.1016/j.ijpharm.2011.01.058.
- [135] R.I. Reda, M.M. Wen, A. Hassan El-Kamel, Ketoprofen-loaded eudragit electrospun nanofibers for the treatment of oral mucositis, *Int. J. Nanomedicine*. 12 (2017) 2335–2351. doi:10.2147/IJN.S131253.

- [136] P.S. Giram, A. Shitole, S.S. Nande, N. Sharma, B. Garnaik, Fast dissolving moxifloxacin hydrochloride antibiotic drug from electrospun Eudragit L-100 nonwoven nanofibrous Mats, *Mater. Sci. Eng. C.* 92 (2018) 526–539. doi:10.1016/j.msec.2018.06.031.
- [137] H.N. Shivakumar, B.G. Desai, G. Deshmukh, Design and Optimization of Diclofenac Sodium Controlled Release Solid Dispersions by Response Surface Methodology, *Indian J. Pharm. Sci.* 70 (2008) 22–30. doi:10.4103/0250-474X.40327.
- [138] R.B. Gandhi, J.R. Robinson, Oral cavity as a site for bioadhesive drug delivery, *Adv. Drug Deliv. Rev.* 13 (1994) 43–74. doi:10.1016/0169-409X(94)90026-4.
- [139] D. Tiwari, R. Sause, P.L. Madan, D. Goldman, Evaluation of polyoxyethylene homopolymers for buccal bioadhesive drug delivery device formulations, *AAPS PharmSci.* 1 (1999) 50–57. doi:10.1208/ps010313.
- [140] H. Takeuchi, J. Thongborisute, Y. Matsui, H. Sugihara, H. Yamamoto, Y. Kawashima, Novel mucoadhesion tests for polymers and polymer-coated particles to design optimal mucoadhesive drug delivery systems, *Adv. Drug Deliv. Rev.* 57 (2005) 1583–1594. doi:10.1016/j.addr.2005.07.008.
- [141] F.C. Carvalho, M.L. Brushi, R.C. Evangelista, M.P.D. Gremiao, Mucoadhesive drug delivery systems, *Brazilian J. Pharm. Sci.* 46 (2010) 1–17. doi:10.4103/0975-7406.76478.
- [142] N. Salamat-Miller, M. Chittchang, T. Johnston, The use of mucoadhesive polymers in buccal drug delivery, *Adv. Drug Deliv. Rev.* 57 (2005) 1666–1691. doi:10.1016/j.addr.2005.07.003.
- [143] G.P. Andrews, T.P. Laverty, D.S. Jones, Mucoadhesive polymeric platforms for controlled drug delivery, *Eur. J. Pharm. Biopharm.* 71 (2009) 505–518. doi:10.1016/j.ejpb.2008.09.028.
- [144] J.O. Morales, J.T. McConville, Manufacture and characterization of mucoadhesive buccal films, *Eur. J. Pharm. Biopharm.* 77 (2011) 187–199. doi:10.1016/j.ejpb.2010.11.023.
- [145] I. Bravo-Osuna, C. Vauthier, A. Farabollini, G.F. Palmieri, G. Ponchel, Mucoadhesion mechanism of chitosan and thiolated chitosan-poly(isobutyl cyanoacrylate) core-shell nanoparticles, *Biomaterials.* 28 (2007) 2233–2243. doi:10.1016/j.biomaterials.2007.01.005.

- [146] D.-G. Yu, J.-J. Li, G.R. Williams, M. Zhao, Electrospun amorphous solid dispersions of poorly water-soluble drugs: A review, *J. Control. Release.* 292 (2018) 91–110. doi:10.1016/j.jconrel.2018.08.016.
- [147] A.J. Meinel, O. Gernershaus, T. Luhmann, H.P. Merkle, L. Meinel, Electrospun matrices for localized drug delivery: Current technologies and selected biomedical applications, *Eur. J. Pharm. Biopharm.* 81 (2012) 1–13. doi:10.1016/j.ejpb.2012.01.016.
- [148] M. Ignatova, K. Starbova, N. Markova, N. Manolova, I. Rashkov, Electrospun nano-fibre mats with antibacterial properties from quaternised chitosan and poly(vinyl alcohol), *Carbohydr. Res.* 341 (2006) 2098–2107. doi:10.1016/j.carres.2006.05.006.
- [149] P. Vrbata, P. Berka, D. Stránská, P. Doležal, M. Musilová, L. Čížinská, Electrospun drug loaded membranes for sublingual administration of sumatriptan and naproxen, *Int. J. Pharm.* 457 (2013) 168–176. doi:10.1016/j.ijpharm.2013.08.085.
- [150] M. Rychter, A. Baranowska-Korczyn, B. Milanowski, M. Jarek, B.M. Maciejewska, E.L. Coy, J. Lulek, & J. Lulek¹, Cilostazol-Loaded Poly(ϵ -Caprolactone) Electrospun Drug Delivery System for Cardiovascular Applications, *Pharm. Res.* 35 (2018) 32–51. doi:https://doi.org/10.1007/s11095-017-2314-0.
- [151] X. Li, C. Wang, S. Yang, P. Liu, B. Zhang, Electrospun PCL/mupirocin and chitosan/lidocaine hydrochloride multifunctional double layer nanofibrous scaffolds for wound dressing applications, *Int. J. Nanomedicine.* 13 (2018) 5287–5299. doi:10.2147/IJN.S177256.
- [152] Z. Sultanova, G. Kaleli, G. Kabay, M. Mutlu, Controlled release of a hydrophilic drug from coaxially electrospun polycaprolactone nanofibers, *Int. J. Pharm.* 505 (2016) 133–138. doi:10.1016/j.ijpharm.2016.03.032.
- [153] Bölgen, Vargel, Korkusuz, Menceloğlu, Pişkin, In vivo performance of antibiotic embedded electrospun PCL membranes for prevention of abdominal adhesions, *J. Biomed. Mater. Res. B. Appl. Biomater.* 83 (2007) 340–344. doi:10.1002/jbmb.
- [154] M. Rasekh, C. Karavasili, Y.L. Soong, N. Bouropoulos, M. Morris, D. Armitage, X. Li, D.G. Fatouros, Z. Ahmad, Electrospun PVP–indomethacin constituents for transdermal dressings and drug delivery devices, *Int. J. Pharm.* 473 (2014) 95–104. doi:10.1016/J.IJPHARM.2014.06.059.

- [155] J. Zeng, L. Yang, Q. Liang, X. Zhang, H. Guan, X. Xu, X. Chen, X. Jing, Influence of the drug compatibility with polymer solution on the release kinetics of electrospun fiber formulation., *J. Control. Release.* 105 (2005) 43–51. doi:10.1016/j.jconrel.2005.02.024.
- [156] J. Xie, C.H. Wang, Electrospun micro- and nanofibers for sustained delivery of paclitaxel to treat C6 glioma in vitro, *Pharm. Res.* 23 (2006) 1817–1826. doi:10.1007/s11095-006-9036-z.
- [157] I. Cantón, R. Mckean, M. Charnley, K.A. Blackwood, C. Fiorica, A.J. Ryan, S. MacNeil, Development of an Ibuprofen-releasing biodegradable PLA/PGA electrospun scaffold for tissue regeneration, *Biotechnol. Bioeng.* 105 (2010) 396–408. doi:10.1002/bit.22530.
- [158] Y. Su, X. Li, H. Wang, C. He, X. Mo, Fabrication and characterization of biodegradable nanofibrous mats by mix and coaxial electrospinning, *J. Mater. Sci. Mater. Med.* 20 (2009) 2285–2294. doi:10.1007/s10856-009-3805-2.
- [159] E.-R. Kenawy, G.L. Bowlin, K. Mansfield, J. Layman, D.G. Simpson, E.H. Sanders, G.E. Wnek, Release of tetracycline hydrochloride from electrospun poly(ethylene-co-vinylacetate), poly(lactic acid), and a blend, *J. Control. Release.* 81 (2002) 57–64. doi:10.1016/S0168-3659(02)00041-X.
- [160] H.J. Haroosh, Y. Dong, K.-T. Lau, Tetracycline hydrochloride (TCH)-loaded drug carrier based on PLA:PCL nanofibre mats: experimental characterisation and release kinetics modelling, *J. Mater. Sci.* 49 (2014) 6270–6281. doi:10.1007/s10853-014-8352-7.
- [161] H.S. Kim, H.S. Yoo, MMPs-responsive release of DNA from electrospun nanofibrous matrix for local gene therapy: In vitro and in vivo evaluation, *J. Control. Release.* 145 (2010) 264–271. doi:10.1016/j.jconrel.2010.03.006.
- [162] A. Karataş, A. Hilal Algan, N. Pekel-Bayramgil, F. Turhan, N. Altanlar, Ofloxacin Loaded Electrospun Fibers for Ocular Drug Delivery: Effect of Formulation Variables on Fiber Morphology and Drug Release, *Curr. Drug Deliv.* 13 (2016) 433–443. doi:10.2174/1567201812666151030162258.
- [163] P. Balakrishnan, L. Gardella, M. Forouharshad, T. Pellegrino, O. Monticelli, Star poly(ϵ -caprolactone)-based electrospun fibers as biocompatible scaffold for doxorubicin with prolonged drug release activity, *Colloids Surfaces B Biointerfaces.* 161 (2018) 488–496. doi:10.1016/j.colsurfb.2017.11.014.

- [164] D.C. Aduba, J.A. Hammer, Q. Yuan, W. Andrew Yeudall, G.L. Bowlin, H. Yang, Semi-interpenetrating network (sIPN) gelatin nanofiber scaffolds for oral mucosal drug delivery, *Acta Biomater.* 9 (2013) 6576–6584. doi:10.1016/j.actbio.2013.02.006.
- [165] C. Cavallari, A. Fini, F. Ospitali, Mucoadhesive multiparticulate patch for the intrabuccal controlled delivery of lidocaine, *Eur. J. Pharm. Biopharm.* 83 (2013) 405–414. doi:10.1016/j.ejpb.2012.10.004.
- [166] F. Cilurzo, P. Minghetti, F. Selmin, A. Casiraghi, L. Montanari, Polymethacrylate salts as new low-swellable mucoadhesive materials, *J. Control. Release.* 88 (2003) 43–53. doi:10.1016/S0168-3659(02)00459-5.
- [167] F. Yao, J.K. Weiyuan, Drug Release Kinetics and Transport Mechanisms of Non-degradable and Degradable Polymeric Delivery Systems, *Expert Opin. Drug Deliv.* 7 (2010) 429–444. doi:10.1517/17425241003602259.Drug.
- [168] L.-L.H. Chen, D.J. Chetty, Y.W. Chien, A mechanistic analysis to characterize oramucosal permeation properties, *Int. J. Pharm.* 184 (1999) 63–72. doi:10.1016/S0378-5173(99)00091-5.
- [169] U. Kulkarni, R. Mahalingam, S.I. Pather, X. Li, B. Jasti, Porcine Buccal Mucosa as an In Vitro Model: Relative Contribution of Epithelium and Connective Tissue as Permeability Barriers, *J. Pharm. Sci.* 98 (2009) 471–483. doi:10.1002/jps.21436.
- [170] B. Brodin, B. Steffansen, C.U. Nielsen, Passive diffusion of drug substances: The concepts of flux and permeability, in: *Mol. Biopharm. Asp. Drug Charact. Drug Deliv. Dos. Form Eval.*, 2010: pp. 135–151. doi:10.1200/JCO.2003.10.116.
- [171] C.-Y. Cui, W.-L. Lu, L. Xiao, S.-Q. Zhang, Y.-B. Huang, S.-L. Li, R.-J. Zhang, G.-L. Wang, X. Zhang, Q. Zhang, Sublingual delivery of insulin: effects of enhancers on the mucosal lipid fluidity and protein conformation, transport, and in vivo hypoglycemic activity., *Biol. Pharm. Bull.* 28 (2005) 2279–2288. doi:10.1248/bpb.28.2279.
- [172] M. S. Pendekal, P. K. Tegginamat, Formulation and evaluation of a bioadhesive patch for buccal delivery of tizanidine, *Acta Pharm. Sin. B.* 2 (2012) 318–324. doi:10.1016/j.apsb.2011.12.012.
- [173] A. Fini, V. Bergamante, G.C. Ceschel, Mucoadhesive gels designed for the controlled release of chlorhexidine in the oral cavity, *Pharmaceutics.* 3 (2011) 665–679. doi:10.3390/pharmaceutics3040665.

- [174] R.A. Thakur, C.A. Florek, J. Kohn, B.B. Michniak, Electrospun nanofibrous polymeric scaffold with targeted drug release profiles for potential application as wound dressing, *Int. J. Pharm.* 364 (2008) 87–93. doi:10.1016/j.ijpharm.2008.07.033.
- [175] J.G. Rheinwald, H. Green, Serial Cultivation of Strains of Human Epidermal Keratinocytes: the Formation of Keratinizing Colonies from Single Cells, *Cell*. 6 (1975) 331–344.
- [176] F. Mcgregor, A. Muntoni, J. Fleming, J. Brown, D.H. Felix, D.G. Macdonald, E.K. Parkinson, P.R. Harrison, Molecular Changes Associated with Oral Dysplasia Progression and Acquisition of Immortality: Potential for Its Reversal by 5-Azacytidine, *Cancer Res.* 62 (2002) 4757–4766.
- [177] R. Darby, *Chemical Engineering Fluid Mechanics*, 2001.
- [178] M.E. Santocildes-Romero, L. Hadley, K.H. Clitherow, J. Hansen, C. Murdoch, H.E. Colley, M.H. Thornhill, P. V. Hatton, Fabrication of Electrospun Mucoadhesive Membranes for Therapeutic Applications in Oral Medicine, *ACS Appl. Mater. Interfaces*. 9 (2017) 11557–11567. doi:10.1021/acsami.7b02337.
- [179] C.A. Schneider, W.S. Rasband, K.W. Eliceiri, NIH Image to ImageJ: 25 years of image analysis, *Nat. Methods*. 9 (2012) 671–675. doi:10.1038/nmeth.2089.
- [180] T. Schramm, A. Hester, I. Klinkert, J.P. Both, R.M.A. Heeren, A. Brunelle, O. Lapr evote, N. Desbenoit, M.F. Robbe, M. Stoeckli, B. Spengler, A. R ompp, ImzML - A common data format for the flexible exchange and processing of mass spectrometry imaging data, *J. Proteomics*. 75 (2012) 5106–5110. doi:10.1016/j.jprot.2012.07.026.
- [181] G. Robichaud, K.P. Garrard, J.A. Barry, D.C. Muddiman, MSiReader: An open-source interface to view and analyze high resolving power MS imaging files on matlab platform, *J. Am. Soc. Mass Spectrom.* 24 (2013) 718–721. doi:10.1007/s13361-013-0607-z.
- [182] E. de Hoffman, V. Stroobant, *Mass Spectrometry: Principles and Applications*, in: *Mass Spectrom. Princ. Appl.*, 3rd ed., John Wiley & Sons, 2007: pp. 33–41.
- [183] L.R. Jennings, H.E. Colley, J. Ong, F. Panagakos, J.G. Masters, H.M. Trivedi, C. Murdoch, S. Whawell, Development and Characterization of In Vitro Human Oral Mucosal Equivalents Derived from Immortalized Oral Keratinocytes, *Tissue Eng. Part C Methods*. 22 (2016) 1108–1117. doi:10.1089/ten.tec.2016.0310.
- [184] D.H. Reneker, A.L. Yarin, Electrospinning jets and polymer nanofibers, *Polymer (Guildf)*. 49 (2008) 2387–2425. doi:10.1016/j.polymer.2008.02.002.

- [185] L. Du, H. Xu, Y. Zhang, F. Zou, Electrospinning of polycaprolatone nanofibers with DMF additive: The effect of solution properties on jet perturbation and fiber morphologies, *Fibers Polym.* 17 (2016) 751–759. doi:10.1007/s12221-016-6045-3.
- [186] A. Cipitria, A. Skelton, T.R. Dargaville, P.D. Dalton, D.W. Hutmacher, Design, fabrication and characterization of PCL electrospun scaffolds - A review, *J. Mater. Chem.* 21 (2011) 9419–9453. doi:10.1039/c0jm04502k.
- [187] C. Asawahame, K. Sutjarittangtham, S. Eitssayeam, Y. Tragoolpua, B. Sirithunyalug, J. Sirithunyalug, Antibacterial Activity and Inhibition of Adherence of *Streptococcus mutans* by Propolis Electrospun Fibers, 16 (2015) 182–191. doi:10.1208/s12249-014-0209-5.
- [188] Y.N. Jiang, H.Y. Mo, D.G. Yu, Electrospun drug-loaded core-sheath PVP/zein nanofibers for biphasic drug release, *Int. J. Pharm.* 438 (2012) 232–239. doi:10.1016/j.ijpharm.2012.08.053.
- [189] L.Y. Huang, C. Branford-White, X.X. Shen, D.G. Yu, L.M. Zhu, Time-engineered biphasic drug release by electrospun nanofiber meshes, *Int. J. Pharm.* 436 (2012) 88–96. doi:10.1016/j.ijpharm.2012.06.058.
- [190] C.J. Thompson, G.G. Chase, A.L. Yarin, D.H. Reneker, Effects of parameters on nanofiber diameter determined from electrospinning model, *Polymer (Guildf)*. 48 (2007) 6913–6922. doi:10.1016/j.polymer.2007.09.017.
- [191] O. Hardick, B. Stevens, D.G. Bracewell, Nanofibre fabrication in a temperature and humidity controlled environment for improved fibre consistency, *J. Mater. Sci.* 46 (2011) 3890–3898. doi:10.1007/s10853-011-5310-5.
- [192] M. Putti, M. Simonet, R. Solberg, G.W.M. Peters, Electrospinning poly(ϵ -caprolactone) under controlled environmental conditions: Influence on fiber morphology and orientation, *Polym. (United Kingdom)*. 63 (2015) 189–195. doi:10.1016/j.polymer.2015.03.006.
- [193] Rose-Ped, L. Bellm, J.B. Epstein, A. Trotti, C. Gwede, H. Fuchs, Complications of radiation therapy for head and neck cancers, *Cancer Nurs.* 25 (2002) 461–467. doi:10.1097/00002820-200212000-00010.
- [194] D. Wolf, J. Otto, Efficacy and Safety of a Lidocaine Gel in Patients from 6 Months up to 8 Years with Acute Painful Sites in the Oral Cavity: A Randomized, Placebo-Controlled, Double-Blind, Comparative Study, *Int. J. Pediatr.* 2015 (2015) 141767. doi:10.1155/2015/141767.

- [195] M. Bågesund, P. Tabrizi, Lidocaine 20% patch vs lidocaine 5% gel for topical anaesthesia of oral mucosa, *Int. J. Paediatr. Dent.* 18 (2008) 452–460. doi:10.1111/j.1365-263X.2007.00910.x.
- [196] N. Blagden, M. de Matas, P.T. Gavan, P. York, Crystal engineering of active pharmaceutical ingredients to improve solubility and dissolution rates, *Adv. Drug Deliv. Rev.* 59 (2007) 617–630. doi:10.1016/j.addr.2007.05.011.
- [197] C. Asawahame, K. Sutjarittangtham, S. Eitssayeam, Y. Tragoolpua, B. Sirithunyalug, J. Sirithunyalug, Formation of orally fast dissolving fibers containing propolis by electrospinning technique, *Chiang Mai J. Sci.* 42 (2015) 469–480.
- [198] Q. Hu, R.J. Noll, H. Li, A. Makarov, M. Hardman, R. Graham Cooks, The Orbitrap: a new mass spectrometer, *J. Mass Spectrom.* 40 (2005) 430–443. doi:10.1002/jms.856.
- [199] R.H. Perry, R.G. Cooks, R.J. Noll, Orbitrap mass spectrometry: Instrumentation, ion motion and applications, *Mass Spectrom. Rev.* 27 (2008) 661–699. doi:10.1002/mas.20186.
- [200] S.C. Moyer, L.A. Marzilli, A.S. Woods, V. V. Laiko, V.M. Doroshenko, R.J. Cotter, Atmospheric pressure matrix-assisted laser desorption/ionization (AP MALDI) on a quadrupole ion trap mass spectrometer, *Int. J. Mass Spectrom.* 226 (2003) 133–150. doi:10.1016/S1387-3806(02)00972-7.
- [201] N. Sharmin, M. Elias-Al-Mamun, M.S. Islam, R.U. Jalil, Preparation and characterization of lidocaine double layer buccal tablet using mucoadhesive Carbopol® polymers, *Dhaka Univ. J. Pharm. Sci.* 10 (2011) 29–34. doi:10.3329/dujps.v10i1.10012.
- [202] N.A. Nafee, F.A. Ismail, N.A. Boraie, L.M. Mortada, Mucoadhesive delivery systems. I. Evaluation of mucoadhesive polymers for buccal tablet formulation, *Drug Dev. Ind. Pharm.* 30 (2004) 985–993. doi:10.1081/DDC-200037245.
- [203] C. Padula, L. Pozzetti, V. Traversone, S. Nicoli, P. Santi, In vitro evaluation of mucoadhesive films for gingival administration of lidocaine, *AAPS PharmSciTech.* 14 (2013) 1279–1283. doi:10.1208/s12249-013-0020-8.
- [204] M. Palo, K. Kogermann, I. Laidmäe, A. Meos, M. Preis, J. Heinämäki, N. Sandler, Development of oromucosal dosage forms by combining electrospinning and inkjet printing, *Mol. Pharm.* 14 (2017) 808–820. doi:10.1021/acs.molpharmaceut.6b01054.

- [205] V. Sankar, V. Hearnden, K. Hull, D.V. Juras, M. Greenberg, A. Kerr, P. Lockhart, L. Patton, S. Porter, M. Thornhill, Local drug delivery for oral mucosal diseases: Challenges and opportunities, *Oral Dis.* 17 (2011) 73–84. doi:10.1111/j.1601-0825.2011.01793.x.
- [206] T. Maver, M. Kurecic, D.M. Smrke, K.S. Kleinschek, U. Maver, Electrospun nanofibrous CMC/PEO as a part of an effective pain-relieving wound dressing, *J. Sol-Gel Sci. Technol.* 79 (2016) 475–486. doi:10.1007/s10971-015-3888-9.
- [207] D.W. Chen, Y.H. Hsu, J.Y. Liao, S.J. Liu, J.K. Chen, S.W.N. Ueng, Sustainable release of vancomycin, gentamicin and lidocaine from novel electrospun sandwich-structured PLGA/collagen nanofibrous membranes, *Int. J. Pharm.* 430 (2012) 335–341. doi:10.1016/j.ijpharm.2012.04.010.
- [208] C.W. Kao, D. Lee, M.H. Wu, J.K. Chen, H.L. He, S.J. Liu, Lidocaine/ketorolac-loaded biodegradable nanofibrous anti-adhesive membranes that offer sustained pain relief for surgical wounds, *Int. J. Nanomedicine.* 12 (2017) 5893–5901. doi:10.2147/IJN.S140825.
- [209] F.Y. Lee, D. Lee, T.C. Lee, J.K. Chen, R.C. Wu, K.C. Liu, S.J. Liu, Fabrication of multi-layered lidocaine and epinephrine-eluting PLGA/collagen nanofibers: In vitro and in vivo study, *Polymers (Basel).* 9 (2017) 416–427. doi:10.3390/polym9090416.
- [210] H. Okamoto, H. Taguchi, K. Iida, K. Danjo, Development of polymer film dosage forms of lidocaine for buccal administration - I. Penetration rate and release rate, *J. Control. Release.* 77 (2001) 253–260. doi:10.1016/S0168-3659(01)00509-0.
- [211] K. Dvořáčková, P. Doležel, E. Mašková, J. Muselík, M. Kejdušová, D. Vetchý, The effect of acid pH modifiers on the release characteristics of weakly basic drug from hydrophilic–lipophilic matrices, *AAPS PharmSciTech.* 14 (2013) 1341–1348. doi:10.1208/s12249-013-0019-1.
- [212] E. Marxen, M.C. Axelsen, A.M.L. Pedersen, J. Jacobsen, Effect of cryoprotectants for maintaining drug permeability barriers in porcine buccal mucosa, *Int. J. Pharm.* 511 (2016) 599–605. doi:10.1016/j.ijpharm.2016.07.014.
- [213] C. Padula, G. Colombo, S. Nicoli, P.L. Catellani, G. Massimo, P. Santi, Bioadhesive film for the transdermal delivery of lidocaine: in vitro and in vivo behavior, *J. Control. Release.* 88 (2003) 277–285. doi:10.1016/S0168-3659(03)00015-4.
- [214] R. Abu-Huwajj, S. Assaf, M. Salem, A. Sallam, Potential mucoadhesive dosage form of lidocaine hydrochloride: II. In vitro and in vivo evaluation, *Drug Dev. Ind. Pharm.* 33 (2007) 437–448. doi:10.1080/03639040601150211.

- [215] C.A. Squier, The permeability of keratinized and nonkeratinized oral epithelium to horseradish peroxidase, *J. Ultrastruct. Res.* 43 (1973) 160–177. doi:10.1016/S0022-5320(73)90076-2.
- [216] M.J. Rathbone, I.G. Tucker, Mechanisms, barriers and pathways of oral mucosal drug permeation, *Adv. Drug Deliv. Rev.* 12 (1993) 41–60. doi:10.1016/0169-409X(93)90040-B.
- [217] D.E. Becker, K.L. Reed, Essentials of local anesthetic pharmacology., *Anesth. Prog.* 53 (2006) 98–109. doi:10.2344/0003-3006(2006)53[98:EOLAP]2.0.CO;2.
- [218] J. D'Alvise, R. Mortensen, S.H. Hansen, C. Janfelt, Detection of follicular transport of lidocaine and metabolism in adipose tissue in pig ear skin by DESI mass spectrometry imaging, *Anal. Bioanal. Chem.* 406 (2014) 3735–3742. doi:10.1007/s00216-014-7802-z.
- [219] S. Kijima, H. Todo, Y. Matsumoto, R. Masaki, W.R. Kadhum, K. Sugibayashi, A useful technique using imaging mass spectrometry for detecting the skin distribution of topically applied lidocaine, *J. Drug Deliv. Sci. Technol.* 33 (2016) 157–163. doi:10.1016/j.jddst.2016.04.004.
- [220] L.S. Eberlin, J. V Mulcahy, A. Tzabazis, J. Zhang, H. Liu, M.M. Logan, H.J. Roberts, G.K. Lee, D.C. Yeomans, J. Du Bois, R.N. Zare, Visualizing dermal permeation of sodium channel modulators by mass spectrometric imaging, *J. Am. Chem. Soc.* 136 (2014) 6401–6405. doi:10.1021/ja501635u.
- [221] E. Marxen, J. Jacobsen, B. Hyrup, C. Janfelt, Permeability Barriers for Nicotine and Mannitol in Porcine Buccal Mucosa Studied by High-Resolution MALDI Mass Spectrometry Imaging, *Mol. Pharm.* 15 (2018) 519–526. doi:10.1021/acs.molpharmaceut.7b00891.
- [222] E. Marxen, L. Jin, J. Jacobsen, C. Janfelt, B. Hyrup, J.A. Nicolazzo, Effect of permeation enhancers on the buccal permeability of nicotine: Ex vivo transport studies complemented by MALDI MS Imaging, *Pharm. Res.* 35 (2018) 70–81. doi:10.1007/s11095-017-2332-y.
- [223] G. Hamm, D. Bonnel, R. Legouffe, F. Pamelard, J.-M. Delbos, F. Bouzom, J. Stauber, Quantitative mass spectrometry imaging of propranolol and olanzapine using tissue extinction calculation as normalization factor, *J. Proteomics.* 75 (2012) 4952–4961. doi:10.1016/J.JPROT.2012.07.035.

- [224] L.J. Sparvero, A.A. Amoscato, C.E. Dixon, J.B. Long, P.M. Kochanek, B.R. Pitt, H. Bayir, V.E. Kagan, Mapping of phospholipids by MALDI imaging (MALDI-MSI): Realities and expectations, *Chem. Phys. Lipids.* 165 (2012) 545–562. doi:10.1016/j.chemphyslip.2012.06.001.
- [225] S.D. Turker, W.B. Dunn, J. Wilkie, MALDI-MS of drugs: Profiling, imaging, and steps towards quantitative analysis, *Appl. Spectrosc. Rev.* 52 (2017) 73–99. doi:10.1080/05704928.2016.1207659.
- [226] A.J. Taylor, A. Dexter, J. Bunch, Exploring Ion Suppression in Mass Spectrometry Imaging of a Heterogeneous Tissue, *Anal. Chem.* 90 (2018) 5637–5645. doi:10.1021/acs.analchem.7b05005.
- [227] F. Kabi, 2% Xylocaine® Viscous, (2014) 1–11. <https://www.accessdata.fda.gov/scripts/cder/daf/index.cfm?event=overview.process&ApplNo=009470> (accessed May 3, 2019).
- [228] D.J. Greenblatt, D.M. Benjamin, C.R. Willis, J.S. Harmatz, M.A. Zinny, Lidocaine Plasma Concentrations Following Administration of Intraoral Lidocaine Solution, *Arch. Otolaryngol.* 111 (1985) 298–300. doi:10.1001/archotol.1985.00800070050005.
- [229] N.L. Benowitz, W. Meister, Clinical Pharmacokinetics of Lignocaine, *Clin. Pharmacokinet.* 3 (1978) 177–201. doi:10.2165/00003088-197803030-00001.
- [230] S. Patil, R.S. Rao, B. Majumdar, S. Anil, Clinical appearance of oral Candida infection and therapeutic strategies, *Front. Microbiol.* 6 (2015) e1391. doi:10.3389/fmicb.2015.01391.
- [231] C.K. Lee, T. Uchida, K. Kitagawa, A. Yagi, N.S. Kim, S. Goto, Relationship between lipophilicity and skin permeability of various drugs from an ethanol/water/lauric acid system., *Biol. Pharm. Bull.* 17 (1994) 1421–1424. doi:10.1248/bpb.17.1421.
- [232] S.W. Smith, B.D. Anderson, Human skin permeability enhancement by lauric acid under equilibrium aqueous conditions., *J. Pharm. Sci.* 84 (1995) 551–556. doi:10.1002/jps.2600840507.
- [233] B.J. Aungst, Absorption Enhancers: Applications and Advances, *Am. Assoc. Pharm. Sci.* 14 (2011) 10–18. doi:10.1208/s12248-011-9307-4.
- [234] Y. Fang, R.M. Eglen, Three-Dimensional Cell Cultures in Drug Discovery and Development, *SLAS Discov.* 22 (2017) 456–472. doi:10.1177/1087057117696795.

- [235] T. Sun, S. Jackson, J.W. Haycock, S. MacNeil, Culture of skin cells in 3D rather than 2D improves their ability to survive exposure to cytotoxic agents, *J. Biotechnol.* 122 (2006) 372–381. doi:10.1016/j.jbiotec.2005.12.021.
- [236] N.P. Yadev, C. Murdoch, S.P. Saville, M.H. Thornhill, Evaluation of tissue engineered models of the oral mucosa to investigate oral candidiasis, *Microb. Pathog.* 50 (2011) 278–285. doi:10.1016/j.micpath.2010.11.009.
- [237] L.A. Royce, P. Liu, M.J. Stebbins, B.C. Hanson, L.R. Jarboe, The damaging effects of short chain fatty acids on *Escherichia coli* membranes, *Appl. Microbiol. Biotechnol.* 97 (2013) 8317–8327. doi:10.1007/s00253-013-5113-5.
- [238] A.L. Barry, S.D. Brown, Fluconazole Disk Diffusion Procedure for Determining Susceptibility of *Candida* Species, *J. Clin. Microbiol.* 34 (1996) 2154–2157.
- [239] P. Sandven, Detection of fluconazole-resistant *Candida* strains by a disc diffusion screening test, *J. Clin. Microbiol.* 37 (1999) 3856–3859.
- [240] Y. Jin, H.K. Yip, Y.H. Samaranayake, J.Y. Yau, L.P. Samaranayake, Biofilm-forming ability of *Candida albicans* is unlikely to contribute to high levels of oral yeast carriage in cases of human immunodeficiency virus infection, *J. Clin. Microbiol.* 41 (2003) 2961–2967. doi:10.1128/JCM.41.7.2961-2967.2003.
- [241] S. De Nollin, M. Borgers, Scanning electron microscopy of *Candida albicans* after in vitro treatment with miconazole, *Antimicrob. Agents Chemother.* 7 (1975) 704–711. doi:10.1128/AAC.7.5.704.
- [242] F.L. Mayer, D. Wilson, B. Hube, *Candida albicans* pathogenicity mechanisms, *Virulence.* 4 (2013) 119–128. doi:10.4161/viru.22913.
- [243] P.D. Rogers, K.S. Barker, Genome-wide expression profile analysis reveals coordinately regulated genes associated with stepwise acquisition of azole resistance in *Candida albicans* clinical isolates, *Antimicrob. Agents Chemother.* 47 (2003) 1220–1227. doi:10.1128/AAC.47.4.1220-1227.2003.
- [244] C. Chen, L. Wang, Y. Huang, Morphology and thermal properties of electrospun fatty acids/polyethylene terephthalate composite fibers as novel form-stable phase change materials, *Sol. Energy Mater. Sol. Cells.* 92 (2008) 1382–1387. doi:10.1016/j.solmat.2008.05.013.
- [245] E. Ismar, A.S. Sarac, Electrospun polyacrylonitrile–lauric acid composite nanofiber webs as a thermal energy storage material, *J. Eng. Fiber. Fabr.* 14 (2019) 1–6. doi:10.1177/1558925018824890.

- [246] J. Nunthanid, P. Sriamornsak, C. Limmatvapirat, M. Luangtana-Anan, S. Limmatvapirat, N. Chinatangkul, Design and characterization of monolaurin loaded electrospun shellac nanofibers with antimicrobial activity, *Asian J. Pharm. Sci.* 13 (2017) 459–471. doi:10.1016/j.ajps.2017.12.006.
- [247] D.S. Wishart, Y.D. Feunang, A. Marcu, A.C. Guo, K. Liang, R. Vázquez-Fresno, T. Sajed, D. Johnson, C. Li, N. Karu, Z. Sayeeda, E. Lo, N. Assempour, M. Berjanskii, S. Singhal, D. Arndt, Y. Liang, H. Badran, J. Grant, A. Serra-Cayuela, Y. Liu, R. Mandal, V. Neveu, A. Pon, C. Knox, M. Wilson, C. Manach, A. Scalbert, HMDB 4.0: The human metabolome database for 2018, *Nucleic Acids Res.* 46 (2018) D608–D617. doi:10.1093/nar/gkx1089.
- [248] National Center for Biotechnology Information, PubChem Compd. Database. (2004). <https://pubchem.ncbi.nlm.nih.gov/compound/3893> (accessed March 15, 2019).
- [249] S.E.W. Grubb, C. Murdoch, P.E. Sudbery, S.P. Savige, J.L. Lopez-Ribot, M.H. Thornhill, Candida albicans-endothelial cell interactions: A key step in the pathogenesis of systemic candidiasis, *Infect. Immun.* 76 (2008) 4370–4377. doi:10.1128/IAI.00332-08.
- [250] D.J. Morse, M.J. Wilson, X. Wei, M.A.O. Lewis, D.J. Bradshaw, C. Murdoch, D.W. Williams, Denture-associated biofilm infection in three-dimensional oral mucosal tissue models, *J. Med. Microbiol.* 67 (2018) 364–375. doi:10.1099/jmm.0.000677.
- [251] D. Seleem, B. Benso, J. Noguti, V. Pardi, R.M. Murata, In vitro and in vivo antifungal activity of licochalcone-A against candida albicans biofilms, *PLoS One.* 11 (2016) e0157188. doi:10.1371/journal.pone.0157188.
- [252] D. Seleem, V.S. Freitas-Blanco, J. Noguti, B.R. Zancope, V. Pardi, R.M. Murata, In vitro evaluation of antifungal activity of monolaurin against Candida albicans biofilms, *Biol. Pharm. Bull.* 41 (2018) 1299–1302. doi:10.7717/peerj.2148.